Characterization of the role of TKTL1 in Acute Monocytic Leukaemia

Inês Viegas Baptista

PhD Thesis

2021

Characterization of the role of TKTL1 in Acute Monocytic Leukaemia

Inês Viegas Baptista

PhD Thesis

2021

UNIVERSITAT DE BARCELONA

UNIVERSITY OF BIRMINGHAM

Doctoral Program in Biotechnology

Department of Biochemistry and Molecular Biomedicine

Faculty of Biology

Characterization of the role of TKTL1 in Acute Monocytic Leukaemia

Doctoral Thesis submitted by Ines do Carmo Viegas Baptista to obtain the Ph.D. degree from the University of Barcelona and University of Birmingham in the frame of a dual degree agreement.

Prof. Marta Cascante Serratosa

Co-supervisor and tutor

Prof. Ulrich Guenther

Co-supervisor

Dr. Silvia Marín Martínez

Co-supervisor

Ines do Carmo Viegas Baptista

Doctoral Student

To my family,

the born and the chosen.

Solid as dreams of a rebel,

We'll always find our way.

Frankie Chavez.

Para ser grande, sê inteiro: nada

Teu exagera ou exclui.

Sê todo em cada coisa. Põe quanto és

No mínimo que fazes.

Assim em cada lago a lua toda

Brilha, porque alta vive.

Fernando Pessoa, Odes de Ricardo Reis.

ABSTRACT

Leukaemia is one of the types of cancer where treatment resistance is prevalent. Better understanding of leukemic cells metabolism opens possibilities for new therapeutic strategies and better prognosis stratification. Leukaemia arises from many different genetic alterations, that affect distinct cellular processes, all driving leukemogenesis. Many of these result in a phenotype that grants metabolic advantages amidst the hypoxic conditions of the haematopoietic niche of the bone marrow, the point of origin of all types of this cancer. In order to understand the metabolic reprogramming that grants these advantages, we performed metabolic characterization in vitro of cell lines of acute monocytic leukaemia (THP1) and chronic myeloid leukaemia (HAP1), with focus on the role of Transketolase-like 1 (TKTL1) and ten-to-eleven Methylcytosine dioxygenase 2 (TET2), respectively, on both normoxic and hypoxic experimental settings.

We revealed that TKTL1 is a key enzyme in the metabolic reprogramming of the hypoxia adaptation, driving proliferation, higher glycolytic rates, higher glutamine consumption and subsequent glutamate production. Our results also showed the altered metabolism of many amino acids and biogenic amines, that grant more substrates for nucleotides synthesis, higher stress tolerance and manipulation of the immune response of the microenvironment. It also highlighted the vulnerabilities that arise from focusing on targeting TKTL1 for therapy and possible secondary targetable metabolic pathways for future therapies.

Additionally, we demonstrated the effects of the loss of TET2 in the leukemic cells through a tracer-based metabolomics approach, showing how its mutation primes the cells to shift their metabolism at a higher cost for their ROS homeostasis, a known hallmark of cancer which increases the risk of more mutations occurring due to genomic instability. This allowed us to create a metabolic map of the changes induced by the loss of TET2,

as a blueprint for new therapeutic venues in leukaemias that have this mutational hit.

Together, the thesis presented here contributes to the knowledge of the mechanisms underlying metabolic reprogramming of leukaemia according to specific mutational genotypes and how they open new possible therapies for patients that develop resistance.

Index

1. INTRODUCTION

1 Introduction

1.1 Leukaemia: The Cancer of the Bone Marrow

1.1.1 Cancer Overview

Cancer has been described as the group of diseases that begins from an abnormal cell growth, uncontrollable and invasive of the adjoining areas from the tissue of origin[1]. According to the World Health Organization (WHO) definition, cancer initiates with an accumulation of genetic mutations that can come from a hereditary background, environmental factors, chemical compounds, diet or infections. The last global report on cancer ordered by WHO in 2018 expected 18.1 million new cases of cancer and 9.6 million deaths derived from it[1]. An update from 2020 was performed by the same team, with the estimations of new cases around 19.3 million and 10 million deaths[2]. These numbers highlight how cancer has become ever more one of the top public health problems, necessary of medical advances on both screening and treatment.

Cancer can be a solid tumour, with a proper mass of cancer cells obstructing the organ or tissue of origin, or they can be considered “liquid tumours”, which consist not of an aggregate of cancer cells but on cells being on the circulatory systems (i.e. leukaemia and lymphoma)[3].

The biology of a tumour has been defined by Hanahan and Weinberg in 10 grouping criteria: The Hallmarks of Cancer. The initial six hallmarks are cell death resistance, evasion of growth suppressors, sustained proliferation, angiogenesis, replicative immortality and capacity for invasion and metastasis[4]. Further scientific breakthroughs led to the addition of 4 remaining hallmarks: inflammatory response activation, cellular energetics dysregulation, immune evasion and genome instability[5]. Different types of cancer manifest these hallmarks distinctly, creating a vast array of subtype classification within a single tumour disease.

1.1.2 Haematopoiesis and the origin of leukaemia

Leukaemia is the denomination of the type of cancer that forms from cells in the bone marrow. It is in the bone marrow that occurs the development and differentiation of the many cellular components of the blood and immune system. This process is called Haematopoiesis. It starts with the Haematopoietic Stem Cells (HSCs), which are self-renewal, multi-potent cells with extremely high proliferative capacity[6]. They exist in the form of two subpopulations: Long-term (LT)-HSCs and Short-term (ST)-HSCs (Figure 1.1.1). The LT-HSCs are the "storage" HSCs that can repopulate the entire haematopoietic system for longer than 3-4 months[7]. Their immediate progeny are the ST-HSCs, which have a limited self-renewal and can only refill the haematopoietic system for one month[8].

It is the ST-HSCs that differentiate into Multipotent Progenitor cells (MPP), with a limited self-renewal, lack of repopulating capacity and still not lineage-committed. The MPP cells then branches out like a tree into 2 types of progenitors: the common myeloid progenitor (CMP) and the common lymphoid progenitor (CLP). It is at this step in the haematopoietic process that lineage-restriction is truly applied, with the CMPs creating the myeloid lineage of blood cells and CLPs originating the lymphoid lineage[9–11]. Further haematological differentiation is described in Figure 1.1.1.

In recent years with the advancement in research on how the haematopoietic process happens thanks to Single-cell Assays evolution, it is now understood that the differentiation is not cut-clear into groups but more of a continuum from progenitor into final cell[12,13]. As such, new representations of haematopoiesis are underway, using trajectory lines of differentiation for each type of cell of the haematopoietic system.

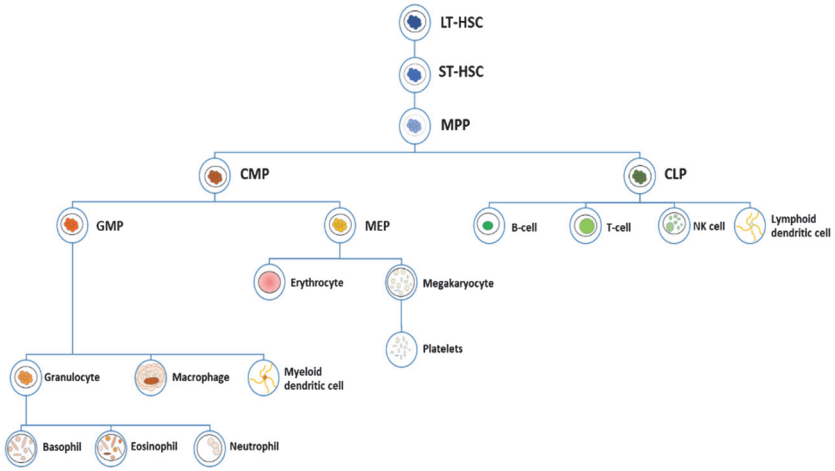

Figure 1.1.1- Schematic of Haematopoiesis. LT-HSCs differentiate into ST-HSCs and sequentially to MPPs. Then it initiates the separate lineages of Myeloid progenitors (CMPs) and Lymphoid progenitors (CLPs). The lymphoid branch generates B-cells, T-cells, Natural killer cells (NK-cells) and lymphoid dendritic cells. The myeloid progenitor differentiates in GMPs and MEPs. The MEPs create Erythrocytes and Megakaryocytes, which in turn makes platelets. The GMPs form Macrophages, Granulocytes and Myeloid dendritic cells. Lastly, granulocytes make basophils, eosinophils and neutrophils. Adapted from Laurenti et al., 2018.

Haematopoiesis is a process that needs very high levels of regulation, finely tuned to control the many different subpopulations of cells and the destiny of HSCs (quiescence, self-renewal and differentiation). This happens with the aid of a complex microenvironment within the bone marrow, denominated as niche[14,15]. The HSC niche has been shown to be responsible for the regulation and maintenance of immune cells and blood production. It is from the niche secretions that the transcription factors and cytokines that regulate HSCs originate[14,16].

Any failure on HSCs regulation, homeostasis of the niche or imbalance on differentiation trajectory can lead to haematological malignancies, such as leukaemia and lymphoma.

1.1.3 Leukaemia epidemiology

As mentioned above, Leukaemia is the cancer that arises from errors during Haematopoiesis, leading to a rapid proliferation of abnormal cells that lack the proper differentiation. Leukaemia is a disease that affects all age brackets, being the 13th place by incidence and 10th by mortality, worldwide, by the end of 2020[2] (Figure 1.1.2).

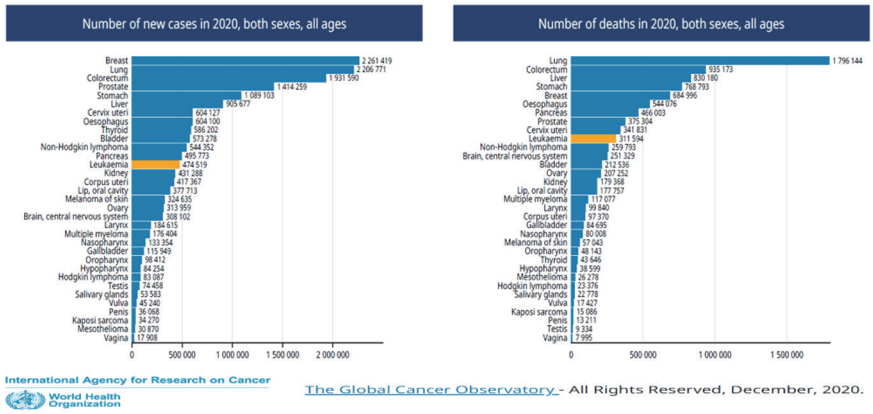

Figure 1.1.2- Cancer Statistics for the year 2020 by WHO. The number of new cases and of deaths, across all ages, for both sexes, for the year 2020 for all main types of cancers. Leukaemia is highlighted in orange. Adapted from Leukaemia fact sheet, available for free use at The Global Cancer Observatory (https://gco.iarc.fr/today/data/factsheets).

Leukaemia has a 5-year relative survival rate of 65%, with the estimations for 2021 of almost 62 thousand new cases and eventual 23.660 deaths[17]. The distribution of leukaemia per age varies according to the leukaemia subtype, with some types occurring almost entirely on children patients and other being specific of old age[18,19].

1.1.4 Leukaemia Classification

The WHO Classification of Tumours of Haematopoietic and Lymphoid Tissues (4th edition, 2008) was revised in 2016 to better structure different types of leukaemias, considering the many haematologic, morphologic, cytogenetic and molecular genetic findings[20].

The classification of Leukaemia is performed using 2 principal criteria: the speed of progression and the nature of the malignant cells found. The speed of progression is defined by how long the disease evolves from acute into the chronic form. The nature of the malignant cells revolves around if it originates from the myeloid or the lymphoid subtypes. The distribution of these characteristics results in 4 major classification of leukaemia: Acute Myeloid Leukaemia (AML), Chronic Myeloid Leukaemia (CML), Acute lymphocytic Leukaemia (ALL) and Chronic lymphocytic Leukaemia (CLL). Within each of these groupings, a more detailed separation of the disease happens according to prevalent genetic events (mutations, translocations, etc.), morphology and other pathophysiological traits[20].

1.1.4.1 Acute Myeloid Leukaemia

AML is the leukaemia that rises from accumulation of mutations on progenitor cells that leads to an increased proliferation of abnormal immature myeloid cells that impede the normal proceedings of Haematopoiesis. These cells infiltrate the bone marrow, bloodstream and subsequently organs. The spreading of the malignant cells leads to a variety of symptoms, such as anaemia, bleeding, infections and organ infiltration[21].

AML is a type of leukaemia that can result from other diseases, such as Myelodysplastic Syndrome (MDS) or Myeloproliferative Neoplasm (MPN)[22,23]. It can also be acquired *de novo*, due to treatments with cytotoxic therapies[24]. AML is further structured in subtypes according to genetic

abnormalities, cytogenetic characterization, due to previous therapies or related to Down Syndrome (Table 1.1-A)[20].

Table WHO Haematological Malignancies Classification (4th Edition
Acute myeloid leukemia (AML) and related neoplasms
AML with recurrent genetic abnormalities
AML with t(8;21)(q22;q22.1);RUNX1-RUNX1T1
AML with inv(16)(p13.1q22) or t(16;16)(p13.1;q22);CBFB-MYH11
APL with PML-RARA
AML with t(9;11)(p21.3;q23.3);MLLT3-KMT2A
AML with t(6;9)(p23;q34.1);DEK-NUP214
AML with inv(3)(q21.3q26.2) or t(3;3)(q21.3;q26.2); GATA2, MECOM
AML (megakaryoblastic) with t(1;22)(p13.3;q13.3);RBM15-MKL1
Provisional entity: AML with BCR-ABL1
AML with mutated NPM1
AML with biallelic mutations of CEBPA
Provisional entity: AML with mutated RUNX1
AML with myelodysplasia-related changes
Therapy-related myeloid neoplasms
AML, NOS (not otherwise specified)
AML with minimal differentiation
AML without maturation
AML with maturation
Acute myelomonocytic leukemia
Acute monoblastic/monocytic leukemia
Pure erythroid leukemia
Acute megakaryoblastic leukemia
Acute basophilic leukemia
Acute panmyelosis with myelofibrosis
Myeloid sarcoma
Myeloid proliferations related to Down syndrome
Transient abnormal myelopoiesis (TAM)
Myeloid leukemia associated with Down syndrome

Table 1.1-A- WHO Classification of AML and related neoplasms. Classification is according to genetic abnormalities (chromosomal translocation, gene mutations), myelodysplasia characteristics, surgency due to therapy, cytogenetic profiling, tissue containment (sarcoma) and relation to Down syndrome complications (from trisomy of chromosome 21). Adapted from Arber et al., 2016.

1.1.4.2 Chronic Myeloid Leukaemia

CML is a Myeloproliferative Neoplasm, defined by a clonal disorder of aberrant myeloid blasts in the bone marrow, with an additional increase of erythrocytes and platelets in peripheral blood[25]. This disorder has its cause on the Philadelphia Chromosome, a genomic abnormality resulting from the translocation of chromosome 9 and 22 (t(9;22) (q34.1;q11.2)). This leads to the formation of the fusion gene BCR-ABL1, detected in almost all CML patients (95% from Philadelphia chromosome, remaining 5% from other translocations). The resulting fusion protein is a constitutively active cytoplasmatic tyrosine kinase, that activates through phosphorylation many signal-transduction cascades for cell growth and differentiation[25].
Symptomologies are fatigue, anorexia and weight loss, but around 40% of patients are asymptomatic[25–27]. Of the total number of new leukaemia cases, around 15% are CML, with an median age of 53 years old at time of presentation but all age groups are affected[25]. The 5-year relative survival rate is at 70.6%, mostly due to the implementation of Tyrosine Kinase Inhibitors (TKIs) as a standard treatment[27].

1.1.5 Mutations in leukaemia and their implication with metabolism

As amply referenced above, Leukemogenesis originates on mutations and errors of the normal haematopoietic process. At which step the abnormality occurs or the order of accumulated errors results in many subtypes of leukaemia. AML is mostly resulting from gene mutations or translocations that disrupt the homeostasis of the cell. The main genetic abnormalities used for classification relate to transcription factors[28–31], epigenetics[30,32–35] and proliferation[36] (Table 1.1-A). But these changes by themselves are not capable of converting the haematopoietic cell into a tumour cell. Other mutations contribute during the tumorigenesis. Many common mutations that happen across all AML subtypes are Fms-like tyrosine kinase 3[37] (FLT-

3) (around 30%), Isocitrate Dehydrogenase 1 (IDH1) and IDH2 (15-20%), NPM-1[35] (around 30%) and CEBPA[33] (5-10%). Other recurrent mutations are NRAS, KRAS, TP53, DNA-methyltransferase 3A (DNMT3A), Ten-to-Eleven Methylcytosine Dioxygenase 2 (TET2) and Additional Sex Combs like 1 Transcriptional Regulator (ASXL1)[19,38,39].

On the same hand, CML with the BCR-ABL1 fusion gene results on the constitutively active tyrosine kinase that initiate the signalling pathways of proliferation (NRAS, KRAS, MAPK)[40,41]. The BCR-ABL1 enzyme itself can also differ depending on where the break of the BCR gene during the translocation process, leading to different isoforms that translate into different CML phenotypes. CML shares some of the same common mutations of AML, such as NRAS, KRAS, TET2, ASXL and RUNX1[41].

The overall range of mutations that happen in leukemogenesis must be detected during prognosis, for they represent separate phenotypes and correlate with different prognosis[42]. For example, the germline mutations of MECOM (MDS1 and EVI1 complex locus protein, also known as positive regulatory domain zinc finger protein 3 (PRDM3)) lead to poor prognosis of both AML and CML adult patients[43].

The fact that many common mutations between AML and CML affect the cellular proliferation pathways and gene expression regulation aids the tumour cells to modulate many bioprocesses to its advantage. This creates a completely different metabolism from the progenitor cells, with high energetic demands and constant proliferation causing upregulation of Glycolysis and the Pentose Phosphate Pathway (PPP), for rapid energy gains and generation of ribonucleic building-blocks, respectively (see section 1.3.1). An extensive repertory of metabolic studies on distinct cancer types, including leukaemia, have identified plenty of key enzymes that cancer cells depend on for survival and to gain resistance to treatments[44–50]. A common example of mutations altering the metabolism in Leukaemia is IDH1 and IDH2, which mutations lead to a gain-of-

function, that generates the metabolite 2-Hydroxyglutarate (2-HG), an antagonist of α-Ketoglutarate (αKG) that competes for the same binding site on αKG-dependent enzymes but blocks their activity (such as TET2)[51–53]. Another case is the overexpression of transketolase-like 1 (TKTL1), an enzyme involved in cellular energetics and DNA-building blocks generation, that correlates with poor prognosis of CML patients[54]. Preliminary analysis of TKTL1 capacity as a biomarker for short remission (under 6 months) in AML patients have shown promise[55] but further studies of that possibility have been almost non-existent.

The tumorigenesis process relies on the synergy of the total of these mutations and its effects on the cellular homeostasis, generating a very distinct metabolic profile from its surrounding niche. Such a change can be exploited, has many research studies have already proven[45]. Studying these changes have helped elucidate vulnerabilities of cancer cells that can aid on the efficiency of standard treatments[56]. Further analysis of how specific metabolic genes are being altered in leukemogenesis must be a priority. As such, the focus of our work will be to elucidate on how the overexpression of TKTL1 and the loss of TET2 influence the metabolism of leukaemia cells.

1.1.5.1 Transketolase-like 1

TKTL1 is an isoform of Transketolase (TKT), a very important enzyme in cellular energetics. The TKT family is composed of TKT, TKTL1 and TKTL2[57]. They belong to the non-oxidative branch of the PPP, that provides energy, generates ribonucleic acids for *de novo* synthesis and aids in the Nicotinamide adenine dinucleotide phosphate ($NADP^+$) pool for use in redox reactions (see section 1.3.2). Of all the transketolases, TKTL1 is the one more commonly found overexpressed in cancer[58].

TKTL1 has a 77% homology with TKT[59] and predicted to perform the same enzymatic activity[57]. TKT acts through dimerization, with homodimers of TKT or heterodimers of TKT-TKTL1[60]. TKT expression is regulated positively by Nuclear factor Erythroid 2-like 2 (NRF2) and negatively by BNB and CNC Homolog 1 (BACH1)[61]. The TKTL1 isoform is expressed through promoter hypomethylation[62,63] and can be induced by hypoxia-inducible factor 1 alfa (HIF1α)[64,65]. Recent reports indicate that TKTL1 exists in a forward-loop with HIF1α, the main transcription factor responsible for cellular adaptation to hypoxia[66] (see section 1.4). A normoxic stabilization of HIF1α occurs from the increase generation of pyruvate and lactate[62]. HIF1α then promotes the expression of TKT (and its isoforms), whose activity feeds substrates back to glycolysis and lead to a positive reinforcement of HIF1α expression and stabilization, maintaining the upregulation of many glycolytic enzymes[67].

Previous studies have also proven that the knockdown of TKTL1 decreased the proliferation rate, lowered the $NADP^+$/NADPH ratio and increased Reactive Oxygen Species (ROS) levels , leading to increased apoptosis and re-sensitizing resistant cell lines back to the treatment[68].

TKTL1 has been found to work as a moonlight enzyme, which are multifunctional proteins with more than one physiologically relevant biochemical function[69,70]. Apart from its enzymatic activity in the non-oxidative PPP, it has been reported that TKTL1 aids on checkpoints of the cell cycle, in order to guarantee the availability of Ribose-5-Phosphate (R5P) to build new ribonucleic acids during S phase[60,63]. It can also interact with the PI3K/AKT pathway, a very important signalling pathway of proliferation and cell survival, with TKTL1 overexpression correlating with higher activation of AKT[71–73]. For the specific case of AML, TKTL1 was tested as a biomarker for complete remission (CR) and was found to be higher in patients that had a CR with less than 6 months[55]. To this day no follow-up studies of this potential in AML has been reported.

As mentioned before, TKTL1 has been correlated with poor prognosis on CML patients[54]. It has also been found across a wide range of different types of solid tumours, such as melanoma[63], nasopharyngeal carcinoma[74], uterine cervix cancer[58,75], glioblastoma[71,76], prostate cancer[77],lung cancer[78] and breast cancer[72], to name a few. Across all these distinct diseases, the overexpression of TKTL1 was reported to influence cell proliferation, tumour progression, invasive capacity, treatment response and survival estimation. Of note, the ascending levels of TKTL1 correlate with tumour stage, with highest levels on cancers on the metastatic stage[77]. Due to this importance, a new biomarker diagnosis test was created, the Epitope-detection in monocytes (EDIM). This blood test screens for macrophages (activated monocytes) that had phagocyted tumour cells, carrying tumoral proteins, through specific antibodies for the biomarkers Apo10 (Apo10-epitope of Desoxyribonuclease X) and TKTL1[79,80].

The fact that HIF1α promotes the actions of the TKT family of enzymes is of most relevance for cancers of the hematopoietic niche. AML and CML both exist in hypoxia states, firstly because that is the natural condition of the bone marrow[15] and secondly because tumours become hypoxic at the centre of their mass over time due to uncontrolled expansion[81,82]. Since TKTL1 has already been reported as a good biomarker to predict behaviour and response to treatments in CML patients, a similar role in AML cases must be investigated more deeply.

The collective research done about TKTL1 have set it up in a position not only as prognosis biomarker but as a cross-section between metabolism, proliferation signalling and hypoxia response. These characteristics makes it a prime target for metabolic profiling. The fact that no body of work has currently looked more in depth on the role of TKTL1 in acute myeloid leukaemia is a lack of knowledge that must be culminated most urgently.

1.1.5.2 Ten-to-Eleven Dioxygenase 2

The TET Dioxygenase family of enzymes have an important role on epigenetic maintenance, more specifically the regulation of the methylation of genes. It is composed of TET1, TET2 and TET3 enzymes[83], that participate on various steps of demethylating cytosine bases of the DNA. The TET enzymes are α-KG-dependent, needing oxygen and Fe-II to perform its function, releasing succinate and CO_2 as a result. The TET enzymes are recruited after the action of DNMT1 (responsible for methylation maintenance) or DNMT3 (responsible for *de novo* methylation), that methylate cytosines. The TET enzymes then make a sequential oxidation of 5-methylcytosine (5mC) into 5-hydroxymethylcytosine (5hmC), 5-formylcytosine (5fC) and 5-carboxylcytosine (5caC)[83] (Figure 1.1.3). The 5fC can also be transformed to 5-hydroxymethyluracil (5hmU) by Activation-induced Deaminase (AID) and by Apolipoprotein B mRNA editing enzyme (APOBEC). All these molecules (5fC, 5caC) can then be transformed by Thymidine DNA Glycosylase (TDG) or go through Base Excision Repair (BER) mechanisms (5hmC, 5fC, 5caC and 5hmU) back into original cytosine. It is through this process that TET enzymes regulate methylation-based silencing and prevent aberrant hypermethylation[84], common in cancer cells. TET2 can interact with a plethora of epigenetic agents. It can recruit O-linked β-D-N-acetylglucosamine transferase (OGT) to the chromatin, regulating gene transcription[85]. Many transcription factors influence its activity, such as Wilms' tumour suppressor 1 (WT1) recruiting TET2 to target genes[86] or Dvl-binding protein IDAX (Inhibition of Dvl and Axin complex) promoting its degradation by caspase activation[85]. It can also be negatively regulated by micro-RNAs at the pre-mRNA level[87]. For example, miR22 can downregulate all TET genes and was found in high levels in AML and MDS patient samples[88].

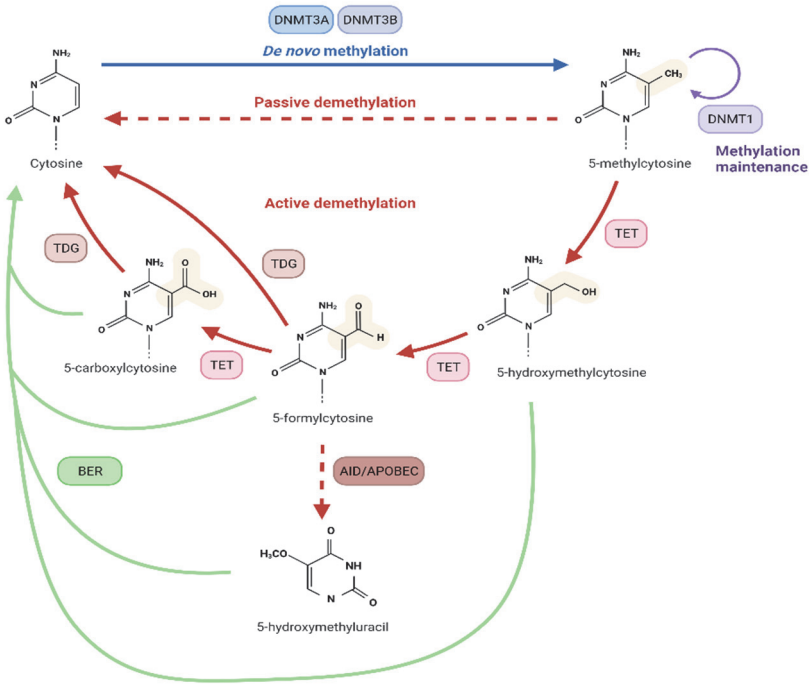

Figure 1.1.3 - Schematic of DNA methylation and demethylation processes. Cytosine base of DNA is methylated by DNMT1, DNMT3A and DNMT3B, resulting in 5-methylcytosine (5mC). Subsequent oxidation by TET enzymes (TET1, TET2 and TET3) generates 5-hydroxymethylcytosine (5hmC), 5-formylcytosine (5fC) and 5-carboxylcytosine (5caC). Additionally, AID/APOBEC converts 5fC into 5-hydromethyluracil (5hmU). TDG then transforms 5fC and 5caC back to cytosine. 5hmC, 5fC,5caC and 5hmU suffer Base Excision Repair (BER) to revert back to cytosine. Adapted from Kunimoto et al., 2014. Created in Biorender.com.

TET enzymes activity can be recovered by Vitamin C (ascorbic acid)[89,90] and by overexpression of NAD-dependent protein deacetylase Sirtuin-1 (SIRT1)[91,92]. Additionally, TET proteins have been found to regulate telomerase shortening. The specific mechanisms of this role are still unclear, but absence of TET enzymes was followed by increased telomere-sister chromatid exchanges[93].

Studies have shown that TET2 mutations are prevalent across multiple types of leukaemia (as mentioned in section 1.1.5), being one of the earlier

mutation hits on the leukemogenesis process. The mutations of TET2 are heterozygous, hemizygous (due to chromosomal defects) or homozygous[94], although the latest is very rare. The loss of 1 allele results in partial or even total inactivation of TET, with the wildtype (WT) copy not being enough to perform its duties[85]. Of note, no distinct phenotype was identified from having a heterozygous or homozygous phenotype, with no difference of Overall Survival (OS) across different cancer patients[85]. The type of mutations that happen are mostly missense mutations, with frameshift and nonsense mutations also occurring[94].

Although the other members of the TET family can perform most of the same functions, it is the loss of TET2 that generally leads to leukemogenesis. While mutations on TET1 and TET3 also occur in tumours, it is TET2 that is the preferred TET enzyme expressed in haematopoietic cells and by default the more mutated in haematological diseases[85]. The loss of TET2 cannot by itself make the full cellular transformation into cancer but it was attested to grant a growth advantage[85]. And since TET2 has such a vital function regulating epigenetic events, from methylation status to scaffolding for DNA "machinery", its loss eventually leads to genomic instability. This creates "fertile ground" for the appearance of other mutations, that will build synergy to start tumorigenesis (Table 1.1-B). For example, TET2 mutations with additional FLT3 mutations induce AML and with ASXL1 mutations generate MPN[83,85].

TET2 mutation frequencies across Haematological Diseases	Frequency (%)
Acute Myeloid Leukaemia (adult)	8-32
Chronic Myeloid Leukaemia	4
B-cell Lymphoma	2-12
T-cell Lymphoma	20-83
Chronic Myelo-monocytic Leukaemia	20-58
Blastic plasmocytoid dendritic neoplasm	25-54
Systemic mastocytosis	20-29
Myelodysplastic Syndrome	6-26
Polycythemia vera / Primary Myelofibrosis/ Essential Thrombocytosis	2-20

Table 1.1-B- Frequencies of TET2 mutations across Haematological Diseases. Adapted from Scourzic et al., 2015 and Rasmussen et al, 2016.

Besides its function on DNA repair mechanisms, TET2 is also linked to immune cells regulation. It is necessary during maturation of T-cells to differentiate to T-helper (Th) cells and T-regulatory (T-reg) cells, maintaining T-cells homeostasis[92]. TET2 deficiencies have been found to impair plasma cell differentiation, promoting B-cell lymphoma[92], and to have deficient-macrophages alter the microenvironment in order to reduce tumour burden in melanoma[95].

On the metabolic front, the fact that TET2 is dependent on αKG, makes any alteration to this metabolite levels affect DNA repair. As mentioned above (see section 1.1.5), mutations of IDH result in the generation of 2-HG, that will compete with αKG for TET2. For these reason, IDH mutations are mutually exclusive of TET2 mutations, i.e., they target the same pathway resulting in the same phenotype[96]. Similarly, mutations on Fumarate Hydratase (FH) and Succinate Dehydrogenase (SDH) can also inhibit TET2 activity, by scarcity of needed metabolites and are also mutually exclusive[51,97]. Ultimately, cancer cells either have a mutated TET2 or an altered mechanism that will block its activity. Another example is Branched-chain amino acids transaminase 1 (BCAT1), with its overexpression leading to low αKG levels, DNA hypermethylation and post-translational stabilization of HIF1α, the same phenotype as IDH and TET2 mutations[98].

The last factor to consider is the link between TET2 and hypoxia. Dioxygenases mandatorily need oxygen for their activity and hypoxic conditions put a strain on their performance. On this category of proteins is not only TET2 but also Prolyl Hydroxylase Domain (PHD) enzymes, which hydroxylate HIF1α, marking it for degradation by ubiquitination[99,100]. Studies have found a link between overexpression of HIF1α and TET2 regulation, resulting in low 5hmC content, leading to gene expression that aids on aggressive phenotypes in melanoma[89]. This regulation can be rescued by silencing of HIF1α, at both the gene and protein level. If the

same can be proven in leukaemia, it could be a major step in developing therapies to impede resistance or rescue pre-leukemic HSCs. At the same time, other research works have found that the reduction in activity of TET enzymes in hypoxia are only resulting from oxygen shortage, showing that 48% of hypermethylation events are hypoxia-related across multiple types of cancer and independent of mutations[101]. A deeper understanding of the role of TET2 activity in hypoxia must be pursued.

Due to its many functions and the resulting array of diseases that comes from its loss, TET2 is a very interesting protein. Add to the fact that its activity relies on the availability of metabolites and oxygen, it can be used to generate diagnose-indicative metabolic profiles. In fact, it is already exploited through immunohistochemistry, by staining of 5mC and 5hmC, whose levels will increase and decrease respectively without TET2[85]. Further elucidation of the metabolic alterations due to TET2 loss on the context of leukaemia, specifically of CML, will be one of the directions of this thesis.

1.2 Epigenetic Instability as a Hallmark of Leukaemia

Genome Instability is one of the newer Hallmarks of Cancer[5]. It mainly consists of mutant genotypes that confer advantages to a subclone cell to eventually dominate the tissue environment. Therefore, cancer can be described as succession of clonal expansions of a mutant genotype. But some clonal expansions can be initiated by non-mutational events such as histone modifications, reshape chromatin for gene expression. All these phenomena that affect DNA reading without altering its sequence are grouped under the term Epigenetics[102]. Coined by Waddington in 1942, these events were found to create a heritable phenotype, that passes on during cell replication. Those changes can be histone modifications, DNA methylation, chromatin remodelling and changes in non-coding RNA[103–107]. These will govern many cellular processes, like embryonic stem cells (ESC)

development[103,105,108] and immune cells differentiation[105,109]. The epigenetic landscape created by these modifications then works in tandem with transcription factors, to determine cell type identity [109,110]. Different stimuli can alter this "identity", with endogenous (genetic inheritance, cell-cell interactions, etc.) or exogenous origins (environmental factors, diet, etc.)[110].

Proteins participating in epigenetic control of gene expression have been separated into three categories: epigenetic readers, epigenetic writers and epigenetic erasers[111]. Simply put, the writers are the enzymes that perform the modification that the reader recognizes and is later removed by the eraser. There is overlap of functions since many writers and erasers also possess reader domains[109].

Tumour cells can arise from altered epigenetic events, that can express oncogenes (genes that promote cancer) or repress tumour suppressor genes (TSG)[104,111]. Tumorigenesis involves epigenetic aberrations, such as hypermethylation of promotor regions while having global DNA hypomethylation status and alterations to histone modifications that disrupts chromatin, affecting accessibility for transcription factors[106,110].

In the case of Leukemogenesis, the epigenetic landscape is highly susceptible to aberrations, because it is essential in HSCs to direct differentiation and the most common mutations of leukaemias are epigenetic participants (DNMT3, TET2, ASXL1) (see section 1.1.5)[112,113]. For tumoral contribution, it is more likely that epigenetic dysregulation is the primary mechanism instead of just an accumulation of somatic mutations of genes of epigenetic modulation members[105].

Cancer Epigenetics is a fast-evolving area, with many directions of growth. Elucidation of the weight of epigenetic aberrations on the formation of tumours, across many cancer types, is a massive undertaking of many research teams across the world. Those endeavourers have already resulted in therapies using chromatin-targeting drugs and hypomethylating

agents[103,111,112,114], with high promising potential to counter-act resistance to standard therapies.

1.2.1 Alterations of DNA methylation status in Leukaemia

DNA methylation is a common epigenetic mechanism of control of gene expression. It occurs by adding methyl groups to 5'-position of cytosine, on CpG islands (Cytosine-phosphate-Guanine), considered a silencing mark[105]. Across the genome, CpG islands mostly occur on promoter regions of genes, with its methylation correlating with silencing transcription. This methylation is performed by DNMTs, by transferring the methyl group from S-Adenosyl-L-methionine (SAM) to create 5mC[105]. Different DNMTs are expressed at different times for distinct functions. DNMT1 is responsible for maintenance of methylation pattern during chromosome replication, DNMT3A and DNMT3B are the *de novo* methyltransferases that make the initial methylation (highly active during embryogenesis)[112,115]. The demethylation process is under the care of TET enzymes, that perform a series of oxidations that eventually revert to unmodified cytosines by BER (see section 1.1.5.2).

As mentioned above, cancer shows aberrant methylation profile of majorly hypomethylated but pockets of hypermethylation (Figure 1.2.1). Global hypomethylation promotes chromosomal instability (deletions, rearrangements), reactivation of transposable elements and loss of imprinting. While the hypermethylation that occurs on CpG islands corresponds to promoters of TSGs[109,110]. This leads to silencing of many important tumour suppressors such as retinoblastoma tumour-suppressor gene (*Rb*), von Hippel-Lindau tumour-suppressor gene (*VHL*), $p16^{INK4a}$, breast-cancer susceptibility gene 1 (*BRCA1*) and *TP53*[109,115].

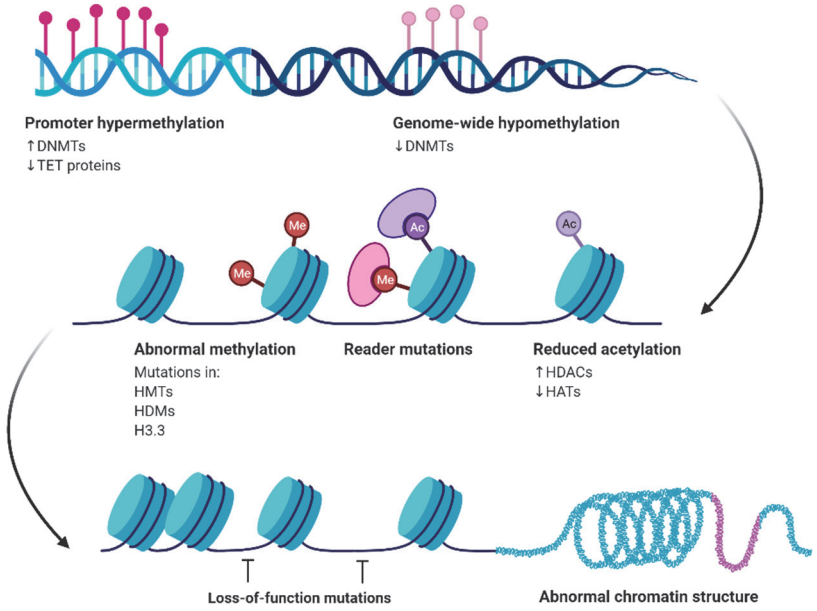

Figure 1.2.1- DNA methylation alterations and the impact on chromatin structure. Promoter hypermethylation occurs by increased DNMTs action and diminishing TET-mediated demethylation while a genome-wide hypomethylation happens. This leads lo alterations to epigenetic writers (DNMTs, HATs, HMTs), readers and erasers (TETs, HDACs, HDMs), that result in mutations of nucleosome packaging and an abnormal chromatin structure. Created in Biorender.com.

In Leukaemia, mutations in participants of both methylation and demethylation have been reported (as mentioned in section 1.1.5). The transcription factor CEBPA (see Table 1.1-A) is commonly mutated in AML but it can also have its expression altered by hypermethylation of its promoter[112]. Mutations in DNMT3 are recurrent in leukaemias and leads to a global hypomethylation profile[114,115]. Contrary effect is the mutations in TET proteins, that result in DNA hypermethylation. And both lead to leukemogenesis, for both are equally essential for HSCs regulation and differentiation. Further elucidation of how the different genetic abnormalities of leukaemia affect the epigenetic events are underway[104,112]. In regards for therapeutic approaches, hypomethylating agents have been

developed, such as Azacitidine and Decitabine. These agents incorporate into DNA of replicant cells and irreversibly bind to DNMTs, depleting them and leading to a hypomethylated status[103,112]. They are currently approved for treatment of AML and MDS and expansion of applications are being pursued[104,109].

1.2.2 Histone Modifications: gatekeeping access to DNA

Another type of epigenetic event is histone modifications. Histones are members of nucleosome, the core unit of chromatin, that consists of 147 base pairs (bp) of DNA wrapped around a histone octamer core[105,106]. The histones are numbered into H1 (the linker), H2A/H2B (dimers) and H3/H4 (central tetramer)[105,106]. These histones have amino termini that act as histone tails that can suffer post-translational modifications (PTMs). These modifications can be acetylation, methylation, phosphorylation, ubiquitination, to name the most relevant and studied[106]. These modifications control genomic DNA condensation and alter access for binding to DNA. Another function of histone modification and their re-structuring of chromatin is regulation of alternative splicing[109,116]. Histone marks are enriched in the borders of exons and their flanking intronic regions[109].

Histone acetylation relates to active transcription and deacetylated status stops it (Figure 1.2.2). This process is mediated by Histone Acetyltransferases (HATs) and Histone Deacetylases (HDACs), many of which are mutated in leukaemia[106,109,116]. Histone methylation can either activate or inactivate transcription, depending on the situation. Another layer to be considered is that histones can be mono-, bi- or trimethylated, with each level of methylation having different effects. These methylations are done by Histone Methyltransferases (HMTs) and removed by Histone Demethylases (HDMs)[106].

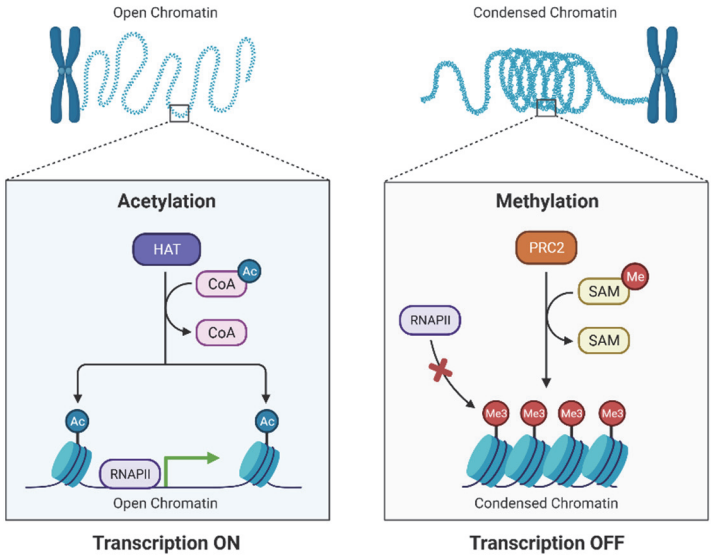

Figure 1.2.2- Histone modifications modulate chromatin condensation for transcription. Acetylation performed by HATs, by transferring the acetyl group from Coenzyme A (CoA) to the histone, opens the chromatin and allows the binding of RNA polymerase II (RNAPII) to initiate transcription. Histone methylation performed by Polycomb Repressive Complex 2 (PRC2), using methyl groups from SAM donors, condenses the chromatin and blocking RNAPII binding, impeding the initiation of transcription. Created in Biorender.com.

Most histone modifications reported and studied to date are to H3. Targeting of H3K4 and H3K36 leads to activation of transcription while H3K92/3 and H3K27me2/3 modifications induce gene silencing[104,117]. Of great relevance is the fact that histone modifications to H3K9 are involved in chromosome X inactivation, gene repression at promoter regions and formation of heterochromatin (condensed DNA usually found in structures such as centromeres and telomeres)[84,85,104,105,116].

Dysregulation of histone modifications are common in cancer. Loss of histone acetylation and increased methylation of histone H3-K9 were found in hypermethylated promoters of TSG[106,116]. Another feature in cancer is that histone dysregulation happens downstream or upstream of DNA methylation, so both events happen in tandem during tumorigenesis[106,116].

In leukaemias, there are many mutations and aberration that affect histone modifications, such as PML-RARA, that induce abnormal recruitment of HDACs[105,116]. Another common mutation in leukaemia occurs on HMTs, such as Enhancer of Zeste Homologue 2 (EZH2), a component of the Polycomb Repressive Complex 2 (PRC2), and Mixed-lineage Leukaemia (MLL) proteins[111,116]. EZH2 losses its HMT activity after chromosomal translocation, leading to PRC2 losing its function of transcriptional silencing maintenance, while KMT2A (an MLL protein) activates gene transcription by modification of H3K4[105,109,116]. EZH2 can also be reduced by mutations to the splicing factors U2AF1 and SRSF2, that dysregulates processing of pre-mRNA[105,109,111,116].

The Food and Drug Administration (FDA) regulatory body have approved several inhibitors of HDACs (HDACi), such as Belinostat and Romidepsin, for treatment of multiple myeloma and T-cell lymphoma[104,109,111,116]. Although they show pleiotropic effects (actions beyond the specifically developed function) that blur the true mechanism of action of these drugs. Alternatives are being developed with EZH2 inhibitors and histone lysine demethylases (KDM) inhibitors, with clinical trials under way[109,116].

1.2.3 Micro-RNAs, the genome "hidden agents"

Of the whole human genome, only 1.2% encodes proteins but most of the genome is still transcribed[118]. The elucidation of this discrepancy lead to the discovery of short and long non-coding RNA (ncRNA) that brought to light new types of RNA to already existing ones (transporter RNA (tRNA), ribosomal RNA (rRNA), small nuclear RNA (snRNA))[107,118]. One of these new RNAs is micro RNA (miRNA), a ncRNA of 22 nucleotides in length that is equivalent to messenger RNA (mRNA) without translating to proteins[107] (Figure 1.2.3). Instead these miRNAs will regulate gene expression by mRNA cleavage, translational inactivation or deadenylation[105,119]. They participate in regulation of many important

functions such as cell division, differentiation and even cardiac function regulation (cardiac rhythm, myocyte growth, etc.)[105,107,120]. Many new miRNAs are discovered each year but there are still a large number of them unbeknownst to us.

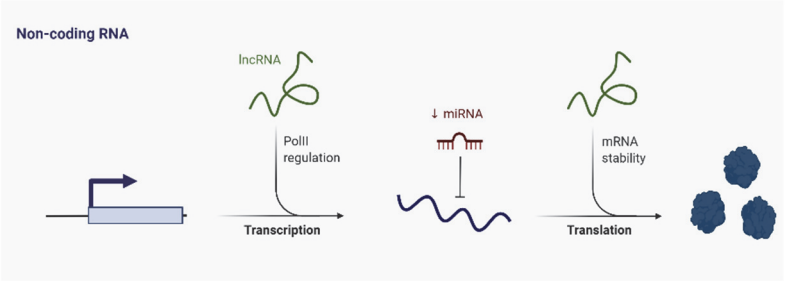

Figure 1.2.3- Epigenetic regulation by Non-coding RNAs. Long non-coding RNAs (lncRNA) can regulate with Polymerase II (PolII), modulating the transcription process. Micro-RNAs (miRNA) can bind to the resulting transcript and impede its translation by directing it for degradation processes. Created in Biorender.com.

The activity of miRNAs is by itself an epigenetic event, but they also interact with the other epigenetic events mentioned above. They can induce DNA methylation or demethylation, the many types of histone modifications or impede the events by blocking access by binding to the target area of DNA[105,110].

In cancer, many miRNAs are being discovered across different types of tumours and correlated with aggressive phenotypes and patient outcome[104].

It has been reported that Leukemogenesis can be triggered by aberrant miRNAs impeding haematopoiesis. Of relevance in AML, Let-7 is a miRNA that can affect many oncogenes (KRAS, MYC, etc)[105,121], miR-29 can induce apoptosis[122] and miR-24 is linked to poor survival and risk of relapse[123].

The research on miRNAs is an ongoing process, with much therapeutic applicability potential, that will revolutionize how we diagnose and treat many types of cancer.

1.2.4 The "symbiosis" of epigenetic events with Transcription Factors in Leukaemia

Epigenetic events are intertwined with the actions of transcription factors. The epigenetic events mentioned above are necessary for granting access to transcription factors for DNA binding. On the other hand, transcription factors can also initiate epigenetic events. For example, the cocktail of 4 transcription factors used to induced cells back into a pluripotency state (Oct4, Sox2, KIf4 and Nanog) happens due to their influence on changing the epigenetic landscape[108]. Transcription factors can also make regulatory loops, that impose epigenetic regulation on that zone and most often are a positive-feedback loop[106,110]. For example, the CCTC-binding factor (CTCF) is responsible for 3-dimensional structures in chromatin, creating the mentioned regulatory loops. These loops can both bring promoters and enhancers closer or isolate regions to avoid transcription (insulator function)[124]. Indirectly, transcription factors can influence epigenetic events through control of ncRNAs[105,107].

Across cancer types, transcription factors have been investigated for their role in tumorigenesis. Cancer cells utilize transcription factors to manipulate a multitude of pathways, from cell proliferation induction to avoiding apoptosis[125–127]. But counteraction of this manipulation is difficult, since transcription factors are regulated by many participants and are necessary very carefully "tailored" treatment regiments with other drugs to avoid resistance[125,126].

In Leukaemia, many transcription factors are implicated with the many genomic abnormalities. The chromosomal translocations that are defining of so many types of leukaemias involve transcription factors, such as PML-RARA, RUNX1, CEBPA, CBFB and GATA2 (see Table 1.1-A). These lead to abnormal activity that can silence TSGs promoters or activate oncogenes[109,124]. Another layer that affects transcription factors on

leukaemias is the common mutations, such as ASXL1 (see section 1.1.5). ASXL1 is a transcriptional regulator, responsible for the recruitment of EZH2 and PRC2 stability. Although the exact effect of mutations to ASXL1 is unclear (loss or gain of function), clear correlations were stablished with higher risk for patients of AML and MDS, and association with RUNX1 and NPM1 mutations[94,116]. Another example is mutations to EZH2, which involve a gain-of-function that leads to abnormal histone modification (H3K27me3) and will block B-cell development[105,116]. Of note is also alterations of CTCF function, occurring by hypermethylation of its binding sites, blocking its activity (correlated with loss of TET2)[124]. CTCF also interacts with other key transcription factors that are commonly mutated in leukaemia, such as NPM1, CEBPA and RUNX1[124,126].

Further research on the interplay between transcription factors and epigenetic events is needed, to discern their interactions and how to use it for therapeutic advantage. Many studies are underway to characterize the effect of epigenetic drugs on the epigenetic activity of transcription factors[104,116,125].

1.2.5 The Epigenetic machinery is dependent on metabolism

The epigenetic machinery is a vast network of many different components that must work in harmony to regulate gene expression of distinct cellular processes. Besides their interaction with transcription factors, there is another cellular process that has input into the activity of epigenetic modulators: the generation of metabolites[104,109]. Many metabolites are used as co-factors of the distinct epigenetic writers and erasers. As such, the availability of such metabolites (i.e. diet stimuli) will influence the epigenetic landscape. As mentioned above, SAM is used as a methyl donor during the DNA methylation performed by DNMTs and acetyl Coenzyme A (acetyl-CoA) is used during histone acetylation[110,128]. Another common crosstalk of epigenome and metabolism in leukaemia is the case of mutated

IDHs. The production of the oncometabolite 2-HG will interfere with the activity of αKG-dependent enzymes, such as TET enzymes (see section 2.1.5.2), KDM enzymes (histone lysine demethylases) and AlkB family members (nucleic acid demethylases)[116,129].

It has also been reported, across many types of cancer, that DNA methylation is used to induce the Warburg Effect (see section 1.3.1). DNA hypermethylation alters expression at gene (direct start of transcription) and protein levels (by avoidance of degradation mechanisms) of many key players of glycolysis, PPP, gluconeogenesis, redox balance and oxygen sensing pathway[130].

Further investigations of the link between DNA methylation status and Warburg effect should be done on a leukemic perspective, especially due to alterations reported to the oxygen sensing pathway (HIF accumulation)[130].

1.3 Metabolic Dysregulation as a Hallmark of Leukaemia

Since many of the molecular alterations involved in the origin of leukaemia manifest in modified phenotypes, a metabolic dysregulation is a natural occurring event arising from those changes.

In general terms, metabolism is the reactions that occur in an organism or cell[131]. These reactions can be catabolic or anabolic. The first is a destructive process that breaks molecules for energy or "building-blocks" while the second is the reverse, involving the synthesis of compounds[131]. The metabolic pathways utilised both types of reactions to generate the many metabolites needed for all cellular functions, such as energy production, proliferation, biosynthesis and homeostasis[131].

Over the many years of studying cancer, a constant factor that researchers highlight is that the tumorigenic process results in a direct or indirect dysregulation of metabolism, leading to a proliferating advantage. Within the Hallmarks of Cancer, this proliferative advantage is characterized

according to the way the advantage is conferred, from deregulating cellular energetics, avoiding apoptosis or growth suppressors, sustaining proliferative signalling or induction of angiogenesis[5].

For the case of leukaemia, many of its originating molecular events are at the epigenetic level, as covered previously (see section 1.1.5 and 1.2). But there are also other types of mutational events during leukemogenesis affecting metabolism, enhancing proliferation or apoptosis evasion. In fact, one of the characteristics used to identify and classify the many types of leukaemia is the abnormal proliferation of a particular type of haematopoietic cell. Another layer of adaptation that leukaemia cells must endure is the hypoxic microenvironment of the bone marrow and haematopoietic niche. Many studies have showed how cancer cells change metabolic processes to support its proliferation and survival such as glycolysis, pentose phosphate pathway, TCA cycle, lipid synthesis and mitochondrial activity[132–135]. The metabolic reprogramming that cancer cells induce is a dynamic interplay between oncogene overexpression and inactivation of TSGs[136]. These genes cover alterations to transcription factors, signalling pathways members, apoptosis inhibitors and inducers, cell cycle regulators, DNA repair and many other processes, resulting in the disrupted metabolism observed.

1.3.1 Glycolysis and the Warburg Effect

Glycolysis is the principal step of many energy production processes. Glucose intake to cells is facilitated by glucose transporters (GLUTs), of which there are 14 known isoforms. These isoforms expression vary according to tissue and intracellular compartment, with the GLUT 1 to 4 being the more studied given their overexpression in cancer[137–140].

Once inside, glucose is broken down by nine reactions, catalysed by specific enzymes at each step (Figure 1.3.1). The flux of this process is regulated by rate-limiting enzymes: hexokinase (HK), phosphofructokinase

(PFK) and pyruvate kinase (PK)[141,142]. The resulting pyruvate at the end of the process is normally transported to mitochondria, where it will produce acetyl-CoA, CO_2 and NADH through the oxidative decarboxylation by the Pyruvate Dehydrogenase Complex (PDC)[142]. The resulting acetyl-CoA is then integrated in the Tricarboxylic Acid Cycle (TCA), also known as Krebs Cycle (see section 1.3.3), followed by the oxidative phosphorylation (OXPHOS) that will lead to production of Adenosine Triphosphate (ATP)[143]. But in the unnormal ways of cancer, most of the pyruvate produced is converted to lactate by Lactate Dehydrogenase (LDH), indifferent if oxygen is present or not[144]. This aerobic glycolysis was denominated as Warburg Effect, in honour of its discovery by Otto Warburg[145]. Although it produces only 2 ATP molecules, this process is a common metabolic reprogramming of cancer cells for a faster energy production and avoiding production of ROS by the mitochondrial processes and subsequent apoptosis activation[146,147].

Many types of cancer show overexpression of many participants of glycolysis, mainly GLUTs, HK, PFK, PK and LDH[142]. Another important factor is the TP53-induced glycolysis and apoptosis regulator (TIGAR), that inhibits glycolysis and redirects its flux into the PPP, for oxidative resistance and to avoid apoptosis[148]. This regulator is usually found overexpressed in many types of cancer such as breast cancer, lung cancer, leukaemia and colon cancer[148].

As for the case of leukaemia, many studies have reported distinct ways that glycolysis is upregulated. In ALL, glycolysis genes are upregulated in addition to down-regulation of TCA cycle genes, driving the Warburg Effect[149]. Leukaemias with FLT3 mutations (see Table 1.1-A) also increases glycolysis, that if blocked can counteract resistance to tyrosine kinase inhibitors treatments[150,151]. Another strong evidence of the metabolic rewiring of leukaemias is that blocking the gene expression of PKM2 and LDHA in HSCs delays the myeloid leukaemia development[152].

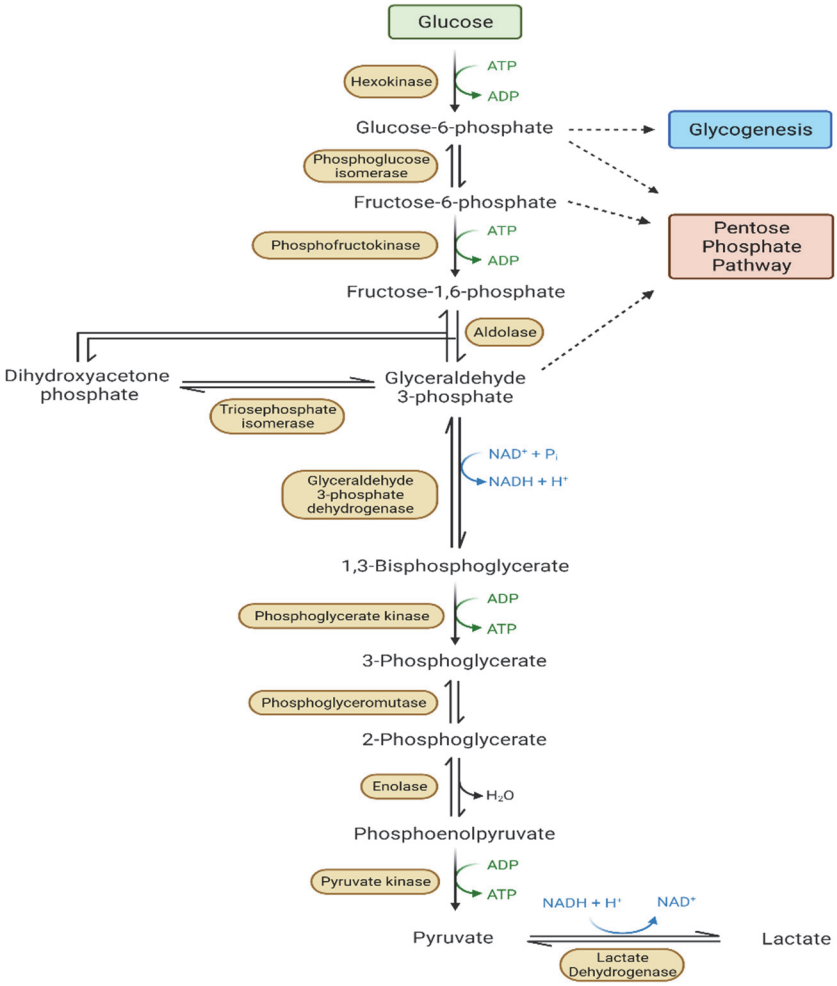

Figure 1.3.1- Schematic of the reactions of glycolysis from glucose to pyruvate and lactate. Glucose is catalyzed into Glucose-6-Phosphate (G6P) by Hexokinase (HK). G6P can be direct into other processes such as glycogenesis and Pentose Phosphate Pathway (PPP) or catalyzed by Phosphoglucose Isomerase (GPI) to form Fructose-6-Phosphate (F6P). The resulting F6P can either be directed to the PPP or catalyzed to Fructose-1,6-phosphate by Phosphofructokinase (PFK). Subsequent reaction catalyzed by Aldolase (ALDO) generates Dihydroxyacetone Phosphate (DHAP) and Glyceraldehyde-3-Phosphate (G3P). DHAP can be converted to G3P by Triosephosphate Isomerase (TPI). G3P can also be directed into PPP or catalyzed into 1,3-Bisphosphoglycerate by Glyceraldehyde-3-Phosphate Dehydrogenase (GAPDH). Following reaction by phosphoglycerate kinase (PGK) produces 3-phosphoglycerate (3PG) and ATP. 3PG is broken down to 2-Phosphoglycerate (2PG) by Phosphoglyceromutase (PGM). Enolase then converts 2PG into Phosphoenolpyruvate (PEP), releasing H_2O. Phosphoenolpyruvate is catalyzed by Pyruvate Kinase (PK) into pyruvate, releasing ATP. Pyruvate can be transferred to mitochondria or can be converted into lactate by Lactate Dehydrogenase (LDH). Created with BioRender.com.

Lastly, leukaemia cells can also influence the glycolysis inside the haematopoietic niche, through stimulation of the production of Insulin-like Growth Factor Binding Protein 1 (IGFBP1) from adipocytes, that desensitizes the surrounding normal cells to insulin, conferring the cancer cells with an advantage in glucose acquisition inside the niche[153]. Another point for the hypothesis of microenvironment regulation of HSCs in the scientific community is the increased expression of GLUT1 without changes at the transcriptomic level[154], allowing more glucose uptake. Further changes have been detailed at various levels in the reviews of Wang *et al* , Unwin *et al* and Rashkovan *et al* [135,152,154].

1.3.2 Pentose Phosphate Pathway

The Pentose Phosphate Pathway is a parallel pathway of glucose metabolism. After the first step of glycolysis catalysed by HK, the resulting Glucose-6-Phosphate (G6P) can be diverted to the PPP (Figure 1.3.2). The initial steps of the PPP are defined as the oxidative branch, with irreversible reactions that produce pentoses, NADPH, CO_2 and protons (H^+). The first reaction is catalysed by Glucose-6-Phosphate Dehydrogenase (G6PD), that oxidizes G6P into 6-phosphogluconolactone, followed by hydrolyzation by Phosphogluconolactonase (6-PGL) and lastly by oxidative decarboxylation of 6-phosphogluconate into Ribulose-5-Phosphate (Ru5P) by 6-phosphogluconate Dehydrogenase (6PGD)[155–157].

The breakdown of Ru5P is then taken over by the non-oxidative branch of PPP (Figure 1.3.2). Ribulose-5-Phosphate can be interconverted both into Xylulose-5-Phosphate (X5P) by Ribulose-5-phosphate Epimerase (RPE) and Ribose-5-Phosphate (R5P) by Ribose-5-phosphate Isomerase (RPI)[155,158]. R5P is utilized in the synthesis of RNA and DNA for cell duplication but both X5P and R5P can be used by Transketolase (TKT), that utilizes thiamine diphosphate (TDP) as a co-factor in order to rearrange 2 carbons from X5P into R5P, generating Sedoheptulose-7-Phosphate

(S7P) and G3P. Both these substrates are then used by Transaldolase (TALDO), that transfers 3 carbons from S7P back into G3P, generating Erythrose-4-Phosphate (E4P) and F6P. There is a secondary reaction performed by TKT, that instead of using R5P to receive the 2 carbons from X5P, it transfers them into E4P, resulting in F6P and G3P[155,156]. As mentioned in section 1.1.5.1, there are isoforms of transketolase, TKTL1 and TKTL2, with active catalytic function[57]. Although it is TKTL1 which is found overexpressed in many types of cancer, reflecting in poor prognosis[54,58,159]. While the oxidative branch is composed of irreversible reactions that generate NADPH for reductive reactions, the non-oxidative branch is reversible at all its steps, allowing more flexibility in adjusting to the requirements of cell. Not only the non-oxidative branch makes components that intersect with glycolysis (F6P and G3P), it produces R5P that serves as the "scaffold" for ribonucleic acids synthesis or converted into adenosine diphosphate ribose[155,156,158].

Cancer cells can use the interplay between PPP and glycolysis to drive their proliferation and survival, directing the flux to produce NADPH, ribonucleic acids building blocks and G3P and F6P for energy production through aerobic glycolysis[158]. Most alterations in the oxidative branch happens to G6PD and to lesser extent to 6PGD. G6PD can have its expression influenced by transcription factor NRF2 and by mTORC1[160,161], by post-translational modifications for activation or dimerization[162–165], degradation by ubiquitination[166] and by epigenetic regulation through $H3K36me^2$ of its promoter[167]. 6PGD aberrant expression is also reported in various cancers, accelerating proliferation, inducing invasiveness and resistance to treatment[168–171]. These alterations mostly lead to increased flux from glycolysis to PPP, increasing the generation of NADPH.

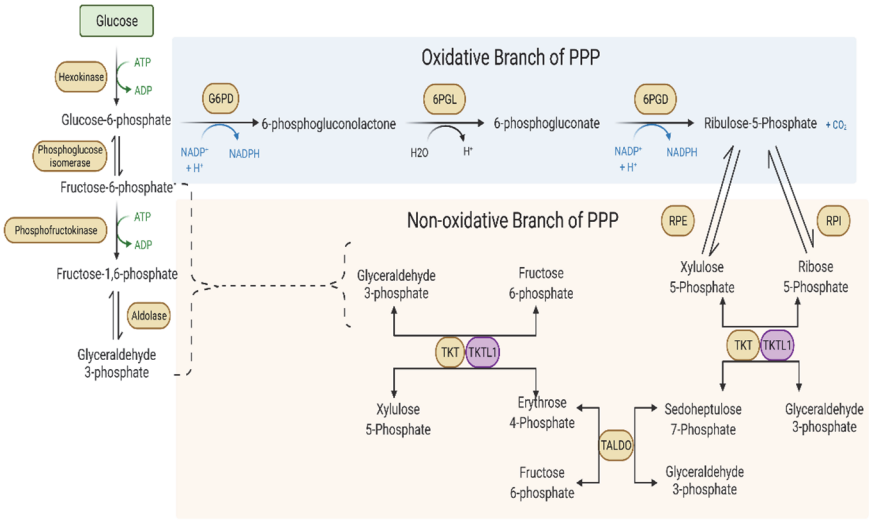

Figure 1.3.2- Interplay of Glycolysis and the branches of the Pentose Phosphate Pathway (PPP). After conversion from glucose by hexokinase (HK), Glucose-6-phosphate (G6P) enters the oxidative branch of the PPP, where it is catalyzed by Glucose-6-phosphate Dehydrogenase (G6PD) into 6-phosphogluconolactone, with side reduction of NADP to produce NADPH. Following reaction catalyzed by Phosphogluconolactonase (6PGL) generates protons (H^+) and 6-phosphogluconate, which in turn is used by 6-phosphogluconate Dehydrogenase (6PGD) to make Ribulose-5-Phosphate (Ru5P), with side byproducts of NADPH and CO_2. Ru5P is then taken into the Non-oxidative branch of the PPP, by conversion into 2 possible substrates: Xylulose-5-Phosphate (X5P) by Ribulose-5-phosphate Epimerase (RPE) and Ribose-5-Phosphate (R5P) by Ribose-5-phosphate Isomerase (RPI). Both substrates are then used by Transketolase (TKT) and Transketolase-like 1 (TKTL1), resulting in Sedoheptulose-7-Phosphate (S7P) and glyceraldehyde-3-phosphate (G3P). A similar reaction is performed by Transaldolase (TALDO), that uses S7P and G3P to form X5P and Erythrose-4-Phosphate (E4P). These substrates are then used by TKT (also TKTL1), that generates G3P and Fructose-6-Phosphate (F6P). These last 2 substrates are a connecting point with glycolysis, flowing between both pathways depending if the cell requires more reductive power (NADPH) and ribonucleic building blocks (R5P) or energy requirements (glycolysis). Adapted from Xuemei Tong et al, 2020. Created with BioRender.com.

Cancer manipulation of the non-oxidative branch is more varied. RPI and RPE expression can be induced by mutated KRAS, a common mutation in various leukaemias[172]. RPI can also be regulated epigenetically, through inhibition by miR-124, resulting in slower cell growth[173]. TALDO overexpression correlates with poor outcome and treatment resistance in

breast cancer[174]. As for TKT, both it and its isoform TKTL1 are found overexpressed across various types of cancer, but not the isoform TKTL2[175,176]. TKT activity is promoted by HIF1α[64], induced by increasing fructose levels[177] and modulated by signalling pathways[61,178,179], resulting in genomic instability[180]. The reprogramming of these enzymes by tumour cells result in the uncoupling of the non-oxidative reactions from the oxidative branch of the PPP. This leads to an increased adaptability to obtain R5P to synthetize *de novo* RNA and DNA without producing NADPH if not necessary.

Leukaemia has been reported to upregulate many members of the PPP. A study reported alterations of the whole PPP gene set in 61% of AML patients (100 out of the 166 patients analysed)[181]. Another study demonstrated in a mouse model that ecotropic viral integration site 1 (EVI1), a nuclear transcription factor encoded on the MECOM gene (commonly translocated in leukaemias, see Table 1.1-A), could bind to enhancer and promoter regions of 6PGD, RPIA and TALDO1, driving the appearance of AML[182]. Another transcription factor commonly mutated in leukaemia, CEBPA increases mRNA and protein levels of G6PD and 6PGD in B-cell malignancies (B-cell ALL and B-cell lymphoma)[183]. TKT is induced in HIF1α-mediated resistance to imatinib in BCR-ABL expressing leukemic cells[64] and TKTL1 overexpression correlates with poor prognosis in CML patients[54].

1.3.3 Mitochondrial Activity

Mitochondrial activity is vital for the cell, for it is a central point of many processes necessary for its survival. It is the "powerhouse" of the cell, where energy production occurs with the fuel obtained from glucose, fatty acids and amino acids[184–187]. This activity is also the source of much of the ROS produced by the cell, as a by-product of OXPHOS[184]. Simultaneously, it is the mitochondria that regulates the intrinsic pathway of apoptosis, by

modulating the release of cytochrome *c* through the formation of pores in its membrane[188,189].

The TCA Cycle occurs inside the mitochondrial matrix, with acetyl-CoA resulting from the PDC conversion of pyruvate being used to form citrate. This is considered the beginning of the process, that consists of 8 main reactions (Figure 1.3.3). Of these 8 reactions, the reaction of Isocitrate Dehydrogenase (IDH), α-Ketoglutarate Dehydrogenase and Malate Dehydrogenase produce NADH, that can be used for redox balance. The reaction of Succinate Dehydrogenase (SDH) transfers 2 hydrogens to Flavin Adenine Dinucleotide (FAD), producing $FADH_2$. The ATP production originates from OXPHOS, with oxidation of nutrients using the previously produced $FADH_2$ and NADH as electron donors and O_2 as the final acceptor, generating water and ROS[184,190]. Of all the TCA cycle reactions, only 3 are irreversible: Citrate Synthase, IDH and α-Ketoglutarate Dehydrogenase. Of note that IDH is considered irreversible due to the negative change in free energy but in certain conditions can be reversible. The remaining enzymes of the cycle can catalyse both directions. While the entirety of the cycle occurs inside the mitochondria, there are both cytosolic and mitochondrial isoforms of some of its enzymes, allowing the production of substrates in both compartments that can be transported in and out according to the needs of the cell[187].

The use of these TCA cycle intermediates from cytosolic production to feed the cycle is called Anaplerosis[184]. For example, pyruvate can be converted to oxaloacetate (OAA) by Pyruvate Carboxylase, if low levels of OAA supersede the requirements of acetyl-CoA for the formation of citrate[184]. Another case is Malic Enzyme, that transforms malate into pyruvate with NADH generation in the cytosol[184,185]. In fact, the TCA cycle is an interconnection of energy production and the metabolism of many amino acids, both synthesis and catabolism, aiding to maintain its intermediates levels.

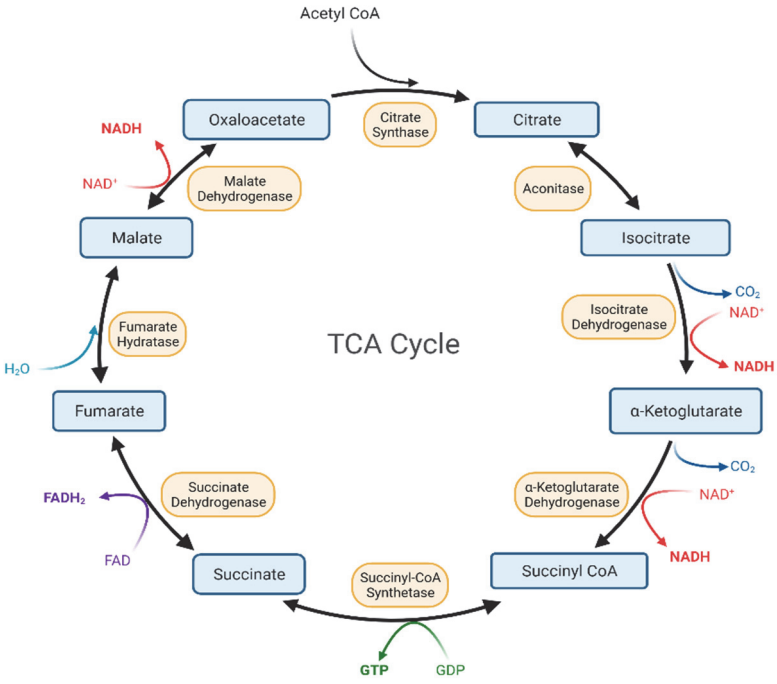

Figure 1.3.3- The reactions and products of the TCA Cycle. Acetyl-CoA is used by Citrate Synthase to generate citrate. Followed by Aconitase producing Isocitrate and subsequent production of α-Ketoglutarate (αKG) by Isocitrate Dehydrogenase (IDH), with side generation of CO_2 and NADH. Same byproducts occur on the following reaction, catalyzed by α-Ketoglutarate Dehydrogenase to produce Succinyl-CoA. The conversion of Succinyl-CoA produces GTP, by transferring the phosphate group into GDP and generating Succinate, catalyzed by Succinyl-CoA Synthetase. Succinate conversion into Fumarate is catalyzed by Succinate Dehydrogenase (SDH), generating $FADH_2$. Fumarate Hydratase (FH) then hydrates fumarate into malate. Malate is then converted into Oxaloacetate by Malate dehydrogenase (MDH), also with generation of NADH. The restarting of the cycle occurs with Citrate Synthase joining Oxaloacetate (OAA) with fresh Acetyl-CoA in the first reaction described. Adapted from Sajnani et al, 2017. Created with BioRender.com.

Initially, it was theorized by Warburg that cancer cells are characterized by dysfunctional mitochondria, given their predilection for aerobic glycolysis[191]. But this hypothesis did not hold true, with evidence showing that cancer cells can suppress respiration and oxidative phosphorylation in a glucose-induced manner[192,193]. This capability is coined the "Crabtree Effect", a reversible and short-term event that allows the cancer cells to

shift between Warburg Effect and respiration, granting adaptability to the microenvironment and the nutrient availability. In reality, mitochondrial activity in cancer cells can be impaired or enhanced, depending on the type of cancer and the specific mutations relating to mitochondrial processes such as TCA cycle[185], apoptotic signalling[194] and ROS production[190].

The direct ways that TCA cycle can be altered in cancer is by mutations of its enzymes. SDH, FH and IDH are commonly mutated in renal cancer and Leukaemias[96,185,195,196]. As mentioned in section 1.1.5, IDH mutations are a gain-of-function that results in the new metabolite 2HG, which impedes the flow of the TCA cycle in the direction of succinyl-CoA production and interferes on epigenetic regulation. Mutations on SDH and FH have similar effects, given that succinate and fumarate also have a role on epigenetics[197–200].

The ROS production native of the mitochondrial activity can both be a result of dysfunction and a tumorigenic factor in cancer transformation, further discussed in section 1.3.6.

Generally, leukemic cells have a mitochondrial phenotype of high TCA Cycle activity as inheritance of HSCs, that use this process for the generation of substrates needed for the epigenetic regulation of differentiation, such as αKG for HDMs and TET enzymes[201].

1.3.4 Metabolism of Amino Acids

As mentioned previously, the metabolism of amino acids is fundamental to many metabolic processes. The existing 20 amino acids are categorized into two groups: essential amino acids (EAAs) and non-essential amino acids (NEAAs). This classification is given according to the ability of synthetization by our human cells, with essential meaning a diet requirement[202]. EAAs consist of Histidine, Lysine, Methionine, Phenylalanine, Threonine, Tryptophan and the Branched-chain amino acids (Isoleucine, Leucine and Valine). NEAAS are all the other remaining amino

acids: Alanine, Aspartate, Asparagine, Arginine, Cysteine, Glutamate, Glutamine, Glycine, Proline, Serine and Tyrosine.

The metabolism of amino acids are a web of interconnected pathways of catabolism and synthesis. As an example, glutamine generates glutamate, which in turn can be used to make alanine, aspartate, serine and proline. EAAs metabolism is mainly catabolic reactions, with their breakdown resulting in NEAAs, such as Phenylalanine producing Tyrosine[203].

This interconnectivity is key for cancer metabolism, allowing the tumour cells to use amino acids to produce intermediates for the TCA cycle, the urea cycle, the One-Carbon metabolism, the methionine salvage pathway and for redox homeostasis[203,204].

1.3.4.1 Glutamine: the addiction of cancer

Glutamine is a NEAA and one of the most consumed nutrients by cells, second only to glucose[205]. Its importance comes from being a doble source of atoms, of both carbons and nitrogens for the synthesis of other molecules[205]. Glutamine uptake occurs through many distinct transporters of amino acids, with the most known being Alanine-Serine-Cysteine Transporter 2 (ASCT2, coded by *SLC1A5*), Sodium-coupled Neutral Amino Acid Transporter 1 (SNAT1, coded by *SLC38A1*) and SNAT2 (coded by *SLC38A2*). Once inside the cells, glutamine can be utilized for 2 main purposes. First as a nitrogen donor, glutamine participates in transaminase reactions for the synthesis of purines and pyrimidines[206]. Secondly, as a carbon donor to generate glutamate at the same time that its nitrogen generates ammonia. It also plays a role on the production of NAD^+, glucosamine-6-phosphate, polyamines and other NEAAs (alanine[207], aspartate[208], serine[209], proline[210] and ornithine[211]. Glutaminolysis begins with the deamination of glutamine into glutamate by Glutaminase (GLS)[212,213], which in turn can be deaminated into αKG by Glutamate Dehydrogenase (GLUD) (see section 1.3.4.2) or can participate in

transaminase reactions transferring the amine group to other metabolites. The resulting ammonia from glutaminolysis must be detoxified, a process further detailed in section 1.3.4.4.

IDH, besides the oxidative reaction during TCA cycle, can also perform reductive carboxylation, that converts αKG back to isocitrate, allowing flexibility in Anaplerosis[205]. Glutaminolysis is also necessary for redox balance (see section 1.3.6), mTOR signalling, autophagy and apoptosis[214–216]. Glutamine can also be produced, by the condensation of glutamate and ammonia, a reaction catalysed by Glutamine Synthetase (GS) that requires ATP[217].

All these characteristics of glutamine metabolism makes it a focal point of metabolic reprogramming in cancer cells[204,205]. In fact, many cancer types have been reported to be glutamine-addicted, with their proliferation and survival depending on glutamine donor role for biosynthesis[218–221] and production for ammonia detoxification and pH balancing[222]. For the case of leukaemias, glutamine also plays a similar essential role for their metabolism for TCA cycle fuel, proliferation signalling and redox control[223]. Another layer of importance is that hypoxia response increases expression and activity of GS[224,225], indicating the relevance of glutamine metabolism on the microenvironment of the bone marrow[204].

1.3.4.2 Glutamate

Glutamate is another NEAA, that can be synthetized through many distinct pathways of metabolism. Glutamate uptake shares many transporters with other amino acids such as Excitatory Amino Acid Transporters (EAATs) and ASCTs[221,226,227]. As mentioned in the previous section, Glutamate is a member of glutaminolysis, that results from the deamination of glutamine and is transformed into αKG by GLUD, but it can also be produced through transaminase reactions[204,205]. One of such reactions is the catabolism of

BCAAs by Branched-Chain Amino Acid Transaminase 1 and 2 (BCAT1 and 2), that convert αKG into glutamate[228].

Glutamate is used in the synthesis of glutathione[229] (see section 1.3.6) and other amino acids such as proline, aspartate, alanine, serine and ornithine[202,230].

1.3.4.3 Serine, Glycine and Methionine: The One-Carbon Metabolism

Serine is a NEAA that is highly consumed by cancer cells[231]. Its uptake is done by many different transporters such as ASCT2 and SNATs[226,227]. It can also be synthetized from 3PG, one of the intermediates of glycolysis, by Phosphoglycerate Dehydrogenase (PHGDH) with conversion of NAD^+ into NADH[202,232] (Figure 1.3.4).

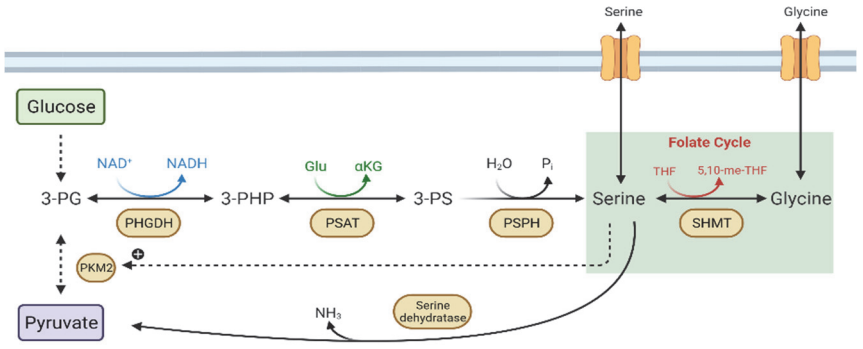

Figure 1.3.4- Schematic of the Serine Synthesis Pathway (SSP). The 3-Phosphoglycerate (3PG) produced from glycolysis is used by Phosphoglycerate Dehydrogenase (PHGDH) to produce 3-Phosphohydroxypyruvate (3PHP), with generation of NADH. Phosphoserine Aminotransferase (PSAT) converts 3PHP into 3-phosphoserine (3PS), through a Glutamate-dependent transamination. The last step that produces serine is the hydrolysis of 3PS by Phosphoserine Phosphatase (PSPH), with the release of an inorganic Phosphate (Pi). Serine is then converted to Glycine by Serine Hydromethyltransferases (SHMT), donating a one carbon unit to Tetrahydrofolate (THF) and making 5,10-methylenetetrahydrofolate (5,10-me-THF), which are members of the Folate Cycle. Serine is used as activator of pyruvate kinase, M2 isoform (PKM2). Serine can be deaminated by Serine Dehydratase, generating pyruvate and ammonia (NH_3). Adapted from Yang et al., 2016. Created with BioRender.com.

Serine can then be utilized as a building block in purine and lipid synthesis, as well as other amino acids such as cysteine and glycine[232]. It also possesses a regulatory function over glycolysis as an allosteric activator of PKM2, an isoform of Pyruvate Kinase. This allows to block the flow of glycolysis at the phosphoenolpyruvate level and redirect it back to 3PG for serine production if its levels are low[202,233]. It can also be transformed into pyruvate by Serine Dehydratase, with side generation of ammonia.

Glycine can be generated from glyoxylate aminotransferase, the Glycine Cleavage System, Threonine and Serine metabolisms[202]. It is used as a precursor in the generation of many metabolites, such as glutathione, nucleic acids, sarcosine and uric acid[202]. Mainly, glycine levels arise through the reaction of Serine Hydromethyltransferases (SHMT) 1 and 2, cytosolic and mitochondrial isoforms respectively[202,232]. This conversion between Serine and Glycine generates one-carbon units (methyl groups), which are then utilized in the cycles of Folate and Methionine. The conjugation of these pathways is denominated the One-Carbon Metabolism[232].

The folate cycle is a key pathway for synthesis of nucleotides, epigenetic events substrates and reductive metabolism[234]. It is initiated when folate (commonly known as vitamin B9) is transformed into Tetrahydrofolate (THF) by Dihydrofolate Reductase (DHFR) in two consecutive reactions[234]. THF is then used on the folate cycle to generate substrates for purine and pyrimidine synthesis and for the methionine cycle (Figure 1.3.5). Although methionine is an EAA, it can be salvaged by Methionine Synthetase (MS), also known as 5-methyltetrahydrofolate-Homocysteine Methyltransferase (MTR). This enzyme uses 5-methyl-THF and homocysteine to make methionine, with the vitamin B12 (cobalamin) as a cofactor[235]. Methionine in turn is catalysed into S-Adenosylmethionine (SAM), a very important metabolite for methyltransferases (MATs) such as DNMTs (as mentioned in section 1.2.1). Not only for MATs, SAM is

essential for the creation of polyamines (see section 1.3.5), a set of important reactions that aid in the salvage of methionine[235] (Figure 1.3.5). The totality of these pathways generate many key substrates for the function of the cells, such as purine and pyrimidine synthesis, redox power in the form of $NADP^+$, FAD and glutathione production (see section 1.3.6), deoxythymidine monophosphate (dTMP) for DNA synthesis and SAM for methylation reactions.

Cancer cells exploit the One-Carbon Metabolism and its partnered pathways in many ways. Overexpression of SHMT2 leads to poor survival and prognosis in breast and hepatic cancer[236,237]. The multifunctional enzyme MTHFD has a cytosolic enzyme (MTHFD1) and two mitochondrial forms (MTHFD1L and 2/L). Upregulation of the MTHFD2 isoform has been reported across many types of cancer, like AML and breast cancer[238,239]. As for MTHFD1, its polymorphisms are indicative of treatment outcome of childhood ALL[240,241].

Alterations of the methionine cycle are a mutational factor in cancer, with methylation reactions for epigenetic regulation becoming compromised[235], as mentioned in section 1.2.1. Lastly, another point of One-Carbon Metabolism in cancer is its connection with the polyamines metabolism, with over expression of Ornithine Decarboxylase (OCD) and Adenosylmethionine Decarboxylase (AMD), aiding tumoral proliferation[242].

Another point of overlap between pathways with One-Carbon Metabolism is the $NADP^+$/NADPH production. MTHFD1 complements the NADPH production in the cytosol and the mitochondrial isoforms assist the generation done by the TCA cycle[234,235]. These interactions aid to control the negative effects of ROS production, allowing to avoid apoptosis[243].

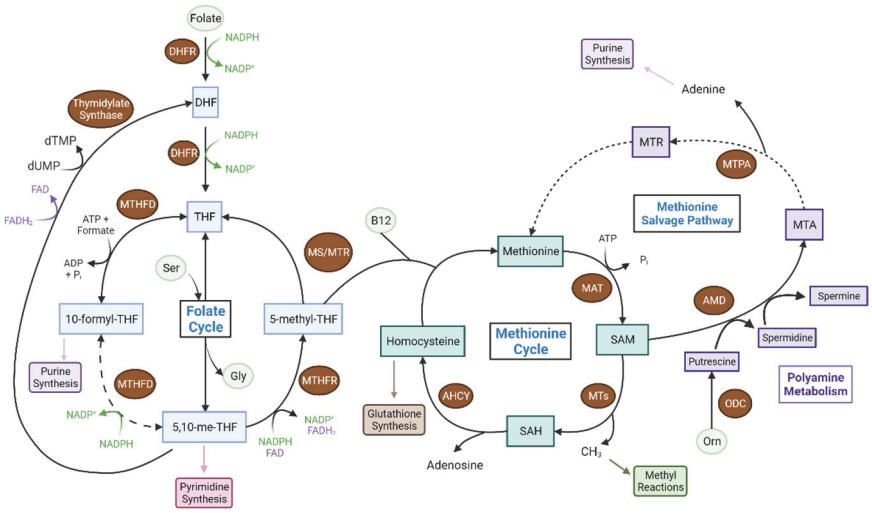

Figure 1.3.5- One Carbon Metabolism and partner metabolisms. Folate is converted to Dihydrofolate (DHF) and Tetrahydrofolate (THF) by the same enzyme, Dihydrofolate Reductase (DHFR). THF can be transformed into 5,10-methylene-THF (5,10-me-THF) by SHMT, using Serine (Ser) as carbon donor and resulting in Glycine (Gly). There are 3 reactions of the Folate Cycle performed by the enzyme Methylenetetrahydrofolate Dehydrogenase (MTHFD). It can transform THF into 10-formyl-THF as a Formate-tetrahydrofolate Ligase, with ATP and Formate as cofactors, releasing ADP and P_i. Next, it can function as Methenyltetrahydrofolate Cyclohydrolase, that converts 10-formyl-THF into 5,10-me-THF by hydrolysis. It can also convert 10-formyl-THF and 5,10-me-THF as a Methylenetetrahydrofolate Dehydrogenase, using $NADP^+$/NADPH. 10-formyl-THF is used for Purine Synthesis and 5,10-me-THF is used for Pyrimidine Synthesis. 5,10-me-THF is either transformed back to DHF by Thymidylate Synthase, with FAD and deoxythymidine Monophosphate (dTMP) as side products or be transformed into 5-methyl-THF by Methylenetetrahydrofolate Reductase (MTHFR), using FAD as cofactor and NADPH as reducing agent. The resulting 5-methyl-THF is then used with Homocysteine by Methionine Synthetase (MS or MTR), with vitamin B12 as cofactor, to produce methionine and THF. Methionine is then catalyzed by Methionine Adenosyltransferase (MAT), to create S-Adenosylmethionine (SAM) in an ATP-dependent manner and generating P_i. SAM can be transformed by Methionine Transferases (MTs) into S-Adenosylhomocysteine (SAH), generating a methyl group for other reactions. SAH is then converted back to homocysteine by Adenosyl-Homocysteinase (AHCY), releasing adenosine. This homocysteine is then used for new methionine or directed for glutathione synthesis. Methionine salvage occurs through the Polyamines metabolism. Putrescine is formed from Ornithine (Orn) by action of Ornithine Decarboxylase (ODC). Then Adenosylmethionine Decarboxylase (AMD) generates Spermidine and Spermine, in a SAM-dependent manner. Both reactions result in Methylthioadenosine (MTA), that can be phosphorylated by Methylthioadenosine Phosphorylase (MTAP), releasing adenine for Purine Synthesis. The remaining Methylthioribose (MTR) is then salvaged back to methionine. Adapted from Sanderson et al., 2019. Created with BioRender.com.

1.3.4.4 The amino acids of the Urea Cycle

The Urea Cycle is an important detoxification process in cells. It requires many NEAAs such as arginine, ornithine, citrulline and aspartate. Ornithine is used by Ornithine Transcarbamylase (OTC) to form citrulline, using Carbamoyl Phosphate (Figure 1.3.6). This molecule is very important in the process of detoxification because it uses toxic products of other biological processes. From respiration, CO_2 is used by Carbonic Anhydrases (CA), in a reversible hydration that regulates intracellular pH[244], which results in bicarbonate ions (HCO_3^-) and protons (H^+). From glutaminolysis, GS and GLUD produce ammonia (NH_4^+). Both these toxic products are used through a reaction catalysed by Carbamoyl Phosphate Synthase 1 (CPS1) to make Carbamoyl Phosphate. CPS1 function is ATP-dependent and requires use of N-Acetyl-Glutamate (NAG), which is produced by N-Acetyl-Glutamate Synthase (NGAS) through joining an Acetyl-CoA to glutamate[245]. The resulting citrulline is transported out of the mitochondria to cytosol by Ornithine Transporter 1 (ORNT1), where it is used by Argininosuccinate Synthetase 1 (ASS1) to make Argininosuccinate, spending ATP and Aspartate. Argininosuccinate is then broken down by Argininosuccinate Lyase (ASL) into arginine, releasing fumarate which is integrated back to the TCA cycle. The reaction of Arginase (ARG1 and ARG2) converts arginine into ornithine[245], producing urea for release (Figure 1.3.6). This cycle of reactions allows for the expulsion of toxic ammonia from the cells in the form of urea, which is normally excreted in urine[245].

Arginine can also be converted into citrulline through Nitric Oxide Synthase (NOS), producing the reactive species Nitric Oxide (NO), that has been reported to both aid or supress tumorigenesis, depending on source and concentration[246–248].

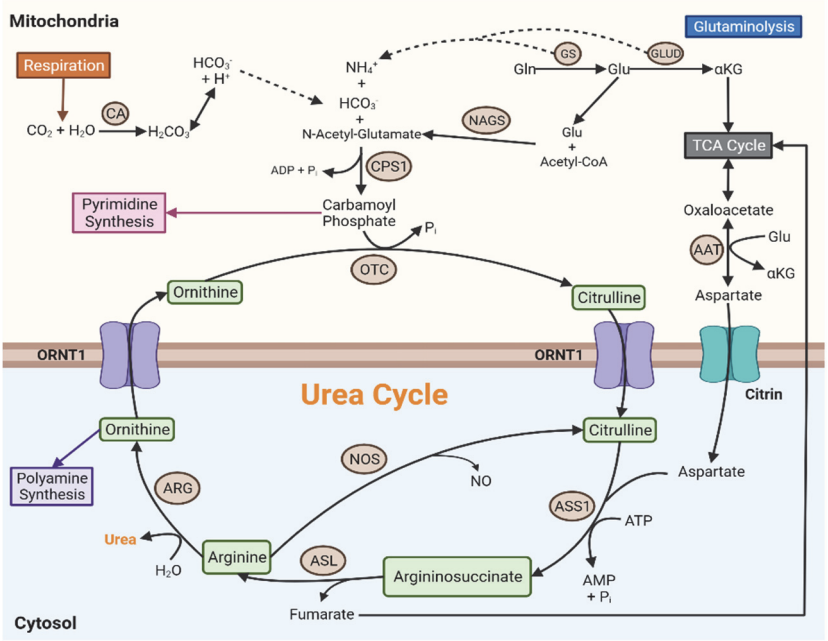

Figure 1.3.6- Urea Cycle mechanisms in cytosol and mitochondria. Urea is formed by hydrolysis of Arginine by Arginase (ARG), resulting in ornithine. Ornithine can be used in polyamine synthesis or transported to mitochondria by Ornithine Transporter 1(ORNT1). There it is used by Ornithine Transcarbamylase (OTC), in conjunction with Carbamoyl Phosphate, producing Citrulline and P_i. Citrulline is then transported by ORNT1 back to cytosol, which is converted to Argininosuccinate by Argininosuccinate Synthetase 1 (ASS1), in an ATP-manner and using aspartate. Argininosuccinate is then broken down by Argininosuccinate Lyase (ASL) into arginine and fumarate. Fumarate can be reutilized by the TCA cycle and Arginine is re-used either to generate new urea or transformed to citrulline by Nitric Oxide Synthase (NOS), with side production of Nitric Oxide (NO). Production of Carbamoyl Phosphate is done by Carbamoyl Phosphate Synthase 1(CPS1), in an ATP-manner using HCO_3^- and NH_4^+, products of Carbonic Anhydrase (CA) and glutaminolysis (both glutaminase (GS) and glutamate dehydrogenase (GLUD), respectively. It also requires N-acetyl-glutamate, that results from joining Acetyl-CoA with Glutamate (Glu), catalyzed by N-Acetyl Glutamate Synthase (NAGS). Carbamoyl Phosphate is also used for Pyrimidine Synthesis. Aspartate can be obtained from Oxaloacetate through Aspartate Aminotransferase (AAT), using Glu and producing α-Ketoglutarate (αKG). Aspartate is then transported by Citrin (SLC25A13) to the cytosol, to be used by ASS1. Adapted from Keshet et al. Created in BioRender.com.

Although the main amino acids used in the Urea Cycle are arginine, ornithine, citrulline and aspartate, in reality its function relies on other amino acid metabolism, such as TCA cycle and Glutaminolysis. In

addition, the resulting substrates of the cycle can be fuel for pyrimidine and polyamines synthesis[245].

Cancer cells can interfere on the urea cycle depending on their necessities, with the majority of tumours shunting the intermediates of this cycle into anabolic routes[245]. Studies have reported overexpression of CPS1 correlates with oncogenic KRAS in lung cancer[249,250] and poor prognosis in colon cancer[251]. ASS1 expression has both been reported to be lowered to increase pyrimidine synthesis[252] or overexpressed to support proliferation[253] and migration[254]. Another common alteration that affects the urea cycle is the use of isoforms CA IX and CA XII by cancer cells to aid migration, invasion and metastasis[244,255].

Leukaemias have been reported to alter their urea cycle by lowering expression of OTC and ORNT1, redirecting ornithine for other uses such as the polyamine synthesis[256–259].

1.3.4.5 Other amino acids interconnections

Besides the many pathways and metabolisms explained previously, there are other amino acids that also have their own role to play in the cellular metabolism and on the tumoral development.

1.3.4.5.1 Branched-chain Amino Acids

BCAAs are essential amino acids which are an important source of nitrogen, participating in the conversion of αKG into glutamate through BCATs but it also contributes as carbon donors to produce TCA cycle intermediares[228]. Inside the mitochondria, Valine generates succinyl-CoA, Leucine generates acetyl-CoA and Isoleucine is able to make both[260].

Besides contributing as nitrogen and carbon donors in metabolism, BCAAs can also play a regulatory role, as the case of Leucine, that functions as an allosteric regulator of GLUD and mTORC1[261,262]. In leukemic cells, alterations of BCAT1 are common, both as overexpression that drives

transformation[263–265] or through its blocking by the oncometabolite 2-HG[266]. The MLL1 fusion protein, known to initiate leukemogenesis, can induce overexpression of BCAT1 by chromatin hyperacetylation[267]. An important point of investigation is that inducing the knockdown of BCAT1 in LSCs results in rising levels of αKG and decreased levels of HIF1α and impaired cell growth[98].

1.3.4.5.2 Alanine

Alanine transamination is done mainly by Glutamate-Pyruvate Transaminase (GPT) (also known as alanine aminotransferase (ALT)) and Alanine-Glyoxylate and Serine-Pyruvate Aminotransferase (AGXT)[268,269]. GPT or ALT can use glutamate, together with pyruvate to produce alanine and αKG[268]. On the other hand, AGXT is responsible for 3 reactions, the first uses alanine and glyoxylate to make pyruvate and glycine (EC 2.6.1.44)[268,269]. The second reaction uses glyoxylate with serine to produce glycine and 3-hydroxypyruvate (EC 2.6.1.45) and the third reaction uses serine and pyruvate to obtain also 3-hydropyruvate and alanine (EC 2.6.1.51)[268,269]. All these reactions are bidirectional, depending on the chemical balance of substrates. Together, these reactions make alanine a focal point between glutamine metabolism, serine-glycine metabolism and generation of pyruvate for use on the TCA cycle. AGXT expression has been correlated with poor survival of hepatocellular carcinoma patients[269] and its polymorphisms can inform on clinical outcome of oxaliplatin treatment of metastatic CRC patients[270]. ALT expression has been associated with higher risk of developing cancer of digestive organs[271].

1.3.4.5.3 Asparagine

Asparagine is mainly utilized for protein synthesis and as an exchange factor in the transport of glutamine, serine, histidine and arginine[272,273]. Its synthesis is done by Asparagine Synthase (ASNS), through an ATP-dependent reaction that requires glutamine and aspartate[274,275]. Asparaginase is the enzyme that breaks asparagine into aspartate and ammonia. Asparagine levels are tightly regulated by cells and has been described that it regulates the activation of the Unfolded Protein Response (UPR), that results in cell death[276]. Of note is the use of asparaginase that can force starvation and block growth of leukemic cells[277,278].

1.3.4.5.4 Proline

Proline metabolism is linked to the metabolism of glutamate. Proline catabolism is done by Proline Dehydrogenase (PRODH) and Pyrroline-5-Carboxylate Dehydrogenase (P5CDH), producing glutamate with the reduction of FAD into $FADH_2$[279]. The reverse reactions for proline production are done by Pyrroline-5-Carboxylate Synthase (P5CS, coded by the gene ALDH18A1) and Pyrroline-5-Carboxylate Reductase (PYCR), utilising NADH/NADPH[279]. PYCR has 2 isoforms, PYCR1 is cytosolic and PYCR2 is mitochondrial[279,280].

Proline metabolism can both be anti- or pro-tumour. PRODH is up-regulated by p-53 and found downregulated in many tumours[281–284]. Its overexpression can diminish DNA synthesis, block cell cycle[280] and suppress HIF-signalling by increasing levels of αKG[285,286]. On the other hand, PRODH aids the survival of breast cancer after HDACs inhibitors treatment[287] and induces migration and metastasis in lung cancer[288]. Proline synthesis also aids tumoral progression, with upregulation of PYCR1 and ALDH18A1 across many cancers[238,289]. Of note is that upregulation of

proline synthesis can modulate an increase in glycolysis and PPP through the ratio of $NAD^+/NADP^+$ [290].

1.3.4.5.5 Lysine

Lysine is an EAA, which catabolism requires αKG and NADPH, producing saccharopine, α-aminoadipic acid (αAAA)[291] and acetyl-CoA[292,293]. This catabolism involves various transamination reactions, resulting in a side production of glutamate. Lysine is necessary for protein synthesis and for a positive nitrogen balance inside the cell[294]. In a cancer setup, lysine is one of the main amino acids that suffers PTMs, especially in epigenetic events regarding histones[295,296].

1.3.4.5.6 Threonine

Threonine is an EAA that can only be catabolised by Threonine Dehydratase in humans, for the genetic loss of the other enzymes[297–299]. Threonine catabolism through threonine dehydratase results in NH_3 and α-Ketobutyrate, with the latter being further transformed into succinyl-CoA, that then feeds the TCA cycle[300]. Furthermore, as it happens with other amino acids, threonine is also an amino acid which relevance in cancer arises from the PTMs that suffers as part of kinases (such as mTOR and AKT).

1.3.4.5.7 Histidine

Histidine is also an EAA, that can function as a pH buffer[301,302]. It has also antioxidant activity, as a scavenger of ROS and Reactive Nitrogen Species (RNS) [303–306]. Histidine catabolism intersects the Folate Cycle, utilizing THF for the conversion of Formiminoglutamate (FIGLU) into glutamate, so it exerts influence on the One-Carbon Metabolism[307,308]. Histidine is required for the synthesis of metabolites such as Histamine through Histidine Decarboxylase (HDC) and Carnosine through Carnosine

Synthase 1 (CARNS1)[302,309]. Histidine is also very important for protein synthesis, being an abundant part of the composition of haemoglobins, cytochromes, Nitric Oxide Synthase (NOS) and catalases[302,310]. Another factor of histidine metabolism is that despite being an EAA, cells can compensate the lack of histidine intake by catabolising haemoglobin and carnosine[311–314].

1.3.4.5.8 Phenylalanine and Tyrosine

Phenylalanine is an EAA that is used in protein synthesis and can be hydroxylated into the NEAA Tyrosine by Phenylalanine Hydroxylase (PAH)[315]. Tyrosine is also a necessary component of many important proteins, such as kinases. Tyrosine catabolism is done by aminotransferases and dioxygenases, with the final products of fumarate and acetoacetate[315], that can fuel the TCA cycle and fatty acids synthesis. In cancer, phenylalanine metabolism has been linked with suppression of T-cell immune response[316] and PAH is found altered in various malignancies[317,318]. Tyrosine is mostly reported in cancer as a phosphorylation site of many important kinases of signalling pathways[319]. The genes of the catabolic reactions of tyrosine have been reported to be downregulated and to suffer epigenetic regulation through miRNAs, aiding the development of hepatocellular carcinoma[320]. Investigations of tyrosine catabolism in cancer appear to be on the rise[317,321,322].

1.3.4.5.9 Tryptophan

Tryptophan is an EAA, used in the synthesis of metabolites such as serotonin and Niacin (vitamin B3) and its catabolism results in the biogenic amine Kynurenine[204,321]. This reaction can be done both by Tryptophan-2,3-dioxygenase (TDO) or Indoleamine-2,3-dioxygenase (IDO). The resulting kynurenine is then further catabolised to generate precursors for NAD^+ production[323]. Tryptophan and Kynurenine play a role on suppressing

immune response[324] and some of the enzymes of this pathway have been reported to correlate with CML progression[325].

1.3.5 Metabolism of Biogenic Amines

Biogenic amines are a vast group of metabolites that arise from the decarboxylation of amino acids, reductive aminations and transamination of aldehydes and ketones[326,327]. They are divided into 3 groups: Monoamines, diamines and polyamines.

Biogenic amines participate in many basic cellular functions such as the synthesis of proteins, hormones and nucleic acids. They also have a supportive role in proliferation, immune response, response to stress and senescence. Additionally, they easily interact with negatively charged molecules (DNA, RNA, phospholipids, etc.), playing a role in their stabilization[328,329]. But their excess is considered carcinogenic, with effects over apoptosis (like pore formation of mitochondria)[330,331] and their catabolism resulting in cytotoxicity (formation of H_2O_2)[332–334]. Of note is the metabolism of polyamines, specially putrescine, spermine and spermidine. Their synthesis is dependent on ornithine and SAM (Figure 1.3.5) and it can be upregulated by C-MYC, cyclin D1, HRAS and KRAS (through upregulation of ODC and AMD1)[335–337]. They have a role on cell cycle, on the transition from G_1 to S phase[338]. Their uptake and synthesis increase have been reported in breast, colon, skin and prostate cancers[339,340].

1.3.6 Redox Balance: The ROS Equilibrium Game

The Redox control inside a cell is a complex process, combining many metabolic pathways in order to achieve a balance between reductive factors and reactive species. These reactive species are grouped in four designations: ROS, RNS, reactive sulphur species (RSS) and reactive chlorine species (RCS), with the first being the more commonly by-product of cellular metabolism[190,341]. The other types of reactive species besides

participating in the redox reactions[342–344], also perform PTMs (like tyrosine nitration by RNS)[344–346] and cause damage to DNA[347].

ROS can be produced primarily from OXPHOS but also inside other organelles such as peroxisomes[348]. It can also arise of the activity of enzymes such as NADPH oxidases (NOXs) and Xanthine Oxidases. This production can be activated by external stimuli such as TNFα, EGF, Interleucin-1β (IL-1β), hypoxia and radiation[349–353].

The ROS scavengers are the Glutathione Peroxidases (GPX), peroxiredoxins, catalases (CATs) and Superoxide Dismutase (SODs)[190,341,354,355]. These enzymes convert free radicals (the highly reactive forms of ROS) into less toxic and stable molecules for excretion. Complementary to their action is the Glutathione Cycle. Glutathione is an antioxidant and one of the most important detoxifying agents for cellular homeostasis[355,356]. Glutathione exists in two forms: the reduced glutathione (GSH) and the oxidised form Glutathione Disulphide (GSSG) (Figure 1.3.7). GSH is used by GPXs to detoxify ROS, resulting in GSSG[355,357].

The glutathione cycle is another interconnection of many paths of metabolism. For the generation of GSH there is the involvement of substrates from glutaminolysis, One-Carbon metabolism and ATP. And during the reduction of GSSG back to GSH, it requires the NADPH generated by the PPP and TCA cycle.

A tight regulation of ROS levels is required in order to use them for signalling, as evident on haematopoiesis, that uses varying levels of oxidative stress to drive the differentiation of HSCs[358] (see section 1.1.2). But ROS can cause damage to DNA leading to genomic instability, with emergence of mutations[359,360]. It can also inactivate important TSGs such as PTEN and activate transcription factors like HIF1α and NRF2, reprogramming the metabolism[361].

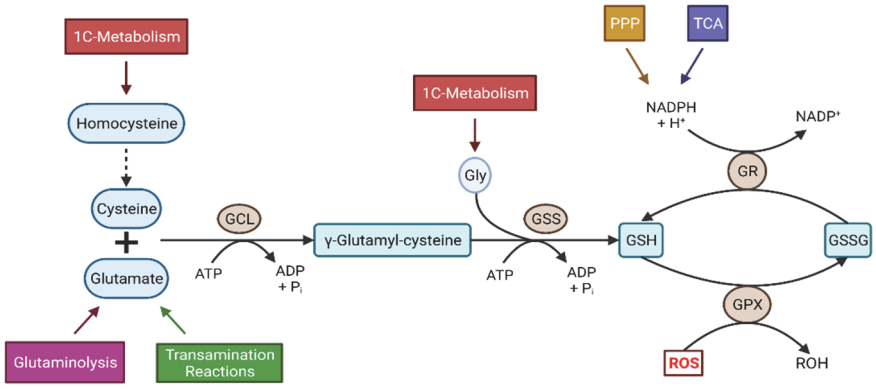

Figure 1.3.7- Glutathione Cycle and its interactions with metabolism. Glutathione (GSH) production starts with the joining of glutamate and cysteine, obtained from glutaminolysis and One-carbon (1C) Metabolism, by Glutamate-cysteine Ligase (GCL), in an ATP-dependent reaction. The resulting γ-Glutamyl-cysteine is then joined with glycine (Gly) by Glutathione Synthetase (GSS), also requiring ATP. GSH (reduced form) is then used by Glutathione Peroxidases (GPX) to detoxify reactive oxygen species (ROS), resulting in Glutathione disulphide (GSSG). The oxidized form GSSG can then be rescued by Glutathione Reductase (GR) back to GSH, using NADPH generated by other metabolisms, mainly the Pentose Phosphate Pathway (PPP) and Tricarboxylic Acid (TCA) Cycle. Adapted from Bansal et al, 2018. Created with BioRender.com.

Cancer cells utilize ROS to drive their tumorigenesis but also its regulation mechanisms in order to avoid apoptosis. They reduce the ROS production from respiration by reducing the entrance of pyruvate to the TCA cycle, through overexpressing PDK1[362]. On the other hand, they increase the expression of SODs, catalases, GPXs and ramping up the production of GSH[355,363], contributing to the increased glutaminolysis observed in tumours[364]. The glutathione cycle in many types of cancer cells is one of the main driving forces to increase the flux of glucose into the PPP. The oxidative branch of the PPP is essential to produce NADPH for the reaction that recovers GSH[365] (see section 1.3.2). Other sources of NADPH are the reactions of IDH, Malic Enzyme and MDH of the TCA cycle[366–368] (see section 1.3.3) and the reactions of MTHFD of the Folate Cycle[369,370] (see section 1.3.4.3). Lastly, cancer cells can exploit the glutathione mechanisms

as a tool for chemotherapeutic resistance, given that GSH is also capable of detoxifying xenobiotics[371–373].

1.4 Hypoxia: A Hallmark of Leukaemia on his own

Hypoxia is the low O_2 state that naturally occurs in living tissues such as the bone marrow and the kidney[374,375]. It is also a regulating factor during embryogenesis[374] and can modulate the cellular metabolism[376]. In the case of cancer, solid tumours usually possess hypoxic regions within their mass, due to a mismatch between rapid proliferation and aberrant vascularization, resulting in bad supply of oxygen[377–379].

As mentioned previously, the main effectors of the oxygen sensing response are the transcription factors HIFs. This group is comprised of HIF1, HIF2 and HIF3, with each dimerizing an α-unit with a β-unit[380,381]. The β-units are constitutively expressed, while the α-units are regulated by hydroxylation from PHDs, that marks it for ubiquitination by VHL and subsequent degradation[99,382]. This hydroxylation occurs in the presence of oxygen, so in normoxia the α-units are very short-lived (Figure 1.4.1). But in the hypoxic setting, the lack of O_2 impedes the degradation of α-units, allowing the joining with β-units and translocation into the nucleus. There is promiscuity between the 3 α-units and HIF1β (also known as Aryl Hydrocarbon Receptor Nuclear Translocator (ARNT))[380]. In the nucleus, the dimers bind to hypoxia-response elements (HREs) in the promoters and enhancers to activate transcription of target genes[381,383].

Of these numerous targets, they range through many cellular functions, from proliferation (growth factors, signalling pathways), angiogenesis (blood vessels formation), metabolic adaptation and avoiding apoptosis[376,384]. All these processes have a great overlap between genes that are regulated by HIF (directly or indirectly) and tumorigenesis. This makes hypoxia as a master regulator of various functions defined as Hallmarks of Cancer[5,378].

Hypoxia can induce tumour cells to make their own growth factors (EGF, IGF1, EPO, etc.), increasing their proliferation and growing independent of exogenous mitogenic growth signals[385]. It can also induce the expression of VEGFs, to initiate angiogenesis and increase the access to nutrients[82,386]. Many signalling pathways of proliferation interact with HIFs, such as MAPK and PI3K/AKT, like the AKT phosphorylation of HIF1α that allows the binding with HIF1β[377,379,387–392].

Hypoxia induces anti-apoptotic proteins[390] and can exert a selective pressure against cells with wildtype p53, aiding on the clonal expansion of cancer cells with p53 mutated[393]. Hypoxic conditions can also favour cell immortalization, by increasing the Human Telomerase (hTERT) activity through MAPK activation[394] and affecting the PHD2-mediated downregulation[395].

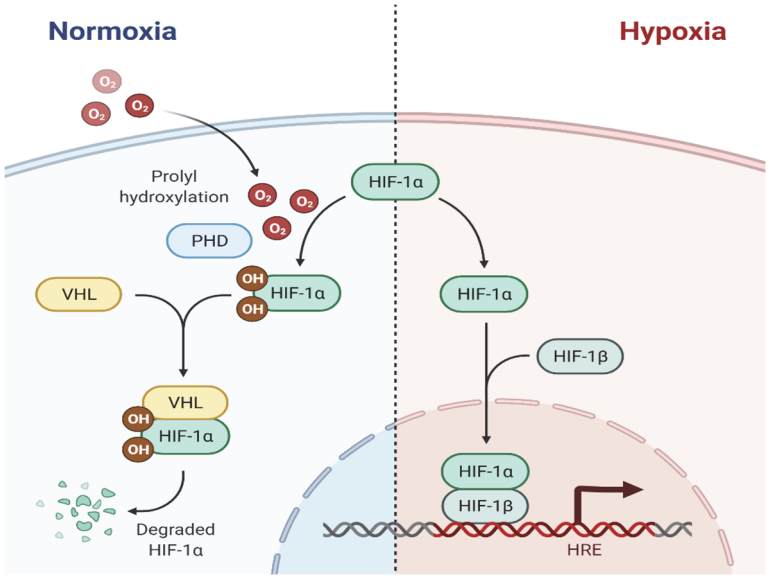

Figure 1.4.1- Destiny of Hypoxia-inducible Factors (HIFs) according to Oxygen presence. In Normoxia, HIF1α is hydroxylated by Prolyl Hydroxylase Domain-containing (PHDs), tagging it for Von Hippel-Lindau (VHL), that binds HIFs to ubiquitination complexes, resulting in their degradation. In hypoxia, lack of O2 impedes PHDs, leaving HIF1α free to form heterodimers with HIF1β, that will translocate into the nucleus and bind to Hypoxia-response Elements (HREs) of various genes promoters and enhancers. Created with BioRender.com.

Hypoxia modulates the microenvironment by signalling tumour-associated macrophages to secrete mitogenic factors, proangiogenic cytokines and immunosuppressive agents through the HIF1 and HIF2 transcription programming[385,386]. This allows tumour cells to escape immune detection and response[385,396]. Hypoxic settings or an overexpression of HIF1α can promote the Epithelial Mesenchymal Transition (EMT), leading to more invasive phenotypes and formation of metastasis[397,398].

In the deregulating of cell energetics, hypoxia induces the Warburg Effect by increasing the expression of GLUT1, PDK1 and many glycolytic enzymes (HKII, GAPDH, ENO, etc). This leads to increased glucose uptake and PDH inhibition to redirect energy production from the TCA cycle[379,387]. The control of ROS levels is one of the main reasons that HSCs have a metabolic profile of low TCA cycle activity and favour anaerobic glycolysis. Studies have proven that an increase in ROS production (from OXPHOS or NOXs) will induce proliferation, differentiation and maturation of the haematopoietic cells in a spectrum, depending on the lineage commitment[388,392,399–402]. Another key factor on this hypoxic regulation is that the changes in metabolism is affecting PHDs. As a dioxygenase, not only are they being directly impeded by the absence of O_2 but also being inhibited by increased ROS, phosphorylation by Protein Kinase C (PKC), Nitric Oxide (NO) and the availability of αKG[99,382] (just like the TET enzymes).

The pathophysiological importance of available O_2 would be counterintuitive for haematological malignancies, given that "blood tumours" is assumed to have direct access to the circulating oxygen. But inside the bone marrow it is a different story. Within the stem niche, the O_2 presence is below 1%. During the hematopoietic differentiation, the cells face a gradient of O_2, from around 1% inside the niche up to 12% when nearing the vascular system[403]. HSCs are in chronic hypoxia for the majority of their lifetime until differentiation[404]. Many studies have showed

that hypoxia is a functional component of the haematopoietic niche but the role of HIFs in stem cells regulation is not so clear. While the impact of HIFs overexpression in solid tumours have been established, with correlations to poor prognosis[405] and therapeutic resistance[406], investigations on their function on leukemic cells are contradictory[391,407,408]. Further investigations are necessary to discern these discrepancies, but it is clear that HIFs play a role on the quiescence of HSCs and the differentiation initiation[382,389,409].

One key factor of interest of leukemic stem cells is their quiescent metabolic phenotype, how they balance the signals of the niche, use anaerobic glycolysis for energy, maintain low levels of ROS without inducing apoptosis and are able of resisting therapy[410], leading to the eventual relapse of many patients. Investigating how leukemic cell lines vary their metabolism from normoxia into chronic hypoxia can elucidate how metabolic reprogramming due to O_2 levels can be hijacked during leukemogenesis at the origin point, the bone marrow. And light a path to breaking the cruel cycle of relapse that persists in many leukaemias nowadays and free leukaemia survivors of that pending doom becoming reality.

1.5 Metabolic Studies Tools

The advancements of science in modern history have allowed a deeper understanding of cancer down to the molecular level. The deciphering of the human genome was a marking event, helping to understand how mutations of genes led to many types of diseases[411]. But it also brought to light that alterations of the genotype do not account directly to the phenotype observed. As such, the research efforts shifted their focus from studying a singular gene, molecule or pathway isolated into an englobing view of the cellular biological system with its many components and their interactions. Thus, the research based in Omics studies emerged. These

"Omics" are composed of genomics, epigenomics, transcriptomics, proteomics, metabolomics and other categories of omics (lipidomics, microbiomics, foodomics, etc.)[412,413].

The main goal of a Multi-Omics approach is to combine the many different layers of knowledge, with high-dimensional datasets of multiple levels of a cell biological system to try to correlate genotype to phenotype (Figure 1.5.1)[414]. But a smooth integration of all these different areas is not yet a reality, with development in each Omics-field at uneven stages, speeds and costs. Starting with genomics, it is the study of all genetic information, with its many variants and abnormalities (mutations, chromosomal rearrangements, etc)[415]. The advances in high-throughput techniques have improved to allow Whole Genome Sequencing (WGS) studies, that have aided in more accurately classifications of cancer subtypes[416,417]. It also created a "repertoire" of sequence variants and mutations that are associated with higher cancer risk and have become part of the routine-testing during tumour-staging and treatment decisions[418]. Despite the many improvements to genomic studies, it is still insufficient in predictive capabilities if used without other Omics for cancer risk assessment, treatment response or recurrence risk.

The second-most advanced Omics study to date is Transcriptomics, that englobes all the gene transcripts (coding and non-coding) being generated in the cell. It complements the genomics information, by revealing which genes are actively being transcribed and if any alternative splicing events are occurring[417]. The development of RNA-sequencing (RNA-Seq) has proven a great tool, that can measure the amount of gene transcripts and their sequence across the genome[419]. Through its datasets, differential expression analysis can be performed and highlight different gene expression signatures, that can be used to understand signalling networks and pathways during different stages of cancer or during treatments[420]. Transcriptomics analysis has many utilities such as genomic interpretation,

identification of biomarkers and discerning new therapeutic avenues from gene interactions[421,422]. A downside of transcriptomics is that to this day it is a high-cost technique, with a very high requirement for data storage and computing processing power[412,423,424]. Another difficulty is when integrating with protein levels, there is only around 40% correlation of transcript-protein[425].

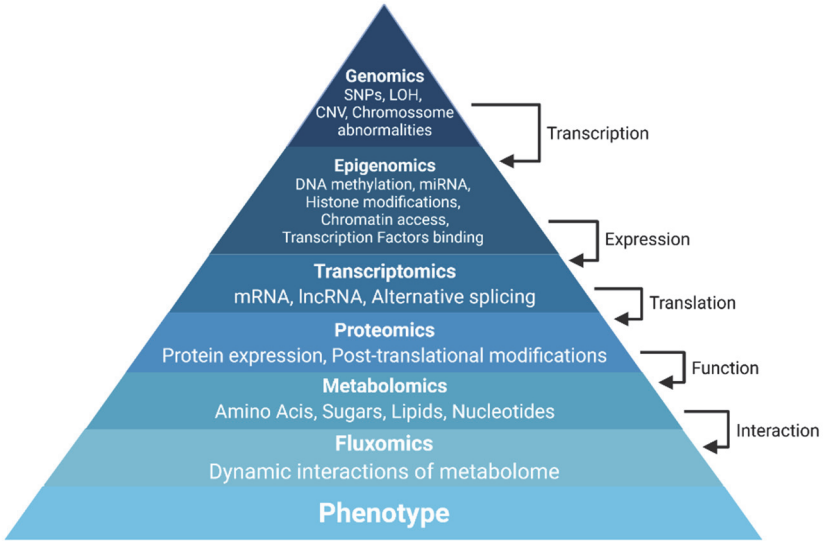

Figure 1.5.1- Multi-Omics Studies Hierarchy. Genomics can identify single nucleotide polymorphisms (SNP), loss of heterogeneity mutations (LOH), copy number variations (CNV) and chromosome abnormalities (translocations, fusions, etc.). Epigenomics can check the status of chromatin access, DNA methylation, histone modifications, activity of micro-RNAs (miRNA) and binding of Transcription factors (TF). Transcriptomics evaluate small RNAs (mRNA), long noncoding RNAs (lncRNA) and if alternative splicing is occurring. Proteomics englobes all the proteins being translated and the many distinct post-translational modifications that they suffer. Metabolomics studies small molecules such as amino acids, sugars, nucleotides and lipids. Fluxomics analyses the real set of intracellular fluxes through all the pathways occurring inside a cell, tissue or organism. All the omics combined can inform on the final phenotype expressed. Adapted from Momeni et al. Created with BioRender.com.

The advancement of Epigenomics is a fast-evolving Omics, younger than Transcriptomics but quickly catching up in developing techniques and clinical translation. The study of how the epigenetic landscape influences

gene expression is necessary as complementary knowledge to interlink genomics and transcriptomics[426]. The complexity of the many modifications that happens to DNA and histones is a layer of difficulty for the evolution of epigenomics (see chapter 1.2). In addition, the epigenetic landscape is influenced by time and spatial factors, with a very tissue-specific response to external stimuli[412]. As such, epigenomics techniques need to be bolstered by transcriptomics performed under the same conditions, to cover these caveats.

The other remaining Omics areas require more development, in both techniques and translation to clinical application, and are not able yet to do an overall massive analysis. Proteomics embodies all the proteins that are translated from the genome, with the many post-translational modifications they suffer[417,427]. Due to these variations, no single technique can assess the whole "proteome" in all its facets. Most proteomic methodologies are focused to identify and quantify specific proteins, mostly through Mass Spectrometry (MS) or affinity-based protein arrays[428,429]. Although proteomics studies have aided in identifying drug target protein pools[430] and established molecular signatures for cancer subtypes[428], showing their promised potential to personalise cancer therapies, the techniques are still demanding in time and resources[429].

Metabolomics is the Omics study that quantifies small molecules such as sugars, lipids, amino acids and nucleotides. It can be applied to all types of cells, tissues and fluids[45,431,432]. It evaluates the levels of metabolites since they are the product of many cellular processes and their changes are reflective of metabolic function (Figure 1.5.1). This makes it more susceptible to external stimuli, from environmental factors, cell-cell interactions or drug targeting effects[424]. In fact, Metabolomics have shown much effectiveness in identifying metabolic biomarkers and to discern metabolic changes during cancer progression and response to treatment[433].

The Achilles' heel of metabolomics lies that it encompasses an enormous amount of metabolites, many still unidentified, with great diversity in concentration levels and chemical composition, complicating its analysis and reproducibility[412,434]. There are many approaches for metabolomic studies that can be separated into 2 categories: targeted and nontargeted studies. The first is a quantitative measure of selected metabolites of a specific pathway or biological process, requiring *a priori* knowledge of the target compounds[435]. The second relates to a global coverage and profiling of the metabolome, with no pre-selection applied in order to obtain a more unbiased analysis[436,437]. Both methodologies utilize MS and Nuclear Magnetic Resonance (NMR) techniques for the metabolite readouts, with MS being less costly and possessing higher sensitivity but NMR being more effective in metabolite identification[438]. In the case of MS, this analytical platform is frequently found being coupled with gas and liquid chromatography (GC and LC) methods in order to resolve large amounts of metabolites from different sample types[439]. At the end, both techniques require specialized bioinformatics software for accurate statistics and analysis of very complex datasets (due to the many species of metabolites amalgamated). Another approach to consider is Stable Isotope Resolved Metabolomics (SIRM), with the objective not of quantify the metabolites levels in samples but to evaluate the incorporation of stable isotopes in specific metabolites known to utilize the tracers given. This approach will be further explained in more detail in section 1.5.1.

Lastly, there is Fluxomics, which is *per-se* a multi-omics approach and is the closest of the "omics" to phenotype (Figure 1.5.1). This is due to the fact that metabolic fluxes are the end result of the interconnections of gene expression, protein expression with its PTMs for regulation and metabolites concentrations[440]. This grants a dynamic picture of phenotype and how it changes in systemic disorders such as diabetes and cancer[441]. Fluxomics makes use of bioinformatics to calculate the map of metabolic fluxes inside

a cell, thus integrating data obtained from other omics such as metabolomics, transcriptomics or proteomics. One of the software analysis most used in Fluxomics is Flux Balance Analysis (FBA)[440,442]. One of its more promising approaches is ^{13}C-Fluxomics, where cells or organisms are incubated or fed in the presence of isotopically enriched substrates. In this case, *a priori* knowledge of labelling transition is needed[440,443], and the analysis of incorporation of the stable isotopes at the different metabolites is done by SIRM. While the use of tracer molecules is a disadvantage due to costs and the available list of molecules currently, the gain of this technique is that it can resolve parallel and cycle pathways, as well as discern reversible reactions[440].

Overall, Multi-Omics studies have aided in a more pathophysiological stratification of cancer subtypes and are a great step in the direction of personalized medicine. There are still limitations to be overcome. The overlap mismatch between the different Omics makes difficult to correlate the data of different methods, making the decision of which omics to perform and how to integrate them a complex one. This could be improved if the generation of the datasets could come from the same biological sample but the sample processing for a distinct Omics makes it unsuitable for the others. On the software front, improvements to analytical and annotation tools are always a must. There are many reviews that summarize the areas of future improvement for Multi-Omics approaches and their contributions for precision medicine[412,413,432].

1.5.1 Stable Isotope Resolved Metabolomics

Stable Isotope Resolved Metabolomics (SIRM), also known as ^{13}C-based Metabolomics or Tracer-based Metabolomics, is a targeted metabolomics technique that relies in the quantification of the incorporation of stable isotopes in metabolites, generated from an enriched precursor, mapping the biological system were the labelled intermediates are present[444–446]. These

stable isotopes are non-radioactive and functionally identical to the natural occurring isotopes. Incorporation of ^{2}H, ^{13}C and ^{15}N into biological precursors, such as glutamine and glucose, are a proven method to trace their metabolism in living systems[447]. The measurement of these isotopes incorporation is done through MS and NMR spectroscopy. Following the isotope labelling, the metabolites are extracted and determined by number of heavy atoms (isotopologues) and the position of those heavy atoms (isotopomers)[439] (Figure 1.5.2).

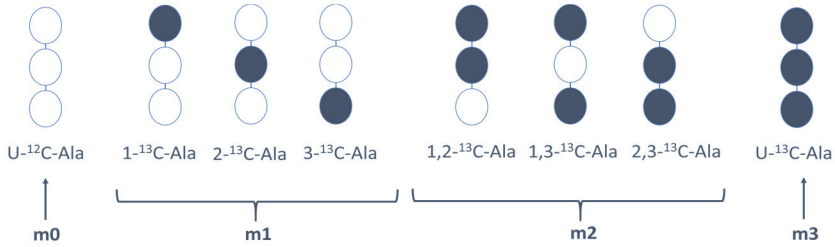

Figure 1.5.2- Permutations of ^{13}C-labelling positions for Alanine. Isotopologues (m_i) are distinguished by the number of atoms labelled (in alanine, from 0 up to 3). Isotopomers distinguish how many and which of the atoms in the molecule are labelled (the 1st, 2nd or 3rd carbon in alanine).

The difference in nominal mass of the heavy atoms from the natural occurring ones allows MS to determine the number of atoms incorporated. High resolution MS equipment (with up to 4 or 5 decimals in m/z determination) or coupling of MS with GC or LC methods is required to quantitatively analyse the less abundant isotopologues. On the other hand, NMR techniques are more suited for determining the positional labelling, due to the magnetic properties of the atomic nuclei, through direct detection or indirectly by their attached protons[439,445]. NMR 1D and 2D methods enable isotopomer analysis capable of discerning distinct patterns in complex biological systems. However, not all the positions and isotopomers are up to date distinguishable from NMR spectra. Due to this, the joining of both NMR and MS methods can enable a more faithful

reconstruction of the pathways and networks of the metabolism under study[439,444–446,448–450].

Another factor that must be considered is the choice of tracer. As mentioned above, *a priori* knowledge is required for this decision, to best match the tracer to the system under study. The distinct possible ^{13}C-tracers available grant different levels of information, with fully labelled tracers (such as U-^{13}C-glucose or U-^{13}C-glutamine) reaching a broader range of labelled metabolites and giving a more global vision of the metabolism under study, or with tracers with specifically labelled positions (such as 1,2-^{13}C-glucose, 4,5-^{13}C-glucose or 3-^{13}C-glutamine). For both cases, *a priori* knowledge comes into play again for the interpretation of the metabolic route the stable isotope travelled and analyse how this results in specific labelled-carbon positioning in other metabolites, informing on the relative contribution of the many metabolic pathways under study.

A specific example of how SIRM aids in discerning the metabolic pathway of production of a metabolite is the use of 1,2-^{13}C-glucose (Figure 1.5.3). The use of this tracer helps to discern how the glucose carbons travel through glycolysis to produce lactate. But it also clarifies if there is use of the PPP, resulting in a different isotopologue of lactate.

SIRM studies have aided in multiple cancer biological models, such as 2D and 3D cell cultures, *in vivo* or *ex vivo* tumour models[446]. SIRM studies have proven once again Warburg's findings and disproven the bias that tumour cells have dysfunctional mitochondria[191]. Thus, SIRM is excellent in profiling metabolic changes and highlighting distinctions between normal tissue and cancer.

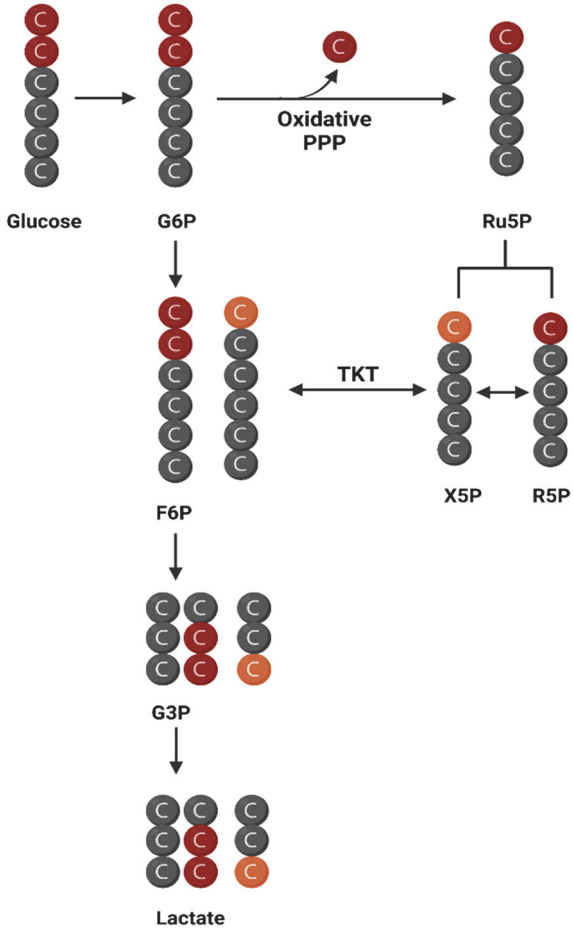

Figure 1.5.3- Example of SIRM using 1,2-^{13}C-glucose and resulting labelling of lactate. 1,2-^{13}C-glucose generates 1,2-^{13}C-glucose-6-phosphate (G6P), which can produce 1,2-^{13}C-fructose-6-phosphate (F6P) or go into the oxidative branch of Pentose Phosphate Pathway (PPP). The Oxidative PPP produces 1-^{13}C-ribulose-5-phosphate (Ru5P), which generates 1-^{13}C-ribose-5-phosphate (R5P) and 1-^{13}C-xylulose-5-phosphate (X5P) in the non-oxidative PPP. Transketolase (TKT) is able to transfer 2 carbons from X5P into Erythrose-4-phosphate (E4P, not shown), producing 1-^{13}C-F6P and 3-^{13}C-glyceraldehyde-3-phosphate (G3P), that can incorporate back into glycolysis. This results in 3 possible molecules of lactate: unlabelled lactate, 2,3-^{13}C-lactate (coming from glycolysis) and 3-^{13}C-lactate (coming from PPP action). Orange carbons represent the carbons that travelled through PPP. Other isotopomers resulting from recombination of labelled fragments are possible but are not shown for simplicity. Adapted from Bruntz et al, 2017. Created with BioRender.com.

2. OBJECTIVES

2 Objectives

Leukaemia is the 10th cancer cause of death worldwide[2]. Although the overall survival rate of Leukaemia has increased across the board due to modernized treatments, there are still extremely aggressive cases that fail to remise. This is due to the capacity to gain resistance to therapy.

Since leukemogenesis is based on various genetic alterations that lead to different subtypes with distinct phenotypes and metabolic profiles, understanding these events can elucidate on new therapeutic targets. Many investigative works have established the important role of studying the metabolism of cancer cells, to improve patient prognosis, risk stratification and counteract eventual resistance to therapy[45].

The present work aims to characterize metabolic adaptations granted by specific enzymes to leukaemia, in both the normal oxygen conditions and a hypoxia state, for closer representation of the haematopoietic niche. The enzymes chosen are TKTL1 and TET2, due to their many peculiar properties listed and to better shed light on their role on leukemogenesis, in order to ultimately aid in help patients with these mutations.

Therefore, the main objectives of the present thesis are the following:

1. Characterization of the role of TKTL1 in the metabolic reprogramming of AML in normoxia and hypoxia, using THP1 Control and THP1 TKTL1-Knockdown as a cell model.
2. Characterization of the role of TET2 in the metabolic reprogramming of CML in normoxia and hypoxia, using HAP1 Parental and HAP1 TET2 Knockout as a cell model.

3. MATERIALS AND METHODS

3 Materials and Methods

3.1 Cell Culture

Human THP-1 acute monocytic leukaemia were obtained from the American Type Culture Collection (Manassas, VA, US). THP-1 WT and THP-1 TKTL1^{KD} cells were generated by Sirion Biotech GmbH (Munich, Germany). The THP-1 cell lines are suspension cells, grown in RPMI 1640 culture medium of 10mM Glucose, 2mM glutamine and supplemented with 10% heat-inactivated Fetal Calf Serum (FCS) and antibiotics: 100 U/ml penicillin, 100 µg/ml streptomycin and 50 µg/ml gentamicin.

Human HAP1 chronic myeloid leukaemia Parental and KO cell lines were obtained from Horizon Discovery©. HAP1 KO cell line was generated using CRISPR/Cas9 technology to delete 19 base pairs in exon 3 of the *TET2* gene (HZGHC001091c010). These cell lines are adherent cells, grown in Iscove's Modified Dulbecco's Medium (IMDM) culture medium with 25 mM glucose, 4mM glutamine and supplemented with 10% heat-inactivated FCS and antibiotics: 100 U/ml penicillin and 100 µg/ml streptomycin.

In hypoxia settings, cells were cultured for 5 days for chronic hypoxic adaptation in Hypoxystation H35 (Don Whitley Scientific Limited, United Kingdom) before any experiment was performed.

3.2 Cell Proliferation Rate Assays

Cell proliferation curves were performed by cell counting with Scepter^{TM} Handheld Automated Cell Counter (Merck Millipore, USA) and Countess II Automated Cell Counter (Thermo Fisher Scientific, Waltham, MA, USA), for both THP-1 and HAP1 cell lines, respectively. THP-1 cell lines were seeded at 3 x 10^5 cells per 25 cm^2 flasks in normoxia and seeded at 4 x 10^5 cells in hypoxia. HAP1 cell lines were seeded at 7.5 x 10^4 cells per p6 well (9.6 cm^2) in normoxia. In hypoxia, HAP1 Parental cells were seeded

at 7.5 x 10^4 cells per p6 well and HAP1 TET2 KO cells were seeded at 1.1 x 10^5 cells per p6 well. Cell counting was done at 24 hours timepoints up until a total of 72h or 96h of incubation. Cell medium was renewed each 24h.

THP-1 counting samples were collected in eppendorfs from seeding flasks, with volumes of 500 µl, centrifuged at 200 x g for 5 min, removed supernatant and cell pellet resuspended in 1 ml PBS solution (Phosphate Buffered Saline). HAP1 counting samples were collected from sacrificing replicate wells, through trypsinization with 1ml trypsin, incubating at 37ºC for 5 min, inactivating trypsin with 3ml media (1:3) and centrifuging at 200 x g for 5 min. Supernatants were discarded and cell pellets were resuspended in 1ml PBS for counting.

3.3 Biochemical Assays by Spectrophotometry

In order to measure the concentration of each metabolite, media samples were collected at all timepoints of growth curves experiments, and frozen at -20ºC or -80ºC until being analysed. Glucose, lactate, glutamine and glutamate concentrations were determined from frozen cell culture medium by using spectrophotometry with an automated autoanalyzer COBAS Mira Plus (Horiba ABX, Japan).

Glucose concentration was measured by calculating NAD(P)H concentration increase (measured at 340 nm) after the conversion of total glucose by hexokinase and conversion of resulting glucose-6-phosphate into D-gluconate-6-phosphate by G6PDH using coupled enzymatic reactions (kit ABX Pentra Glucose HK CP, HORIBA ABX, Japan)[451].

Lactate measurements were performed by mixing media samples with hydrazine buffer (1.55 mg/ml NAD^+ in 0.2 M hydrazine, 12 mM EDTA pH 9 at 37ºC) adding LDH (87.7 U/ml, in 28.6 mM $(NH_4)_2SO_4$). NADH release readouts were done at 340 nm[452].

Before glutamate measurements, the media samples were deproteinated by boiling them at 80ºC for 15 min in a heating block. After cooling for 5 min in ice, samples were centrifuged at 10,000 x g at 4ºC for 10 min. Collected deproteinized supernatants were frozen at -20ºC for future readings.

Glutamate was quantified by mixing the deproteinated medium samples with a glutamate dehydrogenase mix buffer (GLUD1 at 39 U/ml, 2.41 mM ADP, 3.9 mM NAD^+ in 0.5 M hydrazine, 0.5 M glycine pH 9) at 37ºC. NADH release was measured at 340 nm[453].

To determine glutamine concentration in medium samples, glutamine was converted to glutamate through glutaminase reaction. Thus, an aliquot of deproteinated medium was incubated with glutaminase (125 mU/ml of GLS, 125 mM acetate pH 5) at 37ºC for 30 min in constant agitation. Total glutamate concentration (glutamate plus glutamine converted to glutamate) was measured by the same procedure described before.

Consumption and production rates of metabolites were determined by measuring metabolite concentration in incubation media at the beginning and at the end of incubation time and correcting the absolute consumption by time and cell number assuming exponential cell growth.

3.4 Enzymatic Activity Assays

Samples were prepared as indicated: For HAP1 cell lines, fresh cell culture plates were rinsed with PBS and lysed with lysis buffer (20mM Tris-HCL, pH 7.5, 1 mM dithiothreitol, 1mM EDTA, 0.02% (v/v) Triton X-100, 0.02% (v/v) sodium deoxycholate) supplemented with protease and phosphatase inhibitors cocktails (Sigma and Thermo Scientific, respectively) for 30 minutes at 4ºC. Cells were scrapped and collected in eppendorf tubes and the cell lysate was disrupted by sonication using titanium probe (Vibracell, Sonics & Materials Inc., Tune 50, Output 20, 3 cycles of 5 seconds each). For THP-1 cell lines, cell pellets were collected and washed once with PBS before adding lysis buffer and being sonicated.

Once sonicated (both cell lines), the tubes were centrifuged at 10,000 x g at 4ºC for 20 minutes. The supernatant was collected and immediately used for the determination of specific enzyme activities using spectrophotometry (COBAS Mira Plus, Horiba ABX, Japan). All enzymatic activities were determined by monitoring NAD(P)H increase or decrease at 340 nm wavelength. The enzyme activity for each sample was then normalized to the total protein content of the samples quantified by BCA Assay at 550 nm wavelength (Pierce, Thermo Scientific).

3.4.1 TKT and TKTL1

All transketolase activity (both TKT and TKTL1) was determined adding sample to cuvettes containing 5 mM $MgCl_2$, 0.2 U/ml triose phosphate isomerase, 0.2 mM NADH, 0.1 mM thiamine pyrophosphate in 50 mM Tris-HCl, pH 7.6, at 37°C. Reaction started by addition of prepared mixture containing R5P and X5P. This mixture was prepared previously, incubating 50 mM R5P in 50 mM Tris-HCl, pH 7.6, in the presence of 0.1 U/ml ribulose-5-phosphate-3-epimerase and 1.7 mU/ml phosphoriboisomerase, at 37ºC for 1h.

3.4.2 GAPDH

GAPDH activity was obtained by coupling the activities of GAPDH and phosphoglycerate kinase (PGK). Measurements were obtained by adding samples to a cuvette containing 1.1 mM ATP, 0.9 mM EDTA, 1.7 mM MgSO4, 0.2 mM NADH, 14.8 U/ml of PGK in 82.5 mM Triethanolamine-HCl pH 7.6 at 37ºC. Reaction started with the addition of 50 mM G3P up to a final concentration of 6 mM.

3.4.3 LDH

LDH activity was measured by adding samples to a cuvette containing 0.2 mM NADH in 100 mM phosphate buffer, pH 7.4, at 37ºC. Reaction initiated by the addition of pyruvate up to a final concentration of 0.2 mM.

3.4.4 HK

HK activity was determined by coupling HK and G6PD reactions in the following conditions: 3.3 mM $NADP^+$, 14.8 mM ATP, 14.8mM $MgCl_2$, 2.8 U/ml of G6PD and 50mM Tris-HCl, pH 7.6, at 37°C. Reaction was initiated by the addition of glucose up to a final concentration of 10 mM.

3.4.5 G6PD and 6PGD

6-Phosphogluconate dehydrogenase (6PGD) and G6PD specific activities were measured adding samples to a cuvette containing 0.5 mM $NADP^+$ in 50 mM Tris-HCl pH 7.6, at 37ºC. Reactions were initiated by the addition of 6-phosphogluconate (6PG) and glucose-6-phosphate (G6P), respectively, up to a final concentration of 2 mM.

3.4.6 PK

PK activity was determined by coupling PK and LDH reactions in the following conditions: 0.8 mM NADH, 1.6 mM ADP, 12.1 mM $MgCl_2$, 36.8 mM KCl and 5.2 U/ml LDH in 20 mM phosphate buffer pH 7.2 at 37°C. Reaction was initiated by the addition of phosphoenolpyruvate (PEP) up to a final concentration of 3.5 mM.

3.5 Protein Content by Cell Number Assay

Cells were cultured and then collected with different concentrations, starting from 2.5 x 10^5 cells/ml up to 2 x 10^6 cells/ml, for THP1 and HAP1 cell lines, in both normoxia and hypoxia. After cell counting, protein extraction was performed with lysis buffer utilized in enzymatic assays (see

section 3.4) and protein content was measured through BCA Assay at 550 nm wavelength (Pierce, Thermo Scientific). Values were then plotted by cell concentration and protein by cell factors were obtained using linear regression.

3.6 RNA-based Assays

3.6.1 RNA Isolation

RNA was extracted from THP1 cells, both fresh and frozen extracts using Trizol (Sigma) according to manufacturer's protocol. Then chloroform was added to the mixture and centrifuged to generated aqueous and organic phases. The aqueous phase was collected, added cold isopropanol and incubated overnight at 4ºC to precipitate the RNA. The samples were then centrifuged at 13500 x g at 4ºC for 15 min. RNA was purified with several washing steps with 75% ethanol and resuspended in RNAse-free water. Purified RNA was quantified using Nanodrop Spectrophotometer (ND 1000 V3.1.0, Thermo Fisher Scientific Inc.).

3.6.2 RT-PCR

The Reverse Transcription reaction (convert RNA into DNA) was performed at 37ºC using 1 µg of RNA added to mixture containing 5x Buffer (Invitrogen), 0.1 M dithiothreitol (DTT) (Invitrogen), Random Hexamers (Roche), 40 U/µl RNAse inhibitor (Promega, Fitchburg, WI, USA), 40 mM dNTPs (Bioline, London, UK), 200 U/µl M-MLV-RT (Invitrogen).

Gene Expression analysis was performed by RT-PCR system (Applied Biosystems® 7500 Real Time PCR) standard manufacturer's protocol employing TaqMan® (Applied Biosystems) gene specific probes for TKT (Hs00169074_m1), TKTL1 (Hs00202061_m1), GLS (Hs01014019_m1). Reactions were performed in a volume of 20 µl containing 9 µl of cDNA and 11 µl of TaqMan Master Mix (Applied Biosystems). RT-PCR program

set-up parameters were: 1) initial incubation at 50ºC for 2 minutes, 2) denaturalization at 95ºC for 10 minutes, 3) amplification of 40 cycles alternating between 95ºC for 15 seconds and 60ºC for 1 minute. The house-keeping gene used as reference was PP1A (Hs99999904_m1, Applied Biosystems) and expression levels were quantified using ΔΔCt method.

3.6.3 RNA-sequencing

The transcriptomics methodology chosen was RNA-sequencing, to detect differentially expressed genes. Total RNA was extracted from lysates of the THP1 WT and THP1 TKTL1 KD cell lines, with 10 x 10^6 cells, using the RNeasy Kit (Qiagen, Hilden, Germany), with a DNase digestion step. Resulting samples were then sent to the Genomic Platform of the CNIC (National Centre for Cardiovascular Diseases) Institute in Madrid. Data alignment was performed using the Homo sapiens high coverage GRCh37.75.dna.primary_assembly by Juanjo Lozano of the Bioinformatics Platform of CIBEREHD, Institute of Health Carlos III (Madrid, Spain). Data processing and analysis was done in our lab by Effrosyni Karakitsou. The differentially expressed genes were identified using the Differential gene expression analysis based on the negative binomial distribution 2 (DESeq2) package from Bioconductor[454]. Throughout the analyses, a threshold was set for differentially expressed transcripts to be considered as statistically significant if their adjusted p-value or false discovery rate (padj) was lower than 0.05.

3.7 Mitochondrial Activity Assays

Mitochondrial activity assays in HAP1 cell lines were performed on a Seahorse XFe24 Flux Analyzer (Seahorse Bioscience, USA), following the Mitostress Test and Glycolytic Test protocols, and measuring in both cases the Oxygen Consumption Rate (OCR) and the Extracellular Acidification Rate (ECAR). XFe24 sensor cartridges were hydrated overnight using 1ml

per well of XF Calibrant Solution (Seahorse Bioscience, USA), at 37ºC in a non-CO_2 incubator. Both measurements were carried out together, with each plate performing both assays on the same oxygen condition. For data correction, the cells were extracted after measurements, using RIPA buffer and protein content was quantified by BCA assay.

3.7.1 Mito Stress Assay

HAP1 cell lines were seeded at 2.7 x 10^5 cells per ml in normoxia and 2.85 x 10^5 cells per ml in hypoxia, in 24-well plates (Seahorse Biosciences). Plating was done with 100 µL seeding of cell suspension and 150 µL extra addition of medium 2h later once cells had attached to the surface.

After overnight growth, the medium was replaced with Seahorse medium (buffer-free DMEM supplemented with 22 mM glucose, 4 mM glutamine, 1mM pyruvate and antibiotics). The plates were equilibrated in a 37ºC incubator without CO_2 for 60 min. The plate was then joined with the sensor cartridge, previously hydrated and calibrated as described above, and loaded into Analyzer.

The Mito Stress Assay protocol was altered for baseline conditions (25 mM glucose, 4 mM glutamine, 1% streptomycin and penicillin), with injections of 5 µM oligomycin (ATP synthetase inhibitor), 600 nM CCCP (Carbonyl Cyanide m-Chlorophenyl hydrazone, uncoupling agent), and 2 µM rotenone (inhibitor of complex I) together with 2 µM antimycin A (inhibitor of complex III), prepared and loaded into injection ports of cartridge, in order to calculate de different respiratory parameters (see section 3.7.3).

3.7.2 Glycolytic Stress Test

The Glycolytic Stress Test was performed at the same cell concentrations per well as the Mito Stress Test. Assay media was buffer-free DMEM supplemented with 4 mM glutamine and antibiotics. The cell plate went under the same preparing procedure before entering the Analyzer. The

protocol of injections was defined as 22 mM glucose, to initiate glycolysis; 5 μM oligomycin; and 250 mM 2-deoxy-D-glucose (2-DG), to inhibit glycolysis. Glycolytic parameters were then calculated from ECAR and OCR measures.

3.7.3 Calculations from Mito Stress and Glycolytic Stress assays

From each assay data, calculations of each parameter were required. All calculations were done after correction by protein values of each corresponding well.

For the Mito Stress Test Assay:

- Basal mitochondrial respiration was obtained from the subtraction of the non-mitochondrial respiration (OCR value after the injection of rotenone and antimycin A) to the baseline OCR.
- ATP production was calculated from the subtraction of baseline OCR from OCR rate following oligomycin injection.
- Proton leak was the subtraction of non-mitochondrial respiration from the OCR rate after oligomycin injection.
- Maximal respiration resulted from the subtraction of non-mitochondrial respiration to the OCR rate after CCCP injection.
- Spare capacity was calculated by removing the baseline OCR from the OCR rate after CCCP injection.

For the Glycolytic Stress Test Assay:

- Basal acidification without Glucose was the baseline acidification of the medium before any injection.
- Glycolysis rate was obtained from the subtraction of non-glycolytic acidification (ECAR rates after 2-DG injection) to ECAR rates after glucose injection.
- Glycolysis capacity was calculated from removing non-glycolytic acidification values from the ECAR rates after oligomycin injection.

- Glycolytic Reserve was the subtraction of ECAR rates after glucose injection to rates after oligomycin injection.

Crabtree Effect was calculated from OCR levels measured during the Glycolytic Stress Test. It is the subtraction of the baseline OCR to the OCR rate after the glucose injection, divided by the baseline OCR. Next, the logarithm base 2-fold change (log2) of the resulting value was calculated.

3.8 Reactive Oxygen Species (ROS) Assays

Intracellular ROS levels were determined by flow cytometry using the H_2DCFDA reactive (Invitrogen, Thermo Fisher Scientific, USA). HAP1 cell lines were seeded at 1 x 10^5 cells per p6 well, for both normoxia and hypoxia. After 48h incubation, the medium was removed, and cells were incubated with 5 mM glucose and 2 mM glutamine in PBS solution containing 5 μM of H_2DCFDA at 37ºC for 30 min in the cell culture incubator. After probe incorporation in cells, the solution was removed and replaced by standard culture medium, for another incubation at 37ºC for 45 min. This incubation step allows the probe activation, through intracellular esterases. Lastly, cells were washed with PBS, trypsinized and resuspended in PBS with 50 μM of H_2DCFDA and 20 μM of Propidium Iodate (PI), followed immediately by analysis at the Gallios™ Flow Cytometer (Beckman Coulter, USA), which detected the fluorescent probe that was excited at 492 nm and emitted at 520 nm, as well as PI fluorescence.

3.9 Targeted Metabolomics

Intracellular metabolite profiling and determination of uptake and secretion rates of the rest of metabolites apart from glucose, lactate, glutamate and glutamine, were performed using the Biocrates Absolute IDQ™ p180 kit (Biocrates Life Sciences AG, Austria). This kit quantitatively analyses the concentration of 21 amino acids, 19 biogenic amines, 90

glycerophospholipids, 15 sphingolipids, 40 acylcarnitines and hexose sugars.

THP1 cell lines were seeded at 4 x 10^5 cells/ml for both normoxia and hypoxia. After 48h incubation, extracts with 5 x 10^6 cells each were collected. HAP1 cell lines were seeded at high confluence conditions in order to obtain the maximum quantity of cell pellet (in a range of 10 to 15 x 10^6 cells) in 100 mm plates. After 48h incubation, cells were trypsinized and centrifuged at 200 x g for 5 min to obtain the cell pellet and cell medium. Cell pellets and medium aliquots were stored at -80ºC until analysis.

Pellets were resuspended in 70 µL of 85:15 ethanol:PBS buffer and sonicated 3 times for 5 seconds each, then submerged in liquid nitrogen for 30 seconds and thawed at 95ºC. This process was repeated twice. Suspensions were centrifuged at 20,000 x g, at 4ºC for 5 min, and collected the supernatant containing the metabolites. Protein content in cell lysates was measured using BCA assay. For the determination uptake and production of metabolites, metabolites were extracted from cell media taken from beginning and end of incubation in the same conditions as intracellular measurements.

30 to 50 µL of cell lysates and 10 µL of media were plated in the Biocrates plate together with the calibration standards, blanks, and quality controls. The plate was derivatized and processed according to manufacturer's instructions. Once ready, the plate was processed in a AB Sciex 4000 QTRAP MS/MS mass spectrometer coupled to an Agilent HPLC 1200, under two modes of work: HPLCMS reading for determination of amino acids and biogenic amines concentrations, and FIA-MS/MS for determination of lipids, sugars and acylcarnitines concentrations. Analyst and the MetIDQ™ software packages were used to analyse the obtained data and calculate metabolite concentrations. Metabolite concentration in extracts from pellets were normalized by protein. Consumption and

production rates of amino acids and biogenic amines were calculated as previously indicated (see section 3.3).

3.10 Stable Isotope-Resolved Metabolomics (SIRM)

HAP1 cell lines were seeded at 3.8 x 10^6 cells in normoxia and 5.5. x 10^6 cells in hypoxia, in 100 mm plates. After 24h incubation, media was replaced for IMDM culture medium with 22 mM glucose, 4mM glutamine and supplemented with 10% heat-inactivated FCS and antibiotics, with: A) media containing 22 mM glucose 100% enriched in U-^{13}C-glucose, B) media containing 4 mM glutamine 100% enriched in U-^{13}C-glutamine, C) media containing 4 mM glutamine 100% enriched in 3-^{13}C-glutamine, or D) standard media with no tracers. At 0h, 6h and 24h after the labelled substrates were added, cells and media were collected and kept at -80ºC until analysis. Concentration of glucose, lactate, glutamate and glutamine were measured in medium samples according to the methods in section 3.3.

3.10.1 Gas Chromatography Mass Spectrometry (GCMS)

The analyses of isotopologue distribution of ^{13}C-labelled intracellular and extracellular metabolites were performed using an Agilent 7890A gas chromatograph (Agilent Technologies, USA) with an HP-5 capillary column coupled to an Agilent 5975C mass spectrometer. For analysis, 1 µl of each sample was injected together with helium gas as a carrier at a 1 ml/min of flow rate.

3.10.1.1 Extracellular Metabolites Extraction

For extracellular lactate analysis, lactic acid from acidified cell culture media was isolated using ethyl acetate previous to airflow drying. Lactate was derivatized to lactic acid n-propylamide-heptafluorobutyric ester by incubation with 200 µl of 2,2-dimethoxypropane and 50 µl of 0.5 N methanolic HCl at 75ºC for 1 hour and then adding 60 µl of n-propylamine

at 100ºC for 1 hour more. After drying under N_2 flow, samples were filtered using glass wool through a Pasteur pipette and dried again under N_2 flow. Then, samples were resuspended and incubated with 200 µl of dichloromethane and 15 µl of heptafluorobutyric anhydride at room temperature for 10 min, dried under N_2 and resuspended under ethyl acetate before GCMS analysis under chemical ionization mode. The oven temperature variations were programmed as follows: 100ºC for 3 min, then increased to 160ºC at 20ºC/min, and hold for 2 min. The detector was run at single ion monitoring (SIM) mode. Lactate complete fragment C1-C3 was detected at 5.4 minutes of retention time by monitoring m/z ions from 327 to 332.

For amino acids in media, media samples were mixed with milliQ water, added 5 µl of norvaline 1 mg/ml and cold methanol. Then, the samples were vortexed for 60 seconds in cold room and cold chloroform was added. After gentle shaking (30 min at 4ºC) the samples were centrifuged (3,100 x g, at 4ºC for 15 min) and the upper aqueous phase was collected. This phase was then dried under airflow and mixed with dichloromethane (CH_2Cl_2), to completely dehydrate the samples. Samples were then dried using N_2 gas flow. Polar metabolites were derivatized by adding 50 µl of 2% methoxamine hydrochloride in pyridine for 90 minutes at 37ºC, and 30 µl of (N-methyl-N-tert-butyldimethylsilyl) trifluoroacetamide + 1% tertbutyldimethylchlorosilate) for 60 min at 55ºC, before GCMS analysis using electron impact (EI) mode. The oven temperature ramps were programmed as follows: 100ºC for 3 min, then increased to 165ºC at 10ºC/min, to 225ºC at 2.5ºC/min, to 265ºC at 25ºC/min and finally to 300ºC at 7.5ºC/min. The detector was run at single ion monitoring (SIM) mode. Following table lists the extracellular metabolites that were analysed and their retention times (Table 3.10-A).

Compound	Fragment	Retention Time (min)	m/z Cluster	m/z Cluster Range	m/z Control
Pyruvate	C1-C3	7.7	174.1	173.1-179.1	115.1
Lactate	C1-C3	10.8	261.1	260.1-266.1	303.1
Alanine	C1-C3	11.4	260.1	259.1-265.1	232.1
Norvaline	C1-C5	12.9	260.2	259.2-267.2	288.1
Serine	C1-C3	16.1	390.2	389.2-395.2	362.2
Glutamate	C1-C5	17.9	432.3	431.3-439.3	474.3

Table 3.10-A- Extracellular metabolites quantified by GC-MS. Extracellular metabolites and corresponding fragments that were quantified with retention time, monitored clusters and respective ranges. Previously optimized for maximum detection. Extra cluster detected for control purposes.

3.10.1.2 Intracellular Metabolites Extraction

For intracellular ribose analysis, RNA was isolated from cell pellets using Trizol reagent, mixing it with chloroform. The aqueous phase was obtained, and cold isopropanol was added and centrifuged 20,000 x g, at 4ºC for 15 min. The samples were washed several times using cold 75% ethanol. The samples of purified RNA were hydrolysed in 2 ml of 2 M HCl at 100ºC for 2 hours and dried under airflow. The resulting ribose was derivatized into its aldonitrile acetate derivative using 100 µl of 2% hydroxylamine hydrochloride in pyridine at 100ºC for 30 min and 75 µl of acetic anhydride at 100ºC for 1 hour. Then, samples were dried under N_2 flow and resuspended in ethyl acetate before GCMS analysis using chemical ionization mode. The oven temperature ramps were programmed as follows: 150ºC for 1 minute, then increased to 275ºC at 15ºC/min, to 300ºC at 40ºC/min, and hold for 2 min. The detector was run at single ion monitoring (SIM) mode. Ribose complete fragment C1-C5 was detected at 5.3 minutes of retention time monitoring m/z ions from 256 to 261.

For polar intracellular metabolites analysis, cells were washed with ice-cold PBS and scrapped with 1:1 metanol:water (adding first 1 ml of methanol, waiting for 1 minute and adding1 ml of milliQ water afterwards). At that point, 5 µl of norvaline 1 mg/ml was added for quantification purposes to minimize the differences that could be associated with efficiency of extraction. Then, the samples were sonicated (3 cycles of 5 seconds) and 2 ml of cold chloroform was added. After gentle shaking (30 min at 4ºC) the samples were centrifuged (3,100 x g, at 4ºC for 15 min) and the supernatant was completely dried under airflow. The extracted metabolites were derivatized by adding 50 µl of 2% methoxamine hydrochloride in pyridine for 90 minutes at 37ºC and 3 µl of (N-methyl-N-tert-butyldimethylsilyl) trifluoroacetamide + 1% tertbutyldimethylchlorosilate) for 60 min at 55ºC before GCMS analysis using electron impact (EI) mode. The oven temperature ramps were programmed as follows: 100ºC for 3 min, then increased to 165ºC at 10ºC/min, to 225ºC at 2.5ºC/min, to 265ºC at 25ºC/min and finally to 300ºC at 7.5ºC/min. The detector was run at single ion monitoring (SIM) mode. Following table lists the intracellular metabolites that were analysed and their retention times (Table 3.10-B).

Compound	Fragment	Retention Time (min)	m/z Cluster	m/z Cluster Range	m/z Control
Lactate	C1-C3	11.0	261.1	260.1-266.1	303.1
Glycine	C1-C2	12.2	246.1	245.1-250.1	218.1
Norvaline	C1-C5	14.2	260.2	259.2-267.2	288.1
Proline	C2-C5	16.4	258.2	257.2-264.2	286.1
Serine	C1-C3	22.2	390.2	389.2-395.2	362.2
Malate	C1-C4	25.8	419.2	418.2-425.2	461.3
Aspartate	C1-C4	27.1	418.2	417.2-424.2	390.2
Glutamate	C1-C5	30.7	432.3	431.3-439.3	474.3
Citrate	C1-C6	36.9	591.4	590.4-599.4	459.2

Table 3.10-B- Intracellular metabolites quantified by GC-MS. Intracellular metabolites and corresponding fragments that were quantified with retention time, monitored clusters and respective ranges. Previously optimized for maximum detection. Extra cluster detected for control purposes.

3.10.1.3 SIRM data analysis

Raw MS data was examined using MSD5975C Data Analysis (Agilent Technologies). The data obtained by mass spectrometry represents a spectral distribution of ions with its molecular weights (m/z) at each retention time. The ion clusters, which were specified for each case, were used to determine the distribution of ^{13}C at each carbon of the fragment. Manual integration of peak areas was done to quantify the distribution of ribose and lactate. Automated integration using the in-house developed software "Ramid" was used to quantify the distribution of the rest of metabolites[455]. The software, based in "R", allows automatic extraction of the NetCDF files containing the m/z raw time course to isotopologue distributions. All the values of peak areas, which are proportional to the ^{13}C incorporation to each molecule of the compound, needed to be corrected for the presence of natural abundance of ^{13}C as well as Si isotopes that are present from the derivatization reagents and contribute to the mass isotopologue distribution. The correction was performed from isotopologue distributions extracted before, using the "Midcor" software package[455,456]. Afterwards, data was analysed and represented as direct substrate contribution of to specific isotopologues (m1, m2, m3, etc. according to the number of ^{13}C that were labelled).

3.10.2 Nuclear Magnetic Resonance (NMR)

NMR experiments were performed at the University of Birmingham, as part of a secondment under the tutelage of Prof Ulrich Guenther at the Henry Wellcome Building for Nuclear Magnetic Resonance (HWB-NMR). Data processing and analysis was performed by Nuria Vilaplana, as a collaboration within the HaemMetabolome ITN research initiative.

Samples used for NMR analysis were generated in tandem with GCMS samples, as detailed in section 3.10, media samples from the three different

^{13}C-tracers used for GCMS were collected and analysed by NMR. An additional set of samples labelled with U-^{13}C-glucose and 3-^{13}C-glutamine were also analysed using NMR for intracellular metabolite studies.

All NMR data was acquired at Bruker 600 MHz spectrometers equipped with Avance-III consoles using a cooled Bruker SampleJet autosampler. For cell extracts, a triple resonance cryoprobe (TCI) 1.7mm z-axis pulsed field gradient (PFG) cryogenic probe was used, and for media samples, a 5mm TCI z-PFG cryogenic probe was used. Probes were equipped with a cooled SampleJet autosampler (Bruker) and automated tuning and matching.

3.10.2.1 Intracellular Metabolite Extraction

For intracellular metabolite extraction, cells were washed with 5 ml cold PBS, scraped in 600 ul cold Methanol (-20ºC) and collected into glass vials (2 ml). 200 µl HPLC grade chloroform (Merck) and 300 µl Milli-Q water were added with 1 min vortex steps between them. Samples were incubated for 10 min on ice and then centrifuged at 4000 rpm for 15 min at 4ºC. 400 ul of the polar phase (upper phase) were collected into in a new tube. Polar phase samples were dried with vacuum and stored at -80°C.

Dried polar phases samples were reconstituted in 50 µl of 0.1 M phosphate buffer including 3 mM NaN_3, 0.5 mM 3-(Trimethylsilyl) propionic-2,2,3,3-d_4-acid sodium salt (TMSP) and 10% (v/v) D_2O (all from Sigma-Aldrich). Samples were sonicated for 10 min and transferred to 1.7 mm NMR tubes (CortecNet) using the Micro Pipet System 1.7 (New Era Enterprises). Sample preparation was done within 24 hours before the acquisition and kept at 4°C.

3.10.2.2 Extracellular Metabolite Extraction

For the extracellular metabolite extraction, media samples were collected from the adherent cells plates (1 ml per plate) and stored at -80ºC. The day

prior to acquisition, media samples were diluted with a 10% (v/v) 10X phosphate buffer (1 M phosphate buffer with 3 mM NaN3 and 5 mM TMSP in 100% D_2O) to a final concentration equal to the one used with dried polar phases described in the previous section. Buffered samples were transferred to 3 mm NMR tubes (CortecNet) using glass pipettes and stored at 4°C.

3.10.2.3 1D-NMR

Spectra acquisition at 300K using 1D ^{1}H-NOESY (Nuclear Overhauser effect spectroscopy) pulse sequence, with pre-saturated water suppression (noesygppr1d, standard pulse sequence from Bruker). Data point numbers was TD 32,768, the spectral width was 12 parts per million (ppm), with interscan delay of d1 4 seconds and NOE mixing of d8 10 milliseconds. The ^{1}H carrier was set on water frequency, with ^{1}H 90º pulse calibrated at 0.256 W and length of ca 7-8 μs. For medium samples from HAP1 cell lines, 64 transients and 8 steady state transients were acquired. The experimental time for media samples was 7.5 min.

Data processing: 1D ^{1}H-NMR

Spectra processed with *MetaboLab* software[457] within the MATLAB environment (MathWorks). The FID signals were multiplied by 0.3 Hz exponential window function, with zero-filling up to 131,072 data points applied prior to Fourier transformation. Chemical shift was calibrated using the TMSP signal as reference for 0 ppm and spectra were phase corrected manually. The baseline correction was done by applying a spline baseline correction. The TMSP, water and edge regions of the spectra were excluded before scaling, using a probabilistic quotient normalization (PQN). For metabolite identification, utilized Chenomx 7.0 software (Chenomx Inc.) and the Human Metabolome Database (HMDB). Peak intensities were obtained directly from the spectra. Relative metabolite changes were calculated by obtaining the peak intensities of each metabolite at 0 and 24h,

the initial intensity subtracted from the final intensity and the result divided by the initial intensity.

3.10.2.4 ^{13}C-filtered ^{1}H-NMR

Medium samples labelled with U-^{13}C-glucose, U-^{13}C-glutamine and 3-^{13}C-glutamine were analysed with ^{13}C-filtered ^{1}H-NMR spectroscopy as described in Reed et al., 2019. Sample preparation is described in 4.1.1.2. Sample acquisition was done in the Bruker 600 MHz with a 5mm TCI z-PFG cryogenic probe. Spectra acquired at 300 K using a double gradient BIRD filter pulse sequence developed in-house[458]. Used pulse program that combines the ^{1}H[^{12}C] and the all-^{1}H experiments in scan-interleaved mode. The FIDs difference results in the ^{1}H[^{13}C] signal. Spectral width was 12 ppm, data points numbers were 16,384 in each dimension and relaxation delay was 5.3 sec. Acquired 256 transients with 64 steady state transients and the experimental time was 15 min.

Data processing: ^{13}C-filtered ^{1}H-NMR

The ^{13}C-filtered ^{1}H-NMR spectra were processed in *Topspin 4.0.5* (Bruker). Spectra were zero filled to 32,768 data points before Fourier transformation. Phase correction was applied to all the spectra (^{1}H[-^{12}C] and all-^{1}H spectra) and the difference ^{1}H[^{13}C] spectrum was obtained through chemical shift alignment. Metabolites were picked in the ^{1}H[^{13}C] spectrum and integrated in all the spectra (^{1}H[^{12}C], ^{1}H[^{13}C] and all-^{1}H) using the *Topspin 4.0.5* (Bruker) integral tool. For each metabolite label incorporation, we divided the corresponding peak area in the ^{1}H[^{13}C] spectrum by the peak area in the all-^{1}H spectrum.

3.10.2.5 2D ^{1}H-^{13}C HSQC

Sample acquisition was done in Bruker 600 MHz with a 5mm TCI z-PFG cryogenic probe at 300K using a modification of the HSQCGPHPRSP from Bruker, with additional gradient pulses during the insensitive nuclei

enhanced by polarisation transfer (INEPT) echo periods and using soft 180º pulses for ^{13}C. For the 1H dimension: spectral width of 13.018 ppm with 1024 complex points. For the 13C dimension: spectral width of 160 ppm with 2048 complex points. 2 transients were acquired per spectra, with an interscan delay of 1.5 seconds. Generated a non-uniform sampling (NUS) of 25% sampling schedule using the Wagner's schedule generator (Gerhard Wagner Lab, Harvard Medical School), with a tolerance of 0.01 and default values for the other parameters. The total experimental time was 4 hours.

Data processing: 2D ^{1}H-^{13}C HSQC

For the ^{1}H-^{13}C HSQC spectra, processed and phase corrected with *NMRPipe* (National Institute of Standards and Technology of the U.S.)[459]. *MetaboLab* was used to reference using the signal for the methyl group of L-lactic acid, at 1.31/22.9 ppm in the ^{1}H and ^{13}C dimensions, respectively. For the 2D spectra, metabolite identification was carried out using the *MetaboLab* software which includes a chemical shift library for ca. 200 metabolites. Intensities were obtained from signals in the spectra. For normalization, a ^{1}H-NMR spectrum was acquired per each sample and the total area was obtained from *MetaboLab* to normalize the 2D data for differences in cell number. To calculate the % of ^{13}C per metabolite, the normalized intensity of a certain carbon in the labelled sample was divided by the normalized intensity of the same carbon in the unlabelled sample and was multiplied by the natural abundance of ^{13}C (1.1%).

4. RESULTS

4 Results

4.1 Chapter I – Metabolic Characterization of TKTL1 in AML

4.1.1 Introduction

Synthesis of R5P is crucial to ensure the production of nucleotide building blocks for DNA duplication. As explained before, R5P can be synthesised through both branches of the PPP, mediated by G6PD on the oxidative side with the additional production of NADPH and controlled by TKT non-oxidative side, that links glycolysis to the production of R5P[460,461].

Increased expression of TKT and its isoform TKTL1 has been reported in different types of cancers[58,77,78,462] and is related to malignant transformation[463] and poor prognosis[54,464–466]. As described in section 1.1.5.1, the TKTL1 isoenzyme is missing 38 amino acids in the active site compared to TKT and but retains its enzymatic activity[57]. The contribution of TKTL1 to the overall TKT activity has been proven by silencing TKTL1 in different cell lines[463]. Evidence across several cancer tissues up until now have highlighted that TKTL1 is tightly linked to adaptation to hypoxia and its overexpression has been correlated with resistance to ionizing radiation and chemotherapy[467] as well as to the "Warburg effect"[468]. For example, in glioma cells it has been demonstrated that hypoxia lead to TKTL1 induction and that its knockdown decreased flux through the PPP and resulted in cell death[467]. Induction of TKTL1 under hypoxia has also been observed in different cell lines of colorectal cancer (CRC) and upregulation has been demonstrated for a subset of CRC patients[465]. It has also been reported that hypoxia induced dramatic metabolic changes in AML cell lines, including adaptation of both lipid and glycolytic metabolism[469]. In addition, increased levels of TKTL1 haves been reported in response to decitabine (DAC) treatment in primary acute myelogenous leukaemia (AML) samples[470] and

correlated to the acquisition of tyrosine kinase inhibitor resistance in chronic myeloid leukemia[471].

However, to date, there has been less exploration about the role of TKTL1 in the metabolic response triggered by hypoxia in leukaemia and detailed studies on its role during metabolic reprogramming of AML cells to hypoxia are lacking.

One of the objectives of this body of work is to untangle the functional relationship between TKTL1 expression and metabolic adaptation of AML cells to hypoxia. For this purpose, we performed a comparative analysis of hypoxia-induced changes using the THP1 cell line, an monocytic leukemic cell line established in 1980 from the blood of an AML child patient, with an *MLL* fusion[472]. Through the use of THP1 transduced with a lentiviral vector expressing a TKTL1-specific shRNA ($TKTL1^{KD}$) and a wildtype control transduced with an empty vector ($THP\text{-}1^{WT}$), we attested the differences between them both at the transcriptional and metabolic levels. Together, our findings highlight that in response to hypoxia, THP-1 cells deeply rewire central metabolism at the transcriptomic level to sustain an enhanced consumption of glucose and glutamine and that this response is severely impaired in the cells lacking TKTL1.

4.1.2 Results

4.1.2.1 TKTL1 contributes to cell growth in normoxia and hypoxia

To characterize the role of TKTL1 in growth properties and metabolic response to hypoxia of AML cells, we initially evaluated the effect of the shRNA-mediated silencing of TKTL1 on the expression of TKTL1 and TKT genes by RT-PCR. We obtained a knockdown efficiency of 63.3% ± 0.03 for TKTL1 expression whereas the TKT expression has not been significantly affected (Figure 4.1.1).

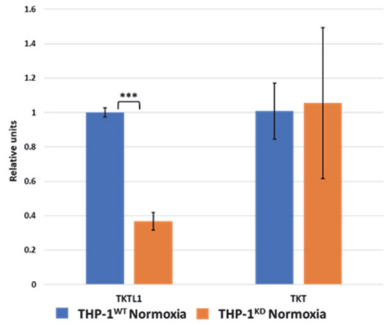

Figure 4.1.1- Effects of TKTL1 silencing on TKTL1 and TKT expression. RT-PCR performed using PPA1 as a housekeeping gene for data normalization. Decrease of TKTL1 expression determined as 63.3% ± 0.03. Data showed is mean ± SD of normalized values of n=2 reads of n=3 replicates of a single experiment. Statistically significant differences were determined by two-tailed independent sample Student's t-test: $p<0.001$ (***).

Next, we evaluated the impact of TKTL1 knockdown on cell proliferation during hypoxia. At 96h of cell incubation, in either normoxia (O_2 at 21%) or hypoxia (O_2 at 1%), an increase in THP-1^{KD} cells duplication time with respect to THP-1^{WT} of around 25 % and 29% respectively was observed (Figure 4.1.2A-B). When compared to normoxia, hypoxia induced a 3-fold increase in duplication time of both THP-1^{wt} and THP-1^{KD} cells.

The protein content per cell was also quantified, to attest that TKTL1 silencing did not affect total cell protein content. The obtained results showed that the protein content of both cell lines in normoxia was not statistically different, which permits us to conclude that the silencing of TKTL1 is not affecting the total cell protein content (Figure 4.1.2C). Same quantification has not been possible in hypoxia due to too much dispersion (data not shown). Altogether, these results reinforce the knowledge that TKTL1 is a necessary enzyme for proliferation as reported in many previous studies, highlighting that its function is essential under normal oxygen conditions, as well as during a hypoxic state.

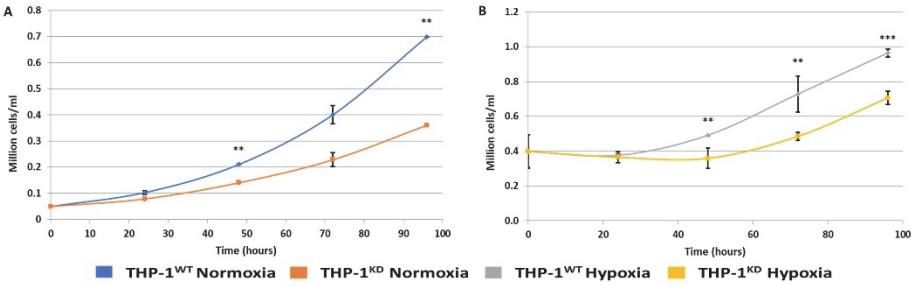

C

Normoxia	THP-1^{WT}	THP-1^{KD}
Duplication time (h)	38.4 ± 2.24	49.37 ± 2.48 **
% of increment vs THP-1^{WT}	-	25.08
Hypoxia	THP-1^{WT}	THP-1^{KD}
Duplication time (h)	113.5 ± 41.81	151.3 ± 19.38
% of increment vs THP-1^{WT}	-	28.56

D

Normoxia	mg protein/ 10^6 cells
THP-1^{WT}	8.54 ± 0.67
THP-1^{KD}	8.89 ± 0.60

Figure 4.1.2- Effect of TKTL1 Knockdown on Proliferation. Growth curve from 0 to 96h incubation in (**A**) normal oxygen conditions and (**B**) in hypoxic conditions (1% O_2). Data shown as representative experiments, with mean ± SD for n=2 reads of n= 3 independent experiments for normoxia condition and n=2 reads of n=2 independent experiments for hypoxia condition. (**C**) Duplication rates calculations in both conditions. (**D**) Cell protein content of THP1 Control and THP1 TKTL1 Knockdown under normoxia. Statistically significant differences in all panels was determined by two-tailed independent sample Student's t-test: $p<0.01$ (**), $p<0.001$ (***).

Since it is through the synthesis of R5P and other pentoses that both branches of the PPP mainly contribute to proliferation, we determined the effect of the TKTL1 knockdown on the total enzymatic activity of TKT, G6PD and 6PGD. TKTL1 knockdown resulted in a decrease of all TKTs activity of around 45% in normoxia and 49% in the hypoxic condition and of total G6PD activity of around 65% (normoxia) and around 75% (hypoxia) (Figure 4.1.3A-B). By contrast, the knockdown did not alter significantly 6PGD activity, neither in normoxia or hypoxia (Figure 4.1.3C).

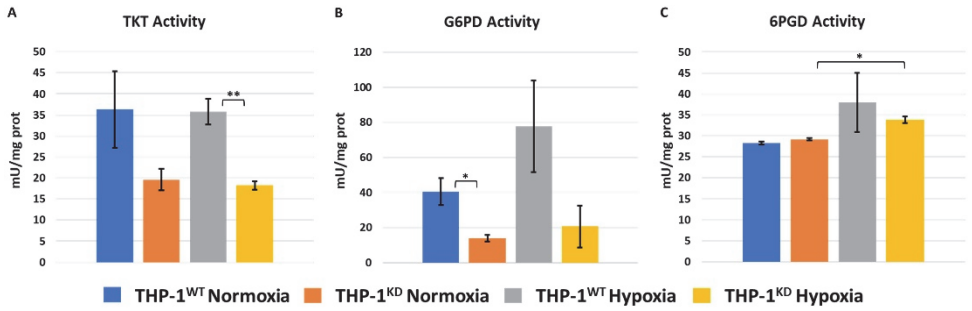

Figure 4.1.3- Changes in total enzyme activity capacity of key enzymes in pentose-phosphate pathway triggered by hypoxia. Enzymatic Activity Assays performed through spectrophotometry in normoxia and hypoxia for **(A)** Transketolase (TKT), **(B)** Glucose-6-Phosphate dehydrogenase (G6PD) and **(C)** 6-phospo-gluconate dehydrogenase (6PGD). Data represented is mean ± SD for n=2 reads of n=2 replicates of n=2 independent experiments. Statistically significant differences in all panels was determined by two-tailed independent sample Student's t-test: $p<0.05$ (*), $p<0.01$ (**), $p<0.001$ (***). The Transketolase activity assay measures both TKT and TKTL1 activity combined, cannot disassociate.

Through transcriptomic analysis we attested if these differences in activity originated from differential gene expression. Consistent with the hypoxia-induced decrease in proliferation rates of these cells, we observed that the G6PD gene expression (quantified as Log2 Fold-Change of hypoxia *versus* normoxia transcript levels (Log2FC)) in hypoxia is decreased significantly for THP-1^{WT} (Log2FC= -0,72) as well as for THP-1^{KD} (Log2FC= -1,24) (Figure 4.4). Taking into account that G6PD is regulated by PTMs, the fact that total G6PD activity did not change could be due to post-transcriptional activation of the enzyme. In fact, it has been described that G6PD is activated by SIRT5-catalyzed deglutarylation[473]. The transcriptomic results show that under hypoxic conditions, SIRT5 levels increase in both THP-1^{WT} (Log2FC= 0,78) and THP-1^{KD} (Log2FC= 1,08) (Figure 4.1.4). In regard to the TKT and TKTL1 genes, there was a very slight increase in gene expression induced by hypoxia which however did not result in effective activity increase, demonstrating that post-translation regulation of the PPP enzymes is occurring and dependent on TKTL1 activity.

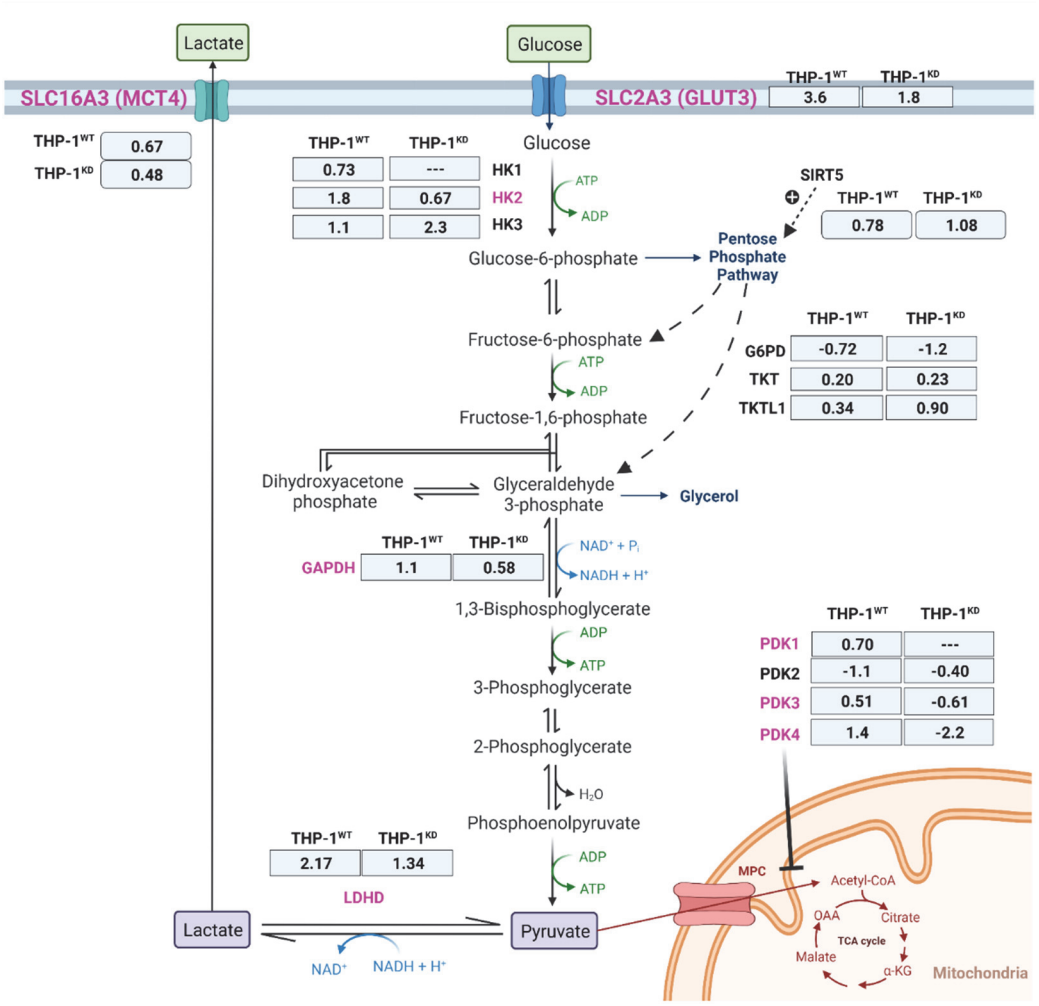

Figure 4.1.4- Gene expression changes of key enzymes and transporters between THP-1^{WT} and THP-1^{KD} in hypoxia. Significant changing genes due to TKTL1 highlighted in pink. Expression changes of normoxia versus hypoxia, indicated in log2-Fold-change of n=3 samples per condition. Abbreviations: G6PD (glucose-6-phosphate dehydrogenase), GAPDH (glyceraldehyde-3-phosphate dehydrogenase), GLUT3 (glucose transporter 3), HK1-3 (hexokinase 1 to 3), LDHD (lactate dehydrogenase D), MCT4 (monocarboxylate transporter 4), PDK1-4 (pyruvate dehydrogenase kinase 1 to 4), SIRT5 (sirtuin 5), SLC (solute carrier family), TKT (transketolase), TKTL1 (transketolase-like 1). Created with BioRender.com.

4.1.2.2 TKTL1 is essential to trigger hypoxia-induced changes to glucose fate in THP-1 cells

A common behaviour of most cancer cells under hypoxic conditions is the increase of the glycolytic pathway flux as a metabolic adaptation to their environment. To see how this feature is dependent on TKTL1, we characterized glucose consumption and lactate production rates, under normoxia and hypoxia conditions in THP-1^{WT} and THP-1^{KD} cells. Results obtained (Figure 4.1.5A-C) showed that in normoxia, THP-1^{WT} glycolytic rates (glucose consumption and lactate production) were around 2-fold higher than in THP-1^{KD} cells. The ratio of lactate production per glucose consumption (Figure 4.1.5C) was significantly different in WT and KD cells in normoxia but not in hypoxia. Nevertheless, the increased values of around 2 for both cell lines in hypoxia indicate that under O_2 restriction, glucose is readily oxidized to lactate.

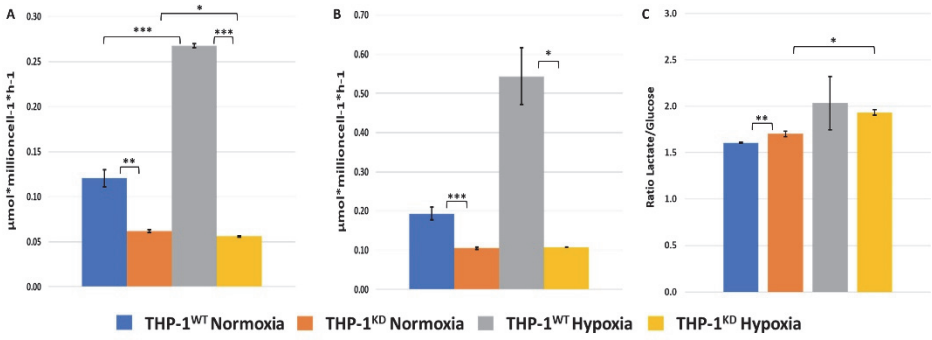

Figure 4.1.5- Loss of TKTL1 impairs hypoxia response. Consumptions and production rates measurements through spectrophotometry from cell culture media after 48h incubation, in both normoxia and hypoxia conditions. (**A**) Glucose consumption. (**B**) Lactate production. (Data represented by mean ± SD of n=3 reads of a representative experiment per normoxia and hypoxia. (**C**) Ratios of lactate produced per glucose consumed. Statistically significant differences in all panels was determined by two-tailed independent sample Student's t-test: $p<0.05$ (*), $p<0.01$ (**), $p<0.001$ (***).

Hypoxia triggered a metabolic switch of around 2.2-fold increase in glucose consumption and lactate production in THP-1^{WT} cells, whereas in THP-1^{KD}

the glycolytic rates were not statistically different in hypoxia with respect to the normoxia measurements (Figure 4.1.5A-B). These results unveil a key role of TKTL1 in the adaptive metabolic switch to glycolysis that THP-1^{WT} cells undergo under hypoxia.

It has been well documented that the hypoxia response induction of glycolysis occurs due to increased gene expression of enzymes, transporters and growth factor receptors (identified in Figure 4.1.4)[474–482]. We investigated if the impaired enhancement of glycolysis in response to hypoxia observed in THP-1^{KD} was due to a failing of upregulation of gene expression.

Results showed that the expression of the isoforms of hexokinase that bind to mitochondria (HK1 and HK2) and the pyruvate dehydrogenase kinase isoenzymes (PDK1, 3 and 4) were strongly up-regulated in THP-1^{WT} in response to hypoxia (see Figure 4.1.4). In the contrary, in THP-1^{KD}, hypoxic conditions induced a decrease of the expression of PDK3 and PDK4 but did not alter the expression of neither HK1 nor PDK1. Worth to note, that the hypoxia-induced increase in gene expression of the hexokinase isoenzyme HK3, that binds to the nucleus, is 2.5-fold higher in THP-1^{KD} than in THP-1^{WT}, which suggests a TKTL1-independent mechanism of regulation of the expression of this gene in hypoxia. In fact, HK3 has been described to have a role in decreasing ROS levels and has been associated with higher levels of transcription factors that regulate mitochondrial DNA content and mitochondrial biogenesis[483].

Other glycolytic enzymes and transporters that are reported to be overexpressed in hypoxia, such as GAPDH, glucose transporter SLC2A3 (GLUT3), lactate dehydrogenase D (LDHD) and lactate transporter SLC16A3 (MCT4), were found to be upregulated under hypoxic conditions in both THP-1^{WT} and in THP-1^{KD} (see Figure 4.1.4).

Measurement of total HK and GAPDH activity in THP-1^{WT} and THP-1^{KD} cells (Figure 4.1.6A-B) showed that activity was higher in THP-1^{WT} than in THP-1^{KD} in both normoxia and hypoxia conditions. In the contrary, we observed that the knock-down of TKTL1 did not affect total LDH activity and that LDH activity was increased in both THP-1^{WT} and THP-1^{KD} cells under hypoxia (Figure 4.1.6C). The results obtained are consistent with the lower K_m for glucose reported for HK3 isoenzyme, when compared to HK1 and HK2[484]. LDHD has been reported to function as a "metabolite repair enzyme" that controls metabolic damage in glycolysis by contributing to the elimination of methylglyoxal formed from another glycolytic enzyme, namely the triose-phosphate isomerase (TPI)[485]. Total GAPDH activity (Figure 4.1.6B) as well as GAPDH gene expression (Figure 4.1.4) increased in both cell lines, in response to hypoxia, favouring the THP-1^{WT}.

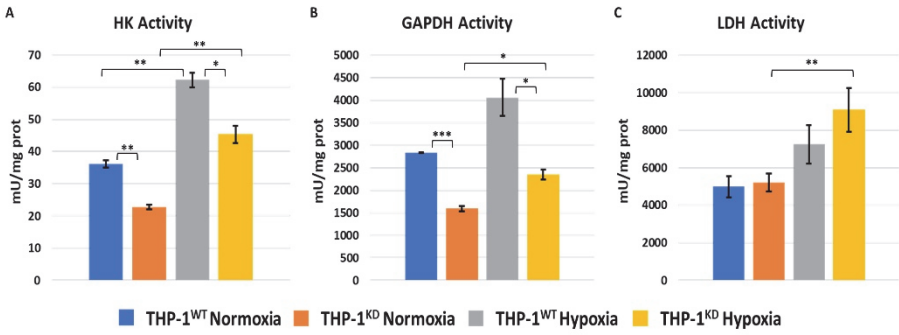

Figure 4.1.6- Changes in total enzyme activity capacity of key glycolytic enzymes triggered by hypoxia. Enzymatic Activity Assays performed through spectrophotometry in normoxia and hypoxia for enzymes (**A**) Hexokinase (HK), (**B**) Glyceraldehyde-3-Phosphate dehydrogenase (GAPDH) and (**C**) Lactate Dehydrogenase (LDH). Data represented is mean ± SD for n=2 reads of n=2 replicates of n=2 independent experiments. Statistically significant differences in all panels was determined by two-tailed independent sample Student's t-test: $p<0.05$ (*), $p<0.01$ (**), $p<0.001$ (***).

Altogether the gene expression profile observed provided strong evidence that the knockdown of TKTL1 impairs the metabolic switch to glycolysis in response to hypoxia, through the downregulation of PDK3 and PDK4

and the increase in the gene expression of HK3. Another factor in the hypoxic response is the use of growth factors and the increase of their receptors. We observed that hypoxia triggered a dramatic increase in Estrogen-Related Receptor b (ESRRb) (log2FC= 4,6) in THP-1^{WT} whereas ESRRb levels remain constant in THP-1 ^{KD}. The family of Estrogen-Related Receptors (ESRRs) has been described to mediate PDKs gene overexpression in hypoxia[479,486], leading to the hypothesis that TKTL1 plays a key role in the switch from OXPHOS to glycolysis, by induction of PDKs that result in PDH inhibition, in an ESRRb-mediated way.

4.1.2.3 TKTL1 is essential to trigger hypoxia-induced changes to glutamine fate in THP-1 cells

Second to glucose, glutamine is a major carbon source for energy production and anabolic processes (see section 1.3.4.1). It has been described that hypoxia enhances cancer cells glutamine synthesis and uptake, by increasing glutamine synthetase (GS, also known as GLUL) and the number of glutamine transporters such as SLC38A2[487]. To attest how TKTL1 could impact glutamine metabolism, we characterised glutamine consumption and glutamate production rates, under normoxia and hypoxia conditions in THP-1^{WT} and THP-1^{KD} cells. The results obtained showed that TKTL1 knockdown resulted in a 20-25% decrease in glutamine consumption and glutamate production under normoxia and in a 70-75% decrease under hypoxia (Figure 4.1.7A-B). When comparing the effect of this knockdown on the ratio of glucose consumption versus glutamine consumption (Figure 4.1.7C), we observed a decrease of around 20% in normoxia and of 27% in hypoxia, which indicates that the overall impact of silencing TKTL1 is more pronounced in hypoxia. In fact, the hypoxic metabolic switch triggered an increase of around 20% of glutamine consumption and glutamate production in THP-1^{WT} cells, while the THP-

1^{KD} cells in hypoxia had around 50-60 % decrease of these metabolites levels (Figure 4.1.7A-B).

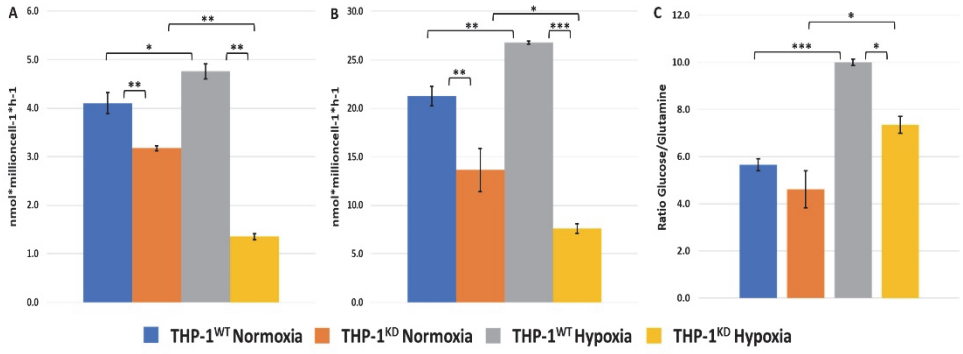

Figure 4.1.7- Loss of TKTL1 impairs hypoxia response. Consumptions and production rates measurements through spectrophotometry from cell culture media after 48h incubation, in both normoxia and hypoxia conditions. (**A**) Glutamate production. (**B**) Glutamine consumption. Data represented by mean ± SD of n=3 reads of a representative experiment per normoxia and hypoxia. (**C**) Ratios of glucose consumed (depicted in Figure 4.1.5A) versus glutamine consumed. Statistically significant differences in all panels was determined by two-tailed independent sample Student's t-test: $p<0.05$ (*), $p<0.01$ (**), $p<0.001$ (***).

Another key characteristic of hypoxia adaptation in cancer cells is changes to expression of key glutamine metabolism genes and transporters[487]. We investigated if the contrary response seen in hypoxia in our results was due to a failure in the upregulation of gene expression (Figure 4.1.8). We observed that GS gene expression was strongly upregulated (log2FC= 1.3) and also *SLC38A2* was slightly upregulated in THP-1^{WT} whereas glutaminase (GLS) expression did not change. By contrast, *GLS* and *SLC38A2* were downregulated in THP-1^{KD} and the observed overexpression of *GS* (log2FC= 0.60) was 50% lower than the observed in the control cells. In addition, *SLC1A3 (*glutamate-aspartate transporter) and *SLC17A7* (glutamate transporter) were strongly overexpressed under hypoxia conditions in THP-1^{WT} whereas in THP-1^{KD} were downregulated or unaltered. Altogether, the observed changes at transcriptomic level relating to glutamine/glutamate intake and metabolism correlate with an

impairment of the metabolic response induced by hypoxia due to TKTL1 knockdown.

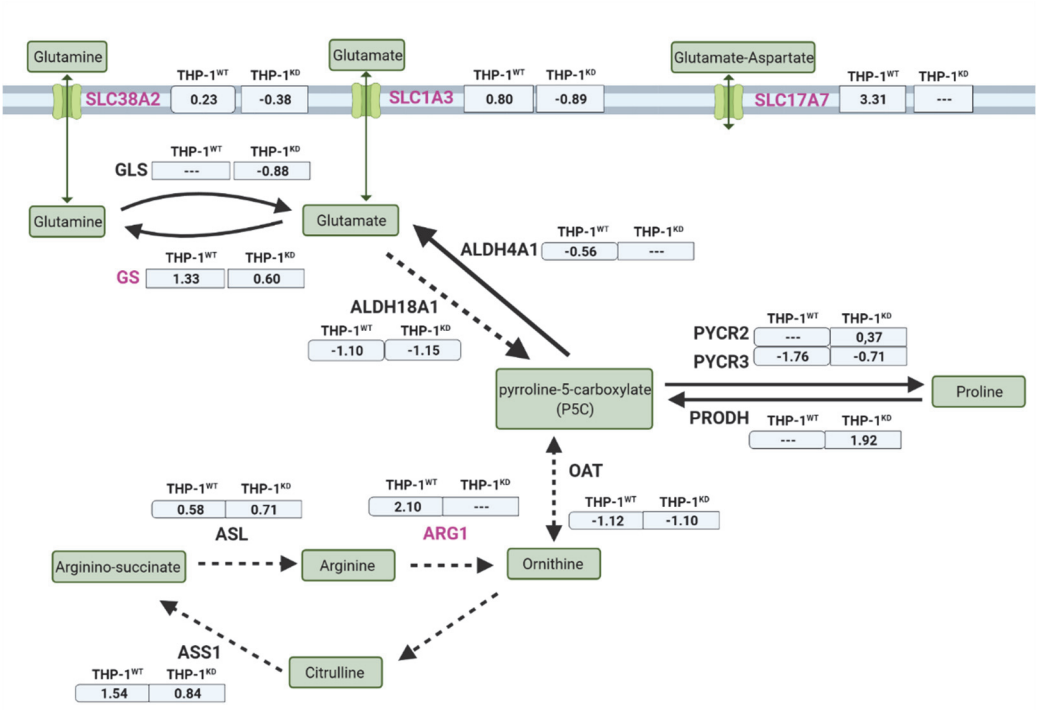

Figure 4.1.8- Gene expression alterations of key players in glutamine and glutamate metabolism and transport between THP-1^{WT} and THP-1^{KD} in hypoxia. Significant changing genes due to TKTL1 highlighted in pink. Expression changes of normoxia versus hypoxia, indicated in log2-Fold-change of n=3 samples per condition. Abbreviations: ALDH (aldehyde dehydrogenase family), ALDH4A1 (pyrroline-5-carboxylate dehydrogenase, mitochondrial), ALDH18A1 (pyrroline-5-carboxylate synthase), ARG1 (arginase 1), ASL (Argininosuccinate lyase), ASS1 (Argininosuccinate synthase 1), GLS (glutaminase), GS (glutamine synthetase), OAT (ornithine aminotransferase), PRODH (proline dehydrogenase), PYCR2 and 3 (pyrroline-5-carboxylate reductase 2 and 3), SLC (solute carrier family). Created with BioRender.com.

4.1.2.4 TKTL1 is essential to trigger hypoxia-induced changes in amino acids fate in THP-1 cells

Besides glutamine and glutamate, we also analysed and compared THP-1^{WT} and THP-1^{KD} consumption/production of additional amino acids in normoxic and hypoxic conditions. THP-1^{WT} produced more proline and ornithine in response to hypoxia than THP-1^{KD} (Figure 4.1.9). The observed dramatic increase in gene expression of PRODH (THP-1^{KD} Log2FC=1.92), that converts proline in pyrroline-5-carboxylate (5PC), and of ARG1 (THP-1^{WT} Log2FC= 2.10), that converts arginine into ornithine, is in accordance with the observed metabolite production differences between THP-1^{WT} and THP-$1^{KD.}$ (Figure 4.1.8). Moreover, in THP-1^{WT} we observed hypoxia inducing a slight decrease in the production of acetylornithine (Figure 4.1.10), an intermediate metabolite between glutamate and ornithine[230], which is consistent with a more active production of ornithine in the wildtype cells in hypoxia conditions. Interestingly we also observed a strong increase in the excretion of total asymmetric dimethylarginine (ADMA) in THP-1^{KD} cells (Figure 4.1.10) which is consistent with a strong overexpression of Arginine Methyltransferase 8 (PRMT8) (log2FC= 5.7). Worth to note that PRMP8 has been recently described as a key player in maintaining stress tolerance by ensuring proper ADMA levels[488].

Regarding BCAAs metabolism, we observed that hypoxia significantly reduced the consumption of isoleucine (Ile) and leucine (Leu) in similar extent in both THP-1^{WT} and THP-1^{KD} and with respect to Valine (Val) we observed that the decrease in cell consumption is only statistically significant in THP-1^{WT} (Figure 4.1.9B). To complete the characterization of the BCAAs metabolism, we further looked at the gene expression of key enzymes in the BCAAs catabolism and we obtained that the expression of BCAT1 and Branched-Chain Keto Acid Dehydrogenase B (BCKDHB)

genes decreased under hypoxia in both cell lines. The inhibition on the expression levels of these enzymes was around 1.6-fold higher in THP-1^{KD} than in THP-1^{WT} (Figure 4.1.11) which is consistent with the observed higher decrease in Ile and Leu consumption induced by hypoxia in THP-1^{KD}.

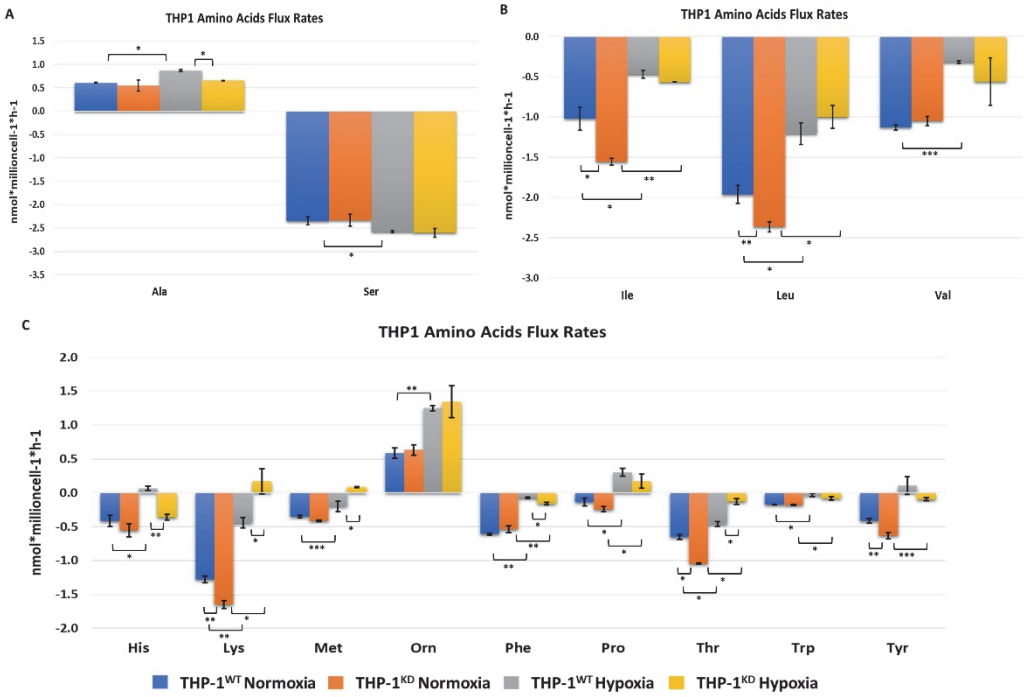

Figure 4.1.9- Flux rates of specific metabolites in extracellular media in normoxia and hypoxic conditions. (**A**) Alanine and Serine flux rates. (**B**) Branched-chain amino acids flux rates (Ile, Leu and Val). (**C**) Histidine, Lysine, Methionine, Ornithine, Phenylalanine, Proline, Threonine, Tryptophan and Tyrosine. Consumption and production rates obtained through Absolute 180 IQ Kit from Biocrates. Data represented is mean ± SD for n=3 reads of n=3 samples of a single experiment. Statistically significant differences were determined by two-tailed independent sample Student's t-test, with p-values of $p< 0.05$ (*), $p< 0.01$ (**) and $p<0.001$ (***).

SLC7A8, an antiport transporter that intakes BCAAs as well as other neutral amino acids (tyrosine, phenylalanine, tryptophan, methionine and glutamine) through obligatory exchange mechanism, as well as

SLC7A7[489], another antiport transporter that similarly exchanges neutral for cationic amino acids, were dramatically overexpressed in response to hypoxia only in THP-1^{WT} (Figure 4.1.11).

Methionine and Tyrosine consumption decreased under hypoxia, but the changes were statistically significant only in THP-1^{KD} cells. In the contrary, with respect to histidine, the decrease in consumption induced by hypoxia was significant only for THP-1^{WT}.

Lysine, threonine and phenylalanine consumption decreased significatively under hypoxia in both cell lines but the changes observed for lysine and threonine uptake were much larger in THP-1^{KD} (Figure 4.1.9C), whereas with respect to phenylalanine , the observed changes were larger in THP-1^{WT}. Worth to note that the consumption of α-aminoadipic acid (αAAA), a biogenic amine generated in the intermediate steps of the catabolism of lysine[291,296], decreased under hypoxia in both cell lines (Figure 4.1.10). But the observed decrease was lower for THP-1^{KD}, consuming significantly more αAAA in hypoxia when compared to THP-1^{WT}. In normoxia conditions there were no significant differences in αAAA consumption between the cell lines.

Tryptophan uptake was slightly decreased in both cell lines under hypoxia (Figure 4.1.9C). Tryptophan can be metabolized to kynurenine, with indoleamine 2,3-dioxygenase 2 (IDO2) being the rate limiting step of this pathway, or to serotonin through TPH1 and TPH2[204,321,323]. Both pathways produce biogenic amines and other active metabolic intermediates with signalling functions. Gene expression of IDO2 was strongly enhanced under hypoxia only in THP-1^{WT} which is consistent with a decreased consumption of kynurenine of these cells (Figure 4.1.10). On the contrary, kynurenine consumption was strongly enhanced under hypoxia in THP-1^{KD} cells which is consistent with the inability of the KD cells to enhance IDO2 in response to hypoxia.

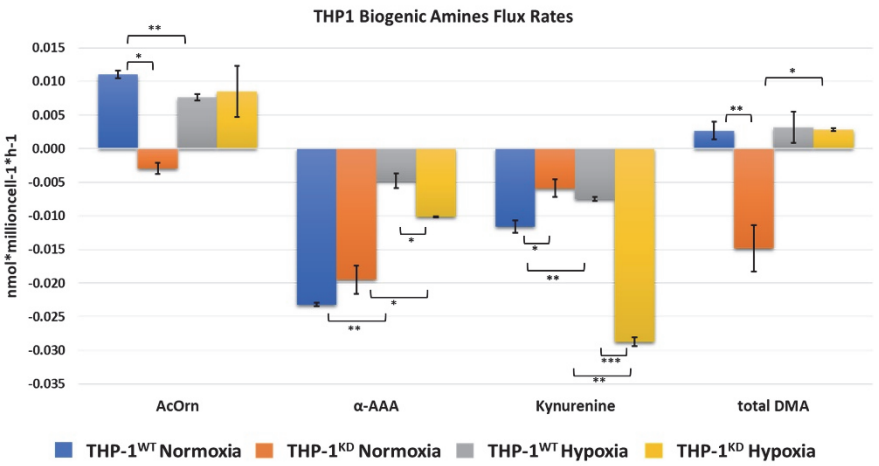

Figure 4.1.10- Flux rates of specific metabolites in extracellular media in normoxia and hypoxic conditions. Acetylornithine (AcOrn), alpha-aminoadipic acid (αAAA), kynurenine and total asymmetric dimethylarginine (total ADMA) flux rates. Consumption and production rates obtained through Absolute 180 IQ Kit from Biocrates. Data represented is mean ± SD for n=3 reads of n=3 samples of a single experiment. Statistically significant differences were determined by two-tailed independent sample Student's t-test, with p-values of $p< 0.05$ (*), $p< 0.01$ (**) and $p<0.001$ (***).

Serine consumption was also slightly enhanced in hypoxia in both cell lines, but the increase was only statistically significant in THP-1^{WT} which is in accordance with the observed bigger increase in PHGDH and SHMT2 gene expression in THP-1^{WT} (Figure 4.1.11).

Secretion of alanine was also enhanced under hypoxia but only for THP-1^{WT} (Figure 4.1.9A), which is consistent with the enhanced glucose and glutamine consumption observed previously with respect to THP-1^{KD}.

Lastly, we measured intracellular amino acid content to see if the alterations to amino acids efflux/consumption pattern observed for THP-1^{KD} under hypoxic conditions, resulted in different net-total amino acids content intracellularly. The THP-1^{WT} cells had three times less aspartate and five times more serine in hypoxia whereas these metabolites levels did not significantly change intracellularly under hypoxia in THP-1^{KD} cells (Appendix I Table 8.1-A). The observed THP-1^{WT} decrease of aspartate

intracellularly under hypoxia is consistent with the reported evidence across different tumours of the negative correlation between hypoxia and aspartate intracellular content[490].

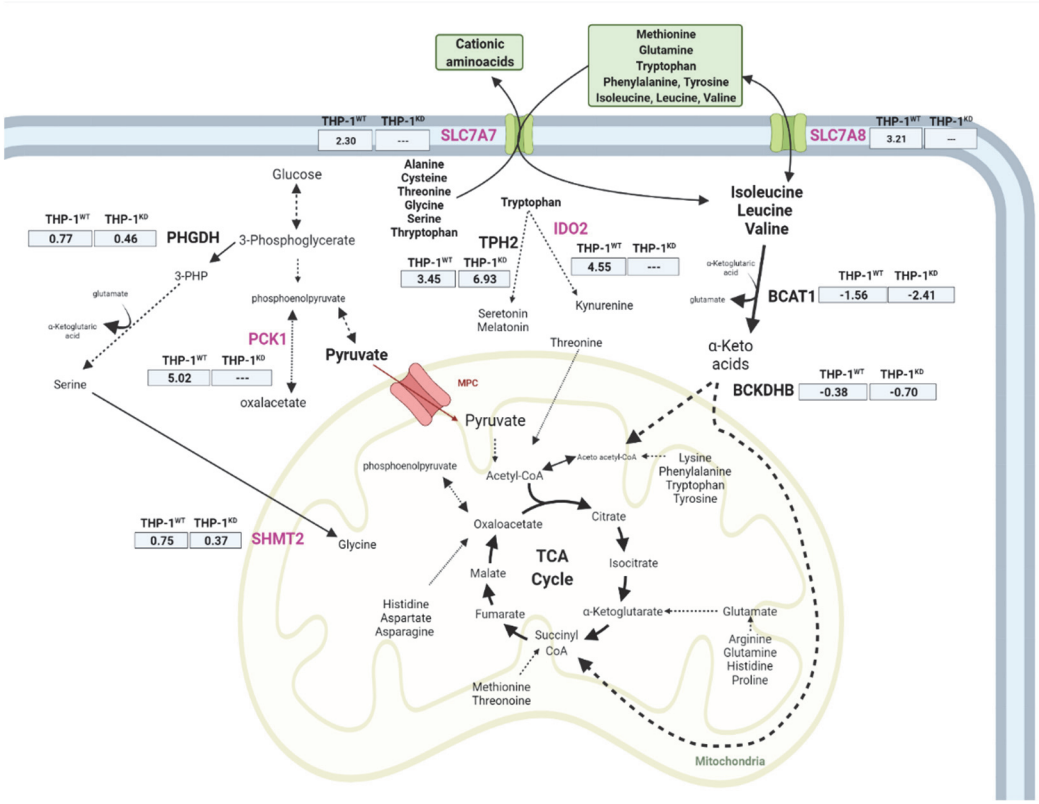

Figure 4.1.11- Gene expression changes of amino acids transport and catabolism between THP-1^{WT} and THP-1^{KD} in hypoxia. Significant changing genes due to TKTL1 highlighted in pink. Expression changes of normoxia versus hypoxia, indicated in log2-Fold-change of n=3 samples per condition. Abbreviations: BCAT1 (branched-chain amino acid transaminase 1), BCKDHB (branched-chain keto acid dehydrogenase B), IDO2 (indoleamine 2,3 dioxygenase 2), PCK1 (phosphoenolpyruvate carboxykinase 1), PHGDH (phosphoglycerate dehydrogenase), SHMT2 (serine hydroxymethyltransferase 2), SLC (solute carrier family), TPH2 (tryptophan hydroxylase 2). Created with BioRender.com.

The rise in intracellular serine content triggered by hypoxia in THP-1^{WT} together with the previously observed increase of serine consumption (Figure 4.1.9A) could be related with the use of this amino acid for pyrimidine synthesis and cell proliferation under hypoxia. In fact, it has

been described that serine synthesis through PHGDH is crucial to ensure appropriate nucleotide levels[491] and a similar effect through PCK1, a key player that drives pyrimidine biosynthesis under hypoxia[492]. Worth to note that PCK1 gene expression was dramatically increased (log2FC=5.0) under hypoxia in THP-1^{WT} whereas hypoxia did not trigger any statistically significant change in THP-1^{KD} (Figure 4.1.11).

The fact that we did not observe these changes in intracellular amino acids content in hypoxia in THP-1^{KD} corroborates the importance of TKTL1 in triggering the switch to enhanced glycolysis and consequent adaptation of amino acids metabolism to support such response. Overall, this new role of TKTL1, beyond its enzymatic function on the non-oxidative branch of the PPP unveiled in this study, opens new opportunities for the design of combined therapies targeting TKTL1 and exploiting the impaired adaptation of these cells to hypoxic stress.

4.2 Chapter II – Metabolic Characterization of TET2 loss of function in a CML cell model

4.2.1 Introduction

In the previous chapter we observed how TKTL1, an isoenzyme of TKT of the non-ox PPP plays a critical role on the switch to glycolysis and glutamine dependency of THP-1 cells to a severe hypoxia setting. Our results highlighted the need to investigate under hypoxic conditions the metabolic role of enzymes that are induced or silenced by the hypoxic response, to unveil new functions beyond the canonical enzymatic role as reaction catalysers.

In this chapter we investigated the role of TET2 in the metabolic adaptation of leukaemia cells to hypoxia. Leukemogenesis arises from many distinct mutations during the haematopoietic process. One of the most prevalent across multiple types of leukaemia is TET2, an epigenetic eraser that is involved in gene expression processes during haematopoietic differentiation (see section 1.1.5.2) and whose activity is proven to be directly influenced by metabolites of the TCA Cycle[200,493]. Moreover, it has been widely demonstrated that hypoxia-induces TET2 loss of activity[494].

Here, taking into account that TET2 activity depends on α-ketoglutarate (αKG) as cofactor and that succinate and fumarate affect TET function by binding site competition, we questioned if the well documented loss of TET activity induced by hypoxia will impact cell metabolism, providing an advantage in metabolic adaptation to hypoxia.

To perform a proof of concept on the impact of the loss of TET2 activity on metabolic adaptation triggered by hypoxia we chose the dual cell lines model HAP1-Wild Type (Parental) and HAP1-TET2 knockout (TET2 KO). The HAP1 cell line is a near-haploid cell line, created from a KBM7 Male Chronic Myelogenous Leukaemia. It has lost most chromosome pairs, except for chromosome 8 and 15. Given this near-haploid nature, it is an

excellent CML cell line for genetic studies, with any mutation or genetic abnormality manifesting as phenotype[495–497]. It was chosen for that characteristic as the cell model to study the metabolic effects of having a simulated loss-of-function mutation in TET2 (see section 3.1). This is because most mutations of TET2 occur in only one allele and it is enough to stop TET2 activity overall.

4.2.2 Results

4.2.2.1 TET2 loss does not affect cell growth or glycolytic dependency

The first step in the characterization of the HAP1 cell lines was to attest how the knockout of TET2 was affecting cell growth, in both normoxia and hypoxia (Figure 4.2.1A). When comparing to the Parental cells, the knock-out cells maintain a similar proliferation in both normoxia and hypoxia, with no significant differences arising. The similarity in cell numbers also translates into protein content, with the only change being due to hypoxia switch (Figure 4.2.1B).

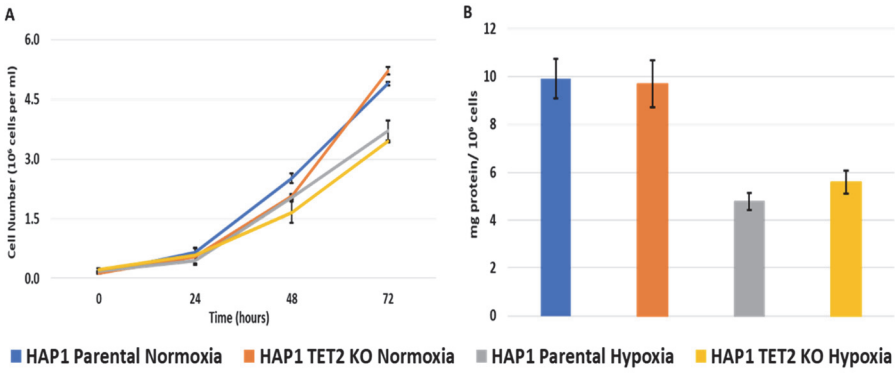

Figure 4.2.1- Effect of TET2 Knockout on Proliferation. Growth curves from 0 to 72h, in normoxia and hypoxia (A). Duplication times (hours) are: Parental Normoxia=25 ± 3.5; TET2 KO Normoxia=25 ± 3.4; Parental Hypoxia=22 ± 1.3 and TET2 KO Hypoxia=26 ± 0.5. Data shown as mean ± SD for n=2 reads of n=2 experiments. (B) Cell protein content of HAP1 Parental and TET2 Knockout under normoxia and hypoxia.

Next, we verify if in spite the similarities in duplication time, the loss of TET2 would translate into differences in cellular metabolic dependency on glucose/glutamine metabolism (Figure 4.2.2). First, we measured glucose consumption and lactate production in both HAP1 Parental and HAP1 TET2 KO cell lines incubated under either normoxic or hypoxic conditions. The consumption of glucose of TET2 KO was the same in normoxia than in hypoxia whereas Parental cells consume less glucose than TET2 KO cells but increase glucose consumption in response to hypoxia up to the same levels observed in Parental cells. (Figure 4.2.2A). The trend of glucose consumption is mirrored in the lactate production (Figure 4.2.2B).

Interestingly, the lactate produced per glucose consumed ratio (ratio lactate/glucose) obtained for each cell line under the different incubation conditions (normoxia or hypoxia) is around 2 which indicates that both cell lines rely strongly in direct cell glucose intake into lactate production even in normoxia conditions (Figure 4.2.2C).

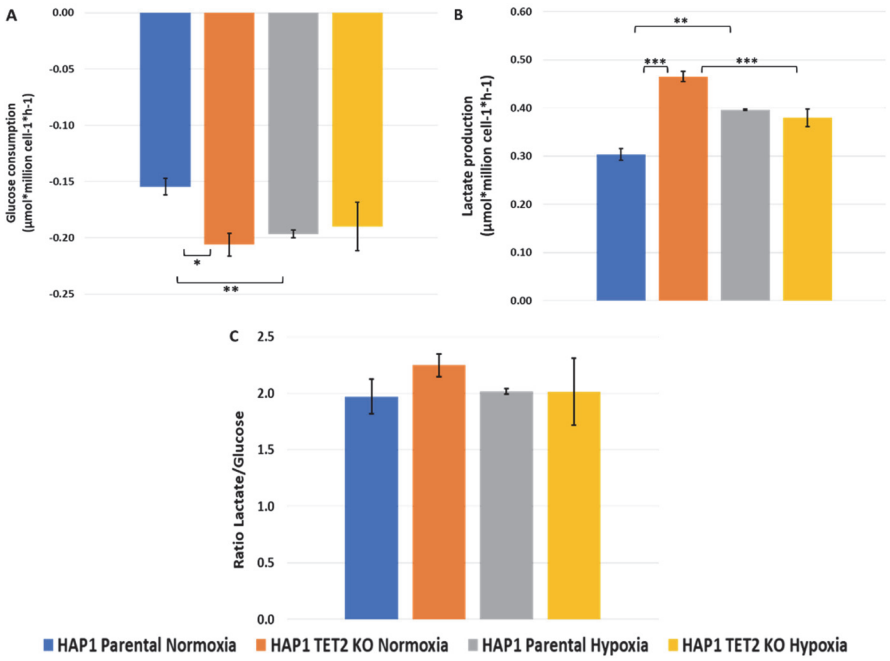

Figure 4.2.2- Loss of TET2 impact on Glucose and Lactate Metabolism. Consumption and production rates of glucose and lactate were determined after 48h incubation, in both normoxia and hypoxia conditions, as described in section 3.3. (A) Glucose consumption. (B) Lactate production. (C) Ratio of lactate produced per glucose consumed (Lac/Glc), determined by dividing the glucose consumption flux rate by lactate production flux rate. Data represented is mean ± SD of n=3 reads of a representative experiment per condition. Statistically significant differences in all panels was determined by two-tailed independent sample Student's t-test: $p<0.05$ (*), $p<0.01$ (**), and $p<0.001$ (***).

Given it has been widely described that HK, GAPDH, PK and LDH are involved in the metabolic response to hypoxia of different cancer cells, we attested if the absence of TET2 would affect the total enzyme activities of these key glycolytic enzymes (Figure 4.2.3). We obtained an increase of activity levels of HK, GAPDH and PK, in response to the hypoxia challenge that was more pronounced in the Parental cell line (Figure 4.2.3A, B and C) which is in accordance with the increase in glucose intake observed in Parental cell line in response to hypoxia (see Figure 4.2.2A).

Altogether, the increase on glucose consumption and the more dramatic increase in HK, GAPDH and PK observed in Parental cells suggest that

glucose-6-phosphate rerouting to pentose-phosphate pathway (PPP), operating as a cycle to generate NADPH, can be higher in Parental cells than in TET2 KO cells.

Worth to note that lactate dehydrogenase activity increase significantly under hypoxia in TET2 KO cells in spite there is not a net increase in the lactate production nor in the lactate/glucose ratio which is indicative of a different metabolic reprogramming due to the loss of TET2 (Figure 4.2.3D) suggesting the possibility that part of the lactate generated in the cytosol, either from glucose or from other sources, is recycled back into pyruvate.

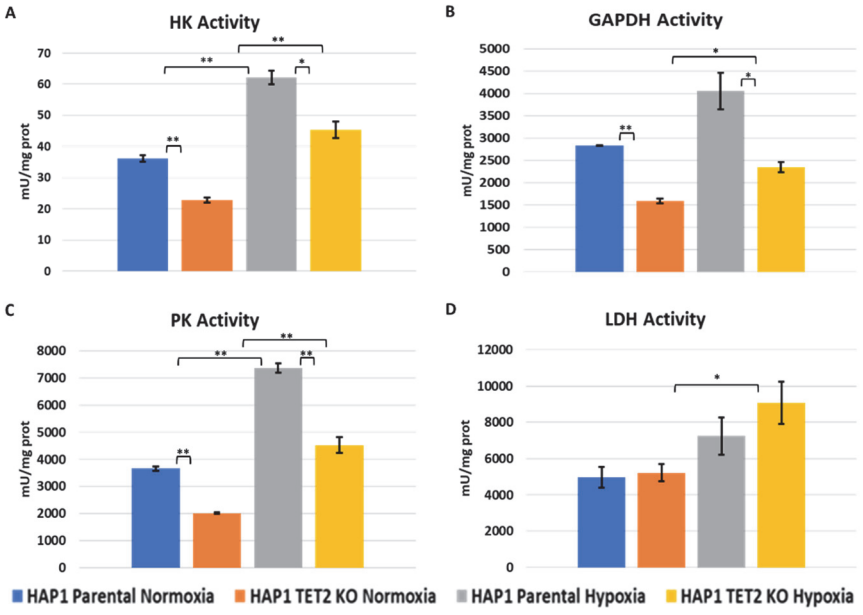

Figure 4.2.3- Impact of loss of TET2 on activity of glycolytic enzymes. Enzymatic Activity Assays performed through spectrophotometry in normoxia and hypoxia for enzymes: (A) Hexokinase (HK), (B) Glyceraldehyde-3-phophate Dehydrogenase (GAPDH), (C) Pyruvate Kinase (PK) and (D) Lactate Dehydrogenase (LDH). Data represented is mean ± SD for n=2 reads of n=2 independent experiments. Statistically significant differences in all panels was determined by two-tailed independent sample Student's t-test: $p<0.05$ (*), $p<0.01$ (**), $p<0.001$ (***).

To investigate more in depth if the differences in TET2 KO cells adaption to hypoxia can be due a different turnover of lactate and ribose pools, we

performed a further characterization using ^{13}C-based metabolomics techniques.

To further explore glucose and lactate metabolism differences in Parental and TET2 KO cells, we incubated the cells with media containing U-^{13}C-glucose and subsequently analysed the incorporation of ^{13}C into pyruvate and lactate using ^{13}C-based metabolomics techniques, under normoxia and hypoxia conditions. In brief, labelling contribution from glucose to pyruvate and lactate was analysed both intra- and extracellularly, using GCMS and NMR (methods in sections 3.10.1 and 3.10.2, respectively) taking into account that metabolism of U-^{13}C-glucose through glycolysis results in U-^{13}C-pyruvate (pyruvate m3) and subsequent conversion of U-^{13}C-pyruvate through LDH reaction results in U-^{13}C-lactate (lactate m3).The obtained ^{13}C-label distributions for both metabolites showed a pattern of higher incorporation of ^{13}C when TET2 is lost, in both normoxia and hypoxia (see Figure 4.2.4).Since intracellular PK activity and extracellular lactate excretion are lower but LDH is higher in TET2 KO cells under hypoxia when comparing to Parental cells, the obtained labelling profile is indicative of a higher recycling of intracellular lactate-pyruvate in TET2 KO cells.

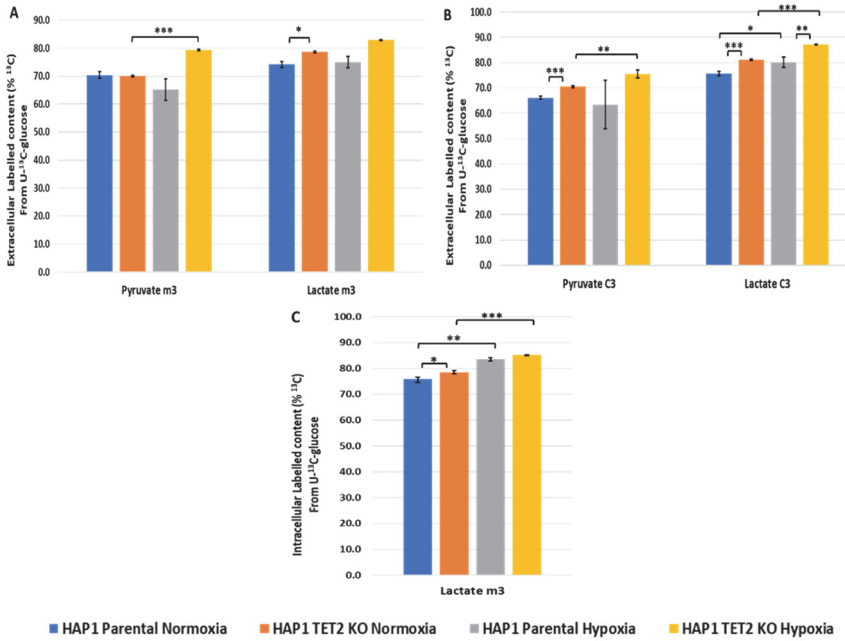

Figure 4.2.4- ^{13}C-Labelling of Pyruvate and Lactate in HAP1 Parental and HAP1 TET2 KO cells incubated with U-^{13}C-glucose. Measurement of ^{13}C-labeled glucose contribution to ^{13}C labelled pyruvate and lactate after 24h incubation with 22,5mM U-^{13}C-glucose. (A) GCMS analysis of labelled extracellular Pyruvate and Lactate from media. m3 indicates that the metabolite is ^{13}C uniformly labelled. Data represented is mean ± SD for n=2 reads of n=3 samples of a single experiment. (B) ^{13}C-filtered ^{1}H-NMR spectroscopy analysis of labelled extracellular Pyruvate and Lactate. C3 refers to the carbon in position 3. Data represented is mean ± SD for n=1 reads of n=3 samples of a single experiment. (C) GCMS analysis of labelled intracellular Lactate. Data represented is mean ± SD for n=2 reads of n=3 samples of a single experiment. Statistically significant differences in all panels were determined by two-tailed independent sample Student's t-test: $p< 0.05$ (*), $p< 0.01$ (**) and $p<0.001$ (***).

4.2.2.2 TET2 loss affects use of G6P and flux of Pentose Phosphate Pathway

Parallel to glycolysis and using its first product G6P is the Pentose Phosphate Pathway. G6PD is the first enzyme and the rate-limiting reaction of the oxidative branch of PPP and it has been recently described that G6PD activity could play a key role in DNA methylation[498], beyond its canonical role in ox-PPP. In brief, it has been recently reported that G6PD inhibition

in hypoxic conditions resulted in αKG increase and SAM (a substrate for methylation reactions, see section 1.2.1) decrease playing a key role in regulating substrates for DNA methylation. To assess if TET2 knockout impacts ox-PPP either in normoxia or hypoxia, we next characterized the total enzyme activities of G6PD and 6PGD (a following enzyme in the ox-PPP). The results obtained showed that G6PD activity is dramatically decreased by the loss of TET2, in both normoxia and hypoxia whereas the following dehydrogenase of the ox-PPP only slightly increases when switching to hypoxia in TET2 KO cells (Figure 4.2.5B). Such impact of TET2 knockdown on G6PD activity could be related with the recently unveiled putative role of G6PD in regulating substrates for DNA methylation[498] and will deserve further studies beyond the scope of the present work.

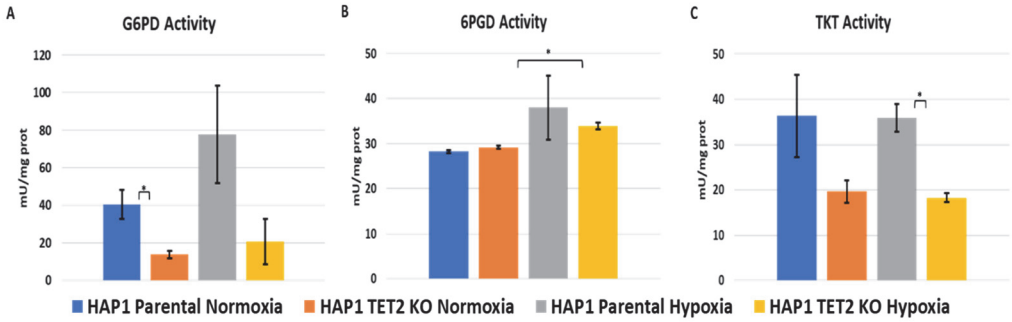

Figure 4.2.5- Decrease of key enzymatic activities of PPP due to loss of TET2. Enzymatic Activity Assays performed through spectrophotometry in normoxia and hypoxia for enzymes: (A) Glucose-6-phosphate Dehydrogenase (G6PD), (B) 6-phosphogluconate Dehydrogenase (6PGD) and (C) Transketolase (TKT). Data represented is mean ± SD for n=2 reads of n=2 independent experiments. Statistically significant differences in all panels was determined by two-tailed independent sample Student's t-test: $p<0.05$ (*), $p<0.01$ (**), $p<0.001$ (***).

To also assess the impact of TET2 silencing on non-ox-PPP, we next analysed global TKT enzyme activity (Figure 4.2.5C) and found that whereas hypoxia did not significantly alter TKT activity levels, knockout of TET2 caused a 35% reduction in total TKT activity. The observed result

is in accordance with the fact that loss of TET2 results in higher degrees of DNA methylation[499] and with the reported increase of TKT expression as a result of its promoter hypomethylation identified in hepatocellular carcinoma[500]. Worth to note that the fact that in Parental cells we observed a hypoxia-triggered increase in G6PD, which is in accordance with the observed increase on glucose consumption that prompt us to hypothesize a higher activity of PPP operating as a cycle. Thus the higher activity in hypoxia of G6PD, which is the key enzyme controlling PPP flux[162–164], will result in an increased rerouting of glucose-6-phosphate through oxidative branch of PPP that will render NADPH and pentose-phosphate with the loss of one CO_2 from each glucose that enters the pathway. The excess of pentose-phosphate generated will return back to glycolytic intermediate metabolites, through non-oxidative PPP contributing to maintain the glucose/lactate optimal balance in hypoxia in Parental cells.

Next, through ^{13}C-based metabolomics experiments in which we incubate the Parental and TET2 KO cells with U-^{13}C-glucose (methods in section 3.10), we investigated how the G6P substrate was traveling from glycolysis to ribose pools or to other pathways. At the level of total ^{13}C-label incorporation in ribose, we observed that TET KO cells display a lower percentage of ^{13}C-labelled ribose both in normoxia and hypoxia conditions (Figure 4.2.6A), which is indicative of a lower turnover of the ribose pool and is in accordance with the lower G6PD and TKT activities reported in TET2 KO cells. Moreover, both cell lines display a decrease in ^{13}C-labelled ribose intracellular content in response to hypoxia challenge being more pronounced for TET2 KO cells than for Parental cells (Figure 4.2.6C). Altogether these results demonstrated that either in normoxia or in hypoxia conditions, TET2 KO appears to impact PPP at both the levels of total G6PD and TKT activities and the turnover of intracellular ribose metabolite pool.

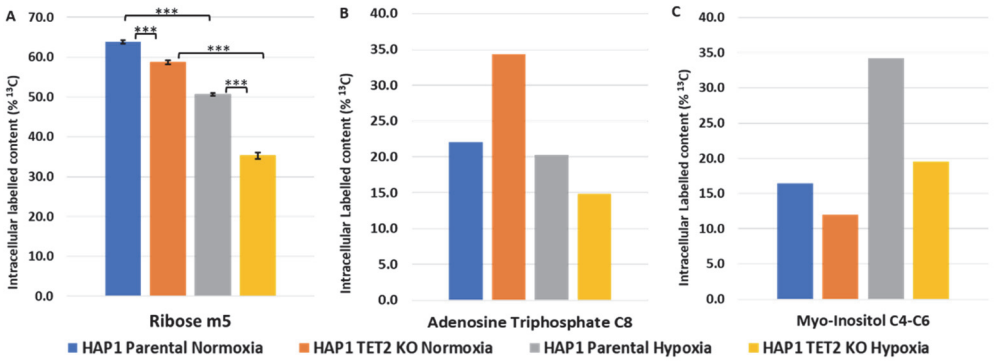

Figure 4.2.6- Loss of TET2 influences different use of PPP substrates. Measurement of glucose contribution to Myo-inositol, Adenosine Triphosphate (ATP) and Ribose after 24h incubation with 22,5mM U-^{13}C-glucose. (A) GCMS analysis of labelled intracellular Ribose m5. Data represented is mean ± SD for n=2 reads of n=3 samples of a single experiment. Statistically significant differences were determined by two-tailed independent sample Student's t-test: $p< 0.05$ (*), $p< 0.01$ (**) and $p<0.001$ (***). (B) ^{1}H-^{13}C-HSQC NMR spectroscopy analysis of labelled intracellular ATP C8 and Myo-Inositol C4-C6 (C). ^{13}C percentages were calculated as a ratio of the labelled and unlabelled sample and multiplied by the natural abundance of ^{13}C (1.1%). Data represented is n=1 read of n=1 sample of a single experiment. Statistical analysis could not be applied due to insufficient replicates.

Through NMR-based techniques, also using U-^{13}C-glucose as a tracer, we also quantified the labelling of ATP (labelling in carbon C8 - one of the carbons of the ribose ring). Results showed that in normoxia TET2 KO cells display a higher percentage of ^{13}C-labelling in C8 of ATP molecule in (34.3%) than Parental cells (22%) (Figure 4.2.6B). By contrary, under hypoxic conditions we observed a strong decrease in ^{13}C-labelling in TET2 KO cells (14.9% of ATP C8) whereas Parental cells maintain a similar percentage of ^{13}C labelling that in normoxia (20.3% of ATP C8) (Figure 4.2.6B). The observed changes are also indicative of an altered ribose pool turnover in TET2 cells and evidenced that TET2 KO impact the metabolic reprogramming triggered by hypoxia through altered PPP enzyme activities that result in an altered ribose-phosphate pool turnover.

Through NMR-based techniques, also using U-^{13}C-glucose as a tracer, we identified also an increased ^{13}C-labelling of Myo-Inositol, only in Parental cells in response to hypoxia (Figure 4.2.6C). Myo-Inositol is an important metabolite for the synthesis of cell signalling molecules (such as Phosphatidylinositol Phosphates, known as PI3P) and many nuclear functions, such as chromatin remodelling, gene transcription and DNA repair of double-strand breaks[501–504].The fact that we see less labelling of this important precursor of Phosphatidylinositol Phosphates synthesis is indicative of an altered response to hypoxia of TET2 KO cells.

4.2.2.3 TET2 loss affects ROS homeostasis

Less G6PD activity directly affects the redox capacity of the cell, through less NADPH production and less reduction of GSSG. This in turn affects the detoxification of reactive oxygen species (ROS).

As such, we checked the ROS levels that showed lower levels on TET2 KO cells in normoxia (Figure 4.2.7). When switching to hypoxia, a rise of ROS levels is expected but the loss of TET2 leads to levels far above the Parental cell line.

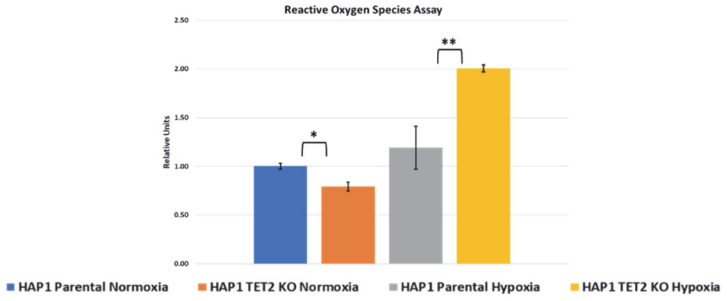

Figure 4.2.7- Loss of TET2 leads to increase of ROS levels. Flow cytometry gate count used was 5000 cells. Data represented is mean ± SD for n=5 samples of n=2 experiments. Statistically significant differences were determined by two-tailed independent sample Student's t-test, with p-values of $p< 0.05$ (*) and $p< 0.01$ (**).

Investigations if this ROS production arises from mitochondrial activity showed that the hypoxia switch drives a similar decrease of oxygen consumption rates (OCR) (Figure 4.2.8A). This is a result of the scarceness of oxygen in this condition, regardless of the TET2 status of the cells.

As for the extracellular acidification rates (ECAR) from glycolytic activity and other non-glycolytic phenomenon, there was no significant change from the absence of TET2, only the influence of the hypoxic setting (Figure 4.2.8B).

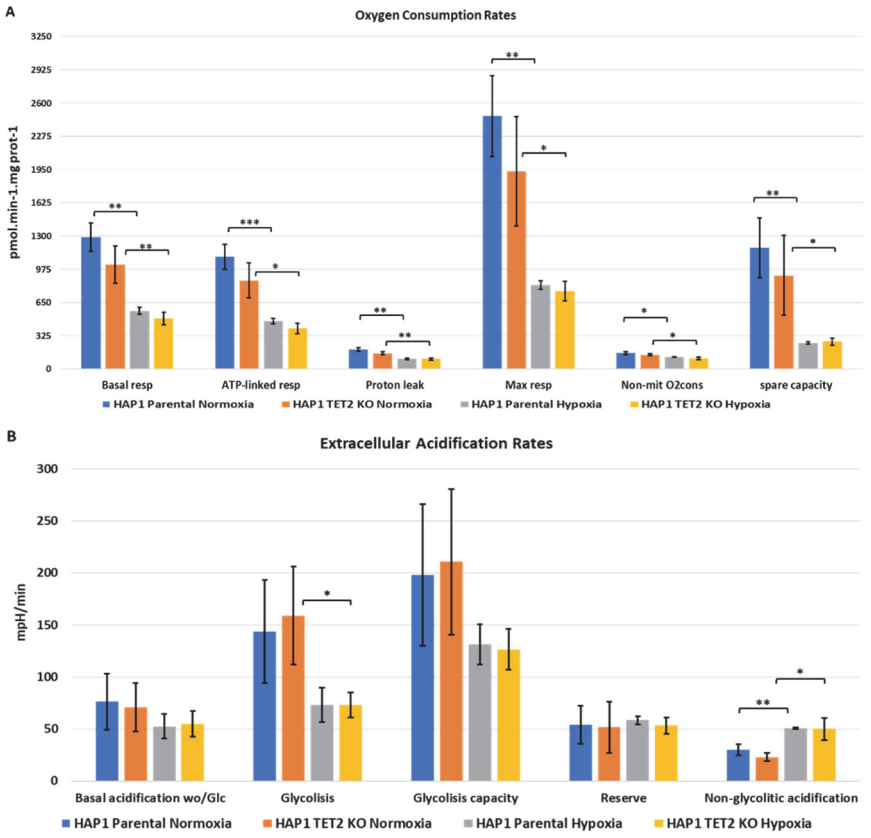

Figure 4.2.8- Loss of TET2 effects over Mitochondrial Activity. Seahorse assays performed using Seahorse XFe24, under Cell Mito Stress Assay and Glycolytic Rate Assay stablished protocol (Agilent ©). Oxygen Consumption Rate (OCR) assay (A), Extracellular Acidification Rate (ECAR) assay (B). Data represented is mean ± SD for n=5 reads of n=3 experiments. Statistically significant differences were determined by two-tailed independent sample Student's t-test, with p-values of $p< 0.05$ (*), $p< 0.01$ (**) and $p<0.001$ (***).

As for the extracellular acidification rates (ECAR) from glycolytic activity and other non-glycolytic phenomenon, there was no significant change from the absence of TET2, only the influence of the hypoxic setting (Figure 4.2.8B).

Next, the Crabtree Effect was quantified from the measurement of the OCR decrease after glucose addition (see section 3.7.3). At the timepoint of glycolysis injection (ΔOCR), we observe a significant difference between the cell lines, indicating that the lack of TET2 results in a partial loss of Crabtree effect in HAP1 cells (Figure 4.2.9). This result showed that HAP1 Parental cells have a higher preference for glycolysis and present lower mitochondrial respiration dependency than HAP1 TET2 KO cells in normoxia. The switch to hypoxia abolishes this difference, indicating that the hypoxia condition resulted in an adaptation to glycolysis that renders TET2 KO cells response to glucose addition similar to Parental cells.

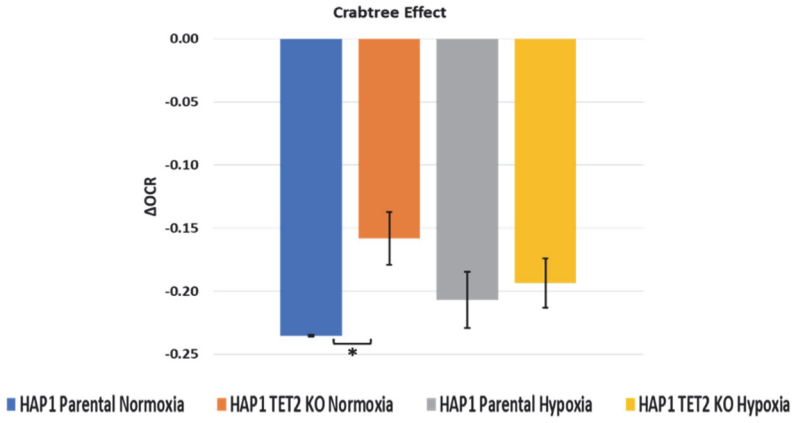

Figure 4.2.9- The Crabtree Effect on HAP1 cell lines. OCR rates measured for both cell lines under normoxia and hypoxia. Data represented is mean ± SD of n=3 experiments. Significance was determined by two-tailed independent sample Student's test, with significance threshold at $p<0.05$ (*).

The similarity of the mitochondrial parameters measured for both cell lines in hypoxia (Figure 4.2.8) let us to conclude that the increase of ROS levels observed in TET2 KO cells (Figure 4.2.7) could be due to the observed

decrease on G6PD total activity of these cells in hypoxia. The fact that TKT activity was also decreased as well as the percentages of ^{13}C enrichment in ribose reinforce this hypothesis as is indicative of a lower activity of ox-PPP and non-ox-PPP pathways acting as a cycle to generate NADPH. Altogether, the totality of the metabolic characterization results shows that the loss of TET2 is clearly driving the cells to manifest a different metabolism, with proliferation and energy production pathways affected, especially in hypoxia.

4.2.2.4 TET2 loss alters the entry point of pyruvate into TCA cycle

With the previous results indicating changes to mitochondrial activity and anaerobic glycolysis in hypoxia, we used tracer-based metabolomics to attest the transition of pyruvate after glycolysis into the TCA cycle. Said entry can be through the PDH complex, where pyruvate is broken down to acetyl-CoA. Another point of entry is through PC reaction, that converts pyruvate into OAA at the cost of ATP. Both paths converge in the formation of citrate, given that CS uses both acetyl-CoA and OAA to produce citrate. The routes of how labelled carbons from glucose can travel across one turn of the TCA cycle is represented in Figure 4.2.10.

Analysis of the isotopologues of citrate from the glucose source fed to the cells shows significant changes to citrate m2, m3, m4 and m5 (Figure 4.2.11 A). Citrate m2, which is the most produced labelled isotopologue and results from labelled pyruvate entering TCA cycle though PDH path, and Citrate m5 isotopologue, that results from condensation of labelled OAA and labelled acetyl-CoA, displayed the same percentage of occurrence in both Parental and TET2 KO cell lines under normoxia. Interestingly, under hypoxia challenge, citrate m2 decreases significantly only in TET2 KO cells, which is indicative of a decrease of PDH activity under hypoxia of TET2 KO cells. By contrary, citrate m5 increases in TET2 KO cells and decreases in Parental cells under hypoxia. Taking into account that citrate

m5 results from the condensation of acetyl-CoA m2 with OAA m3 (formed from carboxylation of pyruvate m3 catalysed by PC), the citrate m5 pattern obtained is indicative of a higher activity of pyruvate carboxylase in TET2 KO cells in response to hypoxia challenge. In the same line, citrate m3 results from the condensation of OAA m3 with an unlabelled acetyl-CoA, obtained from fatty acid metabolism.

Citrate m4, that can be formed in a second turn of TCA cycle either from condensation of OAA m2 with acetyl-CoA m2 or by condensation of OAA m4 with acetyl-CoA m2, increases under the hypoxia challenge in TET2 KO cells and decrease in Parental cells which is indicative of a higher TCA cycle turnover in TET2 KO cells under hypoxia fuelled by pyruvate carboxylase.

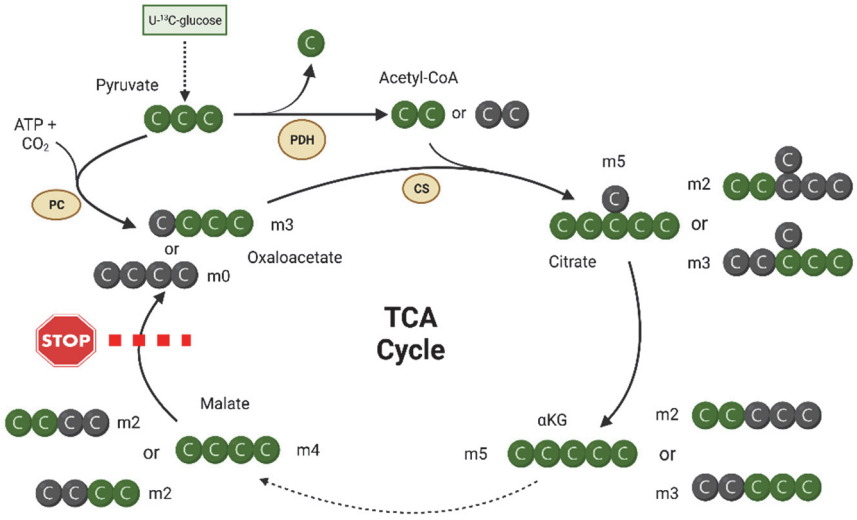

Figure 4.2.10- Scheme of labelling patterns expected in TCA cycle from U-^{13}C-Glucose. Uniformly labelled glucose is converted into fully labelled pyruvate through glycolysis. Said pyruvate can then enter the TCA cycle via pyruvate dehydrogenase (PDH) or via pyruvate carboxylase (PC). In brief, the resulting oxaloacetate and acetyl-CoA is then used by citrate synthase (CS) to generate distinct isotopologues of citrate. Subsequent label patterns travel through α-ketoglutarate (αKG), succinate, fumarate and end up at malate (defined as the stop point of one lop of the cycle). Created with BioRender.com.

Corroborating the citrate labelling profile is the malate isotopologues pattern, given that malate can inherit both the labelling from citrate in the normal turn of the TCA cycle or from the cytosolic conversion from OAA. The significant changes observed were to malate m2, m3 and m4 (Figure 4.2.11B). Thus, consistent with the increase of labelling in citrate under the hypoxic challenge observed in TET2 KO cells, we see also an increase of labelling in malate in this cell line.

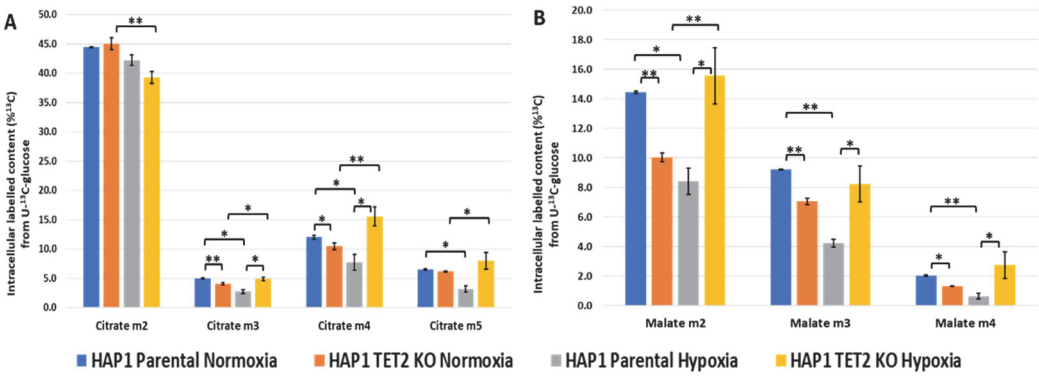

C

U-^{13}C-glucose	Citrate			Malate
Ratios of mZ/ΣM	m2 vs. m3+m5	m3 vs. m5	m4 vs m2	m2 vs. m3+m4
Parental Normoxia	3.86	0.77	0.27	1.28
TET2 KO Normoxia	4.41	0.66	0.23	1.20
Parental Hypoxia	7.19	0.87	0.18	1.73
TET2 KO Hypoxia	3.08	0.62	0.40	1.43

Figure 4.2.11- GCMS analysis of labelled intracellular Citrate and Malate from U-^{13}C-glucose (only 1st turn). Measurement of glucose contributions (% labelled) to intracellular metabolites after 24h incubation with 22,5 mM U-^{13}C-glucose. (A) Represented contribution of glucose to Citrate m2, m3, m4 and m5. (B) Represented contribution of glucose to Malate m2, m3 and m4. Representing labelled isotopologues above 2% labelling and with significant changes. Data represented is mean ± SD for n=3 reads of n=3 samples of a single experiment. Statistically significant differences were determined by two-tailed independent sample Student's t-test, with p-values of $p< 0.05$ (*), $p< 0.01$ (**) and $p<0.001$ (***). (C) Ratios of labelled isotopologues from citrate and malate, from the same experiment represented in A and B. Calculations of PDH activity versus PC activity (m2 vs m3+m5 of citrate; m2 vs m3+m4 of malate); of TCA cycle velocity (m4 vs m2 of citrate) and of β-oxidation contribution of acetyl-CoA (m3 vs m5 of citrate).

Next, we verified the ratios of labelled citrate and malate with the U-^{13}C-glucose tracer to highlight how much the loss of TET2 was influencing

multiple parameters (Figure 4.2.11C). Using the percentage of labelled isotopologues (mZ) per the total labelling occurring in each sample (ΣM), we compared the amount of citrate m2 (from PDH path) versus citrate m3 and m5 (that require OAA made through PC). In normoxia, the contribution of PC and PDH to the TCA cycle is similar in both cell lines (Figure 4.2.11C). But in the hypoxic condition, the Parental cells increase the PDH activity while the TET2 KO sees this ratio decrease, indicating less PDH and more PC activity. Similar ratio calculations using the malate labelling corroborates this tendency of higher PC activity with the loss of TET2 (Figure 4.2.11C).

Another point that confirms the shift in the production of citrate is the contribution of acetyl-CoA from β-oxidation (i.e. unlabelled carbons). This ratio (m3 vs m5 of citrate) shows that in hypoxia the Parental has more entry of acetyl-CoA from β-oxidation while the TET2 KO cells do not change between conditions. This indicates less contribution of fatty acid metabolism to TCA cycle activity in TET2 KO cells in hypoxia.

Lastly, we can also determine how "fast" the TCA cycle reactions are occurring in regard to the absence of TET2. Again, there are equal behaviours between the cell lines in normoxia but in hypoxia, the Parental cells slow down their TCA activity while the cells without TET2 actually increase it. All these results show that the loss of TET2 is altering the mitochondrial activity, increasing the TCA cycle reactions in hypoxic conditions.

4.2.2.5 TET2 loss impairs the hypoxia-triggered switch to reductive carboxylation of glutamine

Glutamine is a non-essential amino acid in normal cells but found to be essential for cancer cells, especially in hypoxic conditions. Given this fact, we inquired how the loss of TET2 would affect the glutamine metabolism.

Measurements of glutamine consumption and glutamate production through spectrophotometry-based methods (see section 3.3) indicated that the hypoxic condition induces a major alteration to these processes (Figure 4.2.12).

Glutamate secretion is slightly higher in cells without TET2 in normoxia and when switching to hypoxia both cell lines increase glutamate production (Figure 4.2.12A).

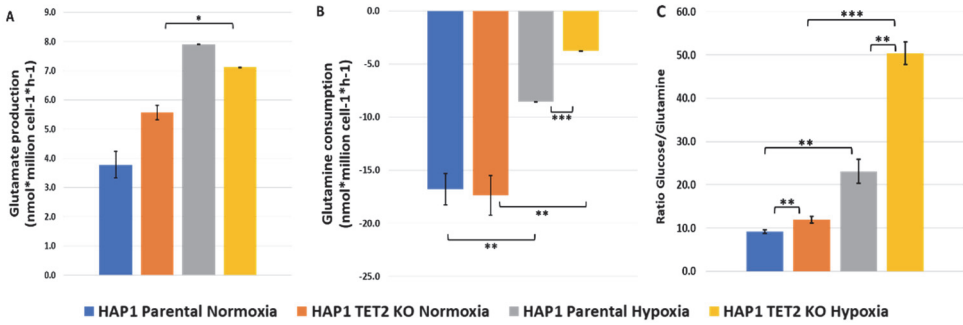

Figure 4.2.12- Loss of TET2 impact on glutamine metabolism. Consumptions and production rates measurements through spectrophotometry from cell culture media after 48h incubation, in both normoxia and hypoxia conditions. (A) Glutamate production and (B) Glutamine consumption and production. (C) Ratio of glucose consumed versus glutamine consumed. Data represented by mean ± SD of n=3 reads of a representative experiment per normoxia and hypoxia. Statistically significant differences in all panels was determined by two-tailed independent sample Student's t-test: $p<0.05$ (*), $p<0.01$ (**), $p<0.001$ (***).

Net glutamine consumption/production is similar between the cell lines in normoxia, (Figure 4.2.12B). with both cell lines consuming much less glutamine than glucose (Figure 4.2.12B-C). In the hypoxia setting, the metabolic adaptation leads to a decreased consumption of glutamine. This decrease is more accentuated in the TET2 KO cells, this indicates that the loss of TET2 could result in a different glutamine metabolism in response to hypoxia in the TET2 KO cells.

This is further evidenced by the ratios of glucose consumption versus glutamine consumption (Figure 4.2.12C) that display a higher increase under hypoxia in TET2 KO cells.

To further investigate cell glutamine dependencies in due to TET2 knockout, we analysed the labelling profile of the metabolites involved in glutaminolysis, using tracer-based metabolomics.

For this purpose, we incubated Parental and TET2 KO cells in parallel biochemical equivalent experiments, with either 22.5 mM U-^{13}C-glucose and unlabelled 4 mM glutamine or with 4 mM U-^{13}C-glutamine and unlabelled 22.5 mM glucose, followed by isotopologue distribution GCMS-based analysis (see section 3.10.1).

The route of incorporation of ^{13}C label into αKG, from U-^{13}C-glucose source has already been depicted in Figure 4.2.10 and the conversion of the ^{13}C-labelled αKG into glutamate and glutamine is catalysed respectively by glutamate dehydrogenase (reversible reaction) and glutamine synthetase. The routes of how isotopologues of glutamate and TCA cycle intermediates originated from the U-^{13}C-glutamine source of labelled carbons are depicted in Figure 4.2.13A. In brief the ^{13}C-label from glutamine can be directly incorporated into glutamate through glutaminase (or through transamination reactions) and into αKG through glutamate dehydrogenase reaction. Next, αKG can enter TCA cycle and be converted into citrate after one turn of the cycle or, alternatively, can follow the reductive carboxylation pathway and be converted into citrate through a reverse IDH reaction. Reductive carboxylation can occur either in cytosol or in the mitochondria and has been described to occur mainly in hypoxic conditions or in cells with defective mitochondria[195].

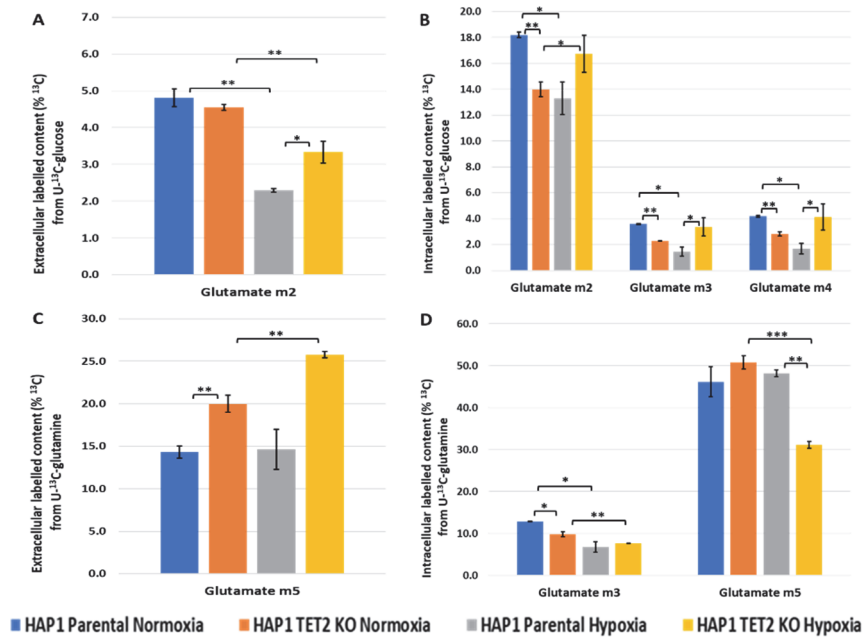

Figure 4.2.13- GCMS analysis of Glutamate isotopologues. Measurement of glucose contribution (% ^{13}C labelled) to extracellular glutamate after 24h incubation with 22.5 mM U-^{13}C-glucose (A) and 4 mM U-^{13}C-glutamine (C). Similar measurements to intracellular glutamate from glucose (B) and glutamine (D) tracer source. Representing labelled isotopologues above 2% labelling and with significant changes. Data represented in all panels is mean ± SD for n=3 reads of n=3 samples of a single experiment. Statistically significant differences were determined by two-tailed independent sample Student's t-test, with p-values of $p< 0.05$ (*), $p< 0.01$ (**) and $p<0.001$ (***).

Glutamate m2, from U-^{13}C-glucose source, excreted to the extracellular media is around 5% in normoxia in both Parental and TET2 KO cells and decreases in both cell lines under hypoxia, being the decrease less pronounced in the KO cells (Figure 4.2.13). The intracellular glutamate m2 is higher in Parental cells in normoxia with a decrease after the switch to hypoxia but an increase in the TET2 KO cells. The same tendencies are observed for intracellular glutamate m3 and m4 (Figure 4.2.13A-B). The higher percentage of glutamate m3 and m4 observed in TET2 KO cell line in hypoxia conditions is in accordance with the ^{13}C-label pattern observed in citrate (see Figure 4.2.11) and corroborate that TET2 KO cells have

higher entry of pyruvate into TCA cycle through pyruvate carboxylase than Parental cells under hypoxia conditions.

Next, we investigated the ^{13}C-label incorporation of glutamate from U-^{13}C-glutamine source. Analysing the glutamate m5, which is the direct product of this tracer source, we observe that under hypoxia TET KO cells the secreted glutamate is more enriched as m5 whereas Parental cells secreted glutamate maintain the same percentage of m5 enrichment in hypoxia than in normoxia. This result is indicative of an increase of glutamine synthetase activity and subsequent export of glutamate triggered by hypoxia only in TET2 KO cells (Figure 4.2.13C).

Intracellular glutamate m5 levels are only lower in TET2 KO cells under hypoxia (Figure 4.2.13D), which is indicative of a higher export of glutamate that can be exchanged for other amino acids through antiport transporters or/and of a higher use of glutamate for glutathione synthesis.

As for glutamate m3 from glutamine source, its formation happens after more than one turn of the TCA cycle and we see much less occurring in hypoxia than normoxia (Figure 4.2.13D).

Put together, these results indicate that without TET2, the cells in hypoxia perform the first deamination of glutamine to obtain nitrogen, with the resulting glutamate being partly directed to the TCA cycle and partly being secreted to the extracellular media.

Following this, we investigated ^{13}C-label incorporation into citrate and malate from U-^{13}C-glutamine. We obtained that citrate m5 and malate m3 increase under hypoxia challenge in Parental cells whereas in TET2 KO cells we observed a decrease of these two isotopologues in response to hypoxia (Figure 4.2.14A-B). These results show that the knockout of TET2 impairs the switch to reductive carboxylation triggered by hypoxia in Parental cells. As depicted in Figure 4.2.15, citrate m5 and malate m3 (generated from oxaloacetate m3) are produced from U-^{13}C-glutamine

through reductive carboxylation pathway and are excellent indicators of the activity of this pathway.

Citrate m4 and Malate m4 are the products of the TCA cycle from the entry point of labelled carbons from αKG, with the hypoxia levels lower than in normoxia for both cell lines (Figure 4.2.14A-B).

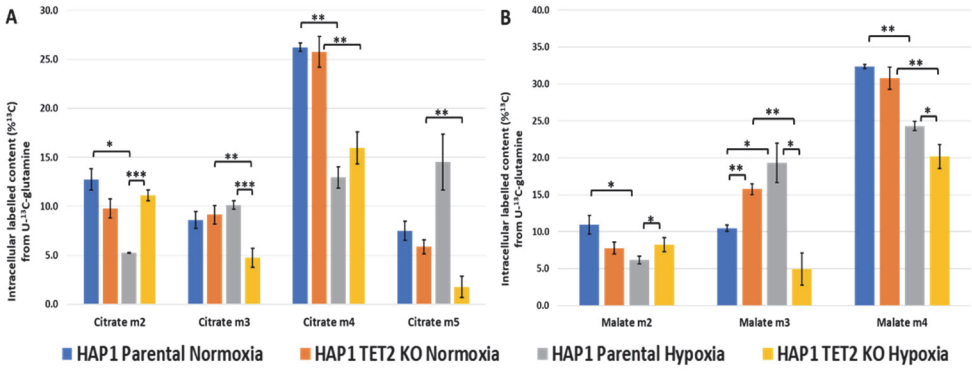

Figure 4.2.14- GCMS analysis of labelled intracellular Citrate and Malate. Measurement of glutamine contributions (% labelled) to intracellular citrate and malate after 24h incubation with 4 mM of U-^{13}C-glutamine. (A) Represented contribution of glutamine to Citrate m2, m3, m4 and m5. (B) Represented contribution of glutamine to Malate m2, m3 and m4. Representing labelled isotopologues above 2% labelling and with significant changes. Data represented is mean ± SD for n=3 reads of n=3 samples of a single experiment. Statistically significant differences were determined by two-tailed independent sample Student's t-test, with p-values of $p< 0.05$ (*), $p< 0.01$ (**) and $p<0.001$ (***).

Lastly, we observed the ratios of the isotopologues of citrate and malate to corroborate our observations (Figure 4.2.15B). Comparing citrate m4 versus citrate m5 indicates the preference for oxidative carboxylation or reductive, respectively. This ratio is similar in normoxia but drastically changes in hypoxia, with the Parental cells favouring the reductive carboxylation while the cells without TET2 favour the oxidative reaction.

From the malate ratios, we can infer the preference from reductive carboxylation or normal TCA cycle, by comparing malate m3 versus m4. This again tells us that while in normoxia there is not much difference, in hypoxia the Parental cells favour the reductive carboxylation path.

A

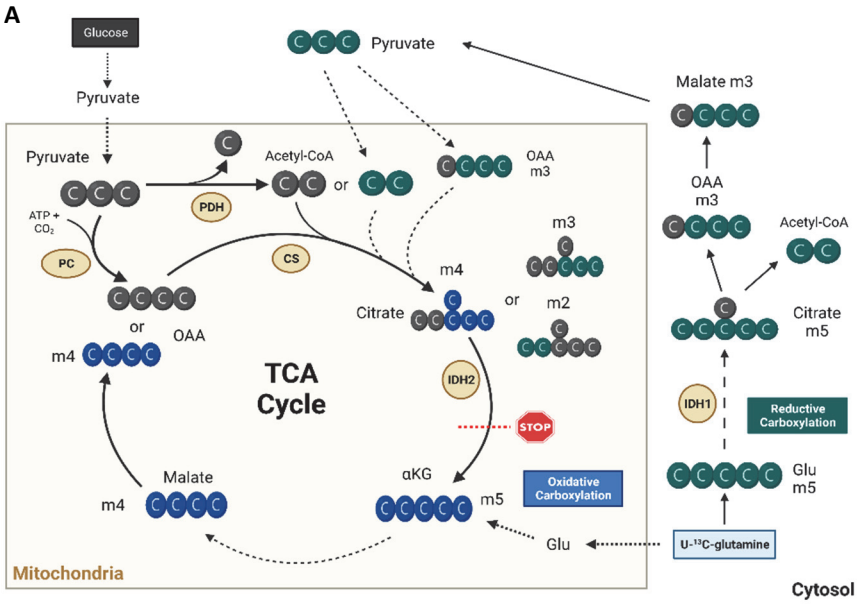

B

U-^{13}C-glutamine	Citrate	Malate
Ratios of mZ/ΣM	m4 vs m5	m4 vs m3
Parental Normoxia	3.50	3.09
TET2 KO Normoxia	4.39	1.95
Parental Hypoxia	0.90	1.26
TET2 KO Hypoxia	9.10	4.17

Figure 4.2.15- Scheme of labelling patterns expected in TCA cycle from U-^{13}C-Glutamine. (A) Uniformly labelled glutamine is converted into fully labelled glutamate (Glu) through glutaminolysis, which then enters the TCA cycle in the form of α-ketoglutarate (αKG), the denominated oxidative carboxylation path (highlighted in blue). Subsequent label patterns travel through succinate, fumarate, malate and end up at oxaloacetate (OAA). This can be used by citrate synthase (CS) to form citrate (defined as the stop point of one lop of the cycle). Alternatively, glutamine can suffer reductive carboxylation (highlighted in green), generating differently labelled Glu, αKG, citrate, OAA, acetyl-CoA and malate. Said malate can be transformed into pyruvate and feed the TCA cycle, in the form of acetyl-CoA (from PDH) or in the form of OAA (from PC). Created with BioRender.com. (B) Ratios of labelled isotopologues from citrate and malate, from the same experiment represented in Figure 4.2.14. Calculations of Reductive carboxylation versus Oxidative carboxylation (m4 vs m5 of citrate; m4 vs m3 of malate).

4.2.2.6 TET2 loss directs One-Carbon Metabolism for Glutathione production

The metabolic characterization results arising from the knockout of TET2 all point to a higher mitochondrial activity and ROS increase. For the cells to maintain their proliferation with these parameters under hypoxia, we can hypothesis that the detoxification systems such as glutathione are also changing.

As mentioned in section 1.3.6, glutathione production is dependent of various other metabolic pathways. It requires glutamate from glutaminolysis, glycine and homocysteine from the One-Carbon metabolism and NADPH to recover GSSG back to GSH, supplied by the PPP and TCA cycle.

From GCMS and NMR-based tracer-based metabolomics approaches and incubating the cells as above described with 22.5 mM U-^{13}C-glucose, we can investigate the flow between glycine and serine. The results presented all the possible isotopologues of serine, both intra and extracellularly (Figure 4.2.16A-B). Serine m3 is a direct product from glycolysis, receiving the labelled carbons from 3-phosphoglycerate (3PG) whereas serine m2 and serine m1 can result from the interconversion of serine and glycine through the reversible serine hydroxymethyltransferase (SHMT) reaction with the participation of labelled or unlabelled substrates. The most significant differences observed, at the level of intracellular isotopologues distribution between the two cell lines in response to hypoxia, are that the Parental cells only increase m3 whereas in TET2 KO cells we observe a significant increase of all serine isotopologues (m1, m2 and m3) under the hypoxic challenge. Worth to note that the percentage of labelled enrichment of the serine isotopologues in extracellular serine also increased in TET2 KO cells in response to hypoxia whereas it is not altered in Parental cells (Figure 4.2.16B). Taking into account that the serine consumption of the cells is not

statistically significant, neither between the two cell lines nor in the different oxygen levels (Figure 4.2.16C) and that glycine m2 (Figure 4.2.16A) is also increased in TET2 KO cells in hypoxia, we concluded that there is a higher interconversion between serine and glycine through SHMT reaction due to an increase in One-Carbon Metabolism in TET2 KO cells under hypoxia. At the level of total glycine consumption, we observed a dramatic increase of glycine consumption in hypoxia in both cell lines that could be due to the fact that hypoxia increased the need of glycine for glutathione synthesis (Figure 4.2.16C).

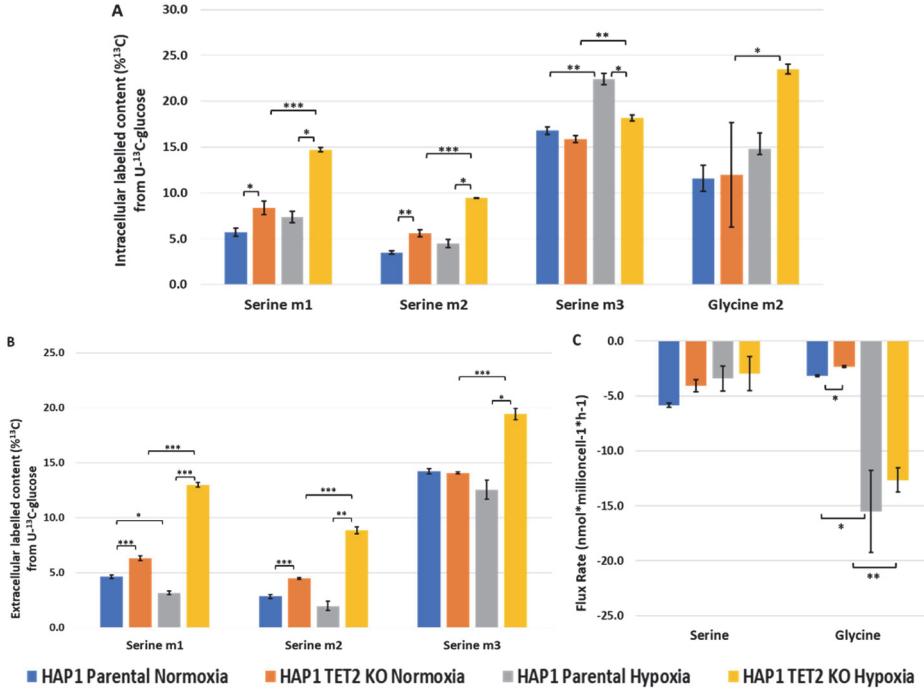

Figure 4.2.16- GCMS analysis of labelled Serine and Glycine. Measurement of glucose contribution (% labelled) to intracellular (A) and extracellular (B) metabolites after 24h incubation with 22.5 mM U-^{13}C-glucose. Representing labelled isotopologues above 2% labelling and significant changes. Data represented is mean ± SD for n=3 reads of n=3 samples of a single experiment. (C) Consumption rates of Serine and Glycine obtained through Absolute 180 IQ Kit from Biocrates. Data represented is mean ± SD for n=3 reads of n=3 samples of a single experiment. Statistically significant differences were determined by two-tailed independent sample Student's t-test, with p-values of $p< 0.05$ (*), $p< 0.01$ (**) and $p<0.001$ (***).

The results obtained using ^{13}C-based NMR metabolomics showed that the percentage of ^{13}C enrichment in carbon C2 of glycine and carbon C3 of serine are also increased under hypoxic challenge in TET2 KO cells corroborating the results obtained by ^{13}C-based GC-MS (Figure 4.2.17). Worth to note that SHMT catalysed conversion of serine into glycine generates 5,10me-THF that can be used as substrate by the 5,10me-THF dehydrogenase activity of MTHFD resulting in the reduction of NADP to NADPH. As TET2 KO cells are not able to increase G6PD under the hypoxia challenge, we hypothesized that the increase observed in glycine m2 can serve the purpose of generating NADPH.

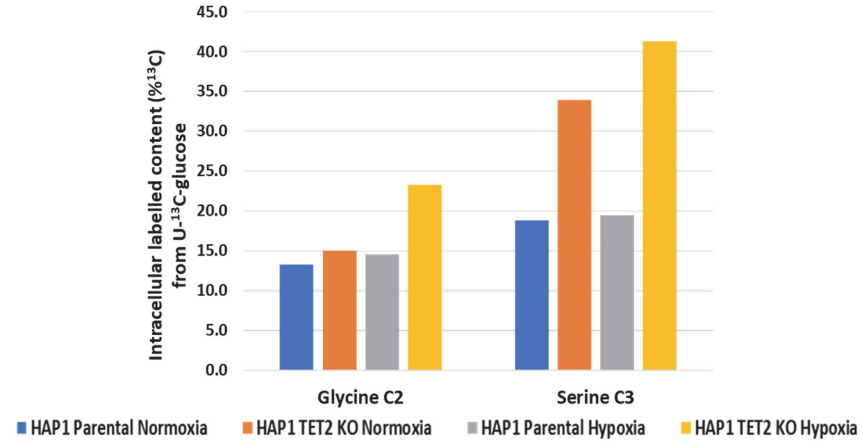

Figure 4.2.17- Labelled Glycine and Serine Isotopomers using ^{13}C-tracer based Metabolomics. Measurement of glucose contribution to intracellular metabolites after 24h incubation with 22,5mM U-^{13}C-glucose, processed and analysed by ^{1}H-^{13}C-HSQC NMR spectroscopy (full procedure in Methods 4.11). ^{13}C percentages were calculated as a ratio of the labelled and unlabelled sample and multiplied by the natural abundance of ^{13}C (1.1%). Data represented is n=1 read of n=1 sample of a single experiment. Statistical analysis could not be applied due to insufficient replicates.

To further investigate if the differences in glutamate and glycine ^{13}C enrichment observed due to TET2 knockout are reflected in the mirror carbons in the glutathione molecule we analysed the differences in ^{13}C enrichment in selected carbons of glutathione. As mentioned before,

glutathione is the joining of three other amino acids, glutamate, cysteine and glycine. Through NMR we are able to see the incorporation of labelled carbons to each specific constituent of GSH (Figure 4.2.18). The carbons C2 and C3 correspond to the 2nd and 3rd carbon of a glutamate molecule. From a glucose source, the C2 labelling correspond to the profile of glutamate m2 attested by GCMS (Figure 4.2.13B). Equal similarities can also be seen on the comparison from the glutamine tracers (Figure 4.2.13D). These results indicate that the use of glutamate for glutathione production is higher in Parental cells, especially in the normoxia setting.

Glutathione C9 correspond to one of the carbons from the glycine utilized in its synthesis. From a glutamine source, the incorporation of this labelled carbon is barely above the natural occurrence of ^{13}C (Figure 4.2.18). As for the carbons from a glucose source, we see high levels in TET2 KO cells, both in normoxia and hypoxia (Figure 4.2.18A). Furthermore, it matches the profile seen of serine C3 and glycine C2 (Figure 4.2.17), showing how this carbon travelled all the way to integrate in glutathione.

Altogether, the obtained results show that the loss of TET2 is affecting glycine and serine metabolism adaptation to the hypoxia challenge which is also reflected in the incorporation of carbons of glucose and glutamine into glutathione. The fact that TET2 KO cells lost the capacity to increase total G6PD activity in response to hypoxia, diminishing its capacity to generate NADPH, is here unveiled as the putative event that trigger the enhanced One-Carbon Metabolism in these cells. Thus, consecutive SHMT and MTHFD reactions will generate glycine and NADPH providing an alternative important source of reductive equivalents to compensate the deficient G6PD total activity of TET KO cells in hypoxia. The enhanced ROS levels observed in TET KO cells in hypoxia could be also related with this primary event of impaired G6PD enhancement under the hypoxic condition of TET2 KO cells.

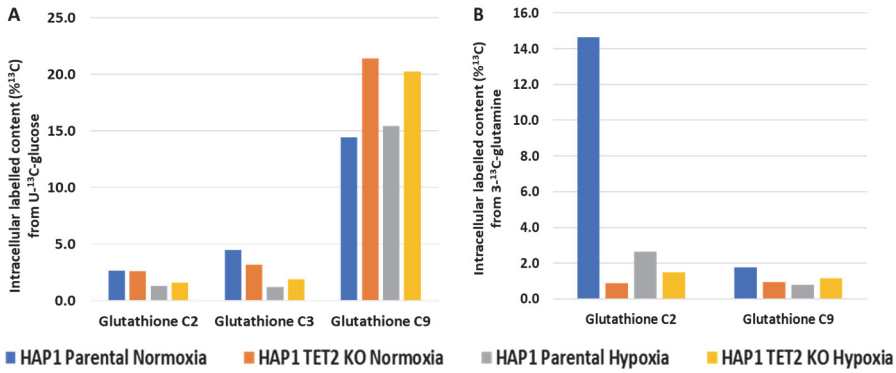

Figure 4.2.18- Label incorporation of intracellular Glutathione using ^{13}C-tracer based Metabolomics. Measurements obtained using cellular extracts after 24h incubation with U-^{13}C-glucose (A) and 3-^{13}C-glutamine (B) tracer, processed and analysed by ^{1}H-^{13}C-HSQC NMR spectroscopy (full procedure in Methods 4.11). ^{13}C percentages were calculated as a ratio of the labelled and unlabelled sample and multiplied by the natural abundance of ^{13}C (1.1%). Data represented is n=1 read of n=1 sample of a single experiment. Statistical analysis could not be applied due to insufficient replicates.

4.2.2.7 TET2 loss influences metabolism of amino acids

With the changes observed to glycolysis, glutamine metabolism and TCA cycle, we pondered how the metabolism of amino acids that interconnects with these pathways were changing as well in response to the loss of TET2. Alanine is a non-essential amino acid that connects the glycolysis pathway with glutamine metabolism because it can be produced from pyruvate carbon-skeleton through alanine aminotransaminase reaction between glutamate and pyruvate that renders αKG in addition to alanine.

Through tracer-based metabolomics, we investigated the incorporation of ^{13}C-label from U-^{13}C-glucose. The incorporation of ^{13}C in C3 position of alanine, attested by NMR (Figure 4.2.19A-B), both intra- and extracellularly, shows the same pattern as pyruvate (see Figure 4.2.4), with higher levels in TET2 KO in hypoxia. This indicates that like the recycling of pyruvate-lactate, a similar process is occurring between alanine and pyruvate. The isotopologues analysed by GCMS corroborate the same

tendency, with alanine m3 being the more present isotopologue for TET2 KO cells, extracellularly (Figure 4.2.19C).

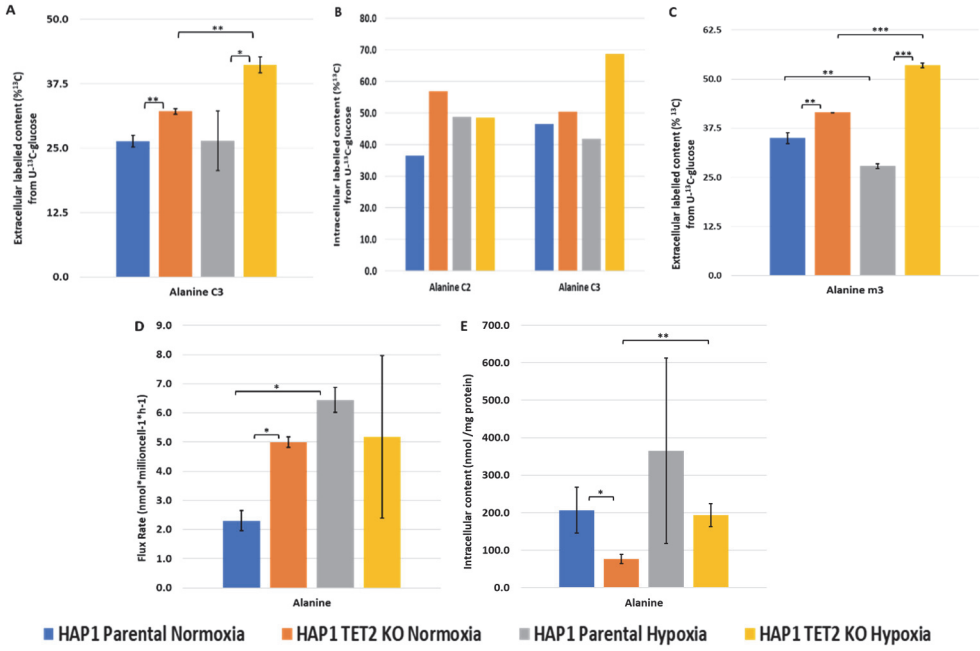

Figure 4.2.19- Impact of TET2 knockout on Alanine metabolism through targeted and ^{13}C-based Metabolomics. (A) ^{13}C-filtered ^{1}H-NMR spectroscopy analysis of labelled extracellular alanine. Data represented is mean ± SD for n=1 reads of n=3 samples of a single experiment. (B) ^{1}H-^{13}C-HSQC NMR spectroscopy analysis of labelled intracellular Alanine. ^{13}C percentages were calculated as a ratio of the labelled and unlabelled sample and multiplied by the natural abundance of ^{13}C (1.1%). Data represented is n=1 read of n=1 sample of a single experiment. Statistical analysis could not be applied due to insufficient replicates. (C) GCMS analysis of labelled extracellular Alanine. Data represented is mean ± SD for n=3 reads of n=3 samples of a single experiment. (D) Consumption and production rates obtained through Absolute 180 IQ Kit from Biocrates. Data represented is mean ± SD for n=3 reads of n=3 samples of a single experiment. (E) Intracellular levels of Alanine (Ala) through Absolute 180 IQ Kit from Biocrates. Data normalized by protein content. Data represented is mean ± SD for n=3 reads of n=3 samples of a single experiment. Statistically significant differences in related panels were determined by two-tailed independent sample Student's t-test: $p< 0.05$ (*) and $p< 0.01$ (**).

The flux rates of alanine show a clear secretion from cells to the extracellular media, with TET2 KO secreting more in normoxia while in hypoxia the differences are not statistically significant as there is a high

error associated to the alanine measurements in hypoxia (Figure 4.2.19D). This higher alanine production in normoxia correlates with the higher glucose consumption observed also in TET2 KO cells in normoxia.

Aspartate is one of the amino acids that had significant changes in our tracer experiments. Given that ^{13}C-labelled aspartate is generated in transamination reactions from oxaloacetate, that in turn is interconverted with malate through malate dehydrogenase reaction, it is expected that aspartate ^{13}C-isotopologues distribution mirror that observed in malate (see the paths of ^{13}C incorporation into oxaloacetate, malate from U-^{13}C-glucose and U-^{13}C-glutamine depicted in Figure 4.2.10 and Figure 4.2.15).

From the experiments using U-^{13}C-glucose we see that m2 and m3 aspartate labelling pattern in Parental and TET2 KO cell lines, in normoxia and hypoxia conditions (Figure 4.2.20A), perfectly mirror those obtained for malate (see Figure 4.2.11B).

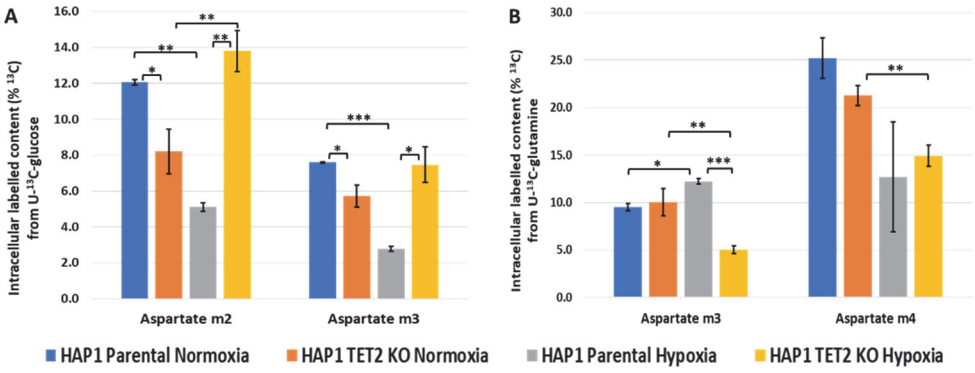

Figure 4.2.20- GCMS analysis of labelled intracellular Aspartate. Measurement of glucose and glutamine contributions (% labelled) to intracellular aspartate after 24h incubation with 22,5 mM U-^{13}C-glucose and 4 mM U-^{13}C-glutamine, respectively. (A) Represented contribution of glucose to Aspartate m2 and m3. (B) Represented contribution of glutamine to Aspartate m3 and m4. Representing labelled isotopologues above 2% labelling and with significant changes. Data represented is mean ± SD for n=3 reads of n=3 samples of a single experiment. Statistically significant differences were determined by two-tailed independent sample Student's t-test, with p-values of $p< 0.05$ (*), $p< 0.01$ (**) and $p<0.001$ (***).

When using the U-^{13}C-glutamine tracer, we obtained changes in aspartate m3 and m4 (Figure 4.2.20B). Again, these are mirrored labels from its precursor malate (see Figure 4.2.14B) as aspartate m4 comes from the oxidative metabolism of glutamine through the TCA cycle whereas aspartate m3 results from the conversion of glutamine into citrate (reductive metabolism of glutamine) and its conversion into oxaloacetate and acetyl-CoA by the action of ATP-citrate lyase (see Figure 4.2.15). These results corroborate that Parental cells enhance the reductive carboxylation in hypoxia and that TET2 knockout impairs the switch to reductive carboxylation of HAP1 cells in response to hypoxia.

Another metabolite which interacts with intermediates of the TCA cycle is proline. ^{13}C-Labelled carbons can incorporate proline when synthesized from glutamate, produced from U-^{13}C-glucose or from U-^{13}C glutamine. From the glucose contribution, proline m2 levels are higher in normoxia than hypoxia, with the Parental cell line displaying higher ^{13}C-enrichment than the TET2 KO cells in both conditions (Figure 4.2.21A). Worth to note that the synthesis of proline molecule from glutamate requires a net consumption of 2 molecules of NADPH. The fact that TET2 KO cells have less capacity to generate NADPH through G6PD due to the decrease of total activity both in normoxia and hypoxia could be the possible mechanism underlying the observed differences.

On the side of U-^{13}C-glutamine contribution to proline, we observe significant labelling changes in isotopologues m2 and m4 of the fragment C2C5 of proline (Figure 4.2.21B). The m4 labelling occurring in the fragment of proline C2C5 is directly from glutaminolysis producing glutamate m5. We can confirm this since the labelling profile is shared with glutamate m5.

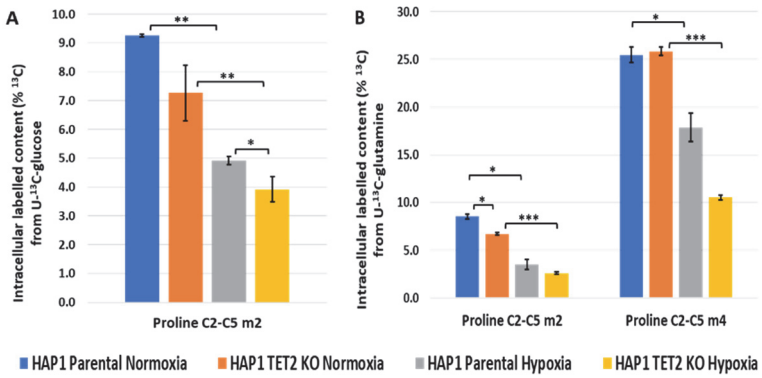

Figure 4.2.21- GCMS analysis of labelled intracellular Proline. Measurement of glucose and glutamine contributions (% labelled) to intracellular proline after 24h incubation with 22,5 mM U-^{13}C-glucose and 4 mM U-^{13}C-glutamine, respectively. Proline fragment C2C5 is represented. (A) Represented contribution of glucose to Proline m2. (B) Represented contribution of glutamine to Proline m2 and m4. Representing labelled isotopologues above 2% labelling and with significant changes. Data represented is mean ± SD for n=3 reads of n=3 samples of a single experiment. Statistically significant differences were determined by two-tailed independent sample Student's t-test, with p-values of $p< 0.05$ (*), $p< 0.01$ (**) and $p<0.001$ (***).

Proline m2 labelling percentages in the C2C5 fragment of proline are much lower than m4 (Figure 4.2.21B), given that such isotopologue results from glutamate coming from second turn of TCA cycle, thus generating forms of glutamate with 2 or 3 ^{13}C. This proline m2 would correlate with glutamate m2 or glutamate m3 molecules (Figure 4.2.13D). The lowering levels of proline m2 attested in hypoxia are then another evidence that the first steps of the TCA cycle are being reduced in both cell lines (Figure 4.2.21B), with less label traveling from αKG back to glutamate.

At the level of the branched chain amino acids (BCAAs) consumptions in normoxia (isoleucine, leucine and valine), we do not see any difference between Parental and TET2 KO cells (Figure 4.2.22B). By contrary, we observed that hypoxia triggers a dramatic increase in isoleucine and leucine consumptions in Parental cells whereas in TET2 KO cells only leucine slightly increase consumption in hypoxia. At the level of intracellular BCAAs content we see higher intracellular levels in Parental cells in

normoxia (Figure 4.2.22A). Interestingly, hypoxia triggers a dramatic increase in isoleucine and leucine content increase in Parental cells and only small changes in TET2 KO cells. The same tendency in lesser extension is observed for Valine.

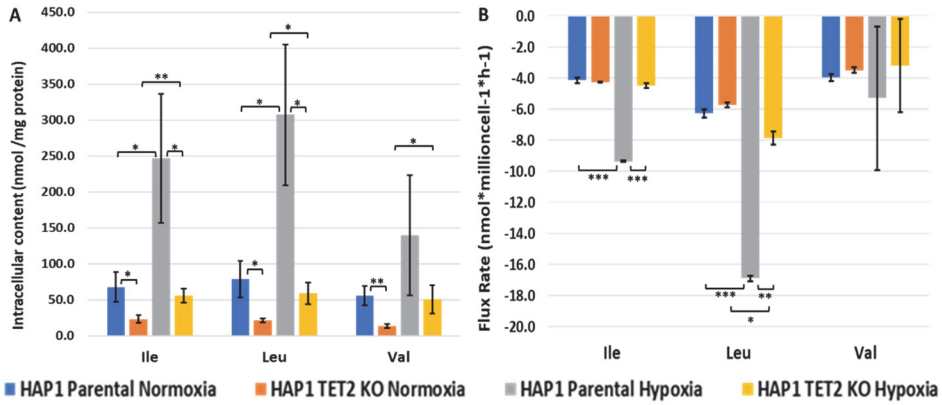

Figure 4.2.22- TET2 knockout effect on Branched-chain amino acids metabolism. (A) Intracellular levels of Isoleucine (Ile), Leucine (Leu) and Valine (Val) through Absolute 180 IQ Kit from Biocrates. Data normalized by protein content. Data represented is mean ± SD for n=3 reads of n=3 samples of a single experiment. (B) Consumption and production rates of Isoleucine (Ile), Leucine (Leu) and Valine (Val), obtained through Absolute 180 IQ Kit from Biocrates. Data represented is mean ± SD for n=3 reads of n=3 samples of a single experiment. Statistically significant differences in related panels were determined by two-tailed independent sample Student's t-test: $p< 0.05$ (*) and $p< 0.01$ (**).

Taking into account that the knockout of TET2 not affect cell proliferation rate neither in normoxia non in hypoxia, the differences observed in BCAAs intracellular content and consumption cannot be related with cell growth needs. The obtained results could be explained at the light of the recent evidence reported in the literature on the role of BCAAs catabolism in activating mTOR and regulating αKG homeostasis. In brief, it has been reported that downregulation of TET2 results in activation of mTOR signalling pathways[505,506] and that the first step in BCAAs catabolism (catalysed by BCAT1 enzyme), is critical for maintaining low levels of αKG that decrease TET2 activity and result in DNA-hypermethylation[98]. Thus, according to these reported evidences the lack of increase of BCAAs

consumption in hypoxia and the low intracellular levels can be due to the fact that leucine and BCAAs are not required by TET2 KO cells neither for increasing mTOR nor to decrease αKG available for TET2-catalysed DNA demethylation.

Finally, we analysed the differences at the level of methionine, which is indirectly related with glutathione synthesis, and polyamines, which are metabolites involved in arginine metabolism and the synthesis of SAM (a key substrate for methylation reactions). We observed that methionine, ornithine and spermine intracellular contents are higher in Parental cells in normoxia and increase under the hypoxic challenge in these cells whereas this effect is not observed in TET2 KO cells (Figure 4.2.23A and C). At the level of cell metabolite consumption/production, the results are not conclusive for neither Methionine and spermine, due to a high experimental error, but a higher net secretion of ornithine to extracellular media is observed for TET2 KO cells which is indicative of a lower utilization of this metabolite for the synthesis of other polyamines or SAM (Figure 4.2.23B). Taking into account that it has been described that exogenous spermine augmented DNA methyltransferase activity and that abnormal gene methylation is triggered by polyamine deficiency[507], it is plausible to conclude that the obtained results, on altered polyamine intracellular levels and consumption/production between the two cell lines, are a consequence of the loss of TET2 activity in KO cells.

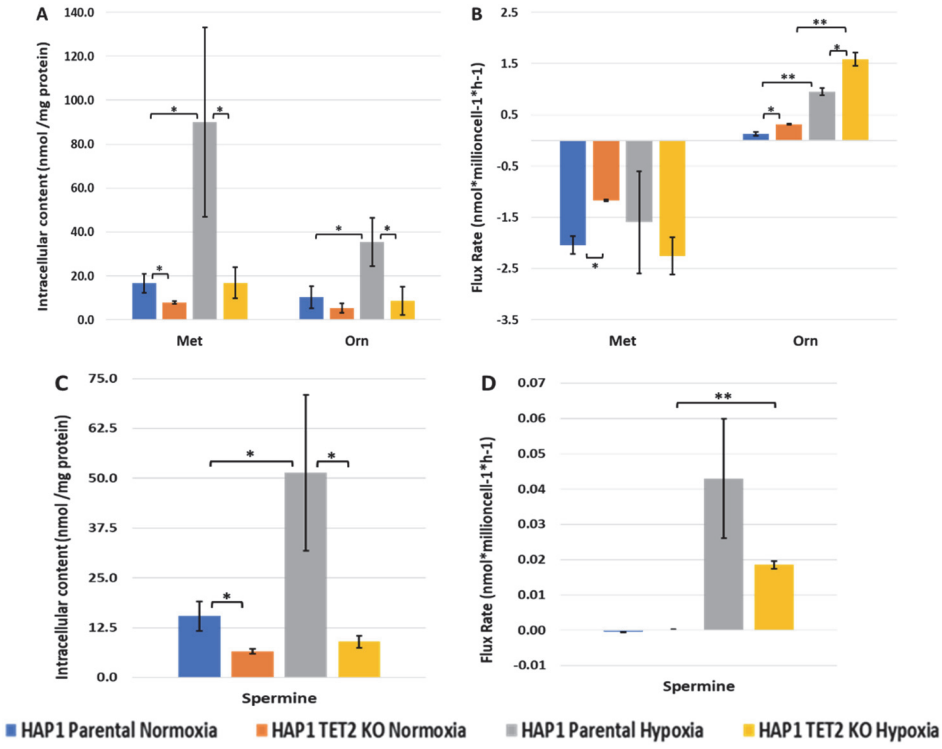

Figure 4.2.23- TET2 knockout effect on Methionine, Ornithine and Spermine metabolism. (A) Intracellular levels of methionine (Met) and ornithine (Orn). Data normalized by protein content. (B) Consumption and production rates of methionine (Met) and ornithine (Orn). (C) Intracellular levels of Spermine. Data normalized by protein content. (D) Consumption and production rates of Spermine. All results obtained through Absolute 180 IQ Kit from Biocrates. Data represented in all panels is mean ± SD for n=3 reads of n=3 samples of a single experiment. Statistically significant differences in all panels were determined by two-tailed independent sample Student's t-test: $p< 0.05$ (*) and $p< 0.01$ (**).

5. DISCUSSION

5 Discussion

Leukaemia is a type of cancer characterized by a rapid expansion of immature haematopoietic cells[20]. This uncontrolled proliferation can arise from many distinct conjugations of mutations, whose compiled synergy drives tumorigenesis[21,24,32,38,42]. The resulting phenotype presents a different metabolism from the surrounding normal cells, granting it advantages in proliferation and survival in the hypoxic conditions of the haematopoietic niche[14,15,39,43,56].

As it has been described in the introduction, metabolism has become one of the main Hallmarks of Cancer[5], and in the last years, new cancer therapies have emerged based on the different metabolic profiles that each tumour displays. But it is true that this new therapeutic strategy based in metabolic inhibitors is not properly working in all type of tumours, thus indicating that this strategy cannot be used in such a general way as other therapies based in directly attacking cell proliferation (for example, therapies based on DNA polymerase inhibitors or DNA intercalating agents). Furthermore, tumour microenvironment, that affects not only nutrients but also oxygen availability, creates a new complication. Thus, some of the metabolic targets identified in *in vitro* studies under normoxia, with great and promising expectations, have scarcely resulted efficient in clinical assays, as the tumour niche or the own three-dimensional structure of the tumour is hypoxic so the real metabolic response of the tumours differ greatly from what was characterized *in vitro*. Due to this, it is becoming more relevant to perform accurate metabolic characterizations not only under normoxia but specially for some types of tumours under hypoxia, so a better understanding of tumour metabolism will be provided, allowing to properly identify their metabolic vulnerabilities to be attacked therapeutically.

In the case of leukemic tumours, the conditions of the hematopoietic niche of the bone marrow of extreme hypoxia is another point to consider in the

formation of this type of cancer. Inside the niche are varying levels of hypoxia, with oxygen present in the range of bellow 1% in the niche and up to 12% when nearing the vascular system[403]. These conditions are favourable to leukemic cells, especially to leukemic stem cells, allowing them to remain quiescent and avoid chemotherapeutic toxicity. Another consideration is that the common mutations that relate to leukaemias are also present in other tumour types, that also become hypoxic over time. For example, breast normal tissue as a physiological oxygen of 8.5% but breast cancer presents only 1.5% of O_2, with this hypoxia correlating with aggressiveness and resistance to treatment[82,508]. Similar correlations between hypoxia and aggressive phenotypes are observed for colorectal cancer (with rectal mucosa oxygen levels of 3.9% dropping to 1.8% after tumorigenesis)[82,509,510], Non-small cells lung cancer (from 5.6% to 0.8%)[82,511] and cervix cancers (from 5.5% to 1.2%)[82,512]. While leukaemias are the type of cancer that originates in the most hypoxic environment, the study of how its mutations aid to adapt to this condition is translational knowledge to other types of cancer that share the same mutations and adaptability to hypoxic conditions during the more aggressive and metastatic phases of disease.

Since leukaemia treatment decisions nowadays account for the mutational profile of the patient, the elucidation of how specific mutations drive the metabolism of leukemic cells, not only in normoxia but also in hypoxia, opens new opportunities of treatment for these patients. Thus, in this thesis we have centred our efforts to better understand the role of TKTL1 and TET2 proteins, which are prevalent mutations in leukaemia, with the intention to open new future therapeutic strategies to patients displaying these mutations.

On the one hand, TKTL1 is a key enzyme of metabolism, linking glycolysis to the production of nucleotides, a necessary component for *de novo* synthesis of RNA and DNA, especially in rapidly proliferating cells[60,158,176].

Although the full scope of its functions is still unknown to this day, a clear correlation of its expression with cancer malignancy and poor prognosis has been established across many types of cancer[54,58,62,77,159,462]. One such type is AML, where the putative role of TKTL1 overexpression remains to be properly pursued[55,470].

The studies presented in chapter 4.1 of this thesis combined target metabolomics and transcriptomics profiling for a comparative analysis of a stable acute monocytic leukemic cell line with a TKTL1 knockdown and a wildtype counterpart with a significant content of this protein, to discern its role on the metabolic adaptation under the state of hypoxia.

The results obtained unveiled that the main metabolic changes triggered by the hypoxic conditions, such as increased glucose and glutamine consumptions and increased lactate production, are impaired by the TKTL1 knockdown. These differences occur as a consequence of changes at the level of gene expression and enzyme activities, thus inducing changes in metabolite exchange with extracellular media and intracellular metabolite homoeostasis.

Thus, TKTL1 knockdown impact not only total TKT activity but also results in a decrease of total G6PD activity thus expanding the metabolic impact to pentose-phosphate and NADPH synthesis capacities of the TKTL1-knockdown cells.

We have observed impaired gene expression and/or total enzyme activity of key metabolic players of glucose metabolism, reported in the literature to be induced under hypoxia[474–478,513], such as lactate and glucose transporters as well as key glycolytic/gluconeogenic enzymes PDKs, HKs, PCK1, GAPDH and LDHs.

At the level of glutamine-glutamate transport and metabolism, we have also observed that the expression of key genes and transporters, reported in the literature to be induced by hypoxia[487], was also impaired in TKTL1 knockdown cells. We have also observed at the level of gene expression,

that key players in glutamine and glutamate transport as well as glutamine synthase were overexpressed in hypoxia in wild type cells, whereas in TKTL1 knockdown cells had an impaired expression or even a downregulation. But we have not only observed changes in the hypoxia response induced in glucose and glutamine metabolism. TKTL1 loss also resulted in a reduction of the hypoxia-triggered switch to proline production when compared with wild type cells and that the pattern of expression of key players in proline metabolism (PYCRs and PRODH) is also altered. Taking into account that TKTL1 knockdown results in a decrease of total G6PD activity and that proline synthesis requires NADPH, these last results could be explained by the expected decreased NADPH pool triggered by G6PD activity deficiency. In fact, there is an increasing evidence that proline synthesis plays a key role in the regulation of cellular redox homeostasis and that is synthesized beyond the cell proliferative need as part of a "redox valve" mechanism[514].

Moreover, we also observed in TKTL1 knockdown cells an impaired expression in hypoxia of PCK1 and key cationic and essential amino acids transporters (SLC7A7 and SLC7A8) as well as an attenuated expression of key players in serine synthesis, that could be related with an altered pyrimidine nucleotide synthesis due to TKTL1 knockdown. In fact, it has been described that PCK1 and PHGDH are key players in ensuring appropriate nucleotide synthesis under hypoxia[491,492].

Even previous evidence exists demonstrating that TKTL1 expression is triggered in hypoxia[467,468], our studies are going beyond the state of the art unveiling that TKTL1 plays a key role in overexpression of key proteins necessary for enhancing glycolysis and glutamine consumption, characteristics of hypoxia adaptation.

Therefore, our results reveal that TKTL1 expression is essential in the adaptation to hypoxia, as it coordinates the metabolic reprogramming of central metabolism triggered by hypoxia not only at the level of glucose but

also contributing to oxidative stress regulation. Further studies should be developed to better understand the mechanisms involved in this new facet of TKTL1 functions on metabolism. Additional investigations of the changes identified here on other AML cell lines and primary patient-derived cells could reveal new approaches for therapies that combine targeting TKTL1 and any of the "weaknesses" that arises from its knock down.

On the other hand, it is known that hypoxia is involved in the epigenetic modification of leukaemia[515]. Although TET2 is one of the prevalent mutations in leukaemia cells, and it is known its role in methylation regulation and epigenetics, it has never been investigated in depth the metabolic impact of the loss of TET2 in leukaemia cells metabolism, and in particular in the metabolic adaptations triggered by hypoxia.

The results obtained in chapter 4.2, on the impact of TET2 knockout at the metabolic level, unveiled that TET2 plays an essential role in the metabolic adaptation HAP1 leukaemia cells to the hypoxia challenge.

In general, at metabolic level, the differences between CML Parental and TET2 KO cells attested in normoxia where minor, with the loss of TET2 barely affecting the cell survival and proliferation.

First major difference is that loss of TET2 decreased the levels of enzymes catalysing key steps of glycolysis (HK, GAPDH and PK) and they shifted under the hypoxia challenge, but also enhanced the increase of LDH activity in hypoxia that did not impact the lactate cellular efflux. Deeper investigation on pyruvate, lactate and ribose intracellular pools allowed us to conclude that knockout of TET2 resulted in a higher recycling of intracellular lactate-pyruvate in KO cells. Moreover, our tracer-based metabolomics data also demonstrated that pyruvate carboxylase flux was higher in TET2 KO cells.

These results unveil a new metabolic vulnerability of TET2 KO cells, as they rely on pyruvate carboxylase to feed TCA cycle, thus letting us to

hypothesize that lactate can enter mitochondria and be converted there to pyruvate to provide the substrate for pyruvate carboxylase. If our hypothesis is true, we would expect that inhibitors of pyruvate carboxylase or alternatively of LDH and lactate and/or pyruvate mitochondria transporters could be appropriate drug to target TET2 mutated tumours. Related with this, overexpression of pyruvate carboxylase has been correlated with bad prognosis in several types of cancer and, recently, potent and selective inhibitors have been developed that displayed promising preclinical results in inhibiting breast cancer progression[516]. Moreover, targeting of pyruvate and/or lactate transporters have also been explored in cancer therapy with promising results[517,518]. At any case, further experiments would need to be done to validate if such inhibitors can be exploited for leukaemia patients harbouring TET2 mutations.

Our metabolic characterization in normoxia and hypoxia also unveiled a dramatic decrease on G6PD activity due to TET2 knockout. Even more interesting, the increase of G6PD activity induced by hypoxia in Parental cells was fully impaired in TET2 KO cells. This loss of activity was not compensated by an increase of non-oxidative branch of PPP because we also observed that TKT activity was lower in TET2 KO cells, both in normoxia and hypoxia. These results pointed to G6PD as a putative target to be explored in combined therapies addressed to patients with tumours with TET2 mutated, because the lower levels of this enzyme can render these tumours more vulnerable to G6PD inhibitors.

The development of G6PD inhibitors and its potential use in different types of cancer is a very active field of research[519] and it has also been described in pre-clinical studies that the inhibition of G6PD could sensitize AML cells to FLT3 inhibitors[520].

Another important difference observed between Parental and TET2 KO cells in response to the hypoxia challenge, is that TET2 KO cells had a decreased capacity to perform reductive carboxylation under hypoxia, as it

is concluded from the ^{13}C labelling patterns observed in citrate, malate and aspartate when U-^{13}C-glutamine was used as a tracer. In accordance with this result, we have also observed that TET2 KO cells dramatically increased the glucose/glutamine consumptions ratio in response to the hypoxia challenge. The observed increase of glutamine consumption under hypoxia in different types of cancer has prompted during the last years to explore glutaminase inhibitors in pre-clinical studies and clinical trials, including leukaemia and other haematological malignancies, with results not as conclusive as expected initially[521,522].

The here obtained results pointed to predict that cancer patients with silenced TET2 will be less sensitive to glutaminase inhibitors. More studies need to be done in the future to validate this hypothesis and to explore if TET2 expression need to be considered as a biomarker to better stratify cancer patients that can benefit from glutaminase inhibitor therapies.

In addition, one-carbon and glutathione metabolism were enhanced in TET2 KO cells, which suggests that tumours with impaired TET2 activity should be more sensitive to therapies targeting one-carbon metabolism. To verify this hypothesis, methotrexate or other inhibitors used in clinics targeting folate metabolism, will be explored in future research in our team.

Not only this, but we have also observed a decrease in proline ^{13}C-label incorporation in TET2 KO cells, that we hypothesize is as a consequence of the decreased total G6PD activity of these cells. In this respect, it should be noted that in chapter 4.1 of this thesis we also observed that TKTL1 knockdown decreased both G6PD activity and proline synthesis. Altogether, the results obtained in both chapters of this thesis unveil a correlation between G6PD activity and proline synthesis that is in accordance with the role of these two pathways in maintaining cell redox homeostasis.

Furthermore, at the level of branched chain amino acids, TET2 KO cells did not experience the dramatic increased consumption of isoleucine and

leucine observed in Parental cells in hypoxia. The increased consumption of BCAAs observed in Parental cells in hypoxia is in accordance with previous evidence reporting that high levels of BCAAs catabolism results in activation of mTOR and subsequently HIF1α. Besides that, it has been described that downregulation of TET2 results in activation of mTOR in prostate cancer cells, but also that BCAT1 is critical for maintaining αKG pool homeostasis in AML stem cells[98,505,506]. Thus, and at the light of these observations, we hypothesize that TET2 KO cells would be less reliant on leucine-isoleucine import for mTOR signalling as the mTOR signalling pathway was already active, and also these cells would not need a so fine tuning of αKG levels to control TET2 activity because the enzyme is already silenced. Although BCAT inhibitors have attracted a lot of interest in the last years in cancer combined therapies[204], our results point out that we expect this therapy to be less efficient in TET2 deficient tumours.

Finally, the differences observed in TET2 KO cells under hypoxia at the level of methionine and polyamines suggest that TET2 downregulation would impact glutathione and/or SAM synthesis and cell methyltransferase activity especially under hypoxia. This conclusion would be in accordance with the well-established link between polyamines intake and global DNA methylation[507]. Of course, further investigation will be necessary to confirm these effects.

Collectively, our results have provided insight into how TKTL1 and TET2 contribute to a different metabolic adaptation in hypoxia. Our results demonstrate that TKTL1 overexpression or TET2 loss of functions mutations can provide advantages to leukaemia cells that co-exist in both normoxic and hypoxic microenvironments. Finally, we also postulate that some of these metabolic advantages may also be putative new metabolic vulnerabilities to be exploited as new drug targets in patients with tumours harbouring these mutations.

6. CONCLUSIONS

6 Conclusions

1. TKTL1 knockdown in THP-1 cells (THP-1^{KD}) impedes hypoxia-induced transcription of genes encoding for hexokinases (HK1 and HK2), glucose and lactate transporter (GLUT3 and MCT4, respectively) and PDK isoenzymes (PDK1, PDK3 and PDK4), resulting in the incapability of THP-1^{KD} to switch to an enhanced glycolysis under the hypoxic challenge.
2. TKTL1 knockdown results not only in a decrease of TKT activity but also in a decrease of G6PD activity in normoxia and impairs the hypoxia-induced expression of G6PD, thus impacting NADPH-related redox capacity of THP-1 cells.
3. TKTL1 knockdown impacts amino acids trafficking and impairs the hypoxia-induced increase of glutamine consumption and the hypoxia-activated transcription of genes encoding for amino acids transporters triggered by hypoxia observed in THP-1 cells.
4. TET2 knockout in HAP1 cells (TET2 KO) results in decreased levels of key glycolytic and pentose phosphate pathway enzymes (HK, GAPDH, PK, G6PD and TKT) and their modulation under the hypoxia challenge.
5. Under the hypoxia condition, TET2 KO cells display a higher recycling of intracellular lactate-pyruvate, a higher flux through pyruvate carboxylase, an increased One-Carbon and Glutathione metabolism, and a decreased capacity to perform reductive carboxylation when compared with TET2 Parental.
6. Hypoxia induces a dramatic increase in isoleucine and leucine cell consumption and corresponding intracellular content in Parental HAP1 cells that are impaired by loss of TET2. Similarly, an increase in methionine, ornithine and spermine intracellular contents under the hypoxic challenge is only observed in Parental cells.

7. BIBLIOGRAPHY

7 Bibliography

1. Bray, F. *et al.* Global cancer statistics 2018: GLOBOCAN estimates of incidence and mortality worldwide for 36 cancers in 185 countries. *CA. Cancer J. Clin.* **68**, 394–424 (2018).
2. Ferlay, J. *et al.* Cancer statistics for the year 2020: An overview. *Int. J. Cancer* **149**, 778–789 (2021).
3. Carbone, A. Cancer Classification at the Crossroads. *Cancers (Basel).* **12**, 10–15 (2020).
4. Hanahan, D. & Weinberg, R. A. The hallmarks of cancer. *Cell* **100**, 57–70 (2000).
5. Hanahan, D. & Weinberg, R. A. Hallmarks of cancer: the next generation. *Cell* **144**, 646–674 (2011).
6. Corces-Zimmerman, M. R. & Majeti, R. Pre-leukemic evolution of hematopoietic stem cells: the importance of early mutations in leukemogenesis. *Leukemia* **28**, 2276–2282 (2014).
7. Morrison, S. J. & Weissman, I. L. The long-term repopulating subset of hematopoietic stem cells is deterministic and isolatable by phenotype. *Immunity* **1**, 661–673 (1994).
8. Yang, L. *et al.* Identification of Lin(-)Sca1(+)kit(+)CD34(+)Flt3- short-term hematopoietic stem cells capable of rapidly reconstituting and rescuing myeloablated transplant recipients. *Blood* **105**, 2717–2723 (2005).
9. Akashi, K., Traver, D., Miyamoto, T. & Weissman, I. L. A clonogenic common myeloid progenitor that gives rise to all myeloid lineages. *Nature* **404**, 193–197 (2000).
10. Kondo, M., Weissman, I. L. & Akashi, K. Identification of clonogenic common lymphoid progenitors in mouse bone marrow. *Cell* **91**, 661–672 (1997).
11. Kondo, M. Lymphoid and myeloid lineage commitment in

multipotent hematopoietic progenitors. *Immunol. Rev.* **238**, 37–46 (2010).

12. Laurenti, E. & Göttgens, B. From haematopoietic stem cells to complex differentiation landscapes. *Nature* **553**, 418–426 (2018).
13. Cheng, H., Zheng, Z. & Cheng, T. New paradigms on hematopoietic stem cell differentiation. *Protein Cell* **11**, 34–44 (2020).
14. Boulais, P. E. & Frenette, P. S. Making sense of hematopoietic stem cell niches. *Blood* **125**, 2621–2629 (2015).
15. Morikawa, T. & Takubo, K. Hypoxia regulates the hematopoietic stem cell niche. *Pflugers Arch.* **468**, 13–22 (2016).
16. Kumar, S. & Geiger, H. HSC Niche Biology and HSC Expansion Ex Vivo. *Trends Mol. Med.* **23**, 799–819 (2017).
17. Surveillance Research Program, N. C. I. SEER*Explorer: An interactive website for SEER cancer statistics. (2021). Available at: https://seer.cancer.gov/explorer/. (Accessed: 26th August 2021)
18. Juliusson, G. *et al.* Acute myeloid leukemia in the real world: why population-based registries are needed. *Blood* **119**, 3890–3899 (2012).
19. Juliusson, G. & Hough, R. Leukemia. *Prog. Tumor Res.* **43**, 87–100 (2016).
20. Arber, D. A. *et al.* The 2016 revision to the World Health Organization classification of myeloid neoplasms and acute leukemia. *Blood* **127**, 2391–2405 (2016).
21. Estey, E. & Döhner, H. Acute myeloid leukaemia. *Lancet (London, England)* **368**, 1894–1907 (2006).
22. De Kouchkovsky, I. & Abdul-Hay, M. 'Acute myeloid leukemia: a comprehensive review and 2016 update'. *Blood Cancer J.* **6**, e441 (2016).
23. Czader, M. & Orazi, A. Acute myeloid leukemia and other types of disease progression in myeloproliferative neoplasms. *Am. J. Clin.*

Pathol. **144**, 188–206 (2015).

24. Lindsley, R. C. *et al.* Acute myeloid leukemia ontogeny is defined by distinct somatic mutations. *Blood* **125**, 1367–1376 (2015).
25. Sawyers, C. L. Chronic myeloid leukemia. *N. Engl. J. Med.* **340**, 1330–1340 (1999).
26. Höglund, M., Sandin, F. & Simonsson, B. Epidemiology of chronic myeloid leukaemia: an update. *Ann. Hematol.* **94**, 241–247 (2015).
27. Apperley, J. F. Chronic myeloid leukaemia. *Lancet* **385**, 1447–1459 (2015).
28. Schnittger, S. *et al.* RUNX1 mutations are frequent in de novo AML with noncomplex karyotype and confer an unfavorable prognosis. *Blood* **117**, 2348–2357 (2011).
29. Liu, P. *et al.* Fusion between transcription factor CBF beta/PEBP2 beta and a myosin heavy chain in acute myeloid leukemia. *Science* **261**, 1041–1044 (1993).
30. Liquori, A. *et al.* Acute Promyelocytic Leukemia: A Constellation of Molecular Events around a Single PML-RARA Fusion Gene. *Cancers (Basel).* **12**, 624 (2020).
31. Leubolt, G., Redondo Monte, E. & Greif, P. A. GATA2 mutations in myeloid malignancies: Two zinc fingers in many pies. *IUBMB Life* **72**, 151–158 (2020).
32. Bill, M. *et al.* Mutational landscape and clinical outcome of patients with de novo acute myeloid leukemia and rearrangements involving 11q23/KMT2A. *Proc. Natl. Acad. Sci. U. S. A.* **117**, 26340–26346 (2020).
33. Mannelli, F. *et al.* CEBPA–double-mutated acute myeloid leukemia displays a unique phenotypic profile: A reliable screening method and insight into biological features. *Haematologica* **102**, 529–540 (2017).
34. Ma, Z. *et al.* Fusion of two novel genes, RBM15 and MKL1, in the

t(1;22)(p13;q13) of acute megakaryoblastic leukemia. *Nat. Genet.* **28**, 220–221 (2001).

35. Falini, B., Sciabolacci, S., Falini, L., Brunetti, L. & Martelli, M. P. Diagnostic and therapeutic pitfalls in NPM1-mutated AML: notes from the field. *Leukemia* **35**, 3113–3126 (2021).
36. Logan, G. E. *et al.* DEK oncogene expression during normal hematopoiesis and in Acute Myeloid Leukemia (AML). *Blood Cells, Mol. Dis.* **54**, 123–131 (2015).
37. Kennedy, V. E. & Smith, C. C. FLT3 Mutations in Acute Myeloid Leukemia: Key Concepts and Emerging Controversies. *Front. Oncol.* **10**, 612880 (2020).
38. DiNardo, C. D. & Cortes, J. E. Mutations in AML: prognostic and therapeutic implications. *Hematol. Am. Soc. Hematol. Educ. Progr.* **2016**, 348–355 (2016).
39. Lagunas-Rangel, F. A., Chávez-Valencia, V., Gómez-Guijosa, M. Á. & Cortes-Penagos, C. Acute myeloid leukemia—genetic alterations and their clinical prognosis. *Int. J. Hematol. Stem Cell Res.* **11**, 329–339 (2017).
40. Kelly, L. M. & Gilliland, D. G. Genetics of myeloid leukemias. *Annu. Rev. Genomics Hum. Genet.* **3**, 179–198 (2002).
41. Zhou, T., Medeiros, L. J. & Hu, S. Chronic Myeloid Leukemia: Beyond BCR-ABL1. *Curr. Hematol. Malig. Rep.* **13**, 435–445 (2018).
42. Adnan-Awad, S., Kankainen, M. & Mustjoki, S. Mutational landscape of chronic myeloid leukemia: more than a single oncogene leukemia. *Leuk. Lymphoma* **0**, 1–15 (2021).
43. Klco, J. M. & Mullighan, C. G. Advances in germline predisposition to acute leukaemias and myeloid neoplasms. *Nat. Rev. Cancer* **21**, 122–137 (2021).
44. Furuta, E., Okuda, H., Kobayashi, A. & Watabe, K. Metabolic genes

in cancer: Their roles in tumor progression and clinical implications. *Biochim. Biophys. Acta - Rev. Cancer* **1805**, 141–152 (2010).

45. Wojcicki, A. V., Kasowski, M. M., Sakamoto, K. M. & Lacayo, N. Metabolomics in acute myeloid leukemia. *Mol. Genet. Metab.* **130**, 230–238 (2020).
46. Li, A. M. *et al.* Metabolic profiling reveals a dependency of human metastatic breast cancer on mitochondrial serine and one-carbon unit metabolism. *Mol. Cancer Res.* **18**, 599–611 (2020).
47. Castro, I., Sampaio-Marques, B. & Ludovico, P. Targeting Metabolic Reprogramming in Acute Myeloid Leukemia. *Cells* **8**, 1–20 (2019).
48. Matre, P. *et al.* Inhibiting glutaminase in acute myeloid leukemia: metabolic dependency of selected AML subtypes. *Oncotarget* **7**, 79722–79735 (2016).
49. Kantarjian, H. *et al.* Acute myeloid leukemia: current progress and future directions. *Blood Cancer J.* **11**, 41 (2021).
50. Stuani, L., Sabatier, M. & Sarry, J. E. Exploiting metabolic vulnerabilities for personalized therapy in acute myeloid leukemia. *BMC Biol.* **17**, 57 (2019).
51. Losman, J.-A. & Kaelin, W. G. What a difference a hydroxyl makes: mutant IDH, (R)-2-hydroxyglutarate, and cancer. *Genes Dev.* **27**, 836–852 (2013).
52. Nakajima, H. & Kunimoto, H. TET2 as an epigenetic master regulator for normal and malignant hematopoiesis. *Cancer Sci.* **105**, 1093–1099 (2014).
53. Xu, W. *et al.* Oncometabolite 2-hydroxyglutarate is a competitive inhibitor of α-ketoglutarate-dependent dioxygenases. *Cancer Cell* **19**, 17–30 (2011).
54. Philipp, M. *et al.* Expression of transketolase-like gene 1 (TKTL1) depends on disease phase in patients with chronic myeloid

leukaemia (CML). *J. Cancer Res. Clin. Oncol.* **140**, 411–417 (2014).

55. Avhandling, A. & Lindberg, M. L. *Acute myeloid leukemia - Apoptotic signalling and gene expression associated with treatment response*. *Dissertation* (Karolinska Institutet, 2013).

56. Jones, C. L. *et al.* Inhibition of Amino Acid Metabolism Selectively Targets Human Leukemia Stem Cells. *Cancer Cell* **34**, 724-740.e4 (2018).

57. Deshpande, G. P., Patterton, H.-G. & Faadiel Essop, M. The human transketolase-like proteins TKTL1 and TKTL2 are bona fide transketolases. *BMC Struct. Biol.* **19**, 2 (2019).

58. Chen, H. *et al.* Overexpression of transketolase-like gene 1 is associated with cell proliferation in uterine cervix cancer. *J. Exp. Clin. Cancer Res.* **28**, 2–9 (2009).

59. Maslova, A. O., Meshalkina, L. E. & Kochetov, G. A. Computer modeling of transketolase-like protein, TKTL1, a marker of certain tumor tissues. *Biochem.* **77**, 296–299 (2012).

60. Li, Y. *et al.* APC/CCDH1 synchronizes ribose-5-phosphate levels and DNA synthesis to cell cycle progression. *Nat. Commun.* **10**, 2502 (2019).

61. Xu, I. M.-J. *et al.* Transketolase counteracts oxidative stress to drive cancer development. *Proc. Natl. Acad. Sci. U. S. A.* **113**, E725-34 (2016).

62. Hutchinson, D. *et al.* TKTL1 is activated by promoter hypomethylation and contributes to head and neck squamous cell carcinoma carcinogenesis via increased aerobic glycolysis and HIF1α stabilization Wenyue. *NIH Public Access* **148**, 825–832 (2008).

63. Jayachandran, A. *et al.* Transketolase-like 1 ectopic expression is associated with DNA hypomethylation and induces the Warburg

effect in melanoma cells. *BMC Cancer* **16**, 134 (2016).

64. Zhao, F. *et al.* Imatinib resistance associated with BCR-ABL upregulation is dependent on HIF-1alpha-induced metabolic reprograming. *Oncogene* **29**, 2962–2972 (2010).
65. Shukla, S. K. *et al.* MUC1 and HIF-1alpha Signaling Crosstalk Induces Anabolic Glucose Metabolism to Impart Gemcitabine Resistance to Pancreatic Cancer. *Cancer Cell* **32**, 71-87.e7 (2017).
66. Bentz, S. *et al.* Hypoxia Induces the Expression of Transketolase-Like 1 in Human Colorectal Cancer. *Digestion* **88**, 182–192 (2013).
67. Belisario, D. C. *et al.* Hypoxia Dictates Metabolic Rewiring of Tumors: Implications for Chemoresistance. *Cells* **9**, 1–29 (2020).
68. Zheng, X. & Li, H. TKTL1 modulates the response of paclitaxel-resistant human ovarian cancer cells to paclitaxel. *Biochem. Biophys. Res. Commun.* **503**, 572–579 (2018).
69. Jeffery, C. J. Moonlighting proteins. *Trends Biochem. Sci.* **24**, 8–11 (1999).
70. Jeffery, C. J. Protein moonlighting: what is it, and why is it important? *Philos. Trans. R. Soc. Lond. B. Biol. Sci.* **373**, 1–19 (2018).
71. Völker, H. U. *et al.* Expression of transketolase-like 1 and activation of Akt in grade IV glioblastomas compared with grades II and III astrocytic gliomas. *Am. J. Clin. Pathol.* **130**, 50–57 (2008).
72. Schmidt, M. *et al.* Glycolytic phenotype in breast cancer: Activation of Akt, up-regulation of GLUT1, TKTL1 and down-regulation of M2PK. *J. Cancer Res. Clin. Oncol.* **136**, 219–225 (2010).
73. Kohrenhagen, N. *et al.* Expression of transketolase-like 1 (TKTL1) and p-Akt correlates with the progression of cervical neoplasia. *J. Obstet. Gynaecol. Res.* **34**, 293–300 (2008).
74. Dong, Y. & Wang, M. Knockdown of TKTL1 additively complements cisplatin-induced cytotoxicity in nasopharyngeal

carcinoma cells by regulating the levels of NADPH and ribose-5-phosphate. *Biomed. Pharmacother.* **85**, 672–678 (2017).

75. Chiarini, A. *et al.* Over Expressed TKTL1, CIP-2A, and B-MYB Proteins in Uterine Cervix Epithelium Scrapings as Potential Risk Predictive Biomarkers in HR-HPV-Infected LSIL/ASCUS Patients. *Front. Oncol.* **9**, 213 (2019).
76. Wanka, C., Steinbach, J. P. & Rieger, J. Tp53-induced glycolysis and apoptosis regulator (TIGAR) protects glioma cells from starvation-induced cell death by up-regulating respiration and improving cellular redox homeostasis. *J. Biol. Chem.* **287**, 33436–33446 (2012).
77. da Costa, I. A. *et al.* Transketolase like 1 (TKTL1) expression alterations in prostate cancer tumorigenesis. *Urol. Oncol. Semin. Orig. Investig.* **36**, 472.e21-472.e27 (2018).
78. Fritz, P. *et al.* TKTL-1 expression in lung cancer. *Pathol. Res. Pract.* **208**, 203–209 (2012).
79. Coy, J. F. EDIM-TKTL1/Apo10 blood test: An innate immune system based liquid biopsy for the early detection, characterization and targeted treatment of cancer. *Int. J. Mol. Sci.* **18**, 1–18 (2017).
80. Saman, S. *et al.* Biomarkers Apo10 and TKTL1: Epitope-detection in monocytes (EDIM) as a new diagnostic approach for cholangiocellular, pancreatic and colorectal carcinoma. *Cancer Biomarkers* **27**, 129–137 (2019).
81. Horsman, M. R. & Vaupel, P. Pathophysiological Basis for the Formation of the Tumor Microenvironment. *Front. Oncol.* **6**, 66 (2016).
82. Muz, B., de la Puente, P., Azab, F. & Azab, A. K. The role of hypoxia in cancer progression, angiogenesis, metastasis, and resistance to therapy. *Hypoxia (Auckland, N.Z.)* **3**, 83–92 (2015).
83. Rasmussen, K. D. & Helin, K. Role of TET enzymes in DNA

methylation, development, and cancer. *Genes Dev.* **30**, 733–750 (2016).

84. Li, W. & Xu, L. Epigenetic Function of TET Family, 5-Methylcytosine, and 5-Hydroxymethylcytosine in Hematologic Malignancies. *Oncol. Res. Treat.* **42**, 309–318 (2019).

85. Scourzic, L., Mouly, E. & Bernard, O. A. TET proteins and the control of cytosine demethylation in cancer. *Genome Med.* **7**, 1–16 (2015).

86. Rampal, R. *et al.* DNA hydroxymethylation profiling reveals that WT1 mutations result in loss of TET2 function in acute myeloid leukemia. *Cell Rep.* **9**, 1841–1855 (2014).

87. Cheng, J. *et al.* An extensive network of TET2-targeting MicroRNAs regulates malignant hematopoiesis. *Cell Rep.* **5**, 471–481 (2013).

88. Song, S. J. *et al.* The oncogenic microRNA miR-22 targets the TET2 tumor suppressor to promote hematopoietic stem cell self-renewal and transformation. *Cell Stem Cell* **13**, 87–101 (2013).

89. Fischer, A. P. & Miles, S. L. Silencing HIF-1α induces TET2 expression and augments ascorbic acid induced 5-hydroxymethylation of DNA in human metastatic melanoma cells. *Biochem. Biophys. Res. Commun.* **490**, 176–181 (2017).

90. Cimmino, L. *et al.* Restoration of TET2 Function Blocks Aberrant Self-Renewal and Leukemia Progression. *Cell* **170**, 1079-1095.e20 (2017).

91. Sun, J. *et al.* SIRT1 Activation Disrupts Maintenance of Myelodysplastic Syndrome Stem and Progenitor Cells by Restoring TET2 Function. *Cell Stem Cell* **23**, 355-369.e9 (2018).

92. Feng, Y., Li, X., Cassady, K., Zou, Z. & Zhang, X. TET2 Function in Hematopoietic Malignancies, Immune Regulation, and DNA Repair. *Front. Oncol.* **9**, 210 (2019).

93. Lu, F., Liu, Y., Jiang, L., Yamaguchi, S. & Zhang, Y. Role of Tet proteins in enhancer activity and telomere elongation. *Genes Dev.* **28**, 2103–2119 (2014).

94. Makishima, H. *et al.* CBL, CBLB, TET2, ASXL1, and IDH1/2 mutations and additional chromosomal aberrations constitute molecular events in chronic myelogenous leukemia. *Blood* **117**, e198-206 (2011).

95. Pan, W. *et al.* The DNA Methylcytosine Dioxygenase Tet2 Sustains Immunosuppressive Function of Tumor-Infiltrating Myeloid Cells to Promote Melanoma Progression. *Immunity* **47**, 284-297.e5 (2017).

96. Figueroa, M. E. *et al.* Leukemic IDH1 and IDH2 mutations result in a hypermethylation phenotype, disrupt TET2 function, and impair hematopoietic differentiation. *Cancer Cell* **18**, 553–567 (2010).

97. Laukka, T. *et al.* Fumarate and Succinate Regulate Expression of Hypoxia-inducible Genes via TET Enzymes. *J. Biol. Chem.* **291**, 4256–4265 (2016).

98. Raffel, S. *et al.* BCAT1 restricts αkG levels in AML stem cells leading to IDHmut-like DNA hypermethylation. *Nature* **551**, 384–388 (2017).

99. Fong, G. H. & Takeda, K. Role and regulation of prolyl hydroxylase domain proteins. *Cell Death Differ.* **15**, 635–641 (2008).

100. Wu, L. Y., He, Y. L. & Zhu, L. L. Possible role of PHD inhibitors as hypoxia-mimicking agents in the maintenance of neural stem cells' self-renewal properties. *Front. Cell Dev. Biol.* **6**, 1–7 (2018).

101. Thienpont, B. *et al.* Tumour hypoxia causes DNA hypermethylation by reducing TET activity. *Nature* **537**, 63–68 (2016).

102. Waddington, C. H. The epigenotype. 1942. *Int. J. Epidemiol.* **41**, 10–13 (2012).

103. Toh, T. B., Lim, J. J. & Chow, E. K. H. Epigenetics in cancer stem

cells. *Mol. Cancer* **16**, 1–20 (2017).

104. Nebbioso, A., Tambaro, F. P., Dell'Aversana, C. & Altucci, L. Cancer epigenetics: Moving forward. *PLoS Genet.* **14**, 1–25 (2018).
105. Shao, S. & Gudjonsson, J. E. Epigenetics of Psoriasis. in *Advances in experimental medicine and biology* (eds. Chang, C. & Lu, Q.) **1253**, 209–221 (Springer Singapore, 2020).
106. Margueron, R., Trojer, P. & Reinberg, D. The key to development: Interpreting the histone code? *Curr. Opin. Genet. Dev.* **15**, 163–176 (2005).
107. Amaral, P. P. & Mattick, J. S. Noncoding RNA in development. *Mamm. Genome* **19**, 454–492 (2008).
108. Yeo, J. C. & Ng, H. H. The transcriptional regulation of pluripotency. *Cell Res.* **23**, 20–32 (2013).
109. Stahl, M. *et al.* Epigenetics in Cancer: A Hematological Perspective. *PLoS Genet.* **12**, 1–21 (2016).
110. Margueron, R. & Reinberg, D. Chromatin structure and the inheritance of epigenetic information. *Nat. Rev. Genet.* **11**, 285–296 (2010).
111. Park, J. W. & Han, J. W. Targeting epigenetics for cancer therapy. *Arch. Pharm. Res.* **42**, 159–170 (2019).
112. Fennell, K. A., Bell, C. C. & Dawson, M. A. Epigenetic therapies in acute myeloid leukemia: Where to from here? *Blood* **134**, 1891–1901 (2019).
113. Ley, T. J. *et al.* Genomic and epigenomic landscapes of adult de novo acute myeloid leukemia. *N. Engl. J. Med.* **368**, 2059–2074 (2013).
114. Liu, K., Liu, Y., Lau, J. L. & Min, J. Epigenetic targets and drug discovery Part 2: Histone demethylation and DNA methylation. *Pharmacol. Ther.* **151**, 121–140 (2015).
115. Lyko, F. The DNA methyltransferase family: A versatile toolkit for

epigenetic regulation. *Nat. Rev. Genet.* **19**, 81–92 (2018).

116. Castelli, G., Pelosi, E. & Testa, U. Targeting histone methyltransferase and demethylase in acute myeloid leukemia therapy. *Onco. Targets. Ther.* **11**, 131–155 (2018).
117. Ross, S. E. & Bogdanovic, O. TET enzymes, DNA demethylation and pluripotency. *Biochem. Soc. Trans.* **47**, 875–885 (2019).
118. Kapranov, P., Willingham, A. T. & Gingeras, T. R. Genome-wide transcription and the implications for genomic organization. *Nat. Rev. Genet.* **8**, 413–423 (2007).
119. Tufarelli, C. *et al.* Transcription of antisense RNA leading to gene silencing and methylation as a novel cause of human genetic disease. *Nat. Genet.* **34**, 157–165 (2003).
120. Calin, G. A. *et al.* Frequent deletions and down-regulation of micro-RNA genes miR15 and miR16 at 13q14 in chronic lymphocytic leukemia. *Proc. Natl. Acad. Sci. U. S. A.* **99**, 15524–15529 (2002).
121. Pelosi, A. *et al.* MiRNA let-7c promotes granulocytic differentiation in acute myeloid leukemia. *Oncogene* **32**, 3648–3654 (2013).
122. Garzon, R. *et al.* MicroRNA 29b functions in acute myeloid leukemia. *Blood* **114**, 5331–5341 (2009).
123. Organista-Nava, J. *et al.* High miR-24 expression is associated with risk of relapse and poor survival in acute leukemia. *Oncol. Rep.* **33**, 1639–1649 (2015).
124. Mujahed, H. *et al.* AML displays increased CTCF occupancy associated with aberrant gene expression and transcription factor binding. *Blood* **136**, 339–352 (2020).
125. Bushweller, J. H. Targeting transcription factors in cancer — from undruggable to reality. *Nat. Rev. Cancer* **19**, 611–624 (2019).
126. Lambert, M., Jambon, S., Depauw, S. & David-Cordonnier, M.-H. Targeting Transcription Factors for Cancer Treatment. *Molecules* **23**, 1479 (2018).

127. Bradner, J. E., Hnisz, D. & Young, R. A. Transcriptional Addiction in Cancer. *Cell* **168**, 629–643 (2017).
128. Kaochar, S. & Tu, B. P. Gatekeepers of chromatin: Small metabolites elicit big changes in gene expression. *Trends Biochem. Sci.* **37**, 477–483 (2012).
129. Gao, S.-S., Naowarojna, N., Cheng, R., Liu, X. & Liu, P. Recent examples of α-ketoglutarate-dependent mononuclear non-haem iron enzymes in natural product biosyntheses. *Nat. Prod. Rep.* **35**, 792–837 (2018).
130. Zhu, X. *et al.* How DNA methylation affects the Warburg effect. *Int. J. Biol. Sci.* **16**, 2029–2041 (2020).
131. Vazquez, A. *et al.* Cancer metabolism at a glance. *J. Cell Sci.* **129**, 3367–3373 (2016).
132. Phan, L. M., Yeung, S.-C. J. & Lee, M.-H. Cancer metabolic reprogramming: importance, main features, and potentials for precise targeted anti-cancer therapies. *Cancer Biol. Med.* **11**, 1–19 (2014).
133. Nemkov, T., D'Alessandro, A. & Reisz, J. A. Metabolic underpinnings of leukemia pathology and treatment. *Cancer reports (Hoboken, N.J.)* **2**, e1139 (2019).
134. Sullivan, L. B., Gui, D. Y. & Vander Heiden, M. G. Altered metabolite levels in cancer: implications for tumour biology and cancer therapy. *Nat. Rev. Cancer* **16**, 680–693 (2016).
135. Rashkovan, M. & Ferrando, A. Metabolic dependencies and vulnerabilities in leukemia. *Genes Dev.* **33**, 1460–1474 (2019).
136. Tarrado-Castellarnau, M., de Atauri, P. & Cascante, M. Oncogenic regulation of tumor metabolic reprogramming. *Oncotarget* **7**, 62726–62753 (2016).
137. Holman, G. D. & Sandoval, I. V. Moving the insulin-regulated glucose transporter GLUT4 into and out of storage. *Trends Cell*

Biol. **11**, 173–179 (2001).

138. Bryant, N. J., Govers, R. & James, D. E. Regulated transport of the glucose transporter GLUT4. *Nat. Rev. Mol. Cell Biol.* **3**, 267–277 (2002).

139. Counihan, J. L., Grossman, E. A. & Nomura, D. K. Cancer Metabolism: Current Understanding and Therapies. *Chem. Rev.* **118**, 6893–6923 (2018).

140. Wilson, W. R. & Hay, M. P. Targeting hypoxia in cancer therapy. *Nat. Rev. Cancer* **11**, 393–410 (2011).

141. Akram, M. Mini-review on glycolysis and cancer. *J. Cancer Educ.* **28**, 454–457 (2013).

142. Abbaszadeh, Z., Çeşmeli, S. & Biray Avcı, Ç. Crucial players in glycolysis: Cancer progress. *Gene* **726**, 144158 (2020).

143. Slavov, N., Budnik, B. A., Schwab, D., Airoldi, E. M. & van Oudenaarden, A. Constant growth rate can be supported by decreasing energy flux and increasing aerobic glycolysis. *Cell Rep.* **7**, 705–714 (2014).

144. Luengo, A., Gui, D. Y. & Vander Heiden, M. G. Targeting Metabolism for Cancer Therapy. *Cell Chem. Biol.* **24**, 1161–1180 (2017).

145. Warburg, O. The Metabolism of Carcinoma Cells. *J. Cancer Res.* **9**, 148–163 (1925).

146. Ahmad, R. *et al.* Induction of ROS-mediated cell death and activation of the JNK pathway by a sulfonamide derivative. *Int. J. Mol. Med.* **44**, 1552–1562 (2019).

147. Kamarajugadda, S. *et al.* Manganese superoxide dismutase promotes anoikis resistance and tumor metastasis. *Cell Death Dis.* **4**, e504 (2013).

148. Geng, J., Yuan, X., Wei, M., Wu, J. & Qin, Z.-H. The diverse role of TIGAR in cellular homeostasis and cancer. *Free Radic. Res.* **52**,

1240–1249 (2018).

149. Boag, J. M. *et al.* Altered glucose metabolism in childhood pre-B acute lymphoblastic leukaemia. *Leukemia* **20**, 1731–1737 (2006).

150. Huang, A. *et al.* Metabolic alterations and drug sensitivity of tyrosine kinase inhibitor resistant leukemia cells with a FLT3/ITD mutation. *Cancer Lett.* **377**, 149–157 (2016).

151. Ju, H. Q. *et al.* ITD mutation in FLT3 tyrosine kinase promotes Warburg effect and renders therapeutic sensitivity to glycolytic inhibition. *Leukemia* **31**, 2143–2150 (2017).

152. Wang, Y.-H. *et al.* Cell-state-specific metabolic dependency in hematopoiesis and leukemogenesis. *Cell* **158**, 1309–1323 (2014).

153. Ye, H. *et al.* Subversion of Systemic Glucose Metabolism as a Mechanism to Support the Growth of Leukemia Cells. *Cancer Cell* **34**, 659-673.e6 (2018).

154. Unwin, R. D. *et al.* Quantitative proteomics reveals posttranslational control as a regulatory factor in primary hematopoietic stem cells. *Blood* **107**, 4687–4694 (2006).

155. Patra, K. C. & Hay, N. The pentose phosphate pathway and cancer. *Trends Biochem. Sci.* **39**, 347–354 (2014).

156. Cho, E. S., Cha, Y. H., Kim, H. S., Kim, N. H. & Yook, J. I. The Pentose Phosphate Pathway as a Potential Target for Cancer Therapy. *Biomol. Ther. (Seoul).* **26**, 29–38 (2018).

157. Ge, T. *et al.* The Role of the Pentose Phosphate Pathway in Diabetes and Cancer. *Front. Endocrinol. (Lausanne).* **11**, 365 (2020).

158. Jin, L. & Zhou, Y. Crucial role of the pentose phosphate pathway in malignant tumors. *Oncol. Lett.* **17**, 4213–4221 (2019).

159. Krockenberger, M. *et al.* Expression of transketolase-like 1 protein (TKTL1) in human endometrial cancer. *Anticancer Res.* **30**, 1653–1659 (2010).

160. Mitsuishi, Y. *et al.* Nrf2 Redirects Glucose and Glutamine into

Anabolic Pathways in Metabolic Reprogramming. *Cancer Cell* **22**, 66–79 (2012).

161. Poulain, L. *et al.* High mTORC1 activity drives glycolysis addiction and sensitivity to G6PD inhibition in acute myeloid leukemia cells. *Leukemia* **31**, 2326–2335 (2017).
162. Rao, X. *et al.* O-GlcNAcylation of G6PD promotes the pentose phosphate pathway and tumor growth. *Nat. Commun.* **6**, 8468 (2015).
163. Jiang, P. *et al.* P53 regulates biosynthesis through direct inactivation of glucose-6-phosphate dehydrogenase. *Nat. Cell Biol.* **13**, 310–316 (2011).
164. Xu, S. N., Wang, T. S., Li, X. & Wang, Y. P. SIRT2 activates G6PD to enhance NADPH production and promote leukaemia cell proliferation. *Sci. Rep.* **6**, 1–13 (2016).
165. Ma, X. *et al.* Polo-like kinase 1 coordinates biosynthesis during cell cycle progression by directly activating pentose phosphate pathway. *Nat. Commun.* **8**, 1506 (2017).
166. Zhang, X. *et al.* Pak4 regulates g6pd activity by p53 degradation involving colon cancer cell growth. *Cell Death Dis.* **8**, 1–9 (2017).
167. Wang, J. *et al.* Reprogramming metabolism by histone methyltransferase NSD2 drives endocrine resistance via coordinated activation of pentose phosphate pathway enzymes. *Cancer Lett.* **378**, 69–79 (2016).
168. Shan, C. *et al.* Lysine acetylation activates 6-phosphogluconate dehydrogenase to promote tumor growth. *Mol. Cell* **55**, 552–565 (2014).
169. Guo, H., Xiang, Z., Zhang, Y. & Sun, D. Inhibiting 6-phosphogluconate dehydrogenase enhances chemotherapy efficacy in cervical cancer via AMPK-independent inhibition of RhoA and Rac1. *Clin. Transl. Oncol.* **21**, 404–411 (2019).

170. Zheng, W. *et al.* Inhibition of 6-phosphogluconate dehydrogenase reverses cisplatin resistance in ovarian and lung cancer. *Front. Pharmacol.* **8**, 1–11 (2017).
171. Bhanot, H. *et al.* Acute myeloid leukemia cells require 6-phosphogluconate dehydrogenase for cell growth and NADPH-dependent metabolic reprogramming. *Oncotarget* **8**, 67639–67650 (2017).
172. Ying, H. *et al.* Oncogenic kras maintains pancreatic tumors through regulation of anabolic glucose metabolism. *Cell* **149**, 656–670 (2012).
173. Qiu, Z. *et al.* MicroRNA-124 Reduces the Pentose Phosphate Pathway and Proliferation by Targeting PRPS1 and RPIA mRNAs in Human Colorectal Cancer Cells. *Gastroenterology* **149**, 1587-1598.e11 (2015).
174. Ding, Y. *et al.* Synthetic lethality between HER2 and transaldolase in intrinsically resistant HER2-positive breast cancers. *Nat. Commun.* **9**, 4274 (2018).
175. Vizán, P. *et al.* Modulation of pentose phosphate pathway during cell cycle progression in human colon adenocarcinoma cell line HT29. *Int. J. cancer* **124**, 2789–2796 (2009).
176. Xu, X., Zur Hausen, A., Coy, J. F. & Löchelt, M. Transketolase-like protein 1 (TKTL1) is required for rapid cell growth and full viability of human tumor cells. *Int. J. cancer* **124**, 1330–1337 (2009).
177. Liu, H. *et al.* Fructose induces transketolase flux to promote pancreatic cancer growth. *Cancer Res.* **70**, 6368–6376 (2010).
178. Qin, Z. *et al.* Transketolase (TKT) activity and nuclear localization promote hepatocellular carcinoma in a metabolic and a non-metabolic manner. *J. Exp. Clin. Cancer Res.* **38**, 154 (2019).
179. Dasgupta, S. *et al.* Metabolic enzyme PFKFB4 activates transcriptional coactivator SRC-3 to drive breast cancer. *Nature*

556, 249–254 (2018).

180. Li, M. *et al.* Transketolase Deficiency Protects the Liver from DNA Damage by Increasing Levels of Ribose 5-Phosphate and Nucleotides. *Cancer Res.* **79**, 3689–3701 (2019).
181. Chen, Y. *et al.* Inhibition of pentose phosphate pathway suppresses acute myelogenous leukemia. *Tumor Biol.* **37**, 6027–6034 (2016).
182. Mizuno, H., Koya, J., Masamoto, Y., Kagoya, Y. & Kurokawa, M. Evi1 upregulates Fbp1 and supports progression of acute myeloid leukemia through pentose phosphate pathway activation. *Cancer Sci.* **112**, 4112–4126 (2021).
183. Xiao, G. *et al.* B-Cell-Specific Diversion of Glucose Carbon Utilization Reveals a Unique Vulnerability in B Cell Malignancies. *Cell* **173**, 470-484.e18 (2018).
184. Corbet, C. & Feron, O. Cancer cell metabolism and mitochondria: Nutrient plasticity for TCA cycle fueling. *Biochim. Biophys. Acta - Rev. Cancer* **1868**, 7–15 (2017).
185. Sajnani, K., Islam, F., Smith, R. A., Gopalan, V. & Lam, A. K. Y. Genetic alterations in Krebs cycle and its impact on cancer pathogenesis. *Biochimie* **135**, 164–172 (2017).
186. Valvezan, A. J. & Manning, B. D. Molecular logic of mTORC1 signalling as a metabolic rheostat. *Nat. Metab.* **1**, 321–333 (2019).
187. Vander Heiden, M. G. & DeBerardinis, R. J. Understanding the Intersections between Metabolism and Cancer Biology. *Cell* **168**, 657–669 (2017).
188. D'Arcy, M. S. Cell death: a review of the major forms of apoptosis, necrosis and autophagy. *Cell Biol. Int.* **43**, 582–592 (2019).
189. Wong, R. S. Y. Apoptosis in cancer: From pathogenesis to treatment. *J. Exp. Clin. Cancer Res.* **30**, 87 (2011).
190. Moloney, J. N. & Cotter, T. G. ROS signalling in the biology of cancer. *Semin. Cell Dev. Biol.* **80**, 50–64 (2018).

191. Warburg, O. On the Origin of Cancer Cells. *Science (80-.).* **123**, 309–314 (1956).
192. Crabtree, H. G. Observations on the carbohydrate metabolism of tumours. *Biochem. J.* **23**, 536–545 (1929).
193. Diaz-Ruiz, R., Rigoulet, M. & Devin, A. The Warburg and Crabtree effects: On the origin of cancer cell energy metabolism and of yeast glucose repression. *Biochim. Biophys. Acta - Bioenerg.* **1807**, 568–576 (2011).
194. Zhou, S., Kachhap, S. & Singh, K. K. Mitochondrial impairment in p53-deficient human cancer cells. *Mutagenesis* **18**, 287–292 (2003).
195. Mullen, A. R. *et al.* Reductive carboxylation supports growth in tumour cells with defective mitochondria. *Nature* **481**, 385–388 (2011).
196. Zong, W.-X., Rabinowitz, J. D. & White, E. Mitochondria and Cancer. *Mol. Cell* **61**, 667–676 (2016).
197. Baysal, B. E. *et al.* Mutations in SDHD , a Mitochondrial Complex II Gene, in Hereditary Paraganglioma. *Science (80-.).* **287**, 848–851 (2000).
198. Tomlinson, I. P. M. *et al.* Germline mutations in FH predispose to dominantly inherited uterine fibroids, skin leiomyomata and papillary renal cell cancer. *Nat. Genet.* **30**, 406–410 (2002).
199. Martínez-Reyes, I. & Chandel, N. S. Mitochondrial TCA cycle metabolites control physiology and disease. *Nat. Commun.* **11**, 1–11 (2020).
200. Xiao, M. *et al.* Inhibition of α-KG-dependent histone and DNA demethylases by fumarate and succinate that are accumulated in mutations of FH and SDH tumor suppressors. *Genes Dev.* **26**, 1326–1338 (2012).
201. Yamashita, M., Dellorusso, P. V., Olson, O. C. & Passegué, E. Dysregulated haematopoietic stem cell behaviour in myeloid

leukaemogenesis. *Nat. Rev. Cancer* **20**, 365–382 (2020).

202. Choi, B.-H. & Coloff, J. L. The Diverse Functions of Non-Essential Amino Acids in Cancer. *Cancers (Basel).* **11**, 675 (2019).

203. Tabe, Y., Lorenzi, P. L. & Konopleva, M. Amino acid metabolism in hematologic malignancies and the era of targeted therapy. *Blood* **134**, 1014–1023 (2019).

204. Fultang, L., Gneo, L., De Santo, C. & Mussai, F. J. Targeting Amino Acid Metabolic Vulnerabilities in Myeloid Malignancies. *Front. Oncol.* **11**, 674720 (2021).

205. Nguyen, T.-L. & Durán, R. V. Glutamine metabolism in cancer therapy. *Cancer Drug Resist.* **1**, 126–138 (2018).

206. Patel, D. *et al.* Aspartate rescues S-phase arrest caused by suppression of glutamine utilization in KRas-driven cancer cells. *J. Biol. Chem.* **291**, 9322–9329 (2016).

207. Hao, Y. *et al.* Oncogenic PIK3CA mutations reprogram glutamine metabolism in colorectal cancer. *Nat. Commun.* **7**, 1–13 (2016).

208. Xu, P. *et al.* LRH-1-dependent programming of mitochondrial glutamine processing drives liver cancer. *Genes Dev.* **30**, 1255–1260 (2016).

209. Vié, N. *et al.* Overexpression of phosphoserine aminotransferase PSAT1 stimulates cell growth and increases chemoresistance of colon cancer cells. *Mol. Cancer* **7**, 1–14 (2008).

210. Liu, W. *et al.* Reprogramming of proline and glutamine metabolism contributes to the proliferative and metabolic responses regulated by oncogenic transcription factor c-MYC. *Proc. Natl. Acad. Sci. U. S. A.* **109**, 8983–8988 (2012).

211. Li, H., Meininger, C. J., Bazer, F. W. & Wu, G. Intracellular sources of ornithine for polyamine synthesis in endothelial cells. *Amino Acids* **48**, 2401–2410 (2016).

212. Brosnan, J. T. Interorgan amino acid transport and its regulation. *J.*

Nutr. **133**, 2068S-2072S (2003).

213. Krebs, H. A. Metabolism of amino-acids. *Biochem. J.* **29**, 1951–1969 (1935).

214. Pennati, M., Folini, M. & Zaffaroni, N. Targeting survivin in cancer therapy: Fulfilled promises and open questions. *Carcinogenesis* **28**, 1133–1139 (2007).

215. Du, Z. X. *et al.* Antisurvivin oligonucleotides inhibit growth and induce apoptosis in human medullary thyroid carcinoma cells. *Exp. Mol. Med.* **38**, 230–240 (2006).

216. Yang, C. T. *et al.* Adenovirus-mediated transfer of siRNA against survivin enhances the radiosensitivity of human non-small cell lung cancer cells. *Cancer Gene Ther.* **17**, 120–130 (2010).

217. Clancy, K. P. *et al.* Localization of the l-glutamine synthetase gene to chromosome 1q23. *Genomics* **38**, 418–420 (1996).

218. Dang, C. V. Glutaminolysis: Supplying carbon or nitrogen or both for cancer cells? *Cell Cycle* **9**, 3884–3886 (2010).

219. Friday, E., Oliver, R., Welbourne, T. & Turturro, F. Glutaminolysis and glycolysis regulation by troglitazone in breast cancer cells: Relationship to mitochondrial membrane potential. *J. Cell. Physiol.* **226**, 511–519 (2011).

220. Van Geldermalsen, M. *et al.* ASCT2/SLC1A5 controls glutamine uptake and tumour growth in triple-negative basal-like breast cancer. *Oncogene* **35**, 3201–3208 (2016).

221. Bröer, A., Rahimi, F. & Bröer, S. Deletion of amino acid transporter ASCT2 (SLC1A5) Reveals an essential role for transporters SNAT1 (SLC38A1) and SNAT2 (SLC38A2) to sustain glutaminolysis in cancer cells. *J. Biol. Chem.* **291**, 13194–13205 (2016).

222. Bott, A. J., Maimouni, S. & Zong, W.-X. The Pleiotropic Effects of Glutamine Metabolism in Cancer. *Cancers (Basel).* **11**, 1–16 (2019).

223. Kreitz, J. *et al.* Metabolic Plasticity of Acute Myeloid Leukemia. *Cells* **8**, 805 (2019).

224. Vats, P. *et al.* Changes in the activity levels of glutamine synthetase, glutaminase and glycogen synthetase in rats subjected to hypoxic stress. *Int. J. Biometeorol.* **42**, 205–209 (1999).

225. Kobayashi, S. & Millhorn, D. E. Hypoxia regulates glutamate metabolism and membrane transport in rat PC12 cells. *J. Neurochem.* **76**, 1935–1948 (2001).

226. Grewer, C., Gameiro, A. & Rauen, T. SLC1 glutamate transporters. *Pflügers Arch. - Eur. J. Physiol.* **466**, 3–24 (2014).

227. Mackenzie, B. & Erickson, J. D. Sodium-coupled neutral amino acid (System N/A) transporters of the SLC38 gene family. *Pflugers Arch. Eur. J. Physiol.* **447**, 784–795 (2004).

228. Neinast, M., Murashige, D. & Arany, Z. Branched Chain Amino Acids. *Annu. Rev. Physiol.* **81**, 139–164 (2019).

229. Meister, A. & Anderson, M. E. Glutathione. *Annu. Rev. Biochem.* **52**, 711–760 (1983).

230. Jones, M. E. Conversion of Glutamate to Ornithine and Proline: Pyrroline-5-Carboxylate, a Possible Modulator of Arginine Requirements. *J. Nutr.* **115**, 509–515 (1985).

231. Dolfi, S. C. *et al.* The metabolic demands of cancer cells are coupled to their size and protein synthesis rates. *Cancer Metab.* **1**, 20 (2013).

232. Yang, M. & Vousden, K. H. Serine and one-carbon metabolism in cancer. *Nat. Rev. Cancer* **16**, 650–662 (2016).

233. Ye, J. *et al.* Pyruvate kinase M2 promotes de novo serine synthesis to sustain mTORC1 activity and cell proliferation. *Proc. Natl. Acad. Sci. U. S. A.* **109**, 6904–6909 (2012).

234. Newman, A. C. & Maddocks, O. D. K. One-carbon metabolism in cancer. *Br. J. Cancer* **116**, 1499–1504 (2017).

235. Sanderson, S. M., Gao, X., Dai, Z. & Locasale, J. W. Methionine

metabolism in health and cancer: a nexus of diet and precision medicine. *Nat. Rev. Cancer* **19**, 625–637 (2019).

236. Ning, S. *et al.* SHMT2 Overexpression Predicts Poor Prognosis in Intrahepatic Cholangiocarcinoma. *Gastroenterol. Res. Pract.* **2018**, 1–6 (2018).
237. Zhang, L. *et al.* Prognostic and therapeutic value of mitochondrial serine hydroxyl-methyltransferase 2 as a breast cancer biomarker. *Oncol. Rep.* **36**, 2489–2500 (2016).
238. Nilsson, R. *et al.* Metabolic enzyme expression highlights a key role for MTHFD2 and the mitochondrial folate pathway in cancer. *Nat. Commun.* **5**, 3128 (2014).
239. Pikman, Y. *et al.* Targeting MTHFD2 in acute myeloid leukemia. *J. Exp. Med.* **213**, 1285–1306 (2016).
240. Erčulj, N., Kotnik, B. F., Debeljak, M., Jazbec, J. & Dolžan, V. Influence of folate pathway polymorphisms on high-dose methotrexate-related toxicity and survival in childhood acute lymphoblastic leukemia. *Leuk. Lymphoma* **53**, 1096–1104 (2012).
241. Krajinovic, M. *et al.* Role of polymorphism in MTHFR and MTHFD1 genes in the outcome of childhood acute lymphoblastic leukemia. *Pharmacogenomics J.* **4**, 66–72 (2004).
242. Casero, R. A., Murray Stewart, T. & Pegg, A. E. Polyamine metabolism and cancer: treatments, challenges and opportunities. *Nat. Rev. Cancer* **18**, 681–695 (2018).
243. Panieri, E. & Santoro, M. M. ROS homeostasis and metabolism: a dangerous liason in cancer cells. *Cell Death Dis.* **7**, e2253 (2016).
244. Pastorek, J. & Pastorekova, S. Hypoxia-induced carbonic anhydrase IX as a target for cancer therapy: From biology to clinical use. *Semin. Cancer Biol.* **31**, 52–64 (2015).
245. Keshet, R., Szlosarek, P., Carracedo, A. & Erez, A. Rewiring urea cycle metabolism in cancer to support anabolism. *Nat. Rev. Cancer*

18, 634–645 (2018).

246. Khan, F. H. *et al.* The role of nitric oxide in cancer: Master regulator or not? *Int. J. Mol. Sci.* **21**, 1–30 (2020).

247. Somasundaram, V. *et al.* Molecular mechanisms of nitric oxide in cancer progression, signal transduction, and metabolism. *Antioxidants Redox Signal.* **30**, 1124–1143 (2019).

248. de la Cruz-Ojeda, P., Flores-Campos, R., Dios-Barbeito, S., Navarro-Villarán, E. & Muntané, J. Role of Nitric Oxide in Gene Expression Regulation during Cancer: Epigenetic Modifications and Non-Coding RNAs. *Int. J. Mol. Sci.* **22**, 6264 (2021).

249. Kim, J. *et al.* CPS1 maintains pyrimidine pools and DNA synthesis in KRAS/LKB1-mutant lung cancer cells. *Nature* **546**, 168–172 (2017).

250. Celiktas, M. *et al.* Role of CPS1 in cell growth, metabolism, and prognosis in LKB1-inactivated lung adenocarcinoma. *J. Natl. Cancer Inst.* **109**, 1–9 (2017).

251. Lee, Y. Y. *et al.* Overexpression of CPS1 is an independent negative prognosticator in rectal cancers receiving concurrent chemoradiotherapy. *Tumor Biol.* **35**, 11097–11105 (2014).

252. Rabinovich, S. *et al.* Diversion of aspartate in ASS1-deficient tumours fosters de novo pyrimidine synthesis. *Nature* **527**, 379–383 (2015).

253. Bateman, L. A. *et al.* Argininosuccinate Synthase 1 is a Metabolic Regulator of Colorectal Cancer Pathogenicity. *ACS Chem. Biol.* **12**, 905–911 (2017).

254. Shan, Y. S. *et al.* Argininosuccinate synthetase 1 suppression and arginine restriction inhibit cell migration in gastric cancer cell lines. *Sci. Rep.* **5**, 1–10 (2015).

255. Daunys, S. & Petrikaitė, V. The roles of carbonic anhydrases IX and XII in cancer cell adhesion, migration, invasion and metastasis. *Biol.*

Cell **112**, 383–397 (2020).

256. Vardon, A. *et al.* Arginine auxotrophic gene signature in paediatric sarcomas and brain tumours provides a viable target for arginine depletion therapies. *Oncotarget* **8**, 63506–63517 (2017).

257. De Santo, C. *et al.* The arginine metabolome in acute lymphoblastic leukemia can be targeted by the pegylated-recombinant arginase I BCT-100. *Int. J. Cancer* **142**, 1490–1502 (2018).

258. Lytovchenko, O. & Kunji, E. R. S. Expression and putative role of mitochondrial transport proteins in cancer. *Biochim. Biophys. Acta - Bioenerg.* **1858**, 641–654 (2017).

259. Sotgia, F. *et al.* Mitochondria 'fuel' breast cancer metabolism: Fifteen markers of mitochondrial biogenesis label epithelial cancer cells, but are excluded from adjacent stromal cells. *Cell Cycle* **11**, 4390–4401 (2012).

260. Green, C. R. *et al.* Branched-chain amino acid catabolism fuels adipocyte differentiation and lipogenesis. *Nat. Chem. Biol.* **12**, 15–21 (2016).

261. Wolfson, R. L. *et al.* Sestrin2 is a leucine sensor for the mTORC1 pathway. *Science (80-.).* **351**, 43–48 (2016).

262. Sener, A. & Malaisse, W. J. L-leucine and a nonmetabolized analogue activate pancreatic islet glutamate dehydrogenase. *Nature* **288**, 187–189 (1980).

263. Hattori, A. *et al.* Cancer progression by reprogrammed BCAA metabolism in myeloid leukaemia. *Nature* **545**, 500–504 (2017).

264. Gu, Z. *et al.* Loss of EZH2 reprograms BCAA metabolism to drive leukemic transformation. *Cancer Discov.* **9**, 1228–1247 (2019).

265. Roela, R. A. *et al.* Gene stage-specific expression in the microenvironment of pediatric myelodysplastic syndromes. *Leuk. Res.* **31**, 579–589 (2007).

266. McBrayer, S. K. *et al.* Transaminase Inhibition by 2-

Hydroxyglutarate Impairs Glutamate Biosynthesis and Redox Homeostasis in Glioma. *Cell* **175**, 101-116.e25 (2018).

267. Oktyabri, D., Ishimura, A., Tange, S., Terashima, M. & Suzuki, T. DOT1L histone methyltransferase regulates the expression of BCAT1 and is involved in sphere formation and cell migration of breast cancer cell lines. *Biochimie* **123**, 20–31 (2016).
268. Kohlmeier, M. Amino Acids and Nitrogen Compounds. in *Nutrient Metabolism* 265–477 (Elsevier, 2015).
269. Sun, Y. *et al.* Loss of alanine-glyoxylate and serine-pyruvate aminotransferase expression accelerated the progression of hepatocellular carcinoma and predicted poor prognosis. *J. Transl. Med.* **17**, 1–16 (2019).
270. Kjersem, J. B. *et al.* AGXT and ERCC2 polymorphisms are associated with clinical outcome in metastatic colorectal cancer patients treated with 5-FU/oxaliplatin. *Pharmacogenomics J.* **16**, 272–279 (2016).
271. Kunutsor, S. K., Apekey, T. A., Van Hemelrijck, M., Calori, G. & Perseghin, G. Gamma glutamyltransferase, alanine aminotransferase and risk of cancer: Systematic review and meta-analysis. *Int. J. Cancer* **136**, 1162–1170 (2015).
272. Curti, A. *et al.* Modulation of tryptophan catabolism by human leukemic cells results in the conversion of CD25- into CD25+ T regulatory cells. *Blood* **109**, 2871–2877 (2007).
273. Arandi, N., Ramzi, M., Safaei, F. & Monabati, A. Overexpression of indoleamine 2,3-dioxygenase correlates with regulatory T cell phenotype in acute myeloid leukemia patients with normal karyotype. *Blood Res.* **53**, 294–298 (2018).
274. Krall, A. S., Xu, S., Graeber, T. G., Braas, D. & Christofk, H. R. Asparagine promotes cancer cell proliferation through use as an amino acid exchange factor. *Nat. Commun.* **7**, 1–13 (2016).

275. Lomelino, C. L., Andring, J. T., McKenna, R. & Kilberg, M. S. Asparagine synthetase: Function, structure, and role in disease. *J. Biol. Chem.* **292**, 19952–19958 (2017).

276. Jiang, J. *et al.* Promoter demethylation of the asparagine synthetase gene is required for ATF4-dependent adaptation to asparagine depletion. *J. Biol. Chem.* **294**, 18674–18684 (2019).

277. Aslanian, A. M. & Kilberg, M. S. Multiple adaptive mechanisms affect asparagine synthetase substrate availability in asparaginase-resistant MOLT-4 human leukaemia cells. *Biochem. J.* **358**, 59–67 (2001).

278. Avramis, V. I. Asparaginases: biochemical pharmacology and modes of drug resistance. *Anticancer Res.* **32**, 2423–2437 (2012).

279. D'Aniello, C., Patriarca, E. J., Phang, J. M. & Minchiotti, G. Proline Metabolism in Tumor Growth and Metastatic Progression. *Front. Oncol.* **10**, 1–14 (2020).

280. Phang, J. M., Liu, W. & Zabirnyk, O. Proline metabolism and microenvironmental stress. *Annu. Rev. Nutr.* **30**, 441–463 (2010).

281. Maxwell, S. A. & Davis, G. E. Differential gene expression in p53-mediated apoptosis-resistant vs. apoptosis-sensitive tumor cell lines. *Proc. Natl. Acad. Sci. U. S. A.* **97**, 13009–13014 (2000).

282. Maxwell, S. A. & Rivera, A. Proline oxidase induces apoptosis in tumor cells, and its expression is frequently absent or reduced in renal carcinomas. *J. Biol. Chem.* **278**, 9784–9789 (2003).

283. Polyak, K., Xia, Y., Zweier, J. L., Kinzler, K. W. & Vogelstein, B. A model for p53-induced apoptosis. *Nature* **389**, 300–305 (1997).

284. Donald, S. P. *et al.* Proline oxidase, encoded by p53-induced gene-6, catalyzes the generation of proline-dependent reactive oxygen species. *Cancer Res.* **61**, 1810–1815 (2001).

285. Tang, L. *et al.* Global metabolic profiling identifies a pivotal role of proline and hydroxyproline metabolism in supporting hypoxic

response in hepatocellular carcinoma. *Clin. Cancer Res.* **24**, 474–485 (2018).

286. Liu, Y. *et al.* Proline oxidase functions as a mitochondrial tumor suppressor in human cancers. *Cancer Res.* **69**, 6414–6422 (2009).

287. Fang, H. *et al.* HDAC inhibitors induce proline dehydrogenase (POX) transcription and anti-apoptotic autophagy in triple negative breast cancer. *Acta Biochim. Biophys. Sin. (Shanghai).* **51**, 1064–1070 (2019).

288. Liu, Y. *et al.* Cancer progression is mediated by proline catabolism in non-small cell lung cancer. *Oncogene* **39**, 2358–2376 (2020).

289. Ding, Z. *et al.* Metabolic pathway analyses identify proline biosynthesis pathway as a promoter of liver tumorigenesis. *J. Hepatol.* **72**, 725–735 (2020).

290. Liu, W., Hancock, C. N., Fischer, J. W., Harman, M. & Phang, J. M. Proline biosynthesis augments tumor cell growth and aerobic glycolysis: Involvement of pyridine nucleotides. *Sci. Rep.* **5**, 1–13 (2015).

291. Crowther, L. M., Mathis, D., Poms, M. & Plecko, B. New insights into human lysine degradation pathways with relevance to pyridoxine-dependent epilepsy due to antiquitin deficiency. *J. Inherit. Metab. Dis.* **42**, 620–628 (2019).

292. Hutzler, J. & Dancis, J. Conversion of lysine to saccharopine by human tissues. *Biochim. Biophys. Acta - Gen. Subj.* **158**, 62–69 (1968).

293. Noda, C. & Ichihara, A. Purification and properties of l-lysine-α-ketoglutarate reductase from rat liver mitochondria. *Biochim. Biophys. Acta - Enzymol.* **525**, 307–313 (1978).

294. Rose, W. C., Borman, A., Coon, M. J. & Lambert, G. F. The Amino Acid Requirements of Man. *J. Biol. Chem.* **214**, 579–587 (1955).

295. Gil, J., Ramírez-Torres, A. & Encarnación-Guevara, S. Lysine

acetylation and cancer: A proteomics perspective. *J. Proteomics* **150**, 297–309 (2017).

296. Matthews, D. E. Review of Lysine Metabolism with a Focus on Humans. *J. Nutr.* **150**, 2548S-2555S (2020).
297. Han, C. *et al.* Regulation of L-threonine dehydrogenase in somatic cell reprogramming. *Stem Cells* **31**, 953–965 (2013).
298. Van Winkle, L. J., Galat, V. & Iannaccone, P. M. Threonine appears to be essential for proliferation of human as well as mouse embryonic stem cells. *Front. Cell Dev. Biol.* **2**, 18 (2014).
299. Edgar, A. J. The human L-threonine 3-dehydrogenase gene is an expressed pseudogene. *BMC Genet.* **3**, 1–13 (2002).
300. Malinovsky, A. V. Reason for indispensability of threonine in humans and other mammals in comparative aspect. *Biochem.* **82**, 1055–1060 (2017).
301. Derave, W., Everaert, I., Beeckman, S. & Baguet, A. Muscle Carnosine Metabolism and β-Alanine Supplementation in Relation to Exercise and Training. *Sport. Med.* **40**, 247–263 (2010).
302. Holeček, M. Histidine in Health and Disease: Metabolism, Physiological Importance, and Use as a Supplement. *Nutrients* **12**, 848 (2020).
303. Dahl, T. A., Midden, W. R. & Hartman, P. E. Some Prevalent Biomolecules As Defenses Against Singlet Oxygen Damage. *Photochem. Photobiol.* **47**, 357–362 (1988).
304. Hartman, P. E., Hartman, Z. & Ault, K. T. Scavenging of Singlet Molecular Oxygen by Imidazole Compounds: High and Sustained Activities of Carboxy Terminal Histidine Dipeptides and exceptional activity of Imidazole-4-Acetic Acid. *Photochem. Photobiol.* **51**, 59–66 (1990).
305. Hipkiss, A. R. On the enigma of carnosine's anti-ageing actions. *Exp. Gerontol.* **44**, 237–242 (2009).

306. Song, B. C., Joo, N. S., Aldini, G. & Yeum, K. J. Biological functions of histidine-dipeptides and metabolic syndrome. *Nutr. Res. Pract.* **8**, 3–10 (2014).

307. Fell, D. & Steele, R. D. Effect of methionine on in vivo histidine metabolism in rats. *J. Nutr.* **113**, 860–866 (1983).

308. Billings, R. E., Noker, P. E. & Tephly, T. R. The role of methionine in regulating folate-dependent reactions in isolated rat hepatocytes. *Arch. Biochem. Biophys.* **208**, 108–120 (1981).

309. Abe, H. Role of Histidine-Related Compounds as Intracellular Proton Buffering Constituents in Vertebrate Muscle. *Biochem.* **65**, 757–765 (2000).

310. Berenbrink, M. Evolution of vertebrate haemoglobins: Histidine side chains, specific buffer value and Bohr effect. *Respir. Physiol. Neurobiol.* **154**, 165–184 (2006).

311. Kopple, J. D. & Swendseid, M. E. Evidence that histidine is an essential amino acid in normal and chronically uremic man. *J. Clin. Invest.* **55**, 881–891 (1975).

312. Kopple, J. D. & Swendseid, M. E. Effect of histidine intake on plasma and urine histidine levels, nitrogen balance and Nτ-methylhistidine excretion in normal and chronically uremic men. *J. Nutr.* **111**, 931–942 (1981).

313. Anderson, H. L., Cho, E. S. & Krause, P. A. Effects of dietary histidine and arginine on nitrogen retention of men. *J. Nutr.* **107**, 2067–2077 (1977).

314. Cho, E. S., Anderson, H. L., Wixom, R. L., Hanson, K. C. & Krause, G. F. Long-term effects of low histidine intake on men. *J. Nutr.* **114**, 369–384 (1984).

315. Matthews, D. E. An overview of phenylalanine and tyrosine kinetics in humans. *J. Nutr.* **137**, 1549S-1555S; discussion 1573S-1575S (2007).

316. Yang, B., Wang, X. & Ren, X. Amino acid metabolism related to immune tolerance by MDSCs. *Int. Rev. Immunol.* **31**, 177–183 (2012).

317. Wiggins, T., Kumar, S., Markar, S. R., Antonowicz, S. & Hanna, G. B. Tyrosine, phenylalanine, and tryptophan in gastroesophageal malignancy: A systematic review. *Cancer Epidemiol. Biomarkers Prev.* **24**, 32–38 (2015).

318. Neurauter, G. *et al.* Serum phenylalanine concentrations in patients with ovarian carcinoma correlate with concentrations of immune activation markers and of isoprostane-8. *Cancer Lett.* **272**, 141–147 (2008).

319. Taddei, M. L., Pardella, E., Pranzini, E., Raugei, G. & Paoli, P. Role of tyrosine phosphorylation in modulating cancer cell metabolism. *Biochim. Biophys. Acta - Rev. Cancer* **1874**, 188442 (2020).

320. Nguyeni, T. N., Nguyen, H. Q. & Duc-Haule. Unveiling prognostics biomarkers of tyrosine metabolism reprogramming in liver cancer by cross-platform gene expression analyses. *PLoS One* **15**, 1–17 (2020).

321. Sikalidis, A. K. Amino Acids and Immune Response: A Role for Cysteine, Glutamine, Phenylalanine, Tryptophan and Arginine in T-cell Function and Cancer? *Pathol. Oncol. Res.* **21**, 9–17 (2015).

322. Yamashita, D. *et al.* Targeting glioma-initiating cells via the tyrosine metabolic pathway. *J. Neurosurg.* **134**, 721–732 (2021).

323. Davis, I. & Liu, A. What is the tryptophan kynurenine pathway and why is it important to neurotherapeutics? *Expert Rev. Neurother.* **15**, 719–721 (2015).

324. Mabuchi, R. *et al.* High serum concentration of L-kynurenine predicts unfavorable outcomes in patients with acute myeloid leukemia. *Leuk. Lymphoma* **57**, 92–98 (2016).

325. Mangaonkar, A. A. *et al.* Bone marrow dendritic cell aggregates

associate with systemic immune dysregulation in chronic myelomonocytic leukemia. *Blood Adv.* **4**, 5425–5430 (2020).

326. Wójcik, W., Łukasiewicz, M. & Puppel, K. Biogenic amines: formation, action and toxicity – a review. *J. Sci. Food Agric.* **101**, 2634–2640 (2021).
327. Bae, D. H., Lane, D. J. R., Jansson, P. J. & Richardson, D. R. The old and new biochemistry of polyamines. *Biochim. Biophys. Acta - Gen. Subj.* **1862**, 2053–2068 (2018).
328. Minois, N. Molecular basis of the 'anti-aging' effect of spermidine and other natural polyamines - A mini-review. *Gerontology* **60**, 319–326 (2014).
329. Igarashi, K. & Kashiwagi, K. Modulation of cellular function by polyamines. *Int. J. Biochem. Cell Biol.* **42**, 39–51 (2010).
330. Gerner, E. W. & Meyskens, F. L. Polyamines and cancer: Old molecules, new understanding. *Nat. Rev. Cancer* **4**, 781–792 (2004).
331. Marcocci, L. *et al.* Tyramine and monoamine oxidase inhibitors as modulators of the mitochondrial membrane permeability transition. *J. Membr. Biol.* **188**, 23–31 (2002).
332. Cohen, S. M., Garland, E. M., St John, M., Okamura, T. & Smith, R. A. Acrolein initiates rat urinary bladder carcinogenesis. *Cancer Res.* **52**, 3577–3581 (1992).
333. Averill-Bates, D. A., Agostinelli, E., Przybytkowski, E. & Mondovi, B. Aldehyde dehydrogenase and cytotoxicity of purified bovine serum amine oxidase and spermine in Chinese hamster ovary cells. *Biochem. Cell Biol.* **72**, 36–42 (1994).
334. Toninello, A., Pietrangeli, P., De Marchi, U., Salvi, M. & Mondovì, B. Amine oxidases in apoptosis and cancer. *Biochim. Biophys. Acta - Rev. Cancer* **1765**, 1–13 (2006).
335. Pegg, A. E., Shantz, L. M. & Coleman, C. S. Ornithine decarboxylase as a target for chemoprevention. *J. Cell. Biochem.* **59**,

132–138 (1995).

336. Nowotarski, S. L., Woster, P. M. & Casero, R. A. Polyamines and cancer: implications for chemotherapy and chemoprevention. *Expert Rev. Mol. Med.* **15**, e3 (2013).

337. Deng, W. *et al.* Role of ornithine decarboxylase in breast cancer. *Acta Biochim. Biophys. Sin. (Shanghai).* **40**, 235–243 (2008).

338. Bettuzzi, S. *et al.* Coordinate changes of polyamine metabolism regulatory proteins during the cell cycle of normal human dermal fibroblasts. *FEBS Lett.* **446**, 18–22 (1999).

339. Lescoat, G. *et al.* Involvement of polyamines in iron(III) transport in human intestinal Caco-2 cell lines. *Mol. Cell. Biochem.* **378**, 205–215 (2013).

340. Cervelli, M., Pietropaoli, S., Signore, F., Amendola, R. & Mariottini, P. Polyamines metabolism and breast cancer: state of the art and perspectives. *Breast Cancer Res. Treat.* **148**, 233–248 (2014).

341. Zhang, J. *et al.* ROS and ROS-Mediated Cellular Signaling. *Oxid. Med. Cell. Longev.* **2016**, 1–18 (2016).

342. Gruhlke, M. C. H. & Slusarenko, A. J. The biology of reactive sulfur species (RSS). *Plant Physiol. Biochem.* **59**, 98–107 (2012).

343. Giles, G. I., Nasim, M. J., Ali, W. & Jacob, C. The reactive sulfur species concept: 15 years on. *Antioxidants* **6**, 1–29 (2017).

344. Sadowska-Bartosz, I., Ott, C., Grune, T. & Bartosz, G. Posttranslational protein modifications by reactive nitrogen and chlorine species and strategies for their prevention and elimination. *Free Radic. Res.* **48**, 1267–1284 (2014).

345. Adams, L., Franco, M. C. & Estevez, A. G. Reactive nitrogen species in cellular signaling. *Exp. Biol. Med.* **240**, 711–717 (2015).

346. Martínez, M. C. & Andriantsitohaina, R. Reactive nitrogen species: Molecular mechanisms and potential significance in health and

disease. *Antioxidants Redox Signal.* **11**, 669–702 (2009).

347. Halliwell, B. Oxygen and nitrogen are pro-carcinogens. Damage to DNA by reactive oxygen, chlorine and nitrogen species: Measurement, mechanism and the effects of nutrition. *Mutat. Res. - Genet. Toxicol. Environ. Mutagen.* **443**, 37–52 (1999).
348. Purohit, V., Simeone, D. M. & Lyssiotis, C. A. Metabolic Regulation of Redox Balance in Cancer. *Cancers (Basel).* **11**, 1–24 (2019).
349. Brand, M. D. The sites and topology of mitochondrial superoxide production. *Exp. Gerontol.* **45**, 466–472 (2010).
350. Roberge, S. *et al.* TNF-α-mediated caspase-8 activation induces ROS production and TRPM2 activation in adult ventricular myocytes. *Cardiovasc. Res.* **103**, 90–99 (2014).
351. Ilatovskaya, D. V., Pavlov, T. S., Levchenko, V. & Staruschenko, A. ROS production as a common mechanism of ENaC regulation by EGF, insulin, and IGF-1. *Am. J. Physiol. Physiol.* **304**, C102–C111 (2013).
352. Clauzure, M. *et al.* Disruption of interleukin-1β autocrine signaling rescues complex I activity and improves ROS levels in immortalized epithelial cells with impaired Cystic Fibrosis Transmembrane Conductance Regulator (CFTR) function. *PLoS One* **9**, 1–17 (2014).
353. Large, M. *et al.* A non-linear detection of phospho-histone H2AX in EA.hy926 endothelial cells following low-dose X-irradiation is modulated by reactive oxygen species. *Radiat. Oncol.* **9**, 1–8 (2014).
354. Srinivas, U. S., Tan, B. W. Q., Vellayappan, B. A. & Jeyasekharan, A. D. ROS and the DNA damage response in cancer. *Redox Biol.* **25**, 101084 (2019).
355. Bansal, A. & Simon, M. C. Glutathione metabolism in cancer progression and treatment resistance. *J. Cell Biol.* **217**, 2291–2298 (2018).

356. Bachhawat, A. K. & Yadav, S. The glutathione cycle: Glutathione metabolism beyond the γ-glutamyl cycle. *IUBMB Life* **70**, 585–592 (2018).

357. Wu, G., Fang, Y. Z., Yang, S., Lupton, J. R. & Turner, N. D. Glutathione Metabolism and Its Implications for Health. *J. Nutr.* **134**, 489–492 (2004).

358. del Río, L. A., Sandalio, L. M., Palma, J., Bueno, P. & Corpas, F. J. Metabolism of oxygen radicals in peroxisomes and cellular implications. *Free Radic. Biol. Med.* **13**, 557–580 (1992).

359. Naik, E. & Dixit, V. M. Mitochondrial reactive oxygen species drive proinflammatory cytokine production. *J. Exp. Med.* **208**, 417–420 (2011).

360. Vafa, O. *et al.* c-Myc Can Induce DNA Damage, Increase Reactive Oxygen Species, and Mitigate p53 Function. *Mol. Cell* **9**, 1031–1044 (2002).

361. Sayin, V. I. *et al.* Activation of the NRF2 antioxidant program generates an imbalance in central carbon metabolism in cancer. *Elife* **6**, 1–23 (2017).

362. Kim, J. W., Tchernyshyov, I., Semenza, G. L. & Dang, C. V. HIF-1-mediated expression of pyruvate dehydrogenase kinase: A metabolic switch required for cellular adaptation to hypoxia. *Cell Metab.* **3**, 177–185 (2006).

363. Rasool, M. *et al.* Assessment of circulating biochemical markers and antioxidative status in acute lymphoblastic leukemia (ALL) and acute myeloid leukemia (AML) patients. *Saudi J. Biol. Sci.* **22**, 106–111 (2015).

364. Vučetić, M., Cormerais, Y., Parks, S. K. & Pouysségur, J. The Central Role of Amino Acids in Cancer Redox Homeostasis: Vulnerability Points of the Cancer Redox Code. *Front. Oncol.* **7**, 319 (2017).

365. Benito, A. *et al.* Glucose-6-phosphate dehydrogenase and transketolase modulate breast cancer cell metabolic reprogramming and correlate with poor patient outcome. *Oncotarget* **8**, 106693–106706 (2017).

366. Jiang, L. *et al.* Reductive carboxylation supports redox homeostasis during anchorage-independent growth. *Nature* **532**, 255–258 (2016).

367. Wise, D. R. *et al.* Hypoxia promotes isocitrate dehydrogenase-dependent carboxylation of -ketoglutarate to citrate to support cell growth and viability. *Proc. Natl. Acad. Sci.* **108**, 19611–19616 (2011).

368. Murai, S. *et al.* Inhibition of malic enzyme 1 disrupts cellular metabolism and leads to vulnerability in cancer cells in glucose-restricted conditions. *Oncogenesis* **6**, e329 (2017).

369. Fan, J. *et al.* Quantitative flux analysis reveals folate-dependent NADPH production. *Nature* **510**, 298–302 (2014).

370. Shin, M., Momb, J. & Appling, D. R. Human mitochondrial MTHFD2 is a dual redox cofactor-specific methylenetetrahydrofolate dehydrogenase/methenyltetrahydrofolate cyclohydrolase. *Cancer Metab.* **5**, 11 (2017).

371. Hangauer, M. J. *et al.* Drug-tolerant persister cancer cells are vulnerable to GPX4 inhibition. *Nature* **551**, 247–250 (2017).

372. Short, S. P. & Williams, C. S. Selenoproteins in Tumorigenesis and Cancer Progression. *Adv. Cancer Res.* **136**, 49–83 (2017).

373. Zhu, Z. *et al.* Glutathione reductase mediates drug resistance in glioblastoma cells by regulating redox homeostasis. *J. Neurochem.* **144**, 93–104 (2018).

374. Fathollahipour, S., Patil, P. S. & Leipzig, N. D. Oxygen regulation in development: Lessons from embryogenesis towards tissue

engineering. *Cells Tissues Organs* **205**, 350–371 (2019).

375. Simon, M. C. & Keith, B. The role of oxygen availability in embryonic development and stem cell function. *Nat. Rev. Mol. Cell Biol.* **9**, 285–296 (2008).

376. Al Tameemi, W., Dale, T. P., Al-Jumaily, R. M. K. & Forsyth, N. R. Hypoxia-Modified Cancer Cell Metabolism. *Front. cell Dev. Biol.* **7**, 4 (2019).

377. Pouysségur, J., Dayan, F. & Mazure, N. M. Hypoxia signalling in cancer and approaches to enforce tumour regression. *Nature* **441**, 437–443 (2006).

378. Ruan, K., Song, G. & Ouyang, G. Role of hypoxia in the hallmarks of human cancer. *J. Cell. Biochem.* **107**, 1053–1062 (2009).

379. Denko, N. C. Hypoxia, HIF1 and glucose metabolism in the solid tumour. *Nat. Rev. Cancer* **8**, 705–713 (2008).

380. Wang, G. L., Jiang, B. H., Rue, E. A. & Semenza, G. L. Hypoxia-inducible factor 1 is a basic-helix-loop-helix-PAS heterodimer regulated by cellular O2 tension. *Proc. Natl. Acad. Sci.* **92**, 5510–5514 (1995).

381. Petrova, V., Annicchiarico-Petruzzelli, M., Melino, G. & Amelio, I. The hypoxic tumour microenvironment. *Oncogenesis* **7**, 10 (2018).

382. Wielockx, B., Grinenko, T., Mirtschink, P. & Chavakis, T. Hypoxia Pathway Proteins in Normal and Malignant Hematopoiesis. *Cells* **8**, 155 (2019).

383. Slemc, L. & Kunej, T. Transcription factor HIF1A: downstream targets, associated pathways, polymorphic hypoxia response element (HRE) sites, and initiative for standardization of reporting in scientific literature. *Tumor Biol.* **37**, 14851–14861 (2016).

384. Goda, N. & Kanai, M. Hypoxia-inducible factors and their roles in energy metabolism. *Int. J. Hematol.* **95**, 457–463 (2012).

385. Lewis, C. & Murdoch, C. Macrophage Responses to Hypoxia. *Am.*

J. Pathol. **167**, 627–635 (2005).

386. Talks, K. L. *et al.* The Expression and Distribution of the Hypoxia-Inducible Factors HIF-1α and HIF-2α in Normal Human Tissues, Cancers, and Tumor-Associated Macrophages. *Am. J. Pathol.* **157**, 411–421 (2000).

387. Testa, U., Labbaye, C., Castelli, G. & Pelosi, E. Oxidative stress and hypoxia in normal and leukemic stem cells. *Exp. Hematol.* **44**, 540–560 (2016).

388. Bigarella, C. L., Liang, R. & Ghaffari, S. Stem cells and the impact of ROS signaling. *Dev.* **141**, 4206–4218 (2014).

389. Pedersen, M. *et al.* Stem cell factor induces HIF-1α at normoxia in hematopoietic cells. *Biochem. Biophys. Res. Commun.* **377**, 98–103 (2008).

390. Schmid, T., Zhou, J. & Brüne, B. HIF-1 and p53: communication of transcription factors under hypoxia. *J. Cell. Mol. Med.* **8**, 423–431 (2004).

391. Tothova, Z. *et al.* FoxOs Are Critical Mediators of Hematopoietic Stem Cell Resistance to Physiologic Oxidative Stress. *Cell* **128**, 325–339 (2007).

392. Piccoli, C. *et al.* To breathe or not to breathe: the haematopoietic stem/progenitor cells dilemma. *Br. J. Pharmacol.* **169**, 1652–1671 (2013).

393. Graeber, T. G. *et al.* Hypoxia-mediated selection of cells with diminished apoptotic potential in solid tumours. *Nature* **379**, 88–91 (1996).

394. Seimiya, H. *et al.* Hypoxia Up-Regulates Telomerase Activity via Mitogen-Activated Protein Kinase Signaling in Human Solid Tumor Cells. *Biochem. Biophys. Res. Commun.* **260**, 365–370 (1999).

395. Kato, H. *et al.* Induction of human endometrial cancer cell senescence through modulation of HIF-1α activity by EGLN1. *Int.*

J. Cancer **118**, 1144–1153 (2006).

396. Murata, Y., Ohteki, T., Koyasu, S. & Hamuro, J. IFN-γ and pro-inflammatory cytokine production by antigen-presenting cells is dictated by intracellular thiol redox status regulated by oxygen tension. *Eur. J. Immunol.* **32**, 2866–2873 (2002).
397. Krishnamachary, B. *et al.* Hypoxia-Inducible Factor-1-Dependent Repression of E-cadherin in von Hippel-Lindau Tumor Suppressor–Null Renal Cell Carcinoma Mediated by TCF3, ZFHX1A, and ZFHX1B. *Cancer Res.* **66**, 2725–2731 (2006).
398. Yang, M.-H. *et al.* Direct regulation of TWIST by HIF-1alpha promotes metastasis. *Nat. Cell Biol.* **10**, 295–305 (2008).
399. Maryanovich, M. *et al.* An MTCH2 pathway repressing mitochondria metabolism regulates haematopoietic stem cell fate. *Nat. Commun.* **6**, 7901 (2015).
400. Daud, H., Browne, S., Al-Majmaie, R., Murphy, W. & Al-Rubeai, M. Metabolic profiling of hematopoietic stem and progenitor cells during proliferation and differentiation into red blood cells. *N. Biotechnol.* **33**, 179–186 (2016).
401. Shinohara, A. *et al.* Intracellular Reactive Oxygen Species Mark and Influence the Megakaryocyte-Erythrocyte Progenitor Fate of Common Myeloid Progenitors. *Stem Cells* **32**, 548–557 (2014).
402. Kwak, H. J. *et al.* Myeloid Cell-Derived Reactive Oxygen Species Externally Regulate the Proliferation of Myeloid Progenitors in Emergency Granulopoiesis. *Immunity* **42**, 159–171 (2015).
403. Rieger, C. T. & Fiegl, M. Microenvironmental oxygen partial pressure in acute myeloid leukemia: Is there really a role for hypoxia? *Exp. Hematol.* **44**, 578–582 (2016).
404. Karigane, D. & Takubo, K. Metabolic regulation of hematopoietic and leukemic stem/progenitor cells under homeostatic and stress conditions. *Int. J. Hematol.* **106**, 18–26 (2017).

405. Vaupel, P. Hypoxia and Aggressive Tumor Phenotype: Implications for Therapy and Prognosis. *Oncologist* **13**, 21–26 (2008).

406. Tredan, O., Galmarini, C. M., Patel, K. & Tannock, I. F. Drug Resistance and the Solid Tumor Microenvironment. *JNCI J. Natl. Cancer Inst.* **99**, 1441–1454 (2007).

407. Manesia, J. K. *et al.* Highly proliferative primitive fetal liver hematopoietic stem cells are fueled by oxidative metabolic pathways. *Stem Cell Res.* **15**, 715–721 (2015).

408. Yalcin, S. *et al.* Foxo3 is essential for the regulation of ataxia telangiectasia mutated and oxidative stress-mediated homeostasis of hematopoietic stem cells. *J. Biol. Chem.* **283**, 25692–25705 (2008).

409. Eliasson, P. *et al.* Hypoxia mediates low cell-cycle activity and increases the proportion of long-term-reconstituting hematopoietic stem cells during in vitro culture. *Exp. Hematol.* **38**, 301-310.e2 (2010).

410. Kocabas, F. *et al.* Hypoxic metabolism in human hematopoietic stem cells. *Cell Biosci.* **5**, 18–25 (2015).

411. Venter, J. C. *et al.* The Sequence of the Human Genome. *Science (80-.).* **291**, 1304–1351 (2001).

412. Tebani, A., Afonso, C., Marret, S. & Bekri, S. Omics-Based Strategies in Precision Medicine: Toward a Paradigm Shift in Inborn Errors of Metabolism Investigations. *Int. J. Mol. Sci.* **17**, 1555 (2016).

413. Olivier, M., Asmis, R., Hawkins, G. A., Howard, T. D. & Cox, L. A. The Need for Multi-Omics Biomarker Signatures in Precision Medicine. *Int. J. Mol. Sci.* **20**, 4781 (2019).

414. Momeni, Z., Hassanzadeh, E., Saniee Abadeh, M. & Bellazzi, R. A survey on single and multi omics data mining methods in cancer data classification. *J. Biomed. Inform.* **107**, 103466 (2020).

415. Yadav, S. P. The wholeness in suffix -omics, -omes, and the word

om. *J. Biomol. Tech.* **18**, 277 (2007).

416. Zhao, E. Y., Jones, M. & Jones, S. J. M. Whole-Genome Sequencing in Cancer. *Cold Spring Harb. Perspect. Med.* **9**, 1–13 (2019).

417. Manzoni, C. *et al.* Genome, transcriptome and proteome: The rise of omics data and their integration in biomedical sciences. *Brief. Bioinform.* **19**, 286–302 (2018).

418. Tomczak, K., Czerwińska, P. & Wiznerowicz, M. The Cancer Genome Atlas (TCGA): an immeasurable source of knowledge. *Contemp. Oncol. (Poznan, Poland)* **19**, A68-77 (2015).

419. Wang, Z., Gerstein, M. & Snyder, M. RNA-Seq: a revolutionary tool for transcriptomics. *Nat. Rev. Genet.* **10**, 57–63 (2009).

420. Byron, S. A., Van Keuren-Jensen, K. R., Engelthaler, D. M., Carpten, J. D. & Craig, D. W. Translating RNA sequencing into clinical diagnostics: Opportunities and challenges. *Nat. Rev. Genet.* **17**, 257–271 (2016).

421. Demircioğlu, D. *et al.* A Pan-cancer Transcriptome Analysis Reveals Pervasive Regulation through Alternative Promoters. *Cell* **178**, 1465-1477.e17 (2019).

422. Moore, D., Simoes, R. de M., Dehmer, M. & Emmert-Streib, F. Prostate Cancer Gene Regulatory Network Inferred from RNA-Seq Data. *Curr. Genomics* **20**, 38–48 (2019).

423. Menyhárt, O. & Győrffy, B. Multi-omics approaches in cancer research with applications in tumor subtyping, prognosis, and diagnosis. *Comput. Struct. Biotechnol. J.* **19**, 949–960 (2021).

424. Sun, Y. V & Hu, Y.-J. Integrative Analysis of Multi-omics Data for Discovery and Functional Studies of Complex Human Diseases. in *Advances in genetics* **93**, 147–190 (2016).

425. Vogel, C. & Marcotte, E. M. Insights into the regulation of protein abundance from proteomic and transcriptomic analyses. *Nat. Rev. Genet.* **13**, 227–232 (2012).

426. Bell, C. G. & Beck, S. The epigenomic interface between genome and environment in common complex diseases. *Brief. Funct. Genomics* **9**, 477–485 (2010).

427. Cesnik, A. J., Shortreed, M. R., Sheynkman, G. M., Frey, B. L. & Smith, L. M. Human Proteomic Variation Revealed by Combining RNA-Seq Proteogenomics and Global Post-Translational Modification (G-PTM) Search Strategy. *J. Proteome Res.* **15**, 800–808 (2016).

428. Law, H. C.-H. *et al.* The Proteomic Landscape of Pancreatic Ductal Adenocarcinoma Liver Metastases Identifies Molecular Subtypes and Associations with Clinical Response. *Clin. Cancer Res.* **26**, 1065–1076 (2020).

429. Duarte, T. & Spencer, C. Personalized Proteomics: The Future of Precision Medicine. *Proteomes* **4**, 29 (2016).

430. Ali, M., Khan, S. A., Wennerberg, K. & Aittokallio, T. Global proteomics profiling improves drug sensitivity prediction: Results from a multi-omics, pan-cancer modeling approach. *Bioinformatics* **34**, 1353–1362 (2018).

431. Jang, C., Chen, L. & Rabinowitz, J. D. Metabolomics and Isotope Tracing. *Cell* **173**, 822–837 (2018).

432. John, A., Qin, B., Kalari, K. R., Wang, L. & Yu, J. Patient-specific multi-omics models and the application in personalized combination therapy. *Futur. Oncol.* **16**, 1737–1750 (2020).

433. Armitage, E. G. & Ciborowski, M. Applications of Metabolomics in Cancer Studies. *Adv. Exp. Med. Biol.* **965**, 209–234 (2017).

434. Wandro, S., Carmody, L., Gallagher, T., LiPuma, J. J. & Whiteson, K. Making It Last: Storage Time and Temperature Have Differential Impacts on Metabolite Profiles of Airway Samples from Cystic Fibrosis Patients. *mSystems* **2**, 1–9 (2017).

435. Roberts, L. D., Souza, A. L., Gerszten, R. E. & Clish, C. B. Targeted

Metabolomics. *Curr. Protoc. Mol. Biol.* **98**, Unit 30.2.1-24 (2012).

436. Vinayavekhin, N. & Saghatelian, A. Untargeted metabolomics. *Curr. Protoc. Mol. Biol.* **Chapter 30**, Unit 30.1.1-24 (2010).

437. Schrimpe-Rutledge, A. C., Codreanu, S. G., Sherrod, S. D. & McLean, J. A. Untargeted Metabolomics Strategies-Challenges and Emerging Directions. *J. Am. Soc. Mass Spectrom.* **27**, 1897–1905 (2016).

438. Cheung, P. K. *et al.* The applications of metabolomics in the molecular diagnostics of cancer. *Expert Rev. Mol. Diagn.* **19**, 785–793 (2019).

439. Higashi, R. M., Fan, T. W. M., Lorkiewicz, P. K., Moseley, H. N. B. & Lane, A. N. Stable isotope-labeled tracers for metabolic pathway elucidation by GC-MS and FT-MS. *Methods Mol. Biol.* **1198**, 147–167 (2014).

440. Winter, G. & Krömer, J. O. Fluxomics - connecting 'omics analysis and phenotypes. *Environ. Microbiol.* **15**, 1901–1916 (2013).

441. Cortassa, S. *et al.* From metabolomics to fluxomics: A computational procedure to translate metabolite profiles into metabolic fluxes. *Biophys. J.* **108**, 163–172 (2015).

442. Cascante, M. & Marin, S. Metabolomics and fluxomics approaches. *Essays Biochem.* **45**, 67–82 (2008).

443. Giraudeau, P. NMR-based metabolomics and fluxomics: Developments and future prospects. *Analyst* **145**, 2457–2472 (2020).

444. Fan, T. W.-M., Tan, J., McKinney, M. M. & Lane, A. N. Stable Isotope Resolved Metabolomics Analysis of Ribonucleotide and RNA Metabolism in Human Lung Cancer Cells. *Metabolomics* **8**, 517–527 (2012).

445. Bruntz, R. C., Lane, A. N., Higashi, R. M. & Fan, T. W. M. Exploring cancer metabolism using Stable isotope-resolved

metabolomics (SIRM). *J. Biol. Chem.* **292**, 11601–11609 (2017).

446. Lane, A. N., Higashi, R. M. & Fan, T. W.-M. Preclinical models for interrogating drug action in human cancers using Stable Isotope Resolved Metabolomics (SIRM). *Metabolomics* **12**, 139–148 (2016).

447. Schoenheimer, R. & Rittenberg, D. Deuterium as an Indicator in the Study of Intermediary Metabolism. *Science (80-.).* **82**, 156–157 (1935).

448. Lane, A. N., Fan, T. W. M. & Higashi, R. M. Isotopomer-Based Metabolomic Analysis by NMR and Mass Spectrometry. *Methods Cell Biol.* **84**, 541–588 (2008).

449. Fan, T. W. & Lane, A. N. NMR-based stable isotope resolved metabolomics in systems biochemistry. *J. Biomol. NMR* **49**, 267–280 (2011).

450. Fan, T. W. *et al.* Stable isotope-resolved metabolomics and applications for drug development. *Pharmacol. Ther.* **133**, 366–391 (2012).

451. Kunst, A., Draeger, B. & Ziegenhorn, J. D-Glucose: UV-methods with hexokinase and glucose-6-phosphate dehydrogenase. in *Methods of Enzymatic Analysis, Vol. VI* (ed. Bergmeyer, H. U.) 163–172 (Weinheim, 1984).

452. Passonneau, J. V. & Lowry, O. H. *Enzymatic Analysis*. *Biochemical Education* **23**, (Humana Press, 1993).

453. Lund, P. L-Glutamine and L-Glutamate. UV-method with Glutaminase and Glutamate Dehydrogenase. in *Methods of Enzymatic Analysis, Vol. VIII: Metabolites 3: Lipids, Amino Acids and Related Compounds* (ed. Bergmeyer, H. U.) 357–363 (Weinheim, 1985).

454. Love, M. I., Huber, W. & Anders, S. Moderated estimation of fold change and dispersion for RNA-seq data with DESeq2. *Genome*

Biol. **15**, 1–21 (2014).

455. Selivanov, V. A. *et al.* Software supporting a workflow of quantitative dynamic flux maps estimation in central metabolism from SIRM experimental data. in *Methods in Molecular Biology* (ed. Nagrath, D.) **2088**, 271–298 (Springer US, 2020).

456. Selivanov, V. A. *et al.* MIDcor, an R-program for deciphering mass interferences in mass spectra of metabolites enriched in stable isotopes. *BMC Bioinformatics* **18**, 1–9 (2017).

457. Ludwig, C. & Günther, U. L. MetaboLab - advanced NMR data processing and analysis for metabolomics. *BMC Bioinformatics* **12**, 366 (2011).

458. Reed, M. A. C. C., Roberts, J., Gierth, P., Kupče, Ē. & Günther, U. L. Quantitative Isotopomer Rates in Real-Time Metabolism of Cells Determined by NMR Methods. *Chembiochem* **20**, 2207–2211 (2019).

459. Hyberts, S. G., Milbradt, A. G., Wagner, A. B., Arthanari, H. & Wagner, G. Application of iterative soft thresholding for fast reconstruction of NMR data non-uniformly sampled with multidimensional Poisson Gap scheduling. *J. Biomol. NMR* **52**, 315–327 (2012).

460. Comín-Anduix, B. *et al.* The effect of thiamine supplementation on tumour roliferation: A metabolic control analysis study. *Eur. J. Biochem.* **268**, 4177–4182 (2001).

461. Berthon, H. A., Kuchel, P. W. & Nixon, P. F. High Control Coefficient of Transketolase in the Nonoxidative Pentose Phosphate Pathway of Human Erythrocytes: NMR, Antibody, and Computer Simulation Studies. *Biochemistry* **31**, 12792–12798 (1992).

462. Li, J. *et al.* TKTL1 promotes cell proliferation and metastasis in esophageal squamous cell carcinoma. *Biomed. Pharmacother.* **74**, 71–76 (2015).

463. Diaz-Moralli, S. *et al.* A key role for transketolase-like 1 in tumor metabolic reprogramming. *Oncotarget* **7**, 51875–51897 (2016).

464. Ahopelto, K. *et al.* TKTL1 as a Prognostic Marker in Pancreatic Ductal Adenocarcinoma and Its Correlation with FDG-PET-CT. *Oncol.* **99**, 177–185 (2021).

465. Peltonen, R. *et al.* High TKTL1 expression as a sign of poor prognosis in colorectal cancer with synchronous rather than metachronous liver metastases. *Cancer Biology and Therapy* **21**, 826–831 (2020).

466. Shi, Z., Tang, Y., Li, K. & Fan, Q. TKTL1 expression and its downregulation is implicated in cell proliferation inhibition and cell cycle arrest in esophageal squamous cell carcinoma. *Tumor Biol.* **36**, 8519–8529 (2015).

467. Heller, S. *et al.* Gene suppression of transketolase-like protein 1 (TKTl1) sensitizes glioma cells to hypoxia and ionizing radiation. *Int. J. Mol. Sci.* **19**, 1–13 (2018).

468. Kämmerer, U. *et al.* TKTL1 expression in human malign and benign cell lines. *BMC Cancer* **15**, 2 (2015).

469. Lodi, A. *et al.* Hypoxia triggers major metabolic changes in AML cells without altering indomethacin-induced TCA cycle deregulation. *ACS Chem. Biol.* **6**, 169–175 (2011).

470. Klco, J. M. *et al.* Genomic impact of transient low-dose decitabine treatment on primary AMLcells. *Blood* **121**, 1633–1643 (2013).

471. Contreras Mostazo, M. G. *et al.* Metabolic plasticity is an essential requirement of acquired tyrosine kinase inhibitor resistance in chronic myeloid leukemia. *Cancers (Basel).* **12**, 1–26 (2020).

472. Tsuchiya, S. *et al.* Establishment and characterization of a human acute monocytic leukemia cell line (THP-1). *Int. J. Cancer* **26**, 171–176 (1980).

473. Zhou, L. *et al.* SIRT 5 promotes IDH 2 desuccinylation and G6 PD

deglutarylation to enhance cellular antioxidant defense . *EMBO Rep.* **17**, 811–822 (2016).

474. Draoui, N. & Feron, O. Lactate shuttles at a glance: from physiological paradigms to anti-cancer treatments. *Dis. Model. Mech.* **4**, 727–732 (2011).

475. Mobasheri, A., Richardson, S., Mobasheri, R., Shakibaei, M. & Hoyland, J. A. Hypoxia inducible factor-1 and facilitative glucose transporters GLUT1 and GLUT3: Putative molecular components of the oxygen and glucose sensing apparatus in articular chondrocytes. *Histol. Histopathol.* **20**, 1327–1338 (2005).

476. Xia, H. *et al.* Hypoxia-induced modulation of glucose transporter expression impacts 18F-fluorodeoxyglucose PET-CT imaging in hepatocellular carcinoma. *Eur. J. Nucl. Med. Mol. Imaging* **47**, 787–797 (2020).

477. Lee, J. H. *et al.* Hypoxia Induces PDK4 Gene Expression through Induction of the Orphan Nuclear Receptor ERRγ. *PLoS One* **7**, e46324 (2012).

478. Su, Z., Liu, Y. & Zhang, H. Adaptive Cardiac Metabolism Under Chronic Hypoxia: Mechanism and Clinical Implications. *Front. Cell Dev. Biol.* **9**, 1–13 (2021).

479. Cunningham, K. F., Beeson, G. C., Beeson, C. C. & McDermott, P. J. Increased expression of estrogen-related receptor β during adaptation of adult cardiomyocytes to sustained hypoxia. *Am. J. Cardiovasc. Dis.* **6**, 46–54 (2016).

480. Leclerc, D. *et al.* Oncogenic role of PDK4 in human colon cancer cells. *Br. J. Cancer* **116**, 930–936 (2017).

481. Riddle, S. R. *et al.* Hypoxia induces hexokinase II gene expression in human lung cell line A549. *Am. J. Physiol. Cell. Mol. Physiol.* **278**, L407–L416 (2000).

482. Lu, C. W., Lin, S. C., Chen, K. F., Lai, Y. Y. & Tsai, S. J. Induction

of pyruvate dehydrogenase kinase-3 by hypoxia-inducible factor-1 promotes metabolic switch and drug resistance. *J. Biol. Chem.* **283**, 28106–28114 (2008).

483. Wyatt, E. *et al.* Regulation and Cytoprotective Role of Hexokinase III. *PLoS One* **5**, e13823 (2010).

484. Wilson, J. E. Isozymes of mammalian hexokinase: Structure, subcellular localization and metabolic function. *J. Exp. Biol.* **206**, 2049–2057 (2003).

485. Bommer, G. T., Van Schaftingen, E. & Veiga-da-Cunha, M. Metabolite Repair Enzymes Control Metabolic Damage in Glycolysis. *Trends Biochem. Sci.* **45**, 228–243 (2020).

486. Zhang, Y. *et al.* Estrogen-related receptors stimulate pyruvate dehydrogenase kinase isoform 4 gene expression. *J. Biol. Chem.* **281**, 39897–39906 (2006).

487. Yoo, H. C., Yu, Y. C., Sung, Y. & Han, J. M. Glutamine reliance in cell metabolism. *Exp. Mol. Med.* **52**, 1496–1516 (2020).

488. Simandi, Z. *et al.* Arginine methyltransferase PRMT8 provides cellular stress tolerance in aging motoneurons. *J. Neurosci.* **38**, 7683–7700 (2018).

489. Bhutia, Y. D. & Ganapathy, V. Glutamine transporters in mammalian cells and their functions in physiology and cancer. *Biochim. Biophys. Acta - Mol. Cell Res.* **1863**, 2531–2539 (2016).

490. Garcia-Bermudez, J. *et al.* Aspartate is a limiting metabolite for cancer cell proliferation under hypoxia and in tumours. *Nat. Cell Biol.* **20**, 775–781 (2018).

491. Reid, M. A. *et al.* Serine synthesis through PHGDH coordinates nucleotide levels by maintaining central carbon metabolism. *Nat. Commun.* **9**, 1–11 (2018).

492. Yamaguchi, N. *et al.* PCK1 and DHODH drive colorectal cancer liver metastatic colonization and hypoxic growth by promoting

nucleotide synthesis. *Elife* **8**, 1–26 (2019).

493. Ko, M. *et al.* Impaired hydroxylation of 5-methylcytosine in myeloid cancers with mutant TET2. *Nature* **468**, 839–843 (2010).

494. Thienpont, B. *et al.* Tumour hypoxia causes DNA hypermethylation by reducing TET activity. *Nature* **537**, 63–68 (2016).

495. Essletzbichler, P. *et al.* Megabase-scale deletion using CRISPR/Cas9 to generate a fully haploid human cell line. *Genome Res.* **24**, 2059–2065 (2014).

496. Shin, J. J. *et al.* Systematic identification of genes involved in metabolic acid stress resistance in yeast and their potential as cancer targets. *DMM Dis. Model. Mech.* **9**, 1039–1049 (2016).

497. Olbrich, T. *et al.* A Chemical Screen Identifies Compounds Capable of Selecting for Haploidy in Mammalian Cells. *Cell Rep.* **28**, 597-604.e4 (2019).

498. Joshi, S. R. *et al.* Hypoxic activation of glucose-6-phosphate dehydrogenase controls the expression of genes involved in the pathogenesis of pulmonary hypertension through the regulation of DNA methylation. *Am. J. Physiol. - Lung Cell. Mol. Physiol.* **318**, L773–L786 (2020).

499. Morinishi, L., Kochanowski, K., Levine, R. L., Wu, L. F. & Altschuler, S. J. Loss of TET2 Affects Proliferation and Drug Sensitivity through Altered Dynamics of Cell-State Transitions. *Cell Syst.* **11**, 86-94.e5 (2020).

500. Zheng, Y. *et al.* Genome-wide DNA methylation analysis identifies candidate epigenetic markers and drivers of hepatocellular carcinoma. *Brief. Bioinform.* **19**, 101–108 (2018).

501. Croze, M. L. & Soulage, C. O. Potential role and therapeutic interests of myo-inositol in metabolic diseases. *Biochimie* **95**, 1811–1827 (2013).

502. Lu, Y. *et al.* Production of myo-inositol from glucose by a novel

trienzymatic cascade of polyphosphate glucokinase, inositol 1-phosphate synthase and inositol monophosphatase. *Enzyme Microb. Technol.* **112**, 1–5 (2018).

503. Dinicola, S. *et al.* Nutritional and Acquired Deficiencies in Inositol Bioavailability. Correlations with Metabolic Disorders. *Int. J. Mol. Sci.* **18**, 2187 (2017).
504. Chatree, S., Thongmaen, N., Tantivejkul, K., Sitticharoon, C. & Vucenik, I. Role of inositols and inositol phosphates in energy metabolism. *Molecules* **25**, 1–18 (2020).
505. Takayama, K. *et al.* TET2 repression by androgen hormone regulates global hydroxymethylation status and prostate cancer progression. *Nat. Commun.* **6**, 8219 (2015).
506. Kamdar, S. *et al.* Exploring targets of TET2-mediated methylation reprogramming as potential discriminators of prostate cancer progression. *Clin. Epigenetics* **11**, 1–19 (2019).
507. Soda, K., Kano, Y., Chiba, F., Koizumi, K. & Miyaki, Y. Increased Polyamine Intake Inhibits Age-Associated Alteration in Global DNA Methylation and 1,2-Dimethylhydrazine-Induced Tumorigenesis. *PLoS One* **8**, 1–7 (2013).
508. Zhang, Y. *et al.* Hypoxia in Breast Cancer—Scientific Translation to Therapeutic and Diagnostic Clinical Applications. *Front. Oncol.* **11**, 1–9 (2021).
509. Yu, S. *et al.* Hypoxia promotes colorectal cancer cell migration and invasion in a SIRT1-dependent manner. *Cancer Cell Int.* **19**, 1–12 (2019).
510. Xu, K. *et al.* Hypoxia Induces Drug Resistance in Colorectal Cancer through the HIF-1α/miR-338-5p/IL-6 Feedback Loop. *Mol. Ther.* **27**, 1810–1824 (2019).
511. Ancel, J. *et al.* Hypoxia in Lung Cancer Management: A Translational Approach. *Cancers (Basel).* **13**, 3421 (2021).

512. Chaudary, N., Mujcic, H., Wouters, B. G. & Hill, R. P. Hypoxia and metastasis in an orthotopic cervix cancer xenograft model. *Radiother. Oncol.* **108**, 506–510 (2013).

513. Nowak, N., Kulma, A. & Gutowicz, J. Up-regulation of key glycolysis proteins in cancer development. *Open Life Sci.* **13**, 569–581 (2018).

514. Zheng, Y., Cabassa-Hourton, C., Planchais, S., Lebreton, S. & Savouré, A. The proline cycle as an eukaryotic redox valve. *J. Exp. Bot.* **72**, 6856–6866 (2021).

515. He, P. *et al.* Effects of hypoxia on DNA hydroxymethylase Tet methylcytosine dioxygenase 2 in a KG-1 human acute myeloid leukemia cell line and its mechanism. *Oncol. Lett.* **22**, 692 (2021).

516. Lin, Q. *et al.* Targeting Pyruvate Carboxylase by a Small Molecule Suppresses Breast Cancer Progression. *Adv. Sci.* **7**, 1903483 (2020).

517. Ruiz-Iglesias, A. & Mañes, S. The Importance of Mitochondrial Pyruvate Carrier in Cancer Cell Metabolism and Tumorigenesis. *Cancers (Basel).* **13**, 1488 (2021).

518. Wang, Z.-H., Peng, W.-B., Zhang, P., Yang, X.-P. & Zhou, Q. Lactate in the tumour microenvironment: From immune modulation to therapy. *EBioMedicine* **73**, 103627 (2021).

519. Yang, H. C., Stern, A. & Chiu, D. T. Y. G6PD: A hub for metabolic reprogramming and redox signaling in cancer. *Biomed. J.* **44**, 285–292 (2021).

520. Gregory, M. A. *et al.* ATM/G6PD-driven redox metabolism promotes FLT3 inhibitor resistance in acute myeloid leukemia. *Proc. Natl. Acad. Sci. U. S. A.* **113**, E6669–E6678 (2016).

521. Guerra, V. *et al.* Interim results from a phase Ib/II clinical study of the glutaminase inhibitor telaglenastat (CB-839) in combination with azacitidine in patients with advanced myelodysplastic syndrome (MDS). *J. Clin. Oncol.* **37**, 7037 (2019).

522. Shen, Y. A. *et al.* Inhibition of glutaminolysis in combination with other therapies to improve cancer treatment. *Curr. Opin. Chem. Biol.* **62**, 64–81 (2021).

8. APPENDIX I

8 Appendix I

8.1 Targeted metabolomics experiments for THP-1 cell models.

The Biocrates Absolute IDQ™ p180 kit (Biocrates Life Sciences AG, Austria) was performed as indicated in section 3.9 (full experimental procedure). Of the metabolites obtained, we analysed the intracellular concentrations and consumption/production rates of amino acids (Table 8.1-A and Table 8.1-C, respectively) and biogenic amines (Table 8.1-B and Table 8.1-D, respectively).

Concentration (nmol/mg protein)								
Metabolite	THP-1^{WT} Normoxia		THP-1^{KD} Normoxia		THP-1^{WT} Hypoxia		THP-1^{KD} Hypoxia	
	Mean	SD	Mean	SD	Mean	SD	Mean	SD
Ala	402.30	143.45	473.60	144.63	346.52	5.56	279.01	79.01
Arg	273.40	77.02	272.04	150.85	292.70	144.44	111.34	86.22
Asn	771.52	228.94	563.26	54.48	474.11	39.58	702.79	395.83
Asp	118.19	37.52	136.50	46.37	36.98	10.07	55.27	44.06
Cit	0.24	0.23	3.20	4.66	2.54	2.93	0.52	0.89
Gln	1636.46	205.69	1760.44	510.50	1377.17	295.79	1100.21	204.71
Glu	ALQ	---	1634.96	1.64	ALQ	---	1609.70	571.89
Gly	915.60	375.13	1075.90	575.77	583.59	285.89	778.96	222.69
His	72.78	13.73	46.93	17.33	58.96	8.22	36.64	16.40
Ile	185.40	38.58	200.03	38.97	210.65	76.16	153.94	44.02
Leu	236.18	55.20	248.53	52.65	249.76	63.02	168.81	66.49
Lys	40.25	17.59	53.42	8.72	63.64	23.21	38.99	25.69
Met	71.61	20.62	66.44	25.40	63.10	21.25	41.63	22.51
Orn	22.30	10.41	21.32	9.00	35.94	6.38	29.14	16.43
Phe	42.47	7.37	39.58	11.15	59.42	22.21	34.28	9.91
Pro	705.55	139.47	743.98	116.06	249.71	37.70	191.38	38.52
Ser	70.15	23.94	129.16	90.81	353.88	116.37	186.89	34.27
Thr	173.83	92.88	142.23	28.16	200.71	89.78	111.91	40.27
Trp	11.02	3.72	12.83	1.75	16.12	6.45	9.69	1.04
Tyr	76.14	26.81	91.19	14.14	89.76	32.79	82.07	19.26
Val	54.40	19.08	40.16	5.70	60.33	7.25	51.91	20.82

Table 8.1-A- Intracellular concentrations of amino acids in THP-1^{WT} and THP-1^{KD} cell models. The intracellular content of these metabolites was obtained using the Biocrates Absolute IDQ™ p180 kit (Biocrates Life Sciences AG, Austria) after 48h incubation with RPMI 1640 10mM Glc and 4mM Gln, 5% S/P and 1% FBS, in both normoxia and hypoxia conditions. ALQ stands for above limit of quantification.

Concentration (nmol/mg protein)								
Metabolite	THP-1^{WT} Normoxia		THP-1^{KD} Normoxia		THP-1^{WT} Hypoxia		THP-1^{KD} Hypoxia	
	Mean	SD	Mean	SD	Mean	SD	Mean	SD
Ac-Orn	2.44	2.34	1.18	1.91	3.27	1.82	2.57	3.02
ADMA	2.17	1.48	1.57	0.75	1.31	0.38	0.74	0.69
alpha-AAA	7.09	2.44	6.27	2.80	5.35	5.40	4.62	0.51
Carnosine	0.84	0.55	0.51	0.19	0.38	0.17	0.21	0.088
Creatinine	16.70	6.86	15.20	2.31	10.38	2.29	11.00	1.91
Histamine	0.32	0.29	0.23	0.40	ULD	---	0.25	0.44
Kynurenine	0.38	0.17	0.43	0.094	0.39	0.17	0.45	0.16
Met-SO	1.88	0.58	1.98	0.95	2.81	1.47	2.79	1.40
Putrescine	2.96	1.32	3.59	1.84	3.003	0.89	3.22	0.51
Serotonin	0.079	0.0404	0.15	0.061	ULD	---	ULD	---
Spermidine	45.35	16.23	36.51	5.33	23.81	8.99	26.50	7.43
Spermine	20.86	11.70	14.61	2.37	13.77	7.30	9.65	4.51
t4-OH-Pro	221.31	22.58	202.10	40.27	130.55	4.57	130.59	58.46
Taurine	469.08	82.46	464.12	361.99	196.01	188.34	219.15	200.75
total DMA	0.12	0.118	0.052	0.053	0.116	0.124	0.202	0.16

Table 8.1-B- Intracellular concentrations of biogenic amines in THP-1^{WT} and THP-1^{KD} cell models. The intracellular content of these metabolites was obtained using the Biocrates Absolute IDQ^{TM} p180 kit (Biocrates Life Sciences AG, Austria) after 48h incubation with RPMI 1640 10mM Glc and 4mM Gln, 5% S/P and 1% FBS, in both normoxia and hypoxia conditions. ULD stands for under limit of detection.

Metabolite	Flux Rates (nmol·millioncell^{-1}·h^{-1})							
	THP-1^{WT} Normoxia		THP-1^{KD} Normoxia		THP-1^{WT} Hypoxia		THP-1^{KD} Hypoxia	
	Mean	SD	Mean	SD	Mean	SD	Mean	SD
Ala	0.61	0.0066	0.55	0.12	0.87	0.023	0.66	0.0005
Arg	-0.43	1.48	-3.21	0.22	-0.95	0.97	-2.69	0.089
Asn	-0.48	0.0071	-1.98	0.26	-0.11	0.023	0.65	0.054
Asp	-0.38	0.33	-0.43	0.032	-0.48	0.094	-0.42	0.17
Cit	0.00998	0.0097	-0.025	0.0055	-0.026	0.0043	-0.0043	0.0043
Gln	-7.60	0.24	-7.04	0.36	-4.60	0.95	-4.91	0.33
Glu	2.24	0.078	1.64	0.0064	1.31	0.11	0.98	0.01
Gly	-0.35	0.048	-0.15	0.55	2.71	3.53	1.14	0.16
His	-0.41	0.0802	-0.55	0.094	0.067	0.031	-0.36	0.039
Ile	-1.02	0.14	-1.55	0.045	-0.47	0.047	-0.56	0.01
Leu	-1.96	0.11	-2.36	0.062	-1.21	0.13	-0.998	0.14
Lys	-1.28	0.0497	-1.65	0.058	-0.44	0.078	0.17	0.18
Met	-0.35	0.018	-0.41	0.011	-0.202	0.079	0.086	0.0083
Orn	0.59	0.078	0.63	0.077	1.25	0.039	1.35	0.24
Phe	-0.61	0.016	-0.54	0.049	-0.075	0.015	-0.16	0.017
Pro	-0.13	0.057	-0.24	0.038	0.304	0.055	0.17	0.103
Ser	-2.35	0.086	-2.33	0.13	-2.57	0.023	-2.60	0.097
Thr	-0.65	0.034	-1.05	0.00804	-0.46	0.036	-0.13	0.042
Trp	-0.18	0.0071	-0.18	0.00703	-0.033	0.021	-0.081	0.026
Tyr	-0.42	0.036	-0.63	0.045	0.11	0.13	-0.095	0.024
Val	-1.13	0.033	-1.05	0.058	-0.32	0.016	-0.56	0.29

Table 8.1-C- Consumption and production rates of amino acids in THP-1^{WT} and THP-1^{KD} cell models. The consumption/production rates of these metabolites was obtained using the Biocrates Absolute IDQ^{TM} p180 kit (Biocrates Life Sciences AG, Austria) to measure culture medium at timepoints 0h and 48h incubation with RPMI 1640 10mM Glc and 4mM Gln, 5% S/P and 1% FBS, in both normoxia and hypoxia conditions. Calculations were done according to section 3.3.

Metabolite	Flux Rates (nmol·millioncell^{-1}·h^{-1})							
	THP-1^{WT} Normoxia		THP-1^{KD} Normoxia		THP-1^{WT} Hypoxia		THP-1^{KD} Hypoxia	
	Mean	SD	Mean	SD	Mean	SD	Mean	SD
Ac-Orn	0.0011	0.00057	-0.0029	0.00083	0.0077	0.00047	0.0085	0.0038
ADMA	ND	---	ND	---	ND	---	ND	---
alpha-AAA	-0.023	0.00028	-0.019	0.0021	-0.0048	0.0011	-0.0101	0.000059
Carnosine	-0.0043	0.0037	-0.0080	0.000895	0.0059	0.0053	-0.0060	0.0012
Creatinine	0.037	0.031	-0.058	0.00895	-0.0028	0.00078	0.013	0.0077
Histamine	ND	---	ND	---	ND	---	ND	---
Kynurenine	-0.012	0.000903	-0.0059	0.0013	-0.0075	0.00027	-0.029	0.00062
Met-SO	-0.011	0.0021	-0.016	0.00064	-0.013	0.031	-0.015	0.016
Putrescine	-0.00015	0.000058	-0.00014	0.000104	0.00033	0.000038	0.0000084	0.000056
Serotonin	ND	---	ND	---	ND	---	ND	---
Spermidine	0.00010	0.000035	0.000014	0.0000064	0.00024	0.00014	0.000042	0.000048
Spermine	ND	---	ND	---	ND	---	ND	---
t4-OH-Pro	-0.11	0.021	-0.42	0.13	0.45	0.12	0.15	0.11
Taurine	-0.041	0.021	-0.099	0.0102	-0.041	0.0063	-0.022	0.0048
total DMA	0.0027	0.0013	-0.015	0.0034	0.0032	0.0023	0.0028	0.00024

Table 8.1-D- Consumption and production rates of biogenic amines in THP-1^{WT} and THP-1^{KD} cell models. The consumption/production rates of these metabolites was obtained using the Biocrates Absolute IDQ^{TM} p180 kit (Biocrates Life Sciences AG, Austria) to measure culture medium at timepoints 0h and 48h incubation with RPMI 1640 10mM Glc and 4mM Gln, 5% S/P and 1% FBS, in both normoxia and hypoxia conditions. Calculations were done according to section 3.3. ND stands for non-detectable.

8.2 Targeted metabolomics experiments for HAP-1 cell models.

The Biocrates Absolute IDQ™ p180 kit (Biocrates Life Sciences AG, Austria) was performed as indicated in section 3.9 (full experimental procedure). Of the metabolites obtained, we analysed the intracellular concentrations and consumption/production rates of amino acids (Table 8.2-A and Table 8.2-C, respectively) and biogenic amines (Table 8.2-B and Table 8.2-D, respectively).

Concentration (nmol/mg protein)								
Metabolite	HAP1 Parental Normoxia		HAP1 TET2 KO Normoxia		HAP1 Parental Hypoxia		HAP1 TET2 KO Hypoxia	
	Mean	SD	Mean	SD	Mean	SD	Mean	SD
Ala	206.69	61.11	76.49	11.89	364.78	247.20	193.26	30.39
Arg	41.51	5.44	12.66	4.01	99.59	50.80	84.84	48.78
Asn	82.38	21.23	37.56	11.00	318.19	185.68	102.17	40.24
Asp	ALQ	---	129.75	34.16	212.53	154.51	160.77	19.00
Cit	0.801	0.21	0.11	0.196	ULD	---	ULD	---
Gln	680.29	350.70	311.57	61.08	2182.00	254.68	520.71	57.65
Glu	ALQ	---	ALQ	---	1503.72	1621.66	ALQ	---
Gly	328.68	284.66	105.42	44.04	497.10	133.95	217.92	197.05
His	35.99	6.93	6.67	3.09	77.16	26.06	22.28	11.38
Ile	68.03	21.06	23.36	5.30	246.85	89.42	55.89	9.68
Leu	78.93	25.16	21.53	2.45	307.36	98.03	59.12	15.27
Lys	147.09	52.96	47.07	13.38	424.76	114.20	91.89	21.97
Met	16.64	4.33	7.97	0.67	90.04	43.12	16.87	7.14
Orn	10.35	5.03	5.42	2.13	35.35	10.99	8.68	6.38
Phe	34.52	12.69	8.21	1.18	107.78	42.76	26.66	8.04
Pro	231.14	48.30	75.69	15.98	321.57	160.79	87.64	8.34
Ser	106.94	28.67	51.06	22.42	412.75	240.95	80.58	67.01
Thr	ALQ	---	95.03	25.00	408.02	103.01	174.50	96.54
Trp	8.10	1.13	0.98	0.11	20.06	13.82	3.60	0.26
Tyr	37.92	10.40	9.74	1.72	147.32	62.78	28.76	5.21
Val	56.26	13.30	13.77	2.50	140.08	83.69	50.52	19.59

Table 8.2-A- Intracellular concentrations of amino acids in HAP-1 Parental and HAP-1 TET2 KO cell models. The intracellular content of these metabolites was obtained using the Biocrates Absolute IDQ™ p180 kit (Biocrates Life Sciences AG, Austria) after 48h incubation with IMDM 25mM Glc and 4mM Gln, 5% S/P and 1% FBS, in both normoxia and hypoxia conditions. ALQ- above limit of quantification; ULD- under limit of detection.

Concentration (nmol/mg protein)								
Metabolite	HAP1 Parental Normoxia		HAP1 TET2 KO Normoxia		HAP1 Parental Hypoxia		HAP1 TET2 KO Hypoxia	
	Mean	SD	Mean	SD	Mean	SD	Mean	SD
Ac-Orn	0.76	0.63	ULD	---	ULD	---	ULD	---
ADMA	1.18	0.24	0.55	0.32	4.19	2.46	0.58	0.195
alpha-AAA	6.80	2.68	11.48	1.86	8.54	5.27	6.75	3.77
Carnosine	0.17	0.065	ULD	---	0.52	0.47	0.081	0.039
Creatinine	9.95	2.37	1.67	0.63	27.78	14.80	10.41	0.96
Histamine	0.045	0.078	ULD	---	ULD	---	0.082	0.14
Kynurenine	0.12	0.080	0.12	0.015	0.55	0.19	0.085	0.059
Met-SO	0.503	0.30	0.095	0.085	2.26	0.56	0.51	0.037
Putrescine	4.67	1.41	9.87	1.46	11.07	3.49	2.53	0.36
Serotonin	0.018	0.0058	0.011	0.0074	ULD	---	ULD	---
Spermidine	29.93	9.97	16.39	2.17	72.39	24.24	16.77	2.77
Spermine	15.39	3.75	6.61	0.596	51.38	19.58	8.96	1.54
t4-OH-Pro	4.36	1.36	1.20	0.14	6.78	1.89	2.30	0.78
Taurine	ALQ	---	86.97	36.09	898.46	591.12	230.56	207.48
total DMA	0.78	0.24	0.077	0.068	0.31	0.46	0.15	0.051

Table 8.2-B- Intracellular concentrations of biogenic amines in HAP-1 Parental and HAP-1 TET2 KO cell models. The intracellular content of these metabolites was obtained using the Biocrates Absolute IDQ™ p180 kit (Biocrates Life Sciences AG, Austria) after 48h incubation with IMDM 25mM Glc and 4mM Gln, 5% S/P and 1% FBS, in both normoxia and hypoxia conditions. ALQ- above limit of quantification; ULD- under limit of detection.

Flux Rates (nmol·millioncell^{-1}·h^{-1})								
Metabolite	HAP1 Parental Normoxia		HAP1 TET2 KO Normoxia		HAP1 Parental Hypoxia		HAP1 TET2 KO Hypoxia	
	Mean	SD	Mean	SD	Mean	SD	Mean	SD
Ala	2.30	0.34	4.996	0.18	6.44	0.43	5.18	2.78
Arg	-4.04	0.0295	-4.86	0.44	-5.46	1.53	-4.36	1.82
Asn	-1.11	0.087	-6.23	0.25	-1.76	1.64	-1.88	0.73
Asp	-0.60	0.16	-0.59	0.13	-2.79	1.78	-2.86	0.76
Cit	0.039	0.012	0.091	0.0901	-0.0069	0.15	-0.093	0.016
Gln	-19.55	0.197	-17.53	0.85	-7.64	19.58	-21.04	2.12
Glu	1.76	0.83	5.05	0.17	4.10	11.07	3.04	3.57
Gly	-3.16	0.079	-2.33	0.099	-15.52	3.74	-12.65	1.09
His	-0.75	0.17	-1.53	0.24	-1.14	0.01	1.13	0.18
Ile	-4.14	0.19	-4.25	0.028	-9.36	0.036	-4.49	0.15
Leu	-6.27	0.26	-5.75	0.15	-16.89	0.18	-7.87	0.42
Lys	-2.96	0.98	-3.93	0.32	-11.12	3.24	-2.92	0.061
Met	-2.04	0.17	-1.17	0.014	-1.59	0.997	-2.25	0.36
Orn	0.13	0.039	0.32	0.0099	0.95	0.068	1.59	0.13
Phe	-1.40	0.069	-1.13	0.21	-2.20	1.14	-0.43	0.045
Pro	1.56	0.14	1.78	1.96	3.60	2.81	1.84	0.01
Ser	-5.85	0.197	-4.06	0.54	-3.41	1.14	-2.96	1.54
Thr	-1.83	0.14	1.40	1.18	7.15	1.50	1.86	0.091
Trp	-0.37	0.0079	-0.45	0.16	-0.89	0.27	-0.21	0.0303
Tyr	-0.75	0.33	-1.95	0.11	-1.66	0.21	-1.28	0.24
Val	-3.97	0.21	-3.49	0.17	-5.30	4.63	-3.20	2.995

Table 8.2-C- Consumption and production rates of amino acids in HAP-1 Parental and HAP-1 TET2 KO cell models. The consumption/production rates of these metabolites was obtained using the Biocrates Absolute IDQ™ p180 kit (Biocrates Life Sciences AG, Austria) to measure culture medium at timepoints 0h and 48h incubation IMDM 25mM Glc and 4mM Gln, 5% S/P and 1% FBS, in both normoxia and hypoxia conditions. Calculations were done according to section 3.3.

Flux Rates (nmol·millioncell^{-1}·h^{-1})								
Metabolite	HAP1 Parental Normoxia		HAP1 TET2 KO Normoxia		HAP1 Parental Hypoxia		HAP1 TET2 KO Hypoxia	
	Mean	SD	Mean	SD	Mean	SD	Mean	SD
Ac-Orn	0.0046	0.000098	0.048	0.0021	0.058	0.0093	0.046	0.000303
ADMA	0.014	0.000098	0.0083	0.0087	ULD	---	ULD	---
alpha-AAA	0.021	0.0049	0.104	0.0044	0.194	0.047	0.156	0.0303
Carnosine	-0.0031	0.00059	-0.024	0.0025	-0.025	0.019	-0.029	0.0203
Creatinine	0.0202	0.00295	0.031	0.028	0.27	0.021	0.13	0.0099
Histamine	ND	---	ND	---	ND	---	ND	---
Kynurenine	-0.00068	0.000098	-0.000501	0.00032	-0.00012	0.0074	0.0027	0.00085
Met-SO	-0.0108	0.000295	-0.024	0.0021	0.0037	0.0306	-0.086	0.0399
Putrescine	0.00099	0.00034	0.0034	0.000085	0.0093	0.0016	0.0102	0.0012
Serotonin	ND	---	ND	---	ND	---	ND	---
Spermidine	-0.0013	0.000059	-0.000299	0.00039	0.037	0.0087	0.014	0.00085
Spermine	-0.00045	0.0000295	0.00024	0.01	0.043	0.017	0.019	0.0011
t4-OH-Pro	-0.013	0.00064	0.074	0.104	0.097	0.15	0.082	0.00303
Taurine	-0.13	0.015	-0.064	0.016	0.43	0.36	0.075	0.033
total DMA	0.0068	0.0018	0.0067	0.000704	0.017	0.019	-0.0304	0.0034

Table 8.2-D- Consumption and production rates of biogenic amines in HAP-1 Parental and HAP-1 TET2 KO cell models. The consumption/production rates of these metabolites was obtained using the Biocrates Absolute IDQ™ p180 kit (Biocrates Life Sciences AG, Austria) to measure culture medium at timepoints 0h and 48h incubation IMDM 25mM Glc and 4mM Gln, 5% S/P and 1% FBS, in both normoxia and hypoxia conditions. Calculations were done according to section 3.3. ND- non-detectable; ULD- under limit of detection.

9. ACKNOWLEDGMENTS

9 Acknowledgments

First of all, I express my gratitude to Prof. Marta Cascante, Prof. Silvia Marín and Prof. Ulrich Guenther for selecting me for such an innovative PhD program. The opportunity you granted me helped me grow both as a scientist and as a person.

Many thanks to all my BQI benchwork colleagues Claudia, Miriam T., Erika, Josep T., Cristina, Ibrahim, Alfonso, Róldan, for all the support during the crazy hours of running experiments, aiding me to settle in a new city and country, the companionship and enduring my endless ringtones. Special thanks to Miriam C., for the guidance and company during the long hypoxia experiments.

My gratitude to our computational group members, Dr. Pedro de Atauri, Dr. Vitaly Selivanov and Dr. Carles Foguet, for the bioinformatic support for my thesis.

To my HaemMetabolome ITN colleagues Nuria, Gaelle, Alan, Johanna, Gregorios, Aysgull and Sam, for sharing precious moments across our travels and the science collaborations.

To the HWB-NMR group of the University of Birmingham, Dr. Michelle Reed, Sarah Whittaker, Mark Jeeves, Jenny and Zuhal, for all the aid during my stay.

A heartfelt thank you to Effrosyni Karakitsou, my "Efifi", for all the friendship and sisterhood during all these years.

I would like to acknowledge my boyfriend Diogo Sousa and my childhood friends Ana de Jesus and Daniela Belela, for all the patience and encouragement.

Lastly, my gratitude to all my family for their belief in me and special thanks to my mother, that "fought" her mother-hen instincts and gave her unconditional support during all those years.